A cell-based study exploring novel therapeutic approaches to target cell stress and cell death pathways in paediatric cancers

A thesis submitted to the National University of Ireland, Galway in fulfilment of the requirement for the degree of

Doctor of Philosophy

By

Nicole McCarthy

Discipline of Biochemistry, School of Natural Sciences,
National University of Ireland, Galway.

Supervisors:
Professor Adrienne Gorman
Professor Afshin Samali
Professor Simone Fulda

August 2020

Table of Contents

Declaration

The experimental work presented in this thesis was performed at the Institute for Experimental Cancer Research in Paediatrics at Goethe University Clinic, Frankfurt, Germany.

The supervision of this thesis was conducted by Adrienne Gorman and Afshin Samali of the National University of Ireland, Galway and Simone Fulda of Goethe University, Frankfurt.

The research work in this thesis is my own original research work. Any additional research conducted by others is clearly specified at the outset of each results section.

Frankfurt am Main, 2020
Nicole McCarthy

Publications

Research Articles:

- **Nicole McCarthy,** Nadezda Dolgikh, Susan Logue, John B Patterson, Qinping Zeng, Adrienne M. Gorman, Afshin Samali, Simone Fulda (2020) The IRE1 and PERK arms of the UPR promote survival of rhabdomyosarcoma cells. Cancer Letters, volume 490, pages 76-88. DOI: 10.1016/j.canlet.2020.07.009

- Behnaz Ahangarian Abhari, **Nicole McCarthy***, Marie Le Berre, Michelle Kilcoyne, Lokesh Joshi, Patrizia Agostinis and Simone Fulda (2019) Smac mimetic suppresses tunicamycin-induced apoptosis via resolution of ER stress. Cell Death and Disease, volume 10, article number 155. DOI: 10.1038/s41419-019-1381-z.

- Behnaz Ahangarian Abhari, **Nicole McCarthy**, Patrizia Agostinis, Simone Fulda (2019) NF-κB contributes to Smac mimetic-conferred protection from tunicamycin-induced apoptosis. Apoptosis, volume 24, pages 269-277. DOI: 10.1007/s10495-018-1507-2.

Reviews:

- Aitor Almanza, Antonio Carlesso, Chetan Chintha, Stuart Creedican, Dimitrios Doultsinos, Brian Leuzzi, Andreia Luís, **Nicole McCarthy*,** Luigi Montibeller, Sanket More, Alexandra Papaioannou, Franziska Püschel, Maria Livia Sassano, Josip Skoko, Patrizia Agostinis, Jackie de Belleroche, Leif A. Eriksson, Simone Fulda, Adrienne M. Gorman, Sandra Healy, Andrey Kozlov, Cristina Muñoz-Pinedo, Markus Rehm, Eric Chevet, Afshin Samali (2018) Endoplasmic Reticulum Stress signalling – from basic mechanisms to clinical applications. FEBSJ, volume 286, Issue 2, pages 241-278. DOI: 10.1111/febs.14608

* Shared first author

Acknowledgments

Firstly I'd like to thank my supervisors Afshin, Adrienne and Simone. Afshin and Adrienne, without you none of this would have been possible. I cannot thank you enough for all you have done for me to allow me to get this far. Thank you to Simone for giving me the opportunity to work in her state of the art lab and allowing me to carry out my research without any boundaries.

Thank you to everyone involved in Train-ERS who were responsible for making this all happen. Thanks to all the PIs, Adrienne, Andrey, Afshin, Cristina, Eric, Jackie, Lief, Marcus, Patrizia and Simone, as well as our project manager Sandra Healy, for putting together this consortium, taking time out of their busy schedules to attend each of the meet-ups and giving their much appreciated input at all of the meetings. To the other ESR's, Aitor, Andreia, Alexandra, Antonio, Brian, Chetan, Dimitrios, Franziska, Josip, Luigi, Maria, Sanket and Stuart, thank you for making this PhD journey such a memorable and entertaining PhD experience. I couldn't have asked for a better consortium group.

Thank you to all in the FKKS who I have had the pleasure of working with and who helped me throughout my research. Thank you to Christina for her help with all the paperwork and publications. Thank you to Nadine for supervising me during my first year and teaching me the basics. Huge thanks to Nadezda for taking me under her wing and watching over me in my final PhD years. Thank you to Svenja for her kindness and help both in the lab and with my thesis. To the 1st floor office gang (Nadezda, Vanessa, Cathinka, Sarah, Jessi, Nadine, Juliane & Vinzenz) thank you for all your help and support throughout the years and thank you for all the laughs. I will miss our absolutely outrageous chats!

I would also like to thank everyone at the Apoptosis Research centre for welcoming me and making my secondment in Galway so enjoyable. I loved being a part of the ASAG gang for a short time. Thank you to all in the lab for their help and guidance during my time there. The feedback and experience I received there was invaluable.

To my crazy Frankfurt friends for making what should have been the four worst years of my life, into some of the best years. Thank you for the endless fun, drinks, distractions and memories. Special shout out to my girls Dani, Ele, Erin, Jade and Kelly for being the best gal friends a girl could ask for, so caring and always so fun. I feel so blessed to have met you all, I really wouldn't have lasted in FFM and got through this PhD without all of you. Dani, thank you especially for being the best company and distraction (from work and life), for always being so positive, understanding and empathetic. Erin, thank you for always listening to me and for being so supportive and encouraging even after you left FFM. Ele, thank you for being such a good listener and a voice of reason, and for always being up for a wild time.

To Matt, who always managed to pull me back whenever I got over stressed, for inspiring and encouraging me to be better and keep going. Thank you for being so understanding and patient with me through this thesis. Lastly, thank you for never failing to put a smile on my face and distracting me when I needed it most.

To all of my wonderful family for just simply being there for me and always believing in me through this whole process. To Michael, Martina, Fionn and Naoise for taking me in when I was in Galway and keeping my brain well nourished, I really appreciate it. To my amazing grandparents, Lena, Richie and Tom for being my biggest fans and always taking such good care of me. Gdad, thank you for coming to visit me so many times, bringing brown bread and making being away from home that little bit easier. Special mention to my mom, Caitlin and Caoimhe, who love me unconditionally even when I've been cranky and stressed. Mom, thank you for always believing in me and supporting every decision I've made, I appreciate you so much. To Lena and Sinead for the endless phone calls of constant support, sympathy, advice and encouragement - for being my absolute rocks. I cannot thank you enough, I would have been absolutely lost without the two of you.

Thank you to everyone who has stood by me over the past four years, which have undoubtably been the toughest four years of my life. I am so lucky to have such an incredible support system. Thank you all for always being so sure of me and constantly reassuring me that I would make it in the end.

Abstract

Paediatric cancer is the leading cause of death by disease in children. In addition to poor survival rates, current treatments for childhood cancers are associated with severe short- and long-term adverse effects suggesting an urgent need for less toxic therapies. The unfolded protein response (UPR) is a cellular stress response, that either restores cellular homeostasis or induces cell death. The UPR has been implicated in a number of pro-tumourigenic processes in various cancers. Inhibitor of Apoptosis (IAP) proteins are also important in cell death and survival signalling and have also been implicated in tumour progression and survival. In this thesis, I investigated UPR and IAP signalling in paediatric cancer cells. The aim was to elucidate their roles in cancer cell survival as well as their roles in response to anticancer treatments. I explored the role of the UPR in rhabdomyosarcoma (RMS), a common childhood soft tissue sarcoma. RMS cell lines exhibited basal IRE1 and PERK signalling and inhibition of this basal activity caused a reduction in viability, proliferation and long-term colony formation of RMS cell lines. Further investigation revealed a robust activation of senescence upon UPR inhibition suggesting that the UPR promotes indefinite replication in RMS cell lines. These data reveal that the UPR is implicated in RMS phenotype and that targeting IRE1 and PERK signalling in RMS could be an attractive therapeutic option. I also examined the cytotoxic effects of ER stress inducers, alone or in combination with other anticancer drugs, on paediatric cancer. A range of ER stress inducers were shown to have cytotoxic effects on several paediatric cancer cell lines. Interestingly, a key observation in this thesis was that IAP antagonists have anti-apoptotic effects on tunicamycin provoked ER stress-induced cell death in paediatric cancer cells. Smac mimetic and IAP inhibitor BV6 resolved tunicamycin-induced ER stress and UPR signalling while also promoting pro-survival signalling through NF-κB. This data provides new insights into the regulation of cellular stress responses by Smac mimetics.

In summary, the findings in this thesis reveal the significance of the UPR in survival and death signalling during anticancer treatment of paediatric cancer cells. This work also highlights the potential of the UPR modulation, with either ER stress inducers or UPR inhibitors, as a therapeutic strategy for paediatric cancers.

Abbreviations

Abbreviation	Long
2-DG	2-Deoxyglucose
AIF	Apoptosis Inducing Factor
ALL	Acute Lymphoblastic Leukemia
AMG	AMGEN44
APAF-1	Apoptosis Protease Activating Factor-1
APS	Ammonium Persulfate
ARMS	Alveolar Rhabdomyosarcoma
ASK1	Apoptosis-Signalling Kinase 1
ATCC	American Type Culture Collection
ATF6	Activating Transcription Factor 6
ATG	Autophagy Related Gene
ATP	Adenosine Triphosphate
Bak	Bcl-2 Homologous antagonist/killer
Bax	Bcl-2 Associated Protein x
Bcl-2	B-cell Lymphoma 2
Bcl-xL	B-cell Lymphoma-extra Large
BECN-1	Beclin-1
BH3	Bcl-2 Homology 3
BID	BH3 Interacting Domain Death Agonist
Bim	Bcl-2 Interacting Mediator of Cell Death
BiP	Binding Immunoglobulin Protein
BFA	Brefeldin A
BRUCE	BIR Repeat Containing Ubiquitin-conjugating Domain Enzyme
BSA	Bovine Serum Albumin
Btz	Bortezomib
bZIP	Basic Leucine Zipper
CAM	Chick Chorioallantoic Membrane
C/EBP	CCAAT/Enhancer-Binding Protein
Ca^{2+}	Calcium
CARD	Caspase Activation and Recruitment Domain
Carf	Carfilzomib
CAR-T	Chimeric Antigen Receptor
cFLIP	Cellular FLICE (FADD-like IL-1β-converting enzyme)-inhibitory Protein

CHOP	C/EBP Homologous Protein
cIAP	Cellular Inhibitor of Apoptosis
CREB	cAMP Response Element Binding Protein
CST	Cell Signalling Technologies
DD	Death Domain
DIABLO	Direct IAP Binding Protein
DISC	Death Inducing Signalling Complex
DMEM	Dulbecco's Modified Eagle Medium
DMSO	Dimethyl Sulfoxide
DNA	Deoxyribonucleic acid
DR5	Death Receptor 5
DSMZ	Deutsche Sammlung von Mikroorganismen und Zellkulturen
DTT	Dithiothreitol
e.g.	Exempli gratia (latin); For Example
ECL	Enhanced Chemiluminescence
EDEM	ER-Degradation-Enhancing-α-Mannidose-like Protein
EDTA	Ethylenediaminetetraacetate
eIF2α	Eukaryotic Translation Initiation Factor 2 Alpha
ER	Endoplasmic Reticulum
ERAD	Endoplasmic Reticulum Associated Degradation
ERK	Extracellular Signal-regulated Kinase
ERMS	Embryonal Rhabdomyosarcoma
ERO1	ER Oxidoreductin 1
FACS	Fluorescent Activated Cell Sorter
FADD	Fas Associated Death Domain Protein
FAS	Apoptosis Stimulating Factor
FCS	Fetal Calf Serum
FKHR	Forkhead in Rhabdomyosarcoma
FOXO	Forkhead Box O
GAPDH	Glyceraldehyde-3-phosphate Dehydrogenase
GBM	Glioblastoma
GCN2	General Control Non-derepressible protein 2
GFP	Green Fluorescent Protein
GRP78	Glucose Regulated Protein 78 kDa
HEPES	Hydroxyethyl Piperazinylethane Sulfonic Acid
HH	Hedgehog

HIF1α	Hypoxia-Inducing Factor 1 alpha
HRI	Heme-Regulated eIF2α Kinase
HRP	Horseradish Peroxidase
HSP	Heat Shock Protein
IAP	Inhibitor of Apoptosis Protein
IGF-II	Insulin-like Growth Factor Type II
IκBα	NF-kappa B Inhibitor Alpha
IKK	IκB Kinase
ILP-2	IAP-like Protein-2
IRE1	Inositol-Requiring Enzyme 1
JNK	C-JUN N-Terminal Kinase
kDa	Kilodalton
LOH	Loss of Heterozygosity
MAPK	Mitogen-activated Protein Kinase
Mcl-1	Induced Myeloid Leukemia Cell Differentiation Protein
MEF	Mouse Embryonic Fibroblast
ML-IAP	Melanoma IAP
MKC	MKC8866
MM	Multiple Myeloma
MOMP	Mitochondrial Outer Membrane Permeabilization
mRNA	Messenger RNA
NAIP	Neuronal Apoptosis Inhibitory Protein
NEMO	NF-κB Essential Modulator
NF-κB	Nuclear Factor kappa-light-chain-activator of B-cells
NIK	NF-κB Inducing Kinase
Nrf2	Nuclear Factor Erythroid 2, Related Factor 2
PAX	Paired Box
PBS	Phosphate Buffered Saline
PCR	Polymerase Chain Reaction
PDI	Protein Disulfide Isomerase
p-eIF2α	Phosphorylated eIF2α
PERK	Protein Kinase RNA-like (PKR) ER Kinase
PI	Propidium Iodide
PKR	Protein Kinase RNA-activated
PP1	Protein Phosphatase 1
PUMA	p53 Upregulated Modulator of Apoptosis

P/S	Penicillin/Streptomycin
RB	Retinoblastoma
RER	Rough Endoplasmic Reticulum
RIDD	Regulated IRE1 Dependent Decay
RING	Really Interesting New Gene
RIP1	Receptor-interacting Serine/Threonine-protein Kinase 1
RMS	Rhabdomyosarcoma
RNA	Ribonucleic Acid
RNase	Ribonuclease
RPM	Rounds Per Minute
RT-PCR	Reverse Transcription Polymerase Chain Reaction
S1P	Site 1 Protease
S2P	Site 2 Protease
SASP	Senescence-Associated Secretory Phenotype
SD	Standard Deviation
SDS	Sodium Dodecyl Sulfate
SER	Smooth Endoplasmic Reticulum
SERCA	Sarco/Endoplasmic Reticulum Ca2+ ATPase
siRNA	Small Interfering RNA
Smac	Second Mitochondria-derived Activator of Caspase
T-ALL	T cell Acute Lymphoblastic Leukemia
tBID	Truncated BH3 Interacting Domain Death Agonist
TEMED	*N,N,N',N'*-Tetramethylethylenediamine
TG	Thapsigargin
TIS	Therapy Induced Senescence
TM	Tunicamycin
TME	Tumour Microenvironment
TNBC	Triple Negative Breast Cancer
TNF	Tumour Necrosis Factor
TNFR	Tumour Necrosis Factor Receptor
TRADD	TNFR Associated Death Domain Protein
TRAF2	TNFR Associated Factor 2
TRB3	Tribbles Homolog 3
tRNA	Transfer RNA
UBA	Ubiquitin Associated Domain
uORFs	Upstream Open Reading Frames

UPR	Unfolded Protein Response
VAC	Vincristine, Actinomycin D and Cyclophosphamide
VEGFA	Vascular Endothelial Growth Factor A
XBP1	X-box Binding Protein 1
XBP1s	Spliced XBP1
XBP1u	Unspliced XBP1
XIAP	X-linked Inhibitor of Apoptosis
β-Gal	β-Galactosidase

Chapter 1: Introduction

The unfolded protein response (UPR) is critical for a wide range of cellular processes. Both, the pro-survival and pro-death signalling pathways of the UPR, in response to endoplasmic reticulum (ER) stress, have been well documented [1]. Malfunction of the UPR has been implicated in a growing number of diseases including cancer, neurodegenerative diseases and diabetes [2]. As a result, understanding the UPR and exploitation of the UPR is of broad scientific and clinical interest. Several compounds either activating or inhibiting UPR pathways have been developed and investigated for their effects on cells [3, 4]. Treatment of cells with UPR modulators (inducers and inhibitors) has not only allowed us to further our understanding of the signalling pathways but has also enabled the identification of their involvement in diseases including cancer.

For many years, cell death has been the preferred mechanism of action for cancer therapeutics and remains clinically relevant for cancer treatment as it ensures complete elimination of tumour cells [5]. Nonetheless, researchers are constantly searching for novel, alternative and more effective therapies. The UPR has been implicated in several of the hallmarks of cancer including growth, survival and cell death evasion [6]. The UPR's links to cell death, as well as its connection to cancer development and survival, makes it a very promising target for cancer therapy. Thus, UPR targeting drugs, including both inducers and inhibitors, are now being investigated as potential cancer treatments [7].

In this chapter, I will give an in-depth overview of the current understanding of ER stress, the UPR, and cell death and survival signalling. In addition, I will highlight the relevance of the UPR and cell death in cancer and their potential as therapeutic targets. This chapter will provide a substantial background knowledge necessary for a clear understanding of the research undertaken and results discovered in this thesis.

1.1 Endoplasmic Reticulum and ER Stress

1.1.1 Endoplasmic Reticulum

The ER is a cellular organelle composed of a membranous network of tubules and flattened sacs that span a large area of the cytoplasm [8]. This entire network is interconnected and its membrane encloses the ER lumen which separates this compartment from the cytoplasm [9]. The ER is typically divided into the rough ER (RER), the smooth ER (SER) and the nuclear envelope. Contrary to SER, the RER has membrane bound ribosomes on its surface [10]. The RER is primarily responsible for protein folding and the SER is involved in other ER functions including calcium (Ca^{2+}) regulation, lipid synthesis and drug detoxification [11]. The nuclear envelope is a continued extension and specialised part of the ER that encloses chromatin, giving the nucleus its structure [12].

1.1.2 ER Functions

The ER is involved in a plethora of different cellular functions. The best described function of the ER is the synthesis, folding and maturation of both secretory and transmembrane proteins. Approximately one-third of all cellular proteins are translocated into the ER for correct and proper folding and modification [13]. In the ER lumen, proteins are exposed to numerous chaperones and foldases that facilitate their folding, assembly and post-translational modification, before they are exported from the ER to their necessary cellular destinations [14]. Some post-translational modifications carried out in the ER include N-linked glycosylation, disulfide bond formation, proline isomerization and lipid conjugation [15]. Protein misfolding frequently takes place in cells due to errors in processes such as transcription and translation [16]. Since misfolded proteins are potentially harmful, cells have developed tightly regulated quality control systems in the ER that ensure misfolded proteins are appropriately taken care of, thereby maintaining homeostasis [17].

The ER is the main cellular storage compartment for Ca^{2+} and plays a crucial role in Ca^{2+} regulation. Ca^{2+} is involved in many intracellular and extracellular signalling networks, playing an essential role in protein synthesis and trafficking, cell

proliferation, differentiation, metabolism and apoptosis [18]. Thus, the ER ultimately controls the Ca^{2+} homeostasis of the whole cell. Since high Ca^{2+} levels are required for optimum enzyme activity, many ER functions are controlled by Ca^{2+} and so Ca^{2+} is essential for ER function [19]. The ER also plays essential roles in lipid synthesis, fat storage, the production of membrane proteins and the formation of lipid droplets and vesicles [20].

1.1.3 ER Stress

Various intracellular and extracellular stimuli can alter ER homeostasis and disrupt protein folding leading to the accumulation of unfolded and misfolded proteins or protein aggregates. This build-up of unfolded proteins in the lumen of the ER is known as ER stress [21]. Glucose deprivation, disruptions in calcium or redox status, high protein folding demand, viral infection, or the expression of mutant or misfolded proteins can all lead to stress in the ER [22]. The ability of cells to respond to ER stress is extremely important and critical for cell survival [23]. The ER has developed a complex but precise signalling network called the unfolded protein response (UPR) to cope with any accumulation of unfolded or misfolded proteins [24].

1.2 The Unfolded Protein Response

The cellular response to ER stress involves the activation of highly specific and sensitive signalling pathways, collectively referred to as the UPR, which aims to overcome stress and restore homeostasis. The UPR is predominantly controlled by three major sensors: inositol requiring enzyme 1 (IRE1), protein kinase RNA-activated (PKR)-like ER kinase (PERK) and activating transcription factor 6 (ATF6) [22, 25] (see Fig. 1.1). The ER luminal domains of all three ER stress sensors are normally bound to Binding immunoglobulin protein (BiP), also known as glucose-regulated protein 78 (GRP78), an ER resident chaperone, that maintains them in an inactive state. Accumulating misfolded proteins in the ER lumen attract and bind BiP, inducing the activation of the three UPR sensors [26]. In brief, the initial response of the UPR is to decrease the protein load by reducing protein synthesis and protein transport into the UPR. Next, there is an increase in ER capacity to

accommodate the increase in unfolded proteins. Degradation pathways are simultaneously activated to remove any unfolded or misfolded proteins. Lastly, if homeostasis cannot be restored, the UPR switches to pro-death signalling in order to protect the organism from unhealthy and potentially harmful cells [22]. The mechanisms and outputs of the UPR are discussed in more depth in Sections 1.3 and 1.6.

1.2.1 IRE1

IRE1 is a conservative protein found in all organisms. In humans, there are two paralogues of IRE1 (IRE1α and IRE1β). IRE1α is ubiquitously expressed throughout the body whereas, IRE1β is expressed primarily in the gastrointestinal tract and the pulmonary mucosal epithelium [27, 28]. IRE1α (hereafter referred to as IRE1) is a type I transmembrane protein with an N-terminal ER luminal region and a cytosolic domain that possesses kinase and endoribonuclease (RNase) activity [29, 30]. Dissociation of BiP from IRE1 results in the oligomerization of IRE1. The close proximity of the IRE1 oligomers results in their self-auto-phosphorylation, subsequently activating its kinase and RNase domains [31, 32].

Activated IRE1 catalyses the splicing of a 26 nucleotide intron from X-box binding protein 1 (*XBP1*) mRNA to produce a spliced isoform referred to as XBP1s [30]. XBP1s is a basic leucine zipper (bZIP) transcription factor [33]. The translation product of unspliced isoform of *XBP1* mRNA (XBP1u) does not possess a transactivation domain, and is therefore unable to activate gene expression. The splicing of *XBP1* by IRE1 results in an open reading frame shift, which allows translation of XBP1s which is transcriptionally active [34]. XBP1s then translocates to the nucleus where it controls the expression of a number of genes [22]. XBP1s is well established as a key component in relieving ER stress and restoring homeostasis following ER stress. Target genes induced by XBP1s encode protein products that enhance ER protein folding capacity and quality control including chaperones, foldases and components of the ER-associated degradation (ERAD) pathway [35, 36]. XBP1s also influences cell fate by mediating cell survival, cell differentiation and development as well as regulating of numerous pathways such as lipid biosynthesis, glucose metabolism, redox metabolism and insulin signalling [1].

Another consequence of IRE1 RNase activity is regulated IRE1-dependent decay (RIDD) [37]. Through RIDD, IRE1 targets a number of transcripts that contain a 'CUGCAG'-like sequence accompanied by a stem-loop structure [38]. The mRNA encoding cytosolic and ER resident proteins are both targets of RIDD [39]. These target transcripts are cleaved by IRE1 endonuclease and the cleaved RNA fragments are then rapidly degraded by cellular exoribonucleases [37]. In order for IRE1 to carry out this process, the mRNA targets must be either localised at the ER membrane or possess a stem-loop structure similar to that of *XBP1*, which allows them to associate directly with IRE1 [40]. RIDD is essential in the response to ER stress as it reduces the ER client protein load by degrading mRNAs [37]. RIDD has now also been identified to have targets involved in processes such as transcription, lysosomal degradation and energy production [41].

1.2.2 PERK

PERK is another UPR sensor and is also ubiquitously expressed in the body. It is a type I transmembrane protein with a cytosolic kinase domain [42]. Like with IRE1, BiP dissociation following ER stress results in PERK's oligomerization and trans-autophosphorylation, leading to the activation of its kinase domain which is responsible for its catalytic activity [26, 43].

The best known PERK substrate, eukaryotic translation initiation factor 2 subunit alpha (eIF2α) is a subunit of the eIF2 heterotrimer [44]. The eIF2 heterotrimer regulates the first step of protein synthesis initiation by promoting the binding of the initiator transfer RNA (tRNA) to 40S ribosomal subunits [45]. Activated PERK phosphorylates eIF2α (p-eIF2α), preventing eIF2 heterotrimer activity. This results in transient inhibition of mRNA translation and consequently, a downregulation in protein synthesis. The translational block during ER stress reduces the work load on the ER folding machinery giving the cell time to remove the unfolded proteins and repair any issues in the protein folding process [46].

Conversely, the expression of some transcripts is increased during PERK-mediated translation repression, for example, activating transcription factor 4 (ATF4). *ATF4*

mRNA is normally inefficiently translated due to the short upstream open reading frames (uORFs) it contains. Following eIF2α phosphorylation, attenuation of translation of uORFs shifts translation initiation towards the protein coding sequence, resulting in more efficient synthesis of ATF4 [46]. ATF4 is a bZIP transcription factor that regulates genes encoding proteins involved in protein folding, amino acid metabolism and autophagy [47, 48]. ATF4 can bind to the promoter of CCAAT/enhancer-binding protein (C/EBP) homologous protein (CHOP) (also known as GADD153) and induce its expression [46]. ATF4 and CHOP both play an important role in the UPR pro-survival and pro-death response to ER stress (described in sections 1.3 and 1.6, respectively).

Growth arrest and DNA-damage-inducible 34 (GADD34) is upregulated following translational inhibition by p-eIF2α while simultaneously being transcriptionally induced by ATF4 and CHOP. Interestingly, GADD34 interacts with protein phosphatase 1 (PP1) which in turn dephosphorylates eIF2α; creating a negative feedback loop that antagonizes p-eIF2α-dependent translation inhibition and restores protein synthesis [49, 50]. Another well-known substrate phosphorylated by PERK is the transcription factor Nuclear factor 2 (Nrf2). PERK phosphorylation of Nrf2 releases it from an inhibitory E3 ligase complex containing Keap1 and Cullin 3 [51]. Nrf2 is then free to accumulate, translocate to the nucleus. In the nucleus Nrf2 bind increases the gene expression of genes encoding proteins involved in antioxidant response [52, 53]. In this way, PERK function is critical for maintaining cellular redox homeostasis.

1.2.3 ATF6

ATF6 is the least understood sensor of the UPR. Following BiP dissociation during ER stress, ATF6 is activated and immediately exported to the Golgi where it is cleaved by two membrane bound proteases known as site-1 protease (S1P) and site-2 protease (S2P). Cleavage of ATF6 by these two proteases generates a 50-kDa cytosolic bZIP-containing fragment (ATF6f). ATF6f is a bZIP transcription factor that translocates to the nucleus where it can activate the transcription of UPR target genes [54, 55]. Interestingly, ER stress-mediated ATF6 activation upregulates *XBP1* mRNA transcription, allowing further accumulation of XBP1s, increasing the overall

UPR response during ER stress. In line with this, ATF6 can also induce CHOP expression to enhance UPR signalling [34, 56] suggesting a strong overlap of ATF6 signalling with the other UPR signalling pathways.

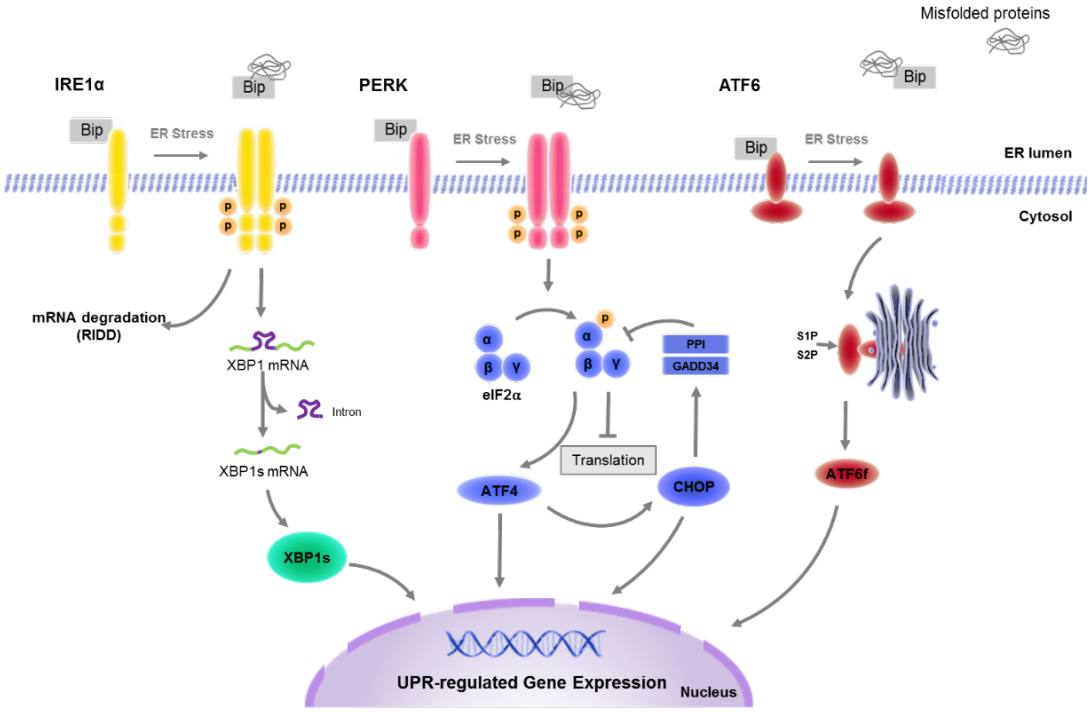

Figure 1.1: UPR sensors and their downstream signalling pathways - Diagram representing the unfolded protein response (UPR) signalling pathway. Following ER stress, three ER stress receptors, IRE1, PERK, and ATF6 are activated. Activation of these 3 stress sensors results in a downstream cascade of signalling events that aim to restore homeostasis or after prolonged stress induce cell death [57].

1.3 UPR Restoring Homeostasis

As outlined above, the UPR is activated in response to misfolded protein accumulation caused by ER stress. The initial response of the UPR is protective, where it acts to alleviate stress and restore homeostasis by reducing the build-up of proteins and improving folding capacity. It does this by three mechanisms; firstly, translation is blocked to limit further production of misfolded proteins. Secondly, the transcription of genes encoding chaperones and foldases are increased in order to ensure correct folding of proteins. Lastly, protein degradation pathways including ERAD and autophagy are activated to dispose of the unfolded proteins.

1.3.1 Translation

The most immediate response following ER stress is the activation of PERK kinase activity. A key target of PERK is eIF2α, which upon phosphorylation, is responsible for blocking translation and thus, reduces the protein load on the ER [46]. Consequently, p-eIF2α liberates ribosomes and translation factors from mRNA allowing those translation factors to exist as free subunits. This availability of translation factors are predicted to help newly synthesized mRNAs that are transcribed by UPR components [46].

1.3.2 Transcription

The next adaptive response signalling wave is controlled by the UPR's major transcription factors, ATF4, XBP1s and ATF6f. ATF4 promotes survival under ER stress by promoting the transcription of genes involved in protein folding, amino acid metabolism, autophagy and redox balance [58]. XBP1s and ATF6f increase the expression of genes encoding chaperones, ERAD components, protein folding modification enzymes and enzymes that regulate lipid synthesis, all of which contribute to the enhancement of cellular folding and degradation capabilities [55]. For example, XBP1s induces ER-degradation-enhancing-α-mannidose-like protein (EDEM), which is a key component of ERAD, and protein disulphide isomerase (PDI), which is key in protein folding [35]. In addition, anti-apoptotic proteins such as myeloid cell leukemia 1 (Mcl-1) are transcriptionally upregulated following ER stress, ensuring cell survival during this stress [59]. Inhibitor of apoptosis (IAP) proteins, which are explained in more detail in section 1.5, are critical in the regulation of apoptosis by preventing caspase activation. It has been shown that ER stress leads to the induction of IAPs. Several papers have reported that cellular IAP1 (cIAP1), cIAP2 and X-linked IAP (XIAP) are induced by ER stress, and that this induction is important for cell survival as it delays the onset of caspase activation and apoptosis. *IAP* mRNA is transcriptionally upregulated during ER stress in a PERK and p-eIF2α-dependent manner [60-62].

Together, this transcriptional upregulation of genes involved in protein folding, processing, and degradation helps reduce the amount of unfolded proteins in the ER,

with the aim of restoring cellular homeostasis. Moreover, the upregulation of anti-apoptotic proteins and IAPs ensures cell survival while the UPR reduces misfolded proteins, enhances protein folding and restores homeostasis.

1.3.3 Protein degradation

In order to reduce the number of misfolded proteins in the ER lumen, the proteins must be removed and disposed of correctly. There are two main protein degradation pathways activated by the UPR following ER stress: ubiquitin-proteasome mediated degradation via ERAD and lysosomal protein degradation via autophagy. Both processes occur naturally in the cell during basal conditions but are also greatly enhanced by UPR signalling during ER stress.

1.3.3.1 ERAD

ERAD involves the translocation of misfolded proteins from the ER to the cytosol where they are targeted for ubiquitination and subsequently degraded by the proteasome. ER chaperones, such as BiP and EDEM1, are responsible for tagging proteins destined for the ERAD pathway [63, 64]. These chaperones are also responsible for escorting the misfolded proteins to the SEL1L-HRD1-SYNV1 complex where substrates can pass through from the ER to the cytoplasm. This complex has an E3 ubiquitin ligase that ubiquitinates the misfolded protein targeting it for proteasomal degradation [65]. In the cytosol, the ubiquitin-tagged misfolded proteins are recognised by the proteasome. The proteasome is a barrel shaped complex composed of two 19S end caps, which recognise ubiquitylated proteins, and a 20S proteolytic core, responsible for protein degradation [66]. As briefly mentioned, XBP1s upregulates the expression of proteins and enzymes of the EDEM family [35]. During ER stress, these EDEMs recognize terminally misfolded glycoproteins and deliver them to the ERAD pathway [67]. In addition, the IRE1-XBP1 signalling pathway transcriptionally upregulates SEL1L and HRD1 [36].

1.3.3.2 Autophagy

When accumulation of misfolded proteins overwhelms ERAD, autophagy is induced as a secondary response to diminish protein build-up [22]. Autophagy is a pathway in which organelles, macromolecules, and unwanted or dysfunctional proteins are degraded. During the autophagy process, targeted substrates are sequestered within double membrane vesicles known as autophagosomes and subsequently delivered to lysosomes where they are degraded. Degradation products are then released and recycled in metabolic pathways [68]. Autophagy is heavily controlled by autophagy-related genes (ATGs). The expression of ATGs are increased following stimuli associated with ER stresses such as, nutrient deprivation, energy shortage, and hypoxia [69]. PERK signalling has been linked to autophagy induction during ER stress, with p-elF2α and ATF4 inducing the expression of ATGs including *ATG12*, *Beclin-1* (BECN-1) and *ATG3* [48, 70, 71]. IRE1 also activates autophagy through its phosphorylation of c-Jun NH2-terminal kinase (JNK). JNK-mediated phosphorylation of B-cell lymphoma 2 (Bcl-2) disrupts the interaction between BECN-1 and Bcl-2, subsequently enabling BECN-1 dissociation and autophagy induction [72, 73]. Furthermore, XBP1s transcriptionally activates BECN-1 [74]. This autophagy induction reduces intracellular stresses on the cell by degrading and at the same time recycling misfolded proteins [75].

Overall, the UPR's induction of translation inhibition, transcriptional upregulation and protein degradation can provide an ER-stress resolving adaptive response. Combined, they reduce ER protein load, enhance ER protein folding capacity, and promote degradation of unfolded proteins. The reduction in misfolded proteins in the ER aims to allow the cell to re-establish homeostasis. As the amounts of improperly folded proteins decrease, the UPR is inactivated. The exact molecular details of UPR attenuation still remain to be further elucidated although negative feedback loops such as GADD34/PPI are thought to play an important role [49, 50]. If homeostasis cannot be restored and the ER stress is unresolved, the UPR switches from pro-survival to pro-death signalling [76].

1.4 Apoptosis

Apoptosis is a programmed form of cell death. Conclusively defined in 1972, it has now become the most extensively studied form of cell death [77]. Apoptosis plays a role in normal biological processes including embryonic development, the immune response, and cellular and tissue homeostasis [78]. The dysregulation of apoptosis is implicated in several pathological conditions including neurodegenerative diseases, autoimmune diseases, cardiovascular diseases and cancer [79]. Typical morphological characteristics of apoptosis include cell shrinkage, nuclear DNA fragmentation, chromatin condensation and membrane blebbing. Biochemical characteristics associated with apoptosis include activation of cysteine-aspartic proteases (collectively referred to as caspases), DNA fragmentation, degradation of cytoskeletal and nuclear proteins and the production of cell surface markers that signal neighbouring and phagocytic cells [80]. Apoptosis can be triggered by a number of stimuli from inside or outside the cell including ER stress. There are two main signalling pathways involved in apoptosis: the extrinsic (death receptor) pathway and the intrinsic (mitochondrial) pathway (illustrated in Fig. 1.2). In both pathways caspases are responsible for signalling and carrying out cell death [81].

1.4.1 Extrinsic Apoptosis

The extrinsic pathway of apoptosis is activated when ligands bind to transmembrane receptors such as tumour necrosis factor receptor (TNFR) and apoptosis stimulating factor (FAS). The cytoplasmic domains of these receptors contain a sequence motif called the death domain (DD) which, following activation, interacts with adaptor proteins that also contain DD motifs. TNFR1 associated protein (TRADD) and receptor interacting protein (RIP) bind to TNFR, and Fas-associated death domain (FADD) and RIP bind to the FAS receptor. Recruitment of these adaptor molecules to their receptors forms the death inducing signalling complex (DISC) [82]. The death domains of TRADD/FADD are not only necessary for their association with their receptors but are also essential for their apoptosis inducing properties i.e., binding to pro-caspase-8. The high concentration of pro-caspase-8 at DISC enables the pro-enzymes to mutually cleave and activate one another [83]. Activated caspase-8 subsequently activates and initiates apoptosis by direct cleavage of

downstream effector caspases-3 and -7, which are responsible for the apoptotic processes including DNA fragmentation [84, 85]. Meanwhile, caspase-8 cleaves and activates BH3 interacting domain death agonist (BID), producing its truncated form (tBID). tBID then translocates to the mitochondria where it stimulates cytochrome *c* release which is involved in the intrinsic pathway, further amplifying the apoptotic response [86].

1.4.2 Intrinsic Apoptosis

The intrinsic pathway of apoptosis is highly regulated by Bcl-2 family proteins [87]. Usually, Bcl-2 family anti-apoptotic proteins including Bcl-2, B-cell lymphoma-extra large (Bcl-xL), and Mcl-1 are at higher levels than pro-apoptotic proteins and prevent apoptosis activation. Following pro-apoptotic signalling, there is an increase in the transcription and/or post-translational activation of pro-apoptotic Bcl-2 family members, such as BH3 only proteins Bcl-2 interacting mediator of cell death (Bim), BID, NOXA and p53 upregulated modulator of apoptosis (PUMA). Once pro-apoptotic Bcl-2 family members outnumber anti-apoptotic members, these BH3-only proteins signal the mitochondrial apoptotic molecules Bcl-2 associated protein x (Bax) and Bcl-2 Homologous antagonist/killer (Bak) to meet at the outer mitochondria membrane [88]. Bax/Bak homo-oligomerization causes pore formation on the mitochondrial membrane resulting in mitochondrial outer membrane permeabilization (MOMP) [87]. MOMP stimulates the release of cytochrome *c* and other pro-apoptotic Bcl-2 members from the mitochondria into the cytosol. Cytochrome *c* then binds to apoptosis protease activating factor-1 (APAF-1) to form the apoptosome [89]. Pro-caspase-9 is activated following binding to this complex. Caspase-9, like caspase-8, is an initiator caspase that activates downstream caspases 3 and 7 [90]. Other molecules released from the mitochondria during MOMP involved in apoptosis include apoptosis inducing factor (AIF) and second mitochondria-derived activator of caspase (Smac)/direct IAP binding protein (DIABLO). Smac promotes caspase activation by binding and neutralising IAPs which normally inhibit caspase activity [91].

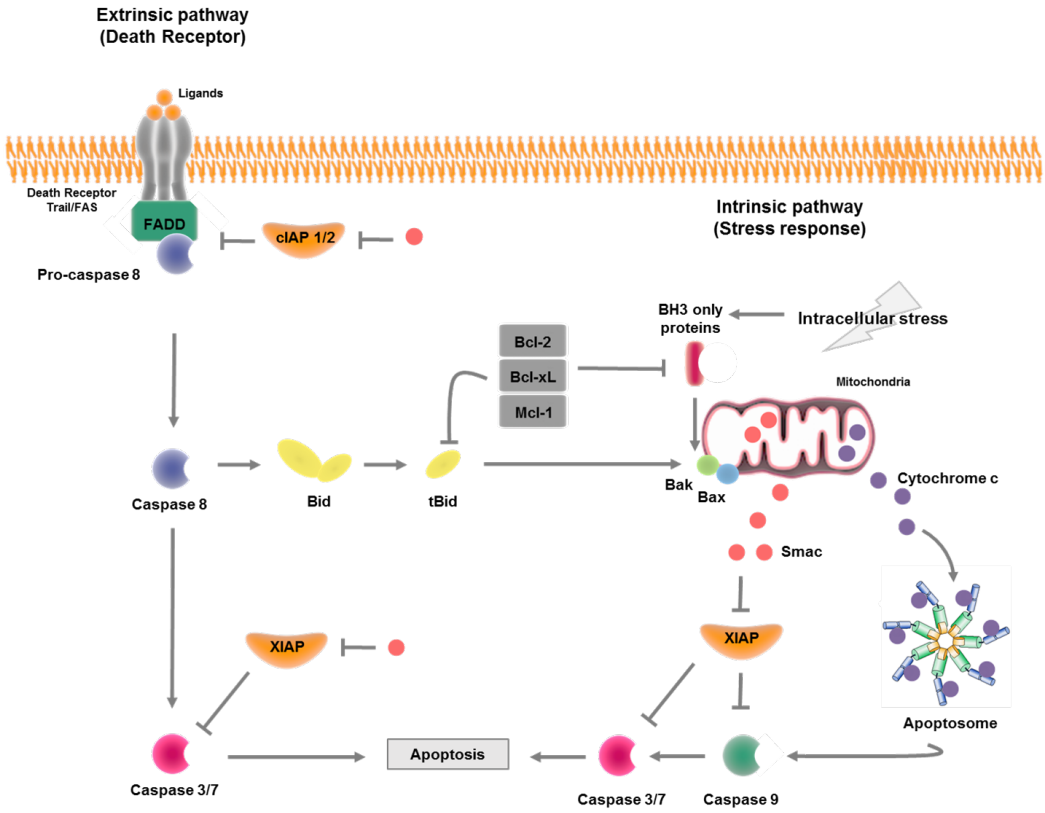

Figure 1.2: Intrinsic and Extrinsic pathways of apoptosis - Diagram representing the extrinsic (death ligand) pathway and the intrinsic (mitochondrial) pathway of apoptosis. Activation of the extrinsic pathway involves ligand binding to a death receptor and subsequent recruitment of adaptor proteins that are responsible for cleaving and activating pro-caspase-8. In response to intracellular stresses, the intrinsic pathway is activated, resulting in cytochrome *c* release from the mitochondria. This is followed by the formation of the apoptosome, the caspase-9 activating complex. Once caspase-9 and -8 are activated, they cleave and activate executioner caspases including caspase-3 and-7.

1.5 Inhibitor of Apoptosis Proteins

Activation of caspases and cell death must be tightly controlled as unwanted activation can be detrimental to cell survival. IAP proteins play a central role in the regulation of cell death and survival signalling. IAPs were originally identified in baculoviruses where they were able to functionally substitute p53 by blocking apoptosis following loss of p53 [92]. IAPs are found in all organisms from viruses to yeast to humans [92-94]. There are currently eight family members of IAPs described in humans: cIAP1, cIAP2, XIAP, neuronal apoptosis inhibitory protein (NAIP), melanoma IAP (ML-IAP), IAP-like protein-2 (ILP-2), survivin and BIR repeat containing ubiquitin-conjugating domain enzyme (BRUCE) (see Fig. 1.3)

[95]. A common feature among all IAPs is the presence of at least one baculovirus IAP repeat (BIR) domain [96]. Several IAP proteins (XIAP, cIAP1, cIAP2, ML-IAP and ILP2) also carry a really interesting new gene (RING) finger domains that function as ubiquitin ligases required for the ubiquitination of substrates [97]. Some IAP proteins, such as cIAP1 and cIAP2, possess a caspase activation and recruitment domain (CARD) that allow binding to caspases and an ubiquitin associated domain (UBA) that ubiquitin residues can bind [92, 98, 99]. The UBA domains of cIAP1 and cIAP2 play an important role in IAP antagonist-stimulated proteasomal degradation of cIAP1 and cIAP2, facilitating their recruitment to the proteasome [100].

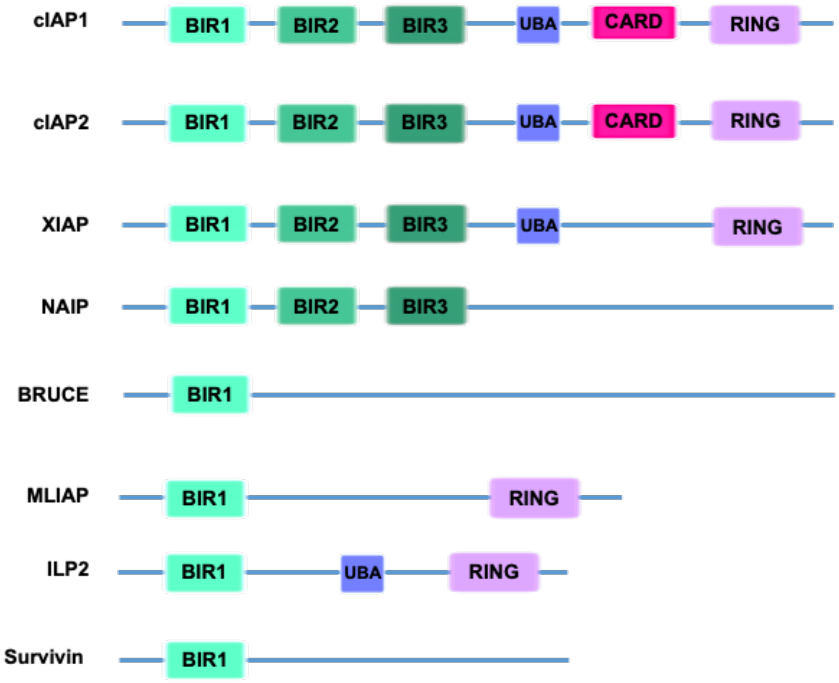

Figure 1.3: Structure of IAP proteins – IAP protein family shown in the structure of their known functional domains BIR: baculovirus IAP repeat, UBA: ubiquitin associated domain, CARD: caspase recruitment domain, RING: really interesting new gene.

Initially it was thought that IAPs anti-apoptotic activity was mediated through binding and inhibition of caspases. However, XIAP is the only IAP that directly inhibits caspases. The XIAP protein regulates both the intrinsic and extrinsic pathways of apoptosis as a result of its direct binding to and inhibition of caspase-3, -7 and -9 [101]. XIAP interacts with caspase-3 and -7 via BIR2 and with caspase-9 via BIR3 [96]. Besides the direct inhibition of caspases, XIAP also promotes proteasomal degradation of caspase-3, caspase-7 and Smac via its E3 ubiquitin ligase

activity [102-104]. Although the BIR domains of cIAP1 and cIAP2 efficiently bind to caspases-3, -7, and -9, they do not possess the precise structural elements required to inhibit them [105, 106]. cIAP1 and cIAP2 regulate the extrinsic pathway of apoptosis through their ubiquitin ligase activity [107]. XIAP, cIAP1 and cIAP2 utilise their E3 ubiquitin ligase activity to alter the stability of various proteins involved in apoptotic signalling such as caspase-3, -7, -9, -8, TNFR, receptor-interacting serine/threonine-protein kinase 1 (RIP1), TNFR-associated factor 2 (TRAF2), TRAF3 and Smac [102, 107-113]. For instance, poly-ubiquitination of RIP1 by cIAPs prevents its ability to form part of the DISC complex with FADD and caspases-8, preventing the induction of extrinsic apoptosis [111].

The ubiquitin ligase activity of IAP proteins can also auto-ubiquitinate and cross-ubiquitinate other IAP proteins resulting in their degradation and inactivation [114, 115]. This suggests that IAPs also regulate each other. For example, cIAP1 can mediate the ubiquitination of cIAP2 and XIAP [114, 115]. IAP protein activity can be inhibited by their endogenous antagonists including Smac. Smac, which is released from the mitochondria to the cytosol following apoptosis activation, is the most studied natural antagonist of IAP proteins [116]. Activated Smac binds to cIAP1 and cIAP2 and promotes their auto-ubiquitination and degradation. Smac also binds to XIAP in the cytosol and consequently interferes with its interaction with caspases [117]. IAP inhibitor Smac interacts with cIAP1/2, XIAP via their BIR domains [96]. Interestingly, Smac does not promote degradation of XIAP [118]. Another role of cIAPs is regulating the nuclear factor kappa-light-chain-activator of B-cells (NF-κB) pathways. cIAP1 and cIAP2 mediated poly-ubiquitination of RIP1 regulates the activation of the canonical NF-κB signalling pathway [111]. cIAP1 and cIAP2 promote poly-ubiquitination of NF-κB inducing kinase (NIK), which in turn blocks non-canonical NF-κB activity [119]. This is described in more detail in section 1.5.1.

1.5.1 NF-κB

As described above, cIAP proteins play an important role in regulating NF-κB signalling. The NF-κB family are a group of transcription factors that regulate the transcription of a broad spectrum of genes involved in cell survival, proliferation,

immunity, inflammation and cell death [120, 121]. There are two NF-κB signalling pathways, the canonical and the non-canonical (illustrated in Fig. 1.4), which are tightly regulated by two crucial post-translational modifications, phosphorylation and ubiquitination. There are five NF-κB transcription factors: p50 (NF-κB1), p52 (NF-κB2), RelA (p65), RelB and c-REL [122].

In the canonical NF-κB pathway, the p50-RelA dimer is bound to IκBα in the cytosol, rendering it inactive and unable to translocate to the nucleus where it can activate target gene expression [123]. In order for NF-κB to be activated, the IkBα inhibitory subunit must be removed through phosphorylation and degradation [122]. Following activation of TNFR, a complex containing TNFR-associated TRADD, RIP1, TRAF2, and cIAPs is formed [124]. In this complex, cIAP protein ubiquitinates RIP1, which then recruits IκB kinase (IKK) complex composed of IKKα, IKKβ and NF-κB essential modulator (NEMO). IKKβ and NEMO are responsible for phosphorylation of IκBα resulting in its removal from NF-κB dimer which is now free to translocate to the nucleus [125].

In contrast, cIAPs are negative regulators of the non-canonical NF-κB pathway. The non-canonical NF-κB signalling pathway is normally maintained in an inactive state due to continuous proteasomal degradation of NF-κB inducing kinase (NIK) by a complex composed of cIAPs, TRAF2, and TRAF3 [126]. Non-canonical signalling is induced by TNF cytokine family proteins, such as CD40 [127]. Disruption of this complex following TNFR activation leads to the accumulation of NIK and its subsequent phosphorylation of IKKα. IKKα is then free to phosphorylate p100, triggering its partial processing and proteasomal degradation generating a p52-RelB dimer that is then free to translocate to the nucleus [128].

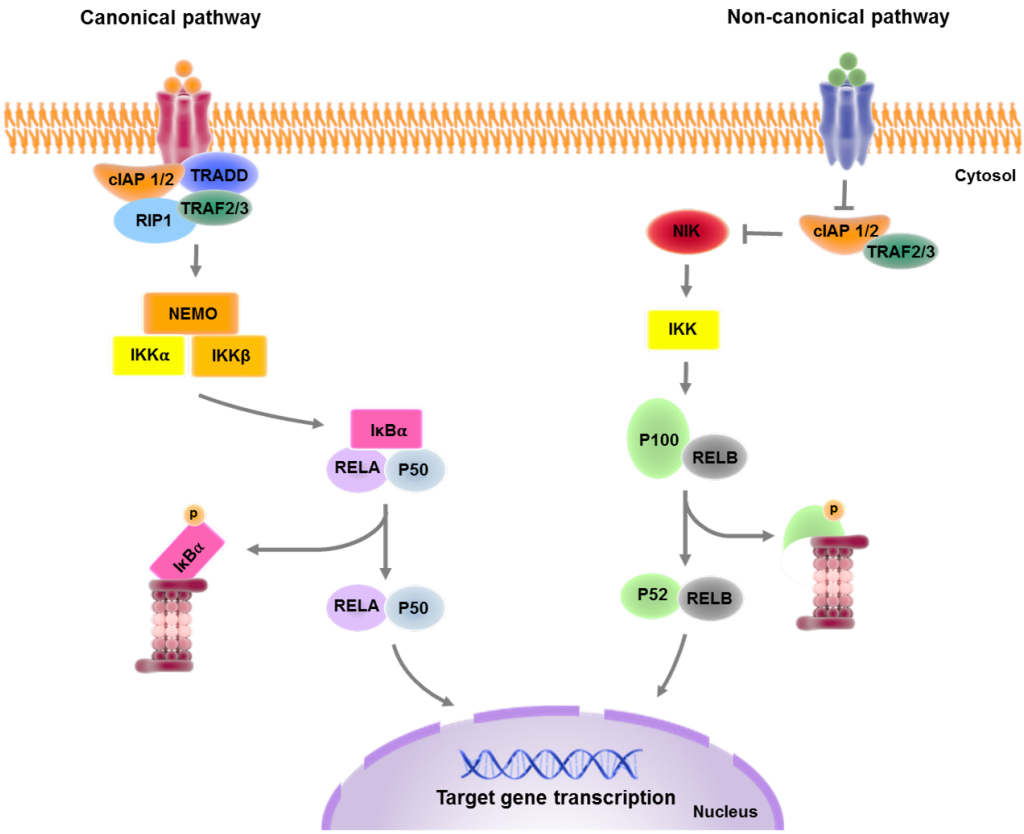

Figure 1.4: NF-κB signalling pathways - A schematic representation of the canonical and non-canonical NF-κB pathways. Activation by external receptors initiate a downstream cascade of signalling events to produce active transcription factors that translocate to the nucleus where they are responsible for activating a number of genes involved in cell survival.

1.6 UPR-induced Cell Death

Initial responses of the UPR aim to reduce protein load and remove unfolded proteins in order to return the cell to a homeostatic state. Following prolonged or extensive activation of the UPR however, the response switches from pro-survival to pro-death [76]. Several types of cell death can be induced following ER stress, including apoptosis, necrosis, necroptosis and autophagic cell death. Unresolved ER stress can lead to the activation of both the intrinsic and extrinsic apoptosis pathways [81] where all three branches of the UPR have been linked to apoptosis induction following ER stress (see Fig. 1.5) [129]. The balance of Bcl-2 proteins is a major player in ER stress induced apoptosis in which there is a clear upregulation of pro-apoptotic Bcl-2 proteins following extensive ER stress [130].

1.6.1 PERK in ER Stress-induced Apoptosis

One of the first components of the UPR signalling pathways reported to be involved in ER stress-induced apoptosis was CHOP [131]. Under ER stress conditions, CHOP reduces the expression of Bcl-2 [132] and upregulates pro-apoptotic BH3-only proteins including Bim, PUMA and NOXA [133-135], all of which tip the balance in favour of apoptosis. Other pro-death targets of CHOP include GADD34, TRB3, Death receptor 5 (DR5) and endoplasmic reticulum oxidoreductase-1 (Ero1α) [136-138]. Upregulation of TRB3, an inhibitor of autophagy, by CHOP causes a further build-up of proteins, intensifying ER stress and promoting cell death [136]. As previously discussed, CHOP-mediated activation of GADD34 promotes dephosphorylation of elF2α, reversing translational inhibition. Termination of translational inhibition promotes continued misfolded protein accumulation in the ER while simultaneously allowing translation of mRNAs encoding pro-apoptotic proteins such as Bim [133, 139]. CHOP is not solely responsible for cell death signalling from the PERK arm. PERK itself also contributes to ER stress-induced cell death. PERK-mediated translational inhibition was shown to downregulate Mcl-1 [140]. ATF4 was also found to post-transcriptionally reduce Mcl-1 levels [141]. Moreover, ATF4 itself has been shown to upregulate PUMA and NOXA proteins under chronic ER stress [135, 142]. IAP proteins are associated with UPR pro-survival signalling (described in section 1.3.2). It has now come to light that IAPs

may be linked to the pro-death side of the UPR in which they are downregulated. XIAP, cIAP1 and cIAP2 translation is reduced in a PERK-p-eIF2α-dependent manner following ER stress. Additionally, ATF4 promotes XIAP degradation. This reduction in XIAP levels could contribute to caspase activation and subsequent cell death [143].

Although numerous data suggests that the PERK arm is crucial in the ER stress-induced cell death pathway, PERK or CHOP deficient cells can still undergo apoptosis indicating that other mechanisms are involved in this cell death process [144].

1.6.2 IRE1 in ER Stress-induced Apoptosis

IRE1 is also associated with ER stress-induced cell death. Activated IRE1 interacts directly with TRAF2, a protein responsible for activating apoptosis signal-regulating kinase 1 (ASK1) [145]. As a result, ASK1 targets JNK and p38 mitogen-activated protein kinases (MAPK) are activated [146, 147]. Phosphorylated JNK has been found to regulate a number of Bcl-2 family members, including the inhibition of anti-apoptotic Bcl-2 family members Bcl-2, Bcl-xL and Mcl-1 and activation of pro-apoptotic Bim [148-150]. The IRE1-JNK-p38 pathway has also been linked to the activation of pro-apoptotic proteins Bax and PUMA [151, 152]. Active IRE1 has been shown to transcriptionally activate CHOP [35]. Furthermore, IRE1-induced p38 MAPK signalling activates CHOP via phosphorylation of its transactivation domain, implying that IRE1 could additionally contribute to CHOP pro-apoptotic activities [131]. In this way, IRE1 potentially enhances the pro-apoptotic effects of CHOP such as Bim and DR5 upregulation [129]. IRE1 signalling may also contribute to apoptosis induction through prolonged RIDD activity by degradation of mRNAs crucial for protein folding, which can further stimulate ER stress, or by the degradation of proteins crucial for survival [153]. For example, the promotion of the caspase-2 translation by RIDD can result in the significant activation of cell death programmes [154, 155].

1.6.3 ATF6 in ER stress-induced Apoptosis

The role of ATF6 in cell death induction is less known. ATF6 has been identified as a CHOP inducer, therefore, ATF6 could support pro-apoptotic signalling through its induction of CHOP [56]. In addition, ATF6 was shown to downregulate the anti-apoptotic Bcl-2 family member Mcl-1, demonstrating the potential of ATF6 to contribute to apoptosis during ER stress [156].

Depending on the cell type and the type or extent of ER stress, different UPR arms may be more prominent in cell death induction. It is possible that two or more UPR branches of the UPR contribute to apoptosis at the same time. As evident from this past section, different UPR branches may separately induce the same pro-apoptotic effector or response, amplifying that specific anti-apoptotic response. Thus, it is no surprise that the silencing of one UPR branch does not always completely rescue ER-stress-induced apoptosis. The exact mechanism in which the UPR switches from pro-survival to pro-death signalling remains unknown. Indeed, extensive or prolonged ER stress is what pushes cells under stress to death, suggesting a threshold that needs to be surpassed to activate cell death signalling [157].

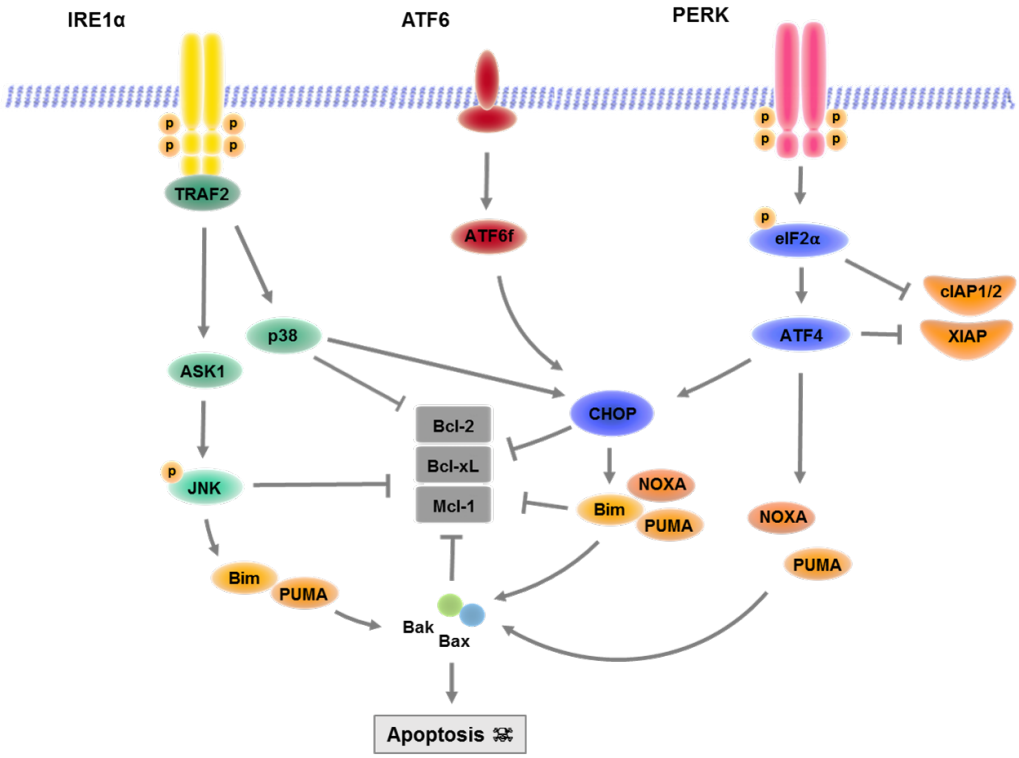

Figure 1.5: UPR induced apoptosis - Schematic representation of links and cross-talk between UPR and cell death players. All three arms of the UPR are associated with the activation of apoptosis following extensive ER stress. The balance of Bcl-2 proteins plays an important role in cell death induction following ER stress where the UPR upregulates pro-apoptotic proteins including PUMA, NOXA and Bim while downregulating anti-apoptotic proteins including Bcl-2, Bcl-xL and Mcl-1.

1.7 Cancer

Cancer is a disease that is defined as a group of cells that have defects in proliferation and homeostasis regulatory processes, which leads to their uncontrolled division and proliferation. According to the World Health Organisation, cancer is among the leading causes of death worldwide [158].

1.7.1 Paediatric Cancers

Paediatric cancer, also referred to as childhood cancer, is defined as cancer that arises in children before the age of 19. Childhood cancer is the leading cause of death by disease in children [159]. Each year, around 360,000 children are diagnosed with cancer worldwide, with approximately 80,000 deaths per year [159-162]. Although the overall five-year survival rate for childhood cancer has significantly improved in recent years, as high as 20% of children and adolescents diagnosed with cancer will not survive, even with access to high quality care [160]. The survival rate for children with cancer in low income countries is as low as 20% [163]. It is important to note that improvements in survival rates have been mostly for the more common childhood cancers such as leukemia and survival rates remain very low for many other cancer types such as neuroblastoma [160]. In addition, side effects of current treatments for paediatric cancers are proven to have damaging short- and long-term side effects [164-167]. Approximately 80% of children that have been treated for high-risk cancers experience severe and life-threatening side effects including pain, nausea, malnutrition, bleeding and ulcers [164]. The majority of children who do survive cancer will suffer lifelong consequences from treatment such as infertility, neurocognitive impairment, mental disabilities, organ toxicities and secondary cancers [165-167]. Both low survival rates and detrimental side effects of current therapies, indicate that new advances and continued research to identify effective treatments are required for paediatric cancers.

1.7.1.1 Rhabdomyosarcoma (RMS)

Rhabdomyosarcoma (RMS) accounts for 4.5% of all childhood cancers [168]. It is a soft tissue sarcoma malignancy that arises from skeletal muscle precursors and is the most common soft tissue sarcoma of children and adolescents [169]. Since RMS

arises from skeletal muscle it can develop in practically every site in the body. The majority of RMS cases occur sporadically, with no known predisposing risk factor. There are a small number of RMS cases where the patient has an identifiable "genetic risk factor" that can be caused by the possession of genetic conditions, such as Li Fraumeni condition [168]. RMS has a particularly low survival rate with the 5-year survival rate near 67% for children younger than 15 years and 51% for adolescents aged 15 to 19 years [165].

RMS can be generally split into two main groups: Embryonal RMS (ERMS) and Alveolar (ARMS). ERMS usually occurs in the first five years of life, predominantly occurs in males and is most often observed in the head and neck region or genitourinary track. This subtype occurs in over 70% of RMS patients [170, 171]. ERMS cases typically possess loss of heterozygosity (LOH) characteristics. This LOH results in an over-expression of the growth promoting gene, insulin-like growth factor Type II (*IGF-II*), located on the short arm of chromosome 11. It is believed that the expression of two copies of this *IGF-II* gene results in excess IGF-II, which in turn leads to the production of a constant proliferative signal that promotes uncontrollable growth and prevents cell death [172, 173]. In addition, ERMS has been shown to have a deregulated hedgehog (HH) signalling pathway where 50% of ERMS tumours have been found to have an activation of GLI1, a transcription factor belonging to the HH pathway [173, 174]. Mutations in *HRAS*, *KRAS* and *NRAS* are observed in over 45% of ERMS cases. The inactivation of p53 and retinoblastoma (Rb) pathways have also been found in number of ERMS cases [168, 173, 175].

ARMS, on the other hand, affects all age groups from 0-19 years, does not vary by sex and accounts for about 30% of children and adolescents with RMS. ARMS usually occurs in tissue of the extremities such as the arms and legs [170, 171]. Alveolar tumours are considered more aggressive and higher risk than ERMS tumours and need more intensive treatment [176]. In contrast to the large amount of mutations seen in ERMS, ARMS are genetically simpler. Approximately 80% of ARMS cases are characterised by specific chromosomal translocations that involve Paired box (*PAX*) genes and Forkhead box protein O1 (*FOXO1*) genes (also known as forkhead in rhabdomyosarcoma (*FKHR*) genes). *PAX* genes are believed to regulate transcription during early neuromuscular development and the *FOXO1* gene

is a transcription factor. This translocation event usually involves the fusion of *PAX3* gene (located on chromosome 2) or *PAX7* gene (located on chromosome 1) to a portion of the *FOXO1* gene (located on chromosome 13) to create a new hybrid gene: *PAX-FOXO1* [177, 178]. The PAX3-FOXO1 fusion is more common than the PAX7-FOXO1 fusion (55% vs 23%) and the PAX7-FOXO1 is linked with a longer event-free survival outcome. This hybrid gene is responsible for turning on growth-stimulating genes that would otherwise be inactive and also switches off growth-inhibitory genes that are usually active [168, 176]. Ultimately, this PAX-FOXO1 hybrid has been found to stimulate proliferation, induce angiogenesis, and inhibit apoptosis [176]. This fusion hybrid appears to be the cause of the bad outcome associated with ARMS [179]. ARMS cells also exhibit a high level of oncogenes *c-Myc* and *MYCN* [180, 181].

Standard current therapy for RMS patients involve surgery, radiation and chemotherapy. The most common chemotherapeutic drugs used to treat RMS is a combination of vincristine, actinomycin D and cyclophosphamide (VAC). VAC has been the standard treatment for RMS for more than four decades now [173]. However, this treatment can have highly toxic effects on patients. Common side effects that are seen with practically all chemotherapy drugs used to treat RMS include hair loss, nausea, vomiting, loss of appetite, fatigue, mouth sores, and the development of low-blood cell counts [168].

1.7.1.2 Neuroblastoma

Neuroblastoma is an extracranial solid tumour that occurs in children. Neuroblastoma represents about 10% of all childhood cancers and accounts for approximately 15% of all childhood cancer deaths [182]. The majority of neuroblastoma cases arise before the age of five and the 5-year survival rates for neuroblastoma patients are around 70% [183, 184]. However, high-risk neuroblastoma cases (defined by *MYCN* amplification status, location and metastasis) have a poor prognosis with a 5-year survival rate of 50% and patients with recurring neuroblastoma show survival rates of less than 10% [185].

Neuroblastoma arises in nerve cells and transformation is usually caused by whole-chromosome gains or segmental chromosomal aberrations. Chromosome gains are usually associated with a favourable prognosis, while chromosomal losses tend to be associated with worse outcomes. For example, gain of chromosome 17q occurs in about 80% of neuroblastomas and is associated with a favourable prognosis. On the other hand, 1p36 chromosomal region deletion occurs in approximately 70% of tumours and correlates with an increased risk of relapse in patients. Likewise, deletions of chromosome 11q have been identified in 20% of neuroblastomas and are also associated with unfavourable patient outcomes and a lower 5 year event free rate. The *MYCN* oncogene is amplified in about 25% of neuroblastoma cases [186, 187]. Current treatments for neuroblastoma include chemotherapy, surgical resection, and/or radiotherapy [182]. Chemotherapy agents typically used for the treatment of neuroblastoma include vincristine, doxorubicin, cyclophosphamide, cisplatin, and etoposide [188].

1.8 UPR in Cancer

The ER and UPR are responsible for a range of cellular and physiological processes. Therefore, it is no surprise that aberrant ER and UPR functions have been linked to a range of pathologies. UPR dysregulation has been implicated in a growing number of diseases, including cancer, Alzheimer's disease, Parkinson's and diabetes [1, 2]. ER stress signalling was first proposed to play a role in cancer development in 2004, after several studies had identified increased UPR activation in tumours [189]. Since then, vast amounts of evidence have implicated the UPR in the formation and advancement of numerous cancers including breast cancer, lung cancer, prostate cancer, skin cancer and brain cancer [190]. Now, the fact that the UPR plays a critical role in the development and sustainability of cancer cells is widely accepted by both scientific and medical communities. The UPR is involved in cancer cells in two ways. Firstly, the UPR can be activated in response to ER stress caused by external stressors such as tumour microenvironment, oncogenic transformation, radiation and pharmacological agents. Secondly, the UPR can be manipulated in order to promote a number of pro-tumourigenic processes including proliferation, oncogenesis, angiogenesis, inflammation, metastasis and invasion [191].

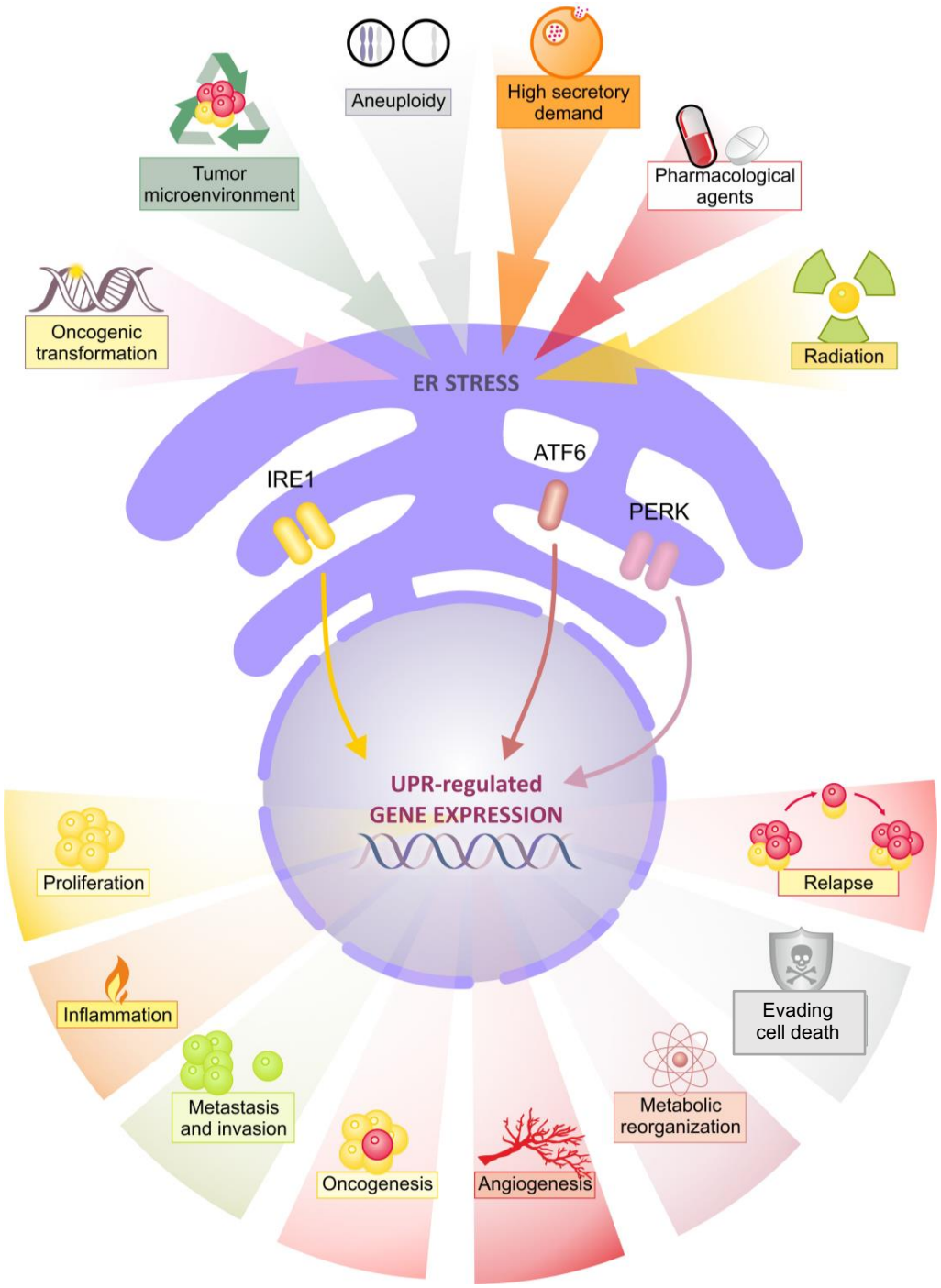

Figure 1.6: UPR involvement in cancer - Diagram highlighting the connections between UPR and cancer. A variety of external and internal stressors lead to UPR activation in cancer. In turn, the UPR drives multiple pro-tumourigenic processes to allow development and survival. Figure prepared by Katarzyna Mnich.

1.8.1 UPR in Cancer Transformation

Neoplastic transformation is a multistep process that involves cancer cells overriding several check points that usually block irregular growth, and manipulating a number of pathways to support growth and ensure survival. This transformation is usually initiated by either loss of tumour suppressors such as p53 and phosphatase and tensin homolog (PTEN) or by the activation of oncogenes including *RAS*, *MYC*, *HER2* and *BRAF*. Regardless of initiation modality, cancer transformation is associated with unrestricted rapid cell division which dramatically enhances protein synthesis rates. Unsurprisingly, this overwhelms the protein folding capacity of the ER, generating ER stress and triggering UPR activation [191-193]. Activation of the IRE1, PERK and to a lesser extent, ATF6 signalling pathways of the UPR have been reported in several cancers following oncogene activation [191]. Initiation of UPR signalling in cancer cells is likely to be an adaptive response utilised to cope with the increased protein folding demands being placed on the ER. For example, loss of p53 expression in various cancer cell lines has been associated with an increase in IRE1 expression and activation of the IRE1-XBP1s signalling pathway. Under normal conditions, wildtype p53 has been shown to regulate IRE1 stability by promoting its proteasomal-mediated degradation. Loss of p53 results in stabilisation of IRE1 allowing its activation if required, which may support higher rates of proliferation. In line with this, in *in vivo* studies, treatment of $TP53^{-/-}$ xenograft tumours with IRE1 RNase inhibitors resulted in a more pronounced tumour growth reduction than similarly treated $TP53^{+/+}$ xenografts [194]. PERK involvement in transformation can be seen in c-Myc transformed cells where increased protein synthesis triggered ER stress and UPR activation, specifically PERK pro-survival signalling. $PERK^{-/-}$ c-Myc transformed xenografts had significantly smaller growth compared to PERK wildtype tumours [195].

1.8.2 UPR in Cancer Growth

The IRE1 pathway has been linked to cell proliferation in several cancers including breast cancer, prostate cancer, colon cancer, glioma, melanoma and multiple myeloma (MM). Genetic and/or pharmacological inhibition of IRE1 in these cancer types reduces cell proliferation *in vitro* and *in vivo* [191, 196-200]. Pharmacological

inhibition of IRE1 RNase activity reduced the proliferation of breast cancer cells *in vitro.* This reduction in proliferation was due to a cell cycle arrest in G1 phase, implying that IRE1 impacts cell cycle signalling in cancer cells [198]. Likewise, IRE1 inhibition in leukemic cells induced G1 cell cycle arrest demonstrating that IRE1 regulates G1 phase controlling proteins including p21, p27 and cyclin D1 [201]. IRE1 activity in prostate cancer has been linked to the cyclin A1, a cell cycle regulating protein, highlighting the role of IRE1 signalling in promoting cell division in cancer cells [202]. PERK is also associated with promoting cancer cell growth. PERK deficiency in human breast cancer cells impeded progression through the cell cycle at the G2/M phase which correlated with a significant decrease in cancer cell proliferation [203].

1.8.3 UPR in Cancer Cell Death Evasion

Although UPR activation promotes adaptive signalling in response to protein folding demands during transformation and survival, cancer cells must be careful not to activate the pro-death signalling potential of the UPR. Cells must achieve the correct balance between adaptive signalling for optimum proliferation without pushing too far towards cell death. Tumour cells have developed multiple mechanisms to limit pro-apoptotic UPR outputs. For example, PERK activation in c-Myc transformed cells suppresses cell death via autophagy. Loss of PERK results in induction of apoptosis, due to decreased autophagy along with increased Ca^{2+} release from the ER [195]. HRAS-transformed mouse embryonic fibroblasts (MEFs) have reduced CHOP levels, a major pro-death signalling component of the UPR [204]. This could be due, in part, to PERK activation of Nrf2 which has been shown to downregulate CHOP, blocking cell death signalling [205]. Other anti-apoptotic mechanisms of the UPR involve signal transducer and activator of transcription 3 (STAT3) and NF-κB, which can be activated by IRE1 and PERK. STAT3 and NF-κB then transcriptionally upregulate multiple anti-apoptotic proteins, including Bcl-2 family members, caspase-8 inhibitor Cellular FADD-like IL-1β-converting enzyme (FLICE)-inhibitory protein (c-FLIP), Mcl-1, and IAPs [193, 206]. If cells successfully limit pro-apoptotic UPR outputs, the UPR can promote survival during tumour progression.

1.8.4 UPR in Cancer Cell Survival

Cancer tumour microenvironments (TME) are characterised by poor vascularization, low oxygen supply (hypoxia), nutrient deprivation, and acidic pH, all of which disturb the protein-folding capacity of the ER and instigate ER stress [207]. The UPR can be activated by hypoxia and nutrient deprivation caused by harsh TME conditions [208]. Tumours rapidly outgrow their available blood supply, therefore, tumours must generate their own vascularisation to supply sufficient oxygen and nutrients necessary for growth and survival. This formation of new blood vessels is termed angiogenesis. All 3 arms of the UPR have been shown to upregulate vascular endothelial growth factor A (VEGFA), a key promoter of angiogenesis [209]. Tumour-generated neovasculature can be inefficient, with slow and inconsistent blood flow. Such poor circulation limits nutrient accessibility, oxygen delivery and waste drainage, thereby driving acute hypoxia, nutrient deprivation and lactic acidosis especially in tumour cores [193]. Cancer cells utilise the UPR to survive these conditions. For example, in triple negative breast cancer (TNBC), XBP1s forms a complex with hypoxia-inducing factor 1 (HIF1α), which was shown to improve cancer cells tolerance to hypoxic conditions [210].

1.8.5 UPR in Senescence

Senescence was first reported by Hayflick in 1965 who discovered that cells in culture have a finite replicative potential [211]. He observed that after cells divide a certain number of times, they stop growing and enter a state of permanent cell cycle arrest, which was later termed replicative senescence. It wasn't until the 90's that it was discovered that this halt in replication was due to shortening of telomeres or telomere dysfunction [212]. Senescent cells possess significant morphological changes including becoming flat, enlarged, vacuolized, and sometimes possess enlarged nuclei or are multinucleated [213]. Since its initial description, our understanding and the definition of senescence has changed considerably. Now, senescence is also recognised as a stress response mechanism that can be induced by a wide range of intrinsic and extrinsic insults including oncogenic activation, oxidative stress, genotoxic stress, mitochondrial dysfunction, irradiation, or chemotherapeutic agents [214, 215]. In addition to the original described

morphological characteristics of senescent cells, several other common characteristics have been established including positive staining for the senescence-associated β-galactosidase (β-Gal) marker and the activation of key effector pathways such as the p53 and Rb pathways [216]. More recently, senescence has become especially complicated with the discovery of senescence-associated secretory phenotype (SASP) which involves the secretion of pro-inflammatory cytokines, growth factors, extracellular matrix components and enzymes from senescent cells [217]. Senescence, like apoptosis, is a protective mechanism when activated by shortened telomeres or certain stress signals, forcing potential harmful cells into a G0-like state and rendering them incapable of further proliferation. Hence, senescence has been recognised as a potent anticancer mechanism that averts malignancies by preventing the replication of pre-neoplastic cells [218, 219]. Cancer cells must find a way to evade senescence in order to indefinitely replicate [220].

The role of UPR in cancer cells with regards to senescence is controversial. Some studies suggest that the UPR induces senescence as an anti-tumourigenic response, other studies demonstrate that the UPR contributes to avoiding senescence (Reviewed in [215]. Unsurprisingly, ER stress induction and UPR activation is evident in all types of senescence. All three arms of the UPR have been found to be activated during senescence, where the UPR has a pro-survival role [215, 221]. For example, increased protein synthesis caused by SASP is believed to be one source of ER stress where PERK induced autophagy aids in cell survival during therapy induced senescence (TIS) [222]. Not only is the UPR found to play a protective role during senescence but it may also contribute to the senescence phenotype. Some studies suggest that UPR signalling is involved in promoting senescence, where knockdown of UPR components results in reduced senescence. For instance, in H-RAS activated melanocytes IRE1 or ATF6 inhibition, or XBP1 or ATF4 knockdown reduced the proportion of cells entering senescence [223], suggesting a pro-senescence role of the UPR. In contrast, the UPR has been suggested to play an anti-senescence role in other studies, where knockdown of UPR components results in senescence induction. For example, genetic silencing of *XBP1* in HRAS-driven senescence in primary murine keratinocytes resulted in an increase in β-Gal positive cells [224].

1.9 IAPs in Cancer

Dysregulation of cell death pathways is commonly seen in cancer [225]. Cell death evasion is one of the well-known hallmarks of cancer [226]. To prevent the induction of apoptosis, cancer cells downregulate pro-apoptotic proteins and reduce levels of anti-apoptotic proteins [225]. IAP proteins are dysregulated in a number of cancers. Alterations in IAP function can be caused by genetic mutations, downregulation of the IAP inhibitor Smac or overexpression of IAP protein or mRNA [227]. For example, genetic amplification of the *cIAP1* and *cIAP2* genes are found in liver cancer, cervical cancer, MM and glioma [228-232]. This upregulation of IAPs is associated with poor prognosis. For instance, high expression of *cIAP2* or *XIAP* correlates with poor prognosis and poor clinical outcome in leukemia patients [233-237]. Moreover, IAP proteins have been implicated in providing resistance of cancer cells to chemotherapy and radiation [95, 238, 239]. Since IAP proteins are aberrantly expressed in many human cancers, IAP proteins are an attractive therapeutic target for these cancers [227]. A number of strategies have been explored targeting IAPs and so far small-molecule IAP inhibitors such as Smac mimetics and IAP antagonists have garnered the most attention (discussed further in section 1.11).

1.10 UPR Targeting Drugs

Since ER and UPR functions are so important in cell signalling, many compounds, including ER stress inducers and UPR inhibitors, have been developed to target the UPR for both basic and translational research. Numerous studies have been carried out on the treatment of cells with ER stress inducers and inhibitors and both the pro-death and pro-survival responses have been well documented. ER stress inducers are beneficial to investigate how cells respond to ER stress and to uncover components involved in stress responses. On the other hand, UPR inhibitors can be valuable for two reasons. Firstly, inhibiting UPR can reveal essential functions of the UPR in cells under normal conditions which can further our understanding of the signalling pathways. Secondly, UPR inhibition can reveal functions of these pathways in pathological conditions furthering our knowledge of the disease under investigation. As previously mentioned, the UPR is activated in a number of cancers and is deemed pro-tumourigenic in many of these cancers. Therefore, pharmacological targeting the UPR is a promising approach for cancer treatment. There are two predominant approaches to harness the UPR as a therapeutic target in cancer. First, induction of ER stress and over-activation of the UPR to force the UPR signalling towards pro-death. Second, inhibition of UPR signalling that cancer cells are reliant on for survival, reducing growth and proliferation or sensitizing the cells towards apoptosis.

1.10.1 ER stress inducers

There are several drugs currently used for the induction of ER stress. Tunicamycin (TM) is one of the most frequently used ER stress inducing drugs. TM is a specific inhibitor that blocks N-glycosylation which is the initial step of glycoprotein biosynthesis in the ER [13]. Blocking this process causes an accumulation of unfolded proteins in the ER, leading to ER stress [3]. Thapsigargin (TG) is another commonly used ER stress inducer. TG is an agent that inhibits sarcoplasmic/endoplasmic reticulum Ca^{2+} ATPase (SERCA) [13]. TG-mediated inhibition of SERCA brings about a decrease in ER calcium levels which results in calcium-dependent ER chaperones losing their chaperone abilities. Reduced chaperone activity leads to the accumulation of unfolded proteins and ER stress [3]. TM and TG are the most commonly used ER stress inducers in experimental

conditions. Another method of ER stress induction is via proteasome inhibition. Proteasomal degradation of misfolded proteins is crucial for cell survival and homeostasis maintenance as it eliminates unwanted or damaged proteins. Proteasome inhibitors cause an accumulation of misfolded proteins and as a consequence stimulate ER stress [240]. Bortezomib (Btz) is a first class proteasome inhibitor that targets the 26S proteasome to induce ER stress and is the most widely utilised proteasome inhibitor [241]. Other commonly used ER stressors include dithiothreitol (DTT), brefeldin A (BFA) and 2-deoxyglucose (2-DG). DTT is a reducing agent that initiates ER stress by blocking disulphide-bond formation, resulting in unfolded proteins. BFA is an inhibitor of ER/Golgi transport causing protein build-up in the ER [3]. 2-DG is an inhibitor of glycolysis which promotes ER stress by interfering with energy production necessary for protein folding [242]. It is important to note that the majority of ER stress inducers are used for research purposes and are not actually used in clinical settings. Nonetheless, their use for basic research is indispensable.

1.10.1.1 ER stress inducers in cancer

As mentioned previously, intense and continuous ER stress can trigger cell death. Inducing cell death in cancer cells via ER stress is a highly attractive therapeutic target. There are numerous drugs currently used that can trigger ER stress-induced cell death. Activation of the UPR due to increased ER stress causes apoptosis in many cancer cell lines, including MM, leukemia, colon, cervical and prostate [243]. Single treatment with TM or TG results in ER stress induced cell death in a number of cancer cell lines [7]. Additionally, several studies have shown that combination of TM or TG with chemotherapeutics enhances cell death in cancer cells [7]. Inhibition of the proteasome also leads to ER stress and UPR activation in cancer cells and it is now well established that proteasome inhibition can stimulate ER stress-induced cell death in several cancers. *In vitro* studies have demonstrated the cytotoxic effects of Btz on a number of cancer cell types, including breast, lung, colon, prostate, and non-Hodgkin's lymphoma [7]. Currently, there are two FDA approved proteasome inhibitors for clinical use, Btz and Carfilzomib (Carf) [244]. Both Btz and Carf are approved for treatment of MM [245, 246].

1.10.2 IRE1 Inhibitors

Several small molecule inhibitors that selectively block the IRE1-XBP1 pathway have been developed. IRE1 activity can be targeted by either binding and inhibiting its RNase domain, or by binding and inhibiting the ATP-binding pocket of the kinase domain. Salicylaldehydes including 4μ8C, MKC3946, STF-083010, and toyocamycin interact with the catalytic core of the RNAase domain and prevent IRE1 RNase activity. These compounds irreversibly bind to IRE1 and inhibit *XBP1* splicing and prevent RIDD activity [247]. The discovery of off target effects for some IRE1 inhibitors has led to the more recent development of a new IRE1 inhibitor named MKC8866 (MKC). MKC8866 is a salicyaldehyde derivative that binds to the RNase domain of IRE1 and blocks any IRE1 RNase activity [4, 248]. MKC8866 has been proven to have efficient and specific effects in preventing *XBP1* splicing in cells with basal XBP1 splicing [198].

1.10.2.1 IRE1 inhibition in cancer

It is now well established that IRE1 signalling is upregulated in several cancers where it supports growth and survival. Therefore, targeting IRE1 signalling is an attractive therapeutic target. Several studies have demonstrated that IRE1 inhibitors have an anticancer effects *in vitro* and *in vivo* [247]. For example, IRE1 RNase inhibitors STF-083010 and MKC3946 have significant cytotoxic activity against MM both *in vitro* and *in vivo* [199, 249]. IRE1 RNase inhibitors including MKC3946, MKC8866, STF-083010, KIRA6 and toyocamycin, suppress proliferation at lower concentrations and trigger cell death at higher concentrations in several leukemic cell lines and patient samples [201, 250]. IRE1 RNase inhibitors, MKC3946 and MKC8866, reduced cell growth in prostate cancer and TNBC cells as a single treatment. Moreover, combination of these IRE1 inhibitors with current therapies synergistically reduced tumour growth and induced cytotoxicity in TNBC, MM and prostate cancer [198, 251, 252].

1.10.3 PERK Inhibitors

Several inhibitors targeting the PERK arm of the UPR have also been developed. GSK2606414 and GSK2656157 are the most widely utilised PERK inhibitors. Both compounds bind to the ATP-binding site cleft of the PERK cytosolic kinase, preventing its kinase activity. These PERK inhibitors are well characterized and display high selectivity for PERK without having any affinity for other eIF2α kinase family members such as heme-regulated eIF2α kinase (HRI), double-stranded RNA-dependent protein kinase (PKR), and general control non-depressible protein 2 (GCN2) from the integrated stress response (ISR) [253, 254]. Unfortunately, GSK2640414 and GSK2656157 activity and specificity is somewhat controversial. Some studies demonstrate that GSK2656157 does not always correlate with reduced eIF2α phosphorylation and that this inhibitor does not recreate the same biological effects of PERK genetic inactivation [255]. Furthermore, studies found that GSK2640414 and GSK2656157 are not as specific as originally thought, as they inhibit RIP1, a protein heavily involved in NF-κB regulation and necroptotic cell death [256]. Since the discovery of this off-target activity, a new structural class of more specific PERK inhibitors were developed known as AMGEN44 (AMG) and AMGEN52 [257]. Although AMGEN44 and AMGEN52 are more selective than GSK2606414 and GSK2656157, they appear to be less potent. Nonetheless, AMGEN44 and AMGEN52 are the recommended compounds to study PERK signalling and pharmacology.

1.10.3.1 PERK inhibition in cancer

As previously discussed (in section 1.8), PERK activity has also been reported to play an important role in several cancers, making it a potential target for cancer therapy. Studies using PERK deficient cells demonstrate reduced pro-tumourigenic activity suggesting that PERK inhibitors may have anticancer activity. Both GSK2606414 and GSK2656157 inhibition of PERK resulted in reduced tumour growth in pancreatic cancer and MM mouse models [258, 259]. However, it has now been discovered that GSK2656157 causes damage to pancreatic cells, which limits its potential use in cancer therapy [253, 258]. No studies into the effect of AMGEN44 on cancer cells have been published as of yet.

1.10.4 ATF6 Inhibitors

Inhibition of ATF6 is difficult because unlike IRE1 and PERK, it is not an enzyme that can be easily targeted. ATF6 contains disulphide bonds in its luminal domain, and since disulphide bond formation requires PDI, most compounds that affect ATF6 signalling are PDI inhibitors [260]. Another option to inhibit ATF6 is by targeting the proteases, S1P and S2P, that are responsible for cleaving and activating ATF6 [261]. However, targeting PDI and protease activity is not specific for ATF6 signalling, and can have substantial effects on multiple other pathways. Pyrazole amides known as ceapins, were recently shown to specifically inhibit ATF6 signalling by blocking ATF6 processing and nuclear translocation in cells under ER stress [262].

1.10.4.1 ATF6 inhibition in cancer

ATF6 expression is upregulated in several cancers including colon cancer, thyroid cancer, and squamous cell head and neck cancer suggesting it can be a potential therapeutic target [247]. Unfortunately, since ATF6 inhibition is difficult, little research into the anticancer effect of its inhibition has been carried out. Nonetheless, melatonin, which has been shown to inhibit ATF6, sensitizes hepatocellular carcinoma to apoptosis, suggesting a potential for ATF6 inhibition in cancer therapy [263]. The discovery of Ceapins as an inhibitor of ATF6 will allow the investigation of the potential for ATF6 inhibition in cancer treatment [262].

The potential of UPR inhibitors in cancer therapy is promising for a number of cancers either as single treatments or in combination with other commonly used treatments. Since UPR inhibitors are relatively new, most studies investigating their anticancer effect are *in vitro* with only a few *in vivo*. Thus, there is limited information on their *in vivo* efficacies and the long-term effects of these inhibitors are unknown. Further investigation into UPR inhibitors for cancer patient treatment is required.

1.11 IAP Antagonists (Smac Mimetics)

Endogenously, IAP protein activity is antagonized by several proteins including Smac, Omi/HtrA or IAP associated factor 1 (XAF1) [116, 264-266]. For example, Smac binding and interaction with the BIR domains of XIAP effectively abrogates its inhibition of caspases-3, -7 and -9 [267, 268]. Smac also induces the autoubiquitination of cIAP1 and cIAP2, causing their proteasomal degradation [119]. The most commonly used IAP antagonists are Smac mimetics such as BV6 and birinipant. Smac mimetics target cIAP1 and cIAP2 by inducing their autoubiquitination, leading to their proteasomal degradation [119]. Smac mimetics also effectively inhibit XIAP activity. These IAP antagonists, like Smac, do not induce the degradation of XIAP [269]. Treatment of cells with Smac mimetics promotes pro-apoptotic signalling by preventing IAP inhibition of caspases. Moreover, the loss of cIAPs stabilizes NIK, promoting non-canonical NF-κB signalling such as the expression of TNFα and subsequent TNFα cell death signalling. Additionally, in the absence of cIAP proteins, RIP1 is deubiquitinated and available for complex formation required for necroptotic cell death induction [119].

1.11.1 Smac Mimetics in Cancer

As previously discussed in section 1.9, IAPs are upregulated in a number of cancers and have been associated with a poor prognosis and clinical outcome for several different cancers [227]. Thus, targeting these proteins in cancer treatment is a promising strategy. A number of Smac mimetics display cytotoxic effects against various cancer cells. For example, Smac mimetic BV6 has demonstrated cytotoxic effects against leukemia, MM, fibrosarcoma and lung cancer cells [238, 270, 271]. Smac mimetics induce cell death in these cancer cells, by binding and inhibiting XIAP, preventing XIAP-mediated inhibition of caspase-3, -7 and -9. Inhibition of cIAP1 and 2 by Smac mimetics results in their proteasomal degradation promoting apoptosis initiation in cancer cells [119, 272, 273]. Furthermore, Smac mimetics in combination with other treatments including chemotherapeutics, death receptor agonists and radiation, show promising results in targeting cancer cells for cell death *in vitro* and *in vivo* [95, 238, 239].

1.12 Aim of the Study

Cancer in children is considered rare, however it is the leading cause of death by disease in children, with over 300,000 children diagnosed each year and an estimated 80,000 deaths annually worldwide [159]. Unsatisfactory cure rates as well as life-altering side effects associated with currently used paediatric treatments, highlight the urgent need for continued research and improved treatments for paediatric cancers.

Since the UPR is implicated in tumourigenesis in many cancers, it is an attractive target for cancer treatment. The aim of this thesis was to determine if the UPR plays an important role in the survival of paediatric cancer cells. We sought to determine the potential of targeting the UPR as a therapeutic strategy, by either inhibition or over-activation, in paediatric cancers, including rhabdomyosarcoma and neuroblastoma. Furthermore, we wanted to investigate the therapeutic potential of combining UPR inhibitors and inducers with other anticancer drugs specifically targeting cell death or survival signalling pathways.

Thus far, the role of the UPR in RMS and its potential as a therapeutic target has not been explored. We decided to investigate basal UPR activity in RMS cells and elucidate the role it plays in RMS survival. We also explored the effect of inhibition of this UPR basal activity and its potential as a therapeutic target. These results are described in Chapter 3.

In this thesis, we also wanted to explore the potential cytotoxic effects of ER stress inducers in paediatric cancer cell lines. ER stress inducer, TM, and Smac mimetic, BV6, are both well-known cell death inducers in cancer cells [7, 274]. Thus, in chapter 4, we aimed to examine the combinatory effects of TM and BV6 in neuroblastoma cells. The results for this investigation are presented in Chapter 4.

Chapter 2: Materials and Methods

2.1 Materials

2.1.1 Cell lines

The cell lines used in this study are shown in Table 1.

Table 1: Paediatric Cell lines

Cell line	Specification	Species	Source
C2C12	non-malignant myoblasts	mouse	American Type Culture Collection (ATCC), Manassas, VA, USA
HEK293T	embryonal Kidney cells	human	ATCC, Manassas, VA, USA
Jurkat FADD$^{-/-}$	T-Cell Acute Lymphoblastic Leukemia (ALL) (T-Cell)	human	kindly provided by Dr. J. Blenis, Department of Cell Biology, Harvard Medical School, Boston, Massachusetts 02115, USA
KYM1	alveolar rhabdomyosarcoma	human	Japanese Collection of Research Bioresources Cell Bank (JCRB), Osaka, Japan.
MRC5	non-malignant lung fibroblast	human	ATCC, Manassas, VA, USA
RH30	alveolar rhabdomyosarcoma	human	Deutsche Sammlung von Mikroorganismen und Zellkulturen (DSMZ), Braunschweig, Germany
RH36	embryonal rhabdomyosarcoma	human	ATCC, Manassas, VA, USA
RH41	alveolar rhabdomyosarcoma	human	ATCC, Manassas, VA, USA
RMS13	alveolar rhabdomyosarcoma	human	ATCC, Manassas, VA, USA
RD	embryonal rhabdomyosarcoma	human	ATCC, Manassas, VA, USA

SH-EP1	neuroblastoma	human	ATCC, Manassas, VA, USA
T174	embryonal rhabdomyosarcoma	human	DSMZ, Braunschweig, Germany
TE381.T	embryonal rhabdomyosarcoma	human	ATCC, Manassas, VA, USA

2.1.2 Stable transfected cell lines

Stably overexpressing cell lines were generated by retroviral transduction. RD-miRNA-146-GFP and RH30-miRNA-146-GFP cells were generated using retroviral transduction (method described in 2.2.5). The pmiR146-eGFP-BSD was kindly gifted by Prof. Dr. Rene Bernards from the Netherlands Cancer Institute with permission from Prof. Steve Elledge, Department of Genetics, Harvard Medical School [275]. *HRAS*, *KRAS* and *NRAS* mutated RMS13 cells were generated by Christina Schott [276].

2.1.3 Cell culture reagents

Cell culture reagents used in this study are shown in Table 2.

Table 2: Cell culture reagents

Reagent	Supplier
Blasticidin (BSD)	Invitrogen, Heidelberg, Germany
Dulbecco's Modified Eagles Medium (DMEM) GlutaMAX-l	Life Technologies, Eggenstein, Germany
Dulbecco's phosphate buffered saline (PBS)	Life Technologies, Eggenstein, Germany
Fetal calf serum (FCS)	Life Technologies, Eggenstein, Germany
4-(2-hydroxyethyl)-1-piperazineethanesulfonic acid (HEPES)	Thermo Fisher Scientific, Dreieich, Germany
Penicillin/Streptomycin (P/S)	Life Technologies, Eggenstein, Germany
Puromycin	Clontech Laboratories, Saint-Germain-en-Laye, France

RPMI 1640 medium, GlutaMAX-l	Life Technologies, Eggenstein, Germany
Sodium pyruvate	Life Technologies, Eggenstein, Germany
Trypsin/EDTA solution (0.05 %), phenol red	Life Technologies, Eggenstein, Germany
Trypan blue solution	Life Technologies, Eggenstein, Germany

2.1.4 Drugs

Inhibitors and compounds used in this study are shown in Table 3.

Table 3: Drugs and inhibitors

Drug	Supplier
2-DG	**Sigma-Aldrich, Taufkirchen, Germany**
Alisertib	Selleck Chemicals, Munich, Germany
AMGEN44	Tocris Bioscience, Bristol, UK
Birinipant	Selleck Chemicals, Munich, Germany, Munich, Germany
Bortezomib	Jansen-Cilag, Neuss, Germany
Brefeldin A	Cell Signaling Technology (CST), Beverly, MA
BV6	Genentech Inc., San Francisco, CA, USA
Carfilzomib	Selleck Chemicals, Munich, Germany
DTT	Sigma-Aldrich, Taufkirchen, Germany
GSK2606414	Tocris Bioscience, Bristol, UK
MKC8866	Fosun Orinove PharmaTech Inc., Westlake Village, CA, USA and MedChemExpress, Cologne, Germany
Necrostatin-1s	Merck Merck Millipore, Cork, Ireland, Cork, Ireland
Tunicamycin	AppliChem, Darmstadt, Germany
Thapsigargin	Sigma-Aldrich, Taufkirchen, Germany
Trametinib	Selleck Chemicals, Munich, Germany
zVAD.fmk	Selleck Chemicals, Munich, Germany

2.1.5 Antibodies

Primary antibodies used for Western blot analysis are shown in Table 4. All antibodies were diluted in 2% bovine serum albumin (BSA).

Table 4: Primary antibodies for Western blot analysis and histology

Target protein	Dilution	Species	Supplier
β-Actin	1:1000	Mouse	Sigma-Aldrich, Taufkirchen, Germany
ATF4	1:1000	Rabbit	CST, Beverly, MA, USA
Bcl-2	1:1000	Rabbit	Abcam, Cambridge, MA, USA
Bcl-xL	1:1000	Rabbit	Abcam, Cambridge, MA, USA
Bim	1:1000	Rabbit	CST, Beverly, MA, USA
Bip (GRP78)	1:500	Rabbit	CST, Beverly, MA, USA
Caspase-3	1:1000	Rabbit	CST, Beverly, MA, USA
Caspase-8	1:1000	Rabbit	Enzo Life Sciences, Loerrach, Germany
Caspase-9	1:1000	Rabbit	CST, Beverly, MA, USA
CHOP (GADD153)	1:500	Mouse	CST, Beverly, MA, USA
cIAP1	1:500	Goat	R&D Systems, Wiesbaden, Germany
cIAP2	1:1000	Rat	Enzo Life Sciences, Loerrach, Germany
E2F1	1:1000	Rabbit	Santa Cruz Biotechnology, Dallas, Texas, USA
eIF2α	1:1000	Rabbit	CST, Beverly, MA, USA
GAPDH	1:10000	Mouse	HyTest, Turku, Finland
IκBα	1:1000	Rabbit	CST, Beverly, MA, USA
IRE1α	1:1000	Rabbit	CST, Beverly, MA, USA
Mcl-1	1:1000	Rabbit	Enzo Life Sciences, Loerrach, Germany
NF-κB p100/p52	1:1000	Mouse	Merck Millipore, Cork, Ireland
NIK	1:1000	Rabbit	CST, Beverly, MA, USA
NOXA	1:1000	Mouse	Enzo Life Sciences, Loerrach, Germany
p21	1:1000	Mouse	BD Biosciences, San Jose, CA, USA
p53	1:1000	Mouse	BD Biosciences, San Jose, CA, USA
PERK	1:1000	Rabbit	CST, Beverly, MA, USA

Phospho-eIF2α	1:1000	Rabbit	CST, Beverly, MA, USA
Phospho-IκBα	1:1000	Mouse	CST, Beverly, MA, USA
Phospho-p53 (Ser15)	1:1000	Mouse	CST, Beverly, MA, USA
PUMA	1:1000	Rabbit	CST, Beverly, MA, USA
Vinculin	1:10000	Mouse	Sigma-Aldrich, Taufkirchen, Germany
XBP1s	1:500	Mouse	Biolegend, San Diego, CA, USA
XIAP	1:1000	Mouse	BD Biosciences, San Jose, CA, USA

Secondary antibodies used for Western blot analysis are shown in Table 5. HPR-conjugated antibodies were diluted in 5% milk in phosphate buffered saline (PBS) with Tween® (PBS-T)

Table 5: Secondary antibodies for Western blot analysis

Antibody	Dilution	Supplier
HRP-conjugated donkey-anti-goat IgG	1:5000	Santa Cruz Biotechnology, Dallas, Texas, USA
HRP-conjugated goat anti-mouse IgG	1:5000	Santa Cruz Biotechnology, Dallas, Texas, USA
HRP-conjugated anti-rabbit IgG	1:5000	Abcam, Cambridge, MA, USA
HRP-conjugated goat anti-rabbit IgG	1:5000	Santa Cruz Biotechnology, Dallas, Texas, USA
HRP-conjugated anti-rat IgG	1:5000	Abcam, Cambridge, MA, USA
HRP-conjugated goat anti-rat IgG	1:5000	Santa Cruz Biotechnology, Dallas, Texas, USA

2.1.6 Fluorescent dyes

Fluorescent dyes used for microscope and Fluorescence Activated Cell Sorter (FACS) are shown in Table 6.

Table 6: Fluorescent dyes for microscope and FACS

Dye	Supplier
Hoechst-33342	Sigma-Aldrich, Taufkirchen, Germany
Ki-67 Antibody Clone	Agilent (Dako), Santa Clara, CA, USA
Mouse IgG FITC-200	R&D Systems, Wiesbaden, Germany
Propidium iodide (PI)	Sigma-Aldrich, Taufkirchen, Germany

2.1.7 Short-interference RNA (siRNA)

Short interference RNA (siRNA) constructs are listed in Table 7. Silencer® siRNA select was purchased from Invitrogen, Karlsruhe, Germany. All siRNAs were diluted to a stock concentration of 20 or 40 μM and used at a final concentration of 10-20 nM.

Table 7: siRNA constructs

siRNA	Target	Catalogue No.	Sequences (5'- 3')
siCtrl	None	4390844	Sequence not provided
siATF4 #1	ATF4	s1702	GCCUAGGUCUCUUAGAUGAtt
siATF4 #2	ATF4	s1703	CCCUGUUGGGUAUAGAUGAtt
siATF4 #3	ATF4	s1704	GAAGCAAGGACAAGACGAGtt
sicIAP1 #1	cIAP1	s1449	CCUCGUAUCAAAACAUUAAtt
sicIAP1 #2	cIAP1	s1450	GGAUAACUGGAAACUAGGAtt
sicIAP1 #3	cIAP1	s1448	GUUAUGCAAUGAGUACUGAtt
sicIAP2 #1	cIAP2	s1451	CACUCAUUACUUCCGGGUAtt
sicIAP2 #2	cIAP2	s1452	GGAGUUCAUCCGUCAAGUUtt
siIRE1 #1	IRE1 (ERN1)	s200430	GAAACUUCCUUUUACCAUCtt
siIRE1 #2	IRE1 (ERN1)	s200431	CCUGCGCUAUCUGACCUUCtt
siIRE1 #3	IRE1 (ERN1)	s200432	CAGGACAUCUGGUAUGUUAtt
siPERK I	PERK	9024S	Sequence not provided
siPERK II	PERK	9026S	Sequence not provided

Amount of siRNA, Lipofectamine, RNAiMAX, OptiMEM, and cell concentrations used for siRNA transfection are listed in Table 8.

Table 8: Preparation of siRNA transfection mix using RNAiMAX reagent

	Per well / dish				
Well plate/dish	Lipofectamine RNAiMAX (µl)	OptiMEM (µl)	siRNA (µl) (10 nM final concentration using 20 mM stock)	OptiMEM (µl)	Cell suspension volume (µl)
96-well	0.3	5	0.025	5	90
24-well	1.5	25	0.125	25	450
12-well	2.5	50	0.25	50	900
6-well	5	100	0.5	100	1800
6 cm	10	200	1	200	3500
10 cm	20	400	2	400	7000

2.1.8 Primer sequences

Primer sequences used for reverse transcription polymerase chain reaction (RT-PCR) are shown in Table 9.

Table 9: List of primer sequences

Target	**Forward Primer (5'-3')**	**Reverse Primer (3'-5')**
XBP1s	GGAATGAAGTGAGGCCAGT.	AGAGTCAATACCGCCAGAATC
GAPDH	TGTAGTTGAGGTCAATGAAGGG	ACATCGCTCAGACACCATG

2.1.9 Plasmids

Plasmids used are shown in Table 10.

Table 10: List of plasmids

Plasmid	**Supplier**
pmiR146-eGFP-BSD	kindly gifted by Prof. Dr. Rene Bernards from the Netherlands Cancer Institute with permission from Prof. Steve Elledge, Department of Genetics, Harvard Medical School

2.1.10 Buffers

Ingredients for buffers used in this study are listed in Table 11.

Table 11: Buffers

Buffer	Ingredients
Blocking buffer	**5% milk powder in PBS-T**
Blotting buffer (1X)	25 mM TrisBase 190 mM Glycine 10% SDS 20% methanol
Nicoletti Buffer	0.05% trisodium citrate dihydrate 0.05% Triton X-100 10% Glycerol 50 mg/ml PI
Phosphate-buffered saline (PBS) (10X)	137 mM NaCl 2.7 mM KCl 2 mM KH_2PO_4 8 mM Na_2HPO_4
PBS-T (0.1%)	1x PBS 0.1% Tween 20
RIPA lysis buffer	50 mM TrisHCl, pH 8 1% NP-40 150 mM NaCl 2mM $MgCl_2$ 0.5% Na-deoxycholate 0.1% SDS PIC 100 mM dithiothreitol (DTT) 1 mM Sodium-orthovanadate Pierce Universal Nuclease
Running buffer (5X)	25 mM TrisBase, pH 6.8 190 mM Glycine 0.1% SDS

SDS loading buffer (6X)	120 mM TrisBase, pH 6.8 10% Glycerol 4% SDS 100 mM DTT Bromophenol blue
Tris Acetate EDTA (TAE) buffer (50X)	2 M Tris Base 1 M Acetic Acid 500 mM EDTA, pH 8

2.1.11 Kits and Ready-to-use-Solutions

Kits and ready-to-use solutions are shown in table 12.

Table 12: Kits

Kit	Supplier
Neon® Transfection System Kit	**Thermo Fisher Scientific, Dreieich, Germany**
Pierce BCA protein assay	Thermo Fisher Scientific, Dreieich, Germany
Pierce ECL Western Blotting Substrate	Thermo Fisher Scientific, Dreieich, Germany
Pure Link HiPure Plasmid Filter Maxiprep Kit	Invitrogen, Heidelberg, Germany
Senescence β-Galactosidase Staining Kit	CST, Beverly, MA, USA

2.1.12 General reagents and chemicals

The general reagents and chemicals used are shown in Table 13.

Table 13: General reagents and chemicals

Reagent/Chemical	Supplier
β-Mercaptoethanol	**Merck Millipore, Cork, Ireland, Cork, Ireland**
0.2 nitrocellulose Western blotting membrane	GE Lifesciences, Freiburg, Germany
Albumin fraction V (BSA)	Carl Roth, Karlsruhe, Germany

Ammonium persulfate (APS)	Carl Roth, Karlsruhe, Germany
Bromphenol blue	Amersham Bioscience, Freiburg, Germany
CasyTon	OMNI Life Science, Bremen, Germany
CasyClean	OMNI Life Science, Bremen, Germany
Cell Titer Glo	Promega, Walldorf, Germany
Chloroform	Sigma-Aldrich, Taufkirchen, Germany
cOmplete™ Protease Inhibitor Cocktail (PIC)	Merck Millipore, Cork, Ireland, Cork, Ireland
Crystal violet (CV)	Carl Roth, Karlsruhe, Germany
Diethyl Pyrocarbonate (DEPC)	Sigma-Aldrich, Taufkirchen, Germany
Dimethyl sulfoxide (DMSO)	Sigma-Aldrich, Taufkirchen, Germany
Disodium hydrogen phosphate dihydrate (Na_2HPO_4)	Carl Roth, Karlsruhe, Germany
Dithiothreitol (DTT)	Merck Millipore, Cork, Ireland
Deoxyribonucleotide triphosphate (dNTP)	Invitrogen, Heidelberg, Germany
DNase buffer	Invitrogen, Heidelberg, Germany
Ethanol	Carl Roth, Karlsruhe, Germany / Sigma-Aldrich, Taufkirchen, Germany
Ethylene diamine tetraacetic acid (EDTA)	Carl Roth, Karlsruhe, Germany
FACS Clean / Rinse solution	BD Biosciences, San Jose, CA, USA
FACS Flow sheath fluid	BD Biosciences, San Jose, CA, USA
FACS Shutdown solution	BD Biosciences, San Jose, CA, USA
Fugene	Invitrogen, Heidelberg, Germany
Formaldehyde	Carl Roth, Karlsruhe, Germany
Glycerol	Carl Roth, Karlsruhe, Germany
Glycine	Carl Roth, Karlsruhe, Germany
HEPES	Sigma-Aldrich, Taufkirchen, Germany

Hyperfilm ECL	GE Lifesciences, Freiburg, Germany
Hybond enhanced chemiluminescence (ECL)	Amersham Bioscience, Freiburg, Germany
Hydrochloric acid (HCl)	Carl Roth, Karlsruhe, Germany
Hydroxyethyl piperazinylethane sulfonic acid (HEPES)	Carl Roth, Karlsruhe, Germany
Isopropanol	Carl Roth, Karlsruhe, Germany
Lipofectamine RNAiMAX	Life Technologies, Eggenstein, Germany
Methanol	Carl Roth, Karlsruhe, Germany
Milk powder (skimmed milk powder, SMP)	Carl Roth, Karlsruhe, Germany
Molecular grade DNase	Invitrogen, Heidelberg, Germany
OligoDt primers	Invitrogen, Heidelberg, Germany
OptiMEM transfection medium	Life Technologies, Eggenstein, Germany
Page Ruler Plus Prestained Protein Ladder	Thermo Fisher Scientific, Dreieich, Germany
Pierce DNase	Thermo Fisher Scientific, Dreieich, Germany
Pierce ECL Western blotting substrate	Thermo Fisher Scientific, Dreieich, Germany
Phenylmethylsulfonyl fluoride (PMSF)	Carl Roth, Karlsruhe, Germany
Potassium chloride (KCl)	Carl Roth, Karlsruhe, Germany
Potassium dihydrogen phosphate (KH_2PO_4)	Carl Roth, Karlsruhe, Germany
Starter for X-ray developer	TETENAL, Norderstedt, Germany
Sodium chloride (NaCl)	Carl Roth, Karlsruhe, Germany
Sodium dodecyl sulfate (SDS)	Carl Roth, Karlsruhe, Germany
Sodium hydroxide (NaOH)	Carl Roth, Karlsruhe, Germany
Sodium-orthovanadate	Sigma-Aldrich, Taufkirchen, Germany
SUPERFIX-MRP x-ray fixer	TETENAL, Norderstedt, Germany
SuperScript II enzyme	Invitrogen, Heidelberg, Germany
Tetramethylethylenediamine (TEMED)	Carl Roth, Karlsruhe, Germany

TRI Reagent	Sigma-Aldrich, Taufkirchen, Germany
TrisBase	Carl Roth, Karlsruhe, Germany
TrisHCl	Carl Roth, Karlsruhe, Germany
Triton X-100	Carl Roth, Karlsruhe, Germany
Tween-20	Carl Roth, Karlsruhe, Germany
UltraPure Agarose	Invitrogen, Heidelberg, Germany

2.1.13 Consumables

Consumables used throughout this study are listed in Table 14.

Table 14: Consumables

Consumable	**Supplier**
µ-slide 8 well ibiTreat	**Ibidi, Planegg, Germany**
Aluminium foil	Carl Roth, Karlsruhe, Germany
Cell culture flasks (25 cm^2, 75 cm^2, 175 cm^2)	Greiner Bio-One, Kremsmünster, Austria
Cell culture plates (96-well, 24-well, 6-well) (clear, black and white)	Greiner Bio-One, Kremsmünster, Austria
Cell scraper	BD Biosciences, San Jose, CA, USA
Combitips (0.5 ml, 1 ml, 5 ml, 10 ml)	Eppendorf, Hamburg, Germany
Centrifuge tubes	Greiner Bio-One, Kremsmünster, Austria
Cover glass	VWR, Dublin, Ireland
Cryogenic vials	Starlab, Milton Keynes, UK, Milton Keynes, UK
Falcon (15 ml, 50 ml) (dark and transparent)	Greiner Bio-One, Kremsmünster, Austria
Filter tips	Starlab, Milton Keynes, UK
Hemocytometer	Marienfeld, Lauda-Königshofen, Germany
Hybond ECL nitrocellulose membrane	GE Lifesciences, Freiburg, Germany
Microcentrifuge tubes	Starlab, Milton Keynes, UK
Parafilm	VWR Darmstadt, Germany

Pasteur pipettes	Carl Roth, Karlsruhe, Germany, Karlsruhe
Pipette tips (10 µl, 200 µl, 1000 µl)	Starlab, Milton Keynes, UK
Reaction tubes (0.5 ml, 1.5 ml, 2 ml)	Starlab, Milton Keynes, UK
Round-bottom tubes (FACS tubes)	BD Biosciences, San Jose, CA, USA
Scalpels	B. Braun, Melsungen, Germany
Sterile culture vials	Carl Roth, Karlsruhe, Germany
Sterile filters (0.45µM)	Merck Millipore, Cork, Ireland
Sterile pipettes (2 ml, 5 ml, 10 ml, 25 ml, 50 ml)	Greiner Bio-One, Kremsmünster, Austria
Syringe (5 ml, 10 ml)	B. Braun, Melsungen, Germany

2.1.14 Equipment

Equipment used throughout this PhD are listed in Table 15.

Table 15: Equipment

Equipment	Supplier
ARE heating magnetic stirrer	**VELP Scientifica, Velate, Italy**
Autoclave VX 150	Systec, Linden, Germany
Avanti J-26 XP ultracentrifuge	Beckman Coulter, Krefeld, Germany
BioRad Pharos FXTM plus Molecular Imager	BioRad, Dreiech, Germany
CC-12 Soft Imaging system	Olympus, Düsseldorf, Germany
Casy Cell Counter	OMNI Life Science, Bremen, Germany
Centrifuge MIKRO 200 R	Hettich, Tuttlingen, Germany
Centrifuge ROTIXA (50 RS & 460 R)	Hettich, Tuttlingen, Germany
CO_2 incubator	SANYO, Bremen, Germany
Easypet® 3	Eppendorf, Hamburg, Germany
Electronic analytical balance	Kern, Balingen
FACS Canto II	BD Biosciences, San Jose, CA, USA
Heating block	Eppendorf, Hamburg, Germany
Heating magnetic stirrer ARE	VELP Scientifica, Velate, Italy
HeraSafe class II biological safety cabinet	Kendro, Hanau, Germany
ImageXpress Micro XLS system	Molecular Devices, Sunnyvale, CA, USA

Infinite M100 microplate reader	Tecan, Männedorf, Switzerland
Micro-centrifuge	Hettich, Tuttlingen, Germany
Microscope CKX41	Olympus, Düsseldorf, Germany
Microscope IX71	Olympus, Düsseldorf, Germany
Mini-Protean Tetra Cell electrophoresis system	BioRad, Dreiech, Germany
Nalgene® Mr Frosty	Sigma-Aldrich, Taufkirchen, Germany
NanoDrop 1000	Peqlab, Erlangen, Germany
Neon® Transfection System	Thermo Fisher Scientific, Dreieich, Germany
PCR-thermocycler	Eppendorf, Hamburg, Germany
pH meter inoLab pH7310	WTW, Oberbayern, Germany
Roller	NeoLab, Heidelberg, Germany
Shaker	NeoLab, Heidelberg, Germany
Sunrise microplate reader	Tecan, Männedorf, Switzerland
Trans-Blot® SD Semi-Dry Transfer Cell	BioRad, Dreiech, Germany
Vacuum pump HLC	Ditabis, Pforzheim, Germany
Vortex mixer (ZX classic; wizard X)	VELP Scientifica, Velate, Italy
Water bath WBT 22	Carl Roth, Karlsruhe, Germany, Karlsruhe, Germany
X-Ray cassette type G	Rego, Gladenbach, Germany

2.1.15 Laboratory-related software

The Software used for data analysis are listed in Table 16.

Table 16: Laboratory-related software

Software	Company
CellSens standard	**Olympus, Düsseldorf, Germany**
FACSDiva version 6.1.3	BD Biosciences, San Jose, CA, USA
FlowJo version 7.6.5	BD Biosciences, San Jose, CA, USA
GraphPad Prism® (version 7.03, GraphPad Software)	GraphPad Prism, San Diego, CA, USA
i-control version 1.10	Tecan, Männedorf, Switzerland
ImageJ version 1.48v	National Institutes of Health, USA

ImageXpress 2015	Molecular Devices, Sunnyvale, CA, USA
Magellan Data Analysis version 7.2	Tecan, Männedorf, Switzerland
MetaXpress®	Molecular Devices, Sunnyvale, CA, USA
MS-Office 2013	Microsoft, Washington, USA
NanoDrop software	Peqlab, Erlangen, Germany

2.2 Methods

2.2.1 Cultivation of cells

RMS cells lines (RH30, RD, KYM1, TE381.T, RMS13, RH36, RH41 and T174) were cultivated in DMEM GlutaMAX^{TM}-l or RPMI 1640 medium, supplemented with 10% foetal calf serum (FCS), 1% penicillin/streptomycin (P/S) and 1% sodium pyruvate. Non-malignant cell lines (C2C12 & MRC5) were cultured in DMEM medium, supplemented with 10% FCS, 1% P/S and 1% sodium pyruvate. Neuroblastoma cells (SH-EP1) were cultured in DMEM medium, supplemented with 10% FCS, 1% P/S and 1% sodium pyruvate. Jurkat FADD$^{-/-}$ cells were cultured in RPMI medium, supplemented with 10% FCS, 1% P/S, 1% sodium pyruvate and 25 mM HEPES buffer. Both, suspension and adherent cell lines were cultured in cell culture flasks in a humidified atmosphere at 37 °C with 5% CO_2. All adherent cells were passaged twice a week. For detachment of adherent cells, medium was removed, cells were washed with sterile PBS and trypsin/EDTA was added for 5 minutes (min). Once all cells were detached, trypsinization was stopped by the addition of fresh growth medium (minimum of twofold ratio to trypsin/EDTA). Suspension cells, on the other hand, were passaged by directly adding the appropriate amount of cell culture into a new flask with fresh media. Cells were discarded after about 30 passages in culture.

2.2.2 Freezing and thawing of cells

As a long-term storage method, cells were frozen in supplemented media containing 10% DMSO and an extra 10% FCS. Cells were put into cryovials and placed into a room temperature Nalgene® Mr Frosty. The container was then placed at -80 °C overnight before being transferred to a nitrogen tank for long-term storage. Cells to be thawed were transferred from defrosted cryovials into a 50 ml falcon with 9ml fresh media. Cells were centrifuged for 5 min at 1800 RPM. The DMSO containing medium was drained off and cells were resuspended in fresh media and placed into culture flasks. Cells were allowed two weeks to adjust before any experiments were performed.

2.2.3 Plating and treating of cells *in vitro*

For plating and treatment of cells, all reagents were pre-warmed to 37°C. Cell densities were determined depending on the well size and the timepoint of measurement. For suspension cells, 20 µl of cell suspension was added to 60 µl of trypan blue dye and counted using a Neubauer chamber. The appropriate number of cells were diluted in growth medium in their required density along with treatment substances in desired concentrations. Adherent cells were seeded in the required density approximately 24 hour (h) before treatment. Cells were trypsinized and then resuspended in fresh growth medium. 20 µl of cell suspension was added to 60 µl of trypan blue dye and counted using a Neubauer chamber. The appropriate number of cells were then diluted in growth medium and seeded in corresponding culture wells or plates. By gently shaking, the cells were distributed evenly in the cell culture plate. After cells were adhered (~ 24 h), medium was removed and replaced by medium containing the treatment substances in desired concentrations. All cells were incubated for indicated timepoints at 37 °C and 5% CO_2.

2.2.4 Transient siRNA transfection

In general, transient knockdown of proteins was performed using SilencerSelect. Cells were transfected with Lipofectamine RNAiMAX and either non-targeting siRNA “siCtrl” or siRNAs targeting specific genes as listed in Table 7. Working volumes and concentrations are described in Table 8. In brief, Lipofectamine RNAiMAX was added to OptiMEM and siRNA (final concentration 10-40 nM) was also added to OptiMEM. The siRNA-OptiMEM mixture was added to Lipofectamine-OptiMEM mixture and incubated for 10 min at room temperature. Next, the transfection mix was distributed to the cell culture wells and the adjusted cell concentration was placed on top. By gently shaking, the cells were distributed evenly in the cell culture plate. The cells were then incubated under usual cell culture conditions (37 °C and 5% CO_2). Six h after transfection, medium was exchanged to avoid toxic effects of the Lipofectamine RNAiMAX. Successful knockdown was verified using Western blot analysis.

For KYM1 cells, transfection with lipofectamine was unsuccessful, therefore, electroporation transfection was performed using a Neon® Transfection System Kit. For electroporation, the appropriate amount of cells from the cell culture flask were centrifuged for 5 min at 1800 RPM. Next, cells were resuspended in PBS (3/4 of previous volume) and centrifuged again for 5 min. PBS was removed and cells were resuspended in Resuspension Buffer. 120 µl cell suspension was then added to the required volume of siRNA (final concentration 20nM) in a 1.5 ml Eppendorf (epi). 100 µl of cell suspension plus siRNA was collected and electroporated using program 14 (1200V, 20ms, 2 pulses). The electroporated cells were subsequently added drop by drop into a falcon with warm P/S free medium. Desired amounts were then transferred to the dish or well plate for measurement of interest. Again, Western blot was used to confirm the knockdown.

2.2.5 Lentiviral transduction

The lentiviral vector pmiR146-eGFP-BSD was introduced into RH30 and RD cells to examine the expression of miRNA-146 as a marker of senescence. The plasmid was a gift from Prof. Dr. Rene Bernard from the Netherlands cancer institute. Preparation of plasmid constructs was carried out using the Pure Link HiPure Plasmid Filter Maxiprep Kit following the user manual's instructions. HEK293T cells were seeded in a 6-well plate (5 x 10^5 cells/cm^2) 24 h prior to transfection. After 24 h, cells were co-transfected with the desired plasmid and packaging plasmids MD2 and PAX2, using OptiMEM and Fugene. After 24 h, medium was changed and at 48 and 72 h, virus containing medium was collected and stored at 4 °C. The virus was then isolated by filtering using syringes, removing any HEK293T cells from the solution. At this point, the virus can be used immediately or flash frozen and stored at -80 °C for long term storage. Parental cell lines (RH30 & RD) were seeded in 6-well plates (1 x 10^5 cells/cm^2) for 24 h to allow cells to attach before the addition of virus. Purified virus from HEK293T cell medium was added to cells (500-1000 µl) along with 2.5µl polybrene. After 48 h, the virus containing medium was removed and fresh growth medium was supplemented. Antibiotic selection using blasticidin (BSD) (15 µg/ml) started after 48 h and was kept on cells continuously during culturing. For experiments with these cells, regular media without BSD was used.

2.2.6 Western Blot

2.2.6.1 Harvesting and lysis of cells for Western Blotting

For Western blotting, cells were seeded in either 6 or 10 cm cell culture dishes and treated with desired drug concentrations for indicated amount of time or transfected with siRNA. At the timepoint of interest, cells were washed once with PBS and additional PBS was added to dish. Cells were collected by scraping the cells from the cell culture dishes and transferred into 2 ml epi's. For suspension cells, all cells and media were directly placed in a falcon without the need for scraping. Cells were centrifuged at 1800 RPM for 5 min in at 4 °C. Supernatant was then removed and the cell pellet was resuspended in 1 ml PBS. Cells were centrifuged again at 1800 RPM for 5 min at 4 °C. Supernatant was removed again, and cell pellets were lysed on ice for 20 min with RIPA lysis buffer (see Table 11) with amounts equaling the size of the pellet. Lysates were then centrifuged for 25 min at 14,000 RPM at 4 °C and the supernatant containing the cellular proteins was transferred into a new tube which was either stored at -20 °C or directly used for determination of protein concentration with Pierce BCA Protein Assay Kit.

2.2.6.2 Protein determination

For protein determination of whole cell lysates, the Pierce BCA Protein Assay Kit was used according to the manufacturer's instructions. In brief, protein concentration was determined in relation to BSA standard curve and absorbance was measured at 550 nM at a microplate reader (Tecan sunrise with Magellan Software).

2.2.6.3 SDS-polyacrylamide gel electrophoresis (PAGE) and Western blot analysis

The polyacrylamide gels consisted of a 5% stacking gel and a resolving gel containing higher percentage polyacrylamide, which is chosen depending on the size of the proteins of interest. The 5% stacking gel consisted of 5% polyacrylamide, 125 mM TrisHCl, pH 6.8, 0.1% SDS, 0.1% APS and 0.1% TEMED. The resolving gels contained either 8%, 10%, 12% or 15% polyacrylamide, 250 mM TrisHCl, pH 8.8,

0.1% SDS, 0.1% APS and 0.04% TEMED. For the SDS-PAGE, 50-80 µg of protein sample were diluted in 6x SDS Loading Dye (see Table 11) and adjusted with ddH_2O to an equal volume, followed by 5 min denaturation at 96 °C before being loaded into the wells of the gel. First, proteins were separated by a constant 100 V until they are passed through the stacking gel. Thereafter, voltage was increased to 140 V for running through the resolving gel. Duration of electrophoresis is chosen depending on the size of the gel and the intended separation of proteins sizes, which is indicated by protein size marker (Page Ruler Plus Prestained Protein Ladder). After satisfactory separation, proteins were transferred to a nitrocellulose membrane using a semi-dry system. Nitrocellulose membrane and Whatman-papers were soaked in blotting buffer (see Table 11) and nitrocellulose membrane and resolving gel were put between two Whatman-papers on each side and placed into the semi-dry system. Transfer of proteins was performed with a constant amperage (1 mA per cm^2 nitrocellulose membrane) for between 1 and 1 h and 40 min depending on the size of the protein to be transferred (shorter time for smaller proteins, longer time for larger proteins). After blotting, the nitrocellulose membrane was removed from the semi-dry system and incubated for 1 h in 5% milk/PBS-T at room temperature for blocking to reduce unspecific antibody binding. Afterwards, the nitrocellulose membrane was washed three times in PBS-T at 10 min each to remove remaining milk before the addition of antibody for protein detection (see Table 4 for list of antibodies used).

2.2.6.4 Protein detection

After blocking and washing, the membrane was incubated with primary antibody diluted in 2% BSA/PBS-T at 4 °C overnight on an orbital shaker. The next day the primary antibody solution was removed and stored at -20 °C for further use. The membrane was washed three times for approximately 10 min with PBS-T. Afterwards, the membrane was incubated with the secondary antibody in 5% milk on a shaker for 1-2 h at room temperature. Next, the membrane was washed again three times in PBS-T for 10 min. Detection of horseradish peroxidase (HRP)-conjugated secondary antibodies using enhanced chemiluminescence (ECL) was performed following the manufacturer's protocol. In brief, ECL solution premixes were mixed in a 1:1 ratio and incubated with the membrane ensuring the whole membrane was

well covered in the solution. The membrane was then placed into an X-Ray developer cassette. In a dark developing room, a film was placed onto the membrane and incubated for a period of time dependent on the signal intensity (this can be between 5 seconds and 1 h). Films were then placed into developing solution. Next, the film was washed and fixed in fixation solution. For digitalization the film was washed, dried and scanned. Before reusing the membrane for the detection of the next protein, the membrane was washed three times in PBS-T for 10 min. For detection of several proteins, membranes were cut and separately incubated or if the same section of membrane is used due to close sizes, primary antibodies of different hosts were chosen in order to avoid overlapping of signals.

2.2.7 PCR

2.2.7.1 RNA Extraction

For RNA extraction, 0.8 x 10^5 cells/cm^2 were seeded in 6-well plates for 24 h before treatment and were subsequently treated for up to 72 h. After harvesting (same as Western blot procedure; section 2.2.6.1), cell pellets were resuspended in 1 ml TRI Reagent and transferred to a 1.5 ml epi. The sample was vortexed for 1 minute and then incubated at room temperature for 5 min. 200 µl of chloroform was added to the samples, shaken vigorously for 15 sec and then incubated for 15 min at room temperature. The samples were spun at maximum speed for 15 min at 4 °C. The upper aqueous layer (~ 400 µl) of the sample was transferred to a new 1.5 ml epi. One volume, equal to the amount of sample, of chilled isopropanol was added dropwise to the sample. The sample was inverted six times and incubated at room temperature for 5-10 min. The sample was then spun again at maximum speed for 15 min at 4 °C. Supernatant was then removed. 1 ml of 85% ethanol in DEPC treated water was added to the pellet. The sample was spun at maximum speed for 15 min at 4 °C. After carefully removing the supernatant, the pellet was allowed to air-dry until all excess liquid had evaporated without the pellet drying up. The pellet was resuspended in RNase free water and heated at 65 °C for 10-15 min for the removal of secondary structures. RNA concentration was determined measuring the absorbance of 260 nM at a NanoDrop Spectrometer. Pureness of RNA was determined by ratio of 260 nm/280 nm for DNA contamination and 260 nm/230 nm

as ratio for protein contamination. RNA was processed immediately or stored at -80 °C.

2.2.7.2 cDNA synthesis and reverse transcription

RNA was dissolved to 2 µg in 10 µl H_20. 1 µl DNase buffer and 1 µl molecular grade DNase was added to the samples and left to incubate for 15 min at room temperature. 1 µl of EDTA was added and the sample was incubated at 65 °C for 8 min. 1 µl of OligoDt primers were added next and samples were incubated at 65 °C for 2 min. 1 µl reverse transcription mastermix including DTT, dNTP's and superscript enzyme was added to the samples and incubated for 50 min at 50 °C followed by 10 min at 85 °C.

2.2.7.3 Conventional PCR

23 µl master mix containing GoTaq polymerase, 10 µM forward primer and 10 µM reverse primer (See Table 9 for primers) were added to 2 µl of previously produced cDNA for PCR reaction in the thermocycler. RT-PCR products for *XBP1s* were run alongside a DNA ladder on a 3% gel using UltraPure Agarose and 1X Tris Acetate EDTA (TAE) buffer. Gels were run in a 30 cm rig at 100 V for approximately 1 h. Gels were imaged using the BioRad Pharos FXTM plus Molecular Imager.

2.2.8 Flow Cytometry

2.2.8.1 Propidium iodide staining

Propidium iodide (PI) uptake due to membrane permeabilization is a marker of cell death and was measured by flow cytometry analysis for suspension cells. For PI staining, suspension cells were seeded in 24-well plates at desired densities and treated for indicated timepoints. Cell suspension was transferred into the round-bottom-tubes and centrifuged at 1800 RPM for 5 min at 4°C. The medium was removed, and the cells were washed with PBS and again centrifuged at 1800 RPM for 5 min at 4 °C. The cell pellet was resuspended in 100 µL PI solution (1 µg/µl). Cell debris was excluded from the measurement in the forward side scatter (FSC)/

side scatter (SSC) and cell death was determined by detecting PI positive population in the PE (red) fluorescence channel.

2.2.8.2 SubG1 fraction assay and cell cycle analysis

Determining the sub-G1 fraction of a sample, allows one to derive the population of apoptotic cells. Cells were seeded in 24-well plates and treated for the required times. At the desired timepoints, the supernatant of each well was transferred into single round-bottom-tubes on ice. The attached cells were trypsinized using Trypsin/EDTA and resuspended in medium and transferred into the corresponding single round-bottom-tube. These round bottom tubes were centrifuged for 5 min at 1800 RPM in 4 °C. Supernatant was removed and the pellet was washed once with PBS and centrifuged again. PBS was then removed, and the cell pellet was resuspended in 100 µl Nicoletti-buffer (see Table 11). Cells were incubated in this hypotonic buffer for at least 30 min at 4°C before flow cytometric measurement. The living cells were gated in the FSC/SSC plot and cell debris was excluded from measurement. SubG1 content was measured to determine apoptotic fraction. For cell cycle analysis, DNA content of the living population was analysed using with FlowJo version 7.6.5 software and the Dean-Jett-Fox model.

2.2.9 Cell viability assay (Cell Titer Glo (CTG))

The Cell Titer Glo (CTG) cell proliferation assay is a colorimetric method for determining the number of viable cells in proliferation by measuring the metabolic activity of cells. Cells were seeded in white 96-well plates and treated for the indicated timepoints or transfected with siRNA. The border wells of the 96-well plate were filled with PBS in order to prevent variations due to evaporation of cell culture medium. Before measurement, the well plate was left at room temperature for 20-30 min to equilibrate to room temperature. 5 µl CTG solution was added to each well and left for 10 min before measurement with a Tecan Infinite M200 plate reader.

2.2.10 Long-term survival assays

2.2.10.1 Casy Cell Counter

RMS cells were seeded in 24-well plates with a cell density of 0.02 x 10^5 cells/cm^2. The next day, cells were treated with the indicated treatment. At two, four and six days, media was removed from cells and trypsinized with 150 µl. Once detached, trypsinization was stopped by the addition of 450 µl fresh growth medium. 100 µl of the cell suspension was added to 10 ml CasyTon solution and measured at the Casy Cell Counter according to manual instructions (Left cursor 10 µM).

2.2.10.2 Colony formation assay

To examine long term survival of cells following treatment, a colony formation assay was used [277]. Cells were seeded in 6-well plates at a density of 400 cells/well and treated with the indicated concentrations or transfected with siRNA. For SH-EP TM/BV6 treated cells, treatment was removed and cells were reseeded at equal concentrations (to rule out differences due to cell death induction) and let grow with normal media for 10 to 12 days. For MKC8866/AMGEN44 treated RMS cells, the treatment containing medium was exchanged for fresh treatment medium every three days. After 10-12 days, medium was removed and the cells were washed one time with PBS. 0.5% crystal violet (CV) staining was added to cells and left for 10-15 min on an orbital shaker (low speed) at room temperature. CV solution was stored at 4 °C to be used 2-3 times more. After washing and drying, 6-well plates were scanned for digitalization of results and colonies were counted manually.

2.2.11 Immunofluorescence

2.2.11.1 PI/Hoechst Staining

PI/Hoechst-33342 double staining was used to determine dead and living cells. Cells were seeded in 96-well plates and treated for the indicated timepoints or transfected with siRNA. The border wells of the 96-well plates were filled with PBS in order to prevent variations due to evaporation of cell culture medium. For PI/Hoechst-33342

double staining, PI and Hoechst-33342 were prediluted 1:100 in PBS and added 1:10 on top of the treatment (final concentration 1 µg/ml) and incubated for 5-15 min at room temperature. PI was measured using TRITC channel and Hoechst-33342 was measured using the DAPI channel at the Molecular Device Microscope. Automated analysis using MetaXpress Software compared PI/Hoechst-33342 double positive stained cells and Hoechst-33342 single positive cells to generate the percentage of dead cells.

2.2.11.2 KI67

RMS cells were seeded in black 96-well plates with a cell density of 0.02 x 10^5 cells/cm^2. The border wells of the 96-well plates were filled with PBS in order to prevent variations due to evaporation of cell culture medium. The next day, cells were treated with the indicated treatment. Treatment was reapplied after 72 h. At desired timepoint, medium was removed from cells using a vacuum pump and cells were incubated in 100 µl paraformaldehyde (PFA) to fix cells to the well plate. After 10 min, cells were washed once with PBS. Cells were then incubated in PBS-(0.1 %) Triton X. Cells were washed once again with PBS-T. Blocking was performed using Antibody Dilution Buffer (ADB) (see Table 11) with 10% FCS for 10 min at room temperature. The well plate was covered with aluminium from this step on. 40 µl of KI-67 antibody (1:200 dilution in ADB) was added to each well and incubated for 1 h at room temperature. After 1 h incubation, cells were washed 3 times with PBS-T. Then, 40 µl of Mouse IgG FITC-200 and Hoechst-33342 (1:800 dilution in ADB) was added to each well and incubated for 30 min at room temperature. After incubation, cells were washed twice with PBS-T and 200 µl PBS-T was added to each well. FITC-tagged KI67 was measured using the FITC channel and Hoechst-33342 was measured using the DAPI channel at the Molecular Device Microscope. Automated analysis using MetaXpress Software compared KI67/Hoechst-33342 double positive stained cells and Hoechst-33342 single positive cells to generate the percentage of KI67 negative and positive cells.

2.2.11.3 miRNA-146-GFP expression

RH30-miR146-GFP and RD-miR146-GFP cells were seeded in black 96-well plates at a cell density of 0.02 x 10^5 cells/cm^2 and treated for six days with the desired concentrations. At the timepoint of interest, cells were stained with Hoechst-33342 (final concentration 1 µg/ml). Green fluorescent protein (GFP) presence was measured using FITC channel and Hoechst-33342 was measured using the DAPI channel at the Molecular Device Microscope. 60X magnification was used to image multiple sites in each well. MetaXpress Software was used to produce DAPI/FITC overlay images. Automated analysis using MetaXpress Software scored the number of cells by counting DAPI positive cells. FITC positive cells were counted manually using overlay images.

2.2.12 β-galactosidase staining (β-Gal)

Build-up of β-Gal is a characteristic of senescence [216], therefore, staining for this can identify senescence. To test this, a Senescence β-Gal Staining Kit was used. Cells were stained following the instructor's manual. In brief, RMS cells were seeded in 24-well plates at a density of 0.02 x 10^5 cells/cm^2 and treated with indicated concentrations for up to six days. At the desired timepoints, cells were fixed and stained according to the kit manual. Once β-Gal solution was added to cells, they were left overnight in a 37 °C incubator (without CO_2). The next day, cells were checked under the microscope and imaged using 10X objective with an IX71 Microscope and CC-12 Soft Imaging system. Quantification performed by manually counting cells.

2.2.13 Statistical analysis

To perform statistical analysis, at least three independent experiments were performed independently including triplicates for each experiment. For comparing two different groups, Student's t-Test (equal variance, two-sample, two-sided distribution) was used to determine significance. All data were expressed as mean +/- standard deviation (SD). P-values indicated statistical significance: p-value ≤

0.05 (significant, *), p-value ≤ 0.01 (very significant, **), p-value ≤ 0.001 (greatly significant, ***).

Chapter 3: The Unfolded Protein Response as a potential therapeutic target in Rhabdomyosarcoma

Publications

Nicole McCarthy, Nadezda Dolgikh, Susan Logue, John B Patterson, Qinping Zeng, Adrienne M. Gorman, Afshin Samali, Simone Fulda (2020) The IRE1 and PERK arms of the UPR promote survival of rhabdomyosarcoma cells. Cancer Letters, volume 490, pages 76-88. DOI: 10.1016/j.canlet.2020.07.009

3.1 Introduction

The low survival rate associated with RMS, as well as severe side effects caused by current RMS treatments, indicates an urgent need for a better understanding of RMS and the identification of new treatment options for RMS patients. As discussed in Chapter 1 (section 1.5), the UPR has been implicated in the development, progression and survival of numerous cancer types including breast, lung, prostate, skin and brain cancer [190].

At present, there is an absence of research investigating basal UPR activity in RMS cells. A small number of papers have been published identifying UPR signalling in RMS cells. These research papers concentrate on the induction of ER stress and the activation of the UPR in treated RMS cells [141, 278-281]. For instance, following inhibition of HSP70 in RMS cells, there is an activation of the PERK-eIF2α-CHOP arm of the UPR subsequently triggering apoptosis in RMS cells [278, 279]. Research from the Muñoz-Pinedo lab demonstrated that glucose deprivation following 2-DG treatment induces cell death in RMS cell lines in a PERK-ATF4 dependent manner [141, 280]. These studies confirm that the UPR is present in RMS cells and that RMS cells have competent UPR signalling. Additionally, these data validate the idea of modulating the UPR as a therapeutic strategy for RMS. For example, since the induction of ER stress and activation of the UPR pro-death signalling components can successfully provoke cell death in RMS cells this could be a therapeutic approach for the treatment of RMS. Proteasome inhibitor and ER stress inducer Btz, which is FDA approved for the use against MM, has previously demonstrated cytotoxic effects against various cancer cells and is a viable option to test against RMS [282-285].

Standard treatment for RMS patients usually involves a combination of chemotherapeutic drugs, with VAC being the most commonly used combination [168, 173]. In recent years, several studies have begun investigating various targeted therapies as potential treatments for RMS patients. These anticancer drugs concentrate on inhibiting pathways that are involved in the transformation and/or progression of the cancer. For RMS, therapeutic targets include the *PAX3-FOXO1* hybrid gene that is responsible for stimulating growth and survival in ARMS [168,

176-178], and aberrant IGF or RAS signalling that promotes differentiation and growth frequently found in ERMS [172, 173]. Several compounds have been identified as potential targeted treatments for RMS. For example, aurora A kinase regulates *PAX3-FOXO1* and inhibition of aurora A kinase using inhibitors such as alisterib, have demonstrated cytotoxic effects against RMS cells [286, 287]. Compounds targeting the RAS-MEK-ERK pathway such as the MEK inhibitor trametinib reduce viability and tumour growth in RMS xenograft models when combined with IGF1R inhibitor [288]. Depending on the role of basal UPR signalling in RMS cells, UPR inhibitors could be therapeutically effective in RMS cells. Cancer cells that exhibit higher basal UPR activity are more sensitive to UPR inhibitors. For example, TNBC cells with higher IRE1 activity displayed reduced tumour growth when treated with IRE1 inhibitor compared to other breast cancer cell lines with lower basal IRE1 activity [198].

The UPR is associated with treatment resistance in which it allows cancer cells to adapt in order to ensure survival [190, 191]. In fact, the UPR has been linked to treatment resistance in RMS [289]. Inhibition of smoothened homolog (SMO), a key protein involved in the HH signalling pathway, caused an activation of several components of the UPR pathway, specifically the PERK arm, which promoted cell invasion in RMS cells [289]. Since the UPR is associated with treatment resistance, UPR inhibitors could sensitise cancer cells to commonly used RMS treatments. For example, Logue and colleagues also demonstrated that the chemotherapeutic paclitaxel induces IRE1 signalling in TNBC, and pharmacological inhibition of IRE1 during paclitaxel treatment significantly decreases tumour growth *in vivo* when compared with paclitaxel alone [198].

The UPR has been implicated in senescence in a number of studies in which the UPR has been suggested to play an anti-senescence role [215, 224, 290, 291]. Senescence is a cellular growth arrest brought about by endogenous or exogenous stress signals [214, 215]. Senescence is utilised as a tumour suppressor mechanism in pre-malignant cells, and cancer cells must actively evade senescence to allow continued survival and indefinite replication [220]. For instance, *PAX3-FOXO1* promotes senescence evasion in ARMS cells through upregulation of Ras-

association domain family (RASSF) member RASSF4 [292]. In more recent years, it has come to light that cellular senescence is also involved in several treatment responses by reducing tumour growth, highlighting its potential as an anticancer therapy [293]. For example, chemotherapeutic drugs cisplatin, cyclophosphamide, doxorubicin and etoposide induce senescence in several different cancer cells including breast, lung and prostate cancers [294-296]. Advantages associated with inducing senescence as cancer therapy include reduced tumour growth, immune stimulation and low toxicity-related side effects [293]. In addition, induction of senescence could be beneficial in apoptosis resistant cancers. Thus, TIS has now emerged as a promising approach that may be used in cancer therapy [293, 297]. Several studies have demonstrated that the UPR plays an anti-senescence role in cancer cells where knockdown of UPR components results in senescence induction [224, 290, 291]. By understanding the mechanisms in which cancer cells avoid senescence, for instance, through UPR signalling, methods to induce senescence can be explored as a therapeutic approach for cancer.

The lack of research into basal UPR signalling in RMS suggests a gap in our knowledge and understanding of RMS. In this chapter I have investigated basal UPR activity in RMS cells and elucidated the role it plays in RMS survival. UPR activity, specifically IRE1 and PERK signalling, was assessed using Western blotting and PCR techniques in both ARMS and ERMS cell lines. For this investigation, the IRE1 RNase inhibitor, MKC8866, and the PERK inhibitor, AMGEN44, were chosen [4, 248, 257]. These UPR inhibitors can be used as experimental tools to investigate downstream UPR signalling and cellular function in RMS cells.

Following confirmation of basal UPR signalling, the effect of UPR inhibition on RMS cells and its potential as a therapeutic target was investigated. The response to UPR inhibitors was compared between both subtypes of RMS. In addition to pharmacological inhibition, genetic silencing approaches were also utilised to confirm the effects observed following IRE1 and PERK inhibition. Moreover, as it is important for targeted drugs to specifically target cancerous tissues and not healthy tissue, the effect of UPR inhibitors on non-malignant cell lines was investigated. Senescence, which is linked to both cancer survival and UPR signalling [291], was

also examined in the context of UPR inhibition in RMS cells. Lastly, since the UPR is also associated with treatment resistance in several cancer types and several studies have demonstrated promising cytostatic and cytotoxic synergism between UPR inhibitors and other anticancer drugs in a number of cancers [198, 250]. I also tested the effects of UPR inhibitors in combination with other anticancer drugs in RMS cells including proteasome inhibitor, Btz, aurora A kinase inhibitor, alisertib, and MEK inhibitor, trametinib.

3.2 Results

3.2.1 RMS cell lines express IRE1 and PERK proteins

First, it was important to verify that the RMS cell lines used in this study expressed the UPR sensors IRE1 and PERK. Using Western blotting, a number of cell lines of both ARMS and ERMS subtypes were confirmed to express both IRE1 and PERK (Fig. 3.1).

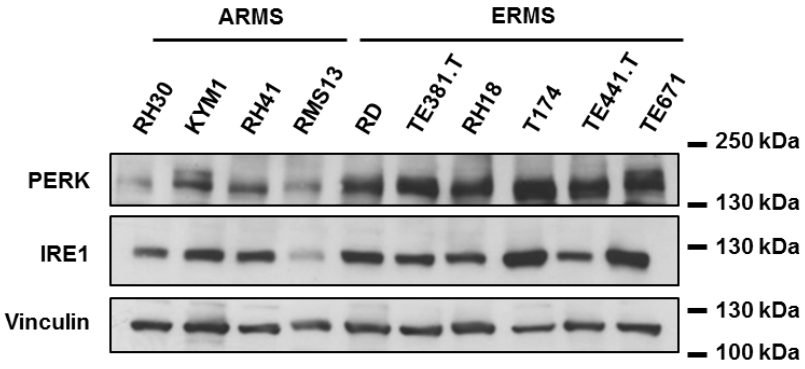

Figure 3.1: RMS cell lines express IRE1 and PERK proteins - Whole cell extracts were harvested from cell lines derived from both ARMS and ERMS, and protein levels of UPR sensors, IRE1 and PERK, were evaluated using Western blot. Vinculin was used as a loading control. The Western blots shown are representative of three independent experiments.

3.2.2 RMS cell lines display basal PERK activity

Next, basal UPR signalling was investigated. For this, two cell lines representative of each subtype were used; RH30 and KYM1 for ARMS, and RD and TE381.T for ERMS. Using Western blotting, PERK phosphorylation (indicated by an upshift in the PERK band) and downstream phosphorylation of eIF2α were investigated. Treatment of RH30 cells with TM was used as a positive control for PERK phosphorylation and treatment of RH30 cells with TM in combination with PERK inhibitor AMGEN44 was used as a negative control. PERK protein levels and phosphorylated eIF2α were observed in all four cell lines (Fig. 3.2A). Several concentrations of PERK inhibitor AMGEN44 were tested to confirm PERK inhibition (See Fig. 3.5 for RH30 and RD, data not shown for KYM1 and TE381.T). Treatment of each of the four cell lines with AMGEN44 revealed a clear reduction in

PERK phosphorylation (indicated by a downshift in the PERK band) confirming PERK basal activity (Fig. 3.2B).

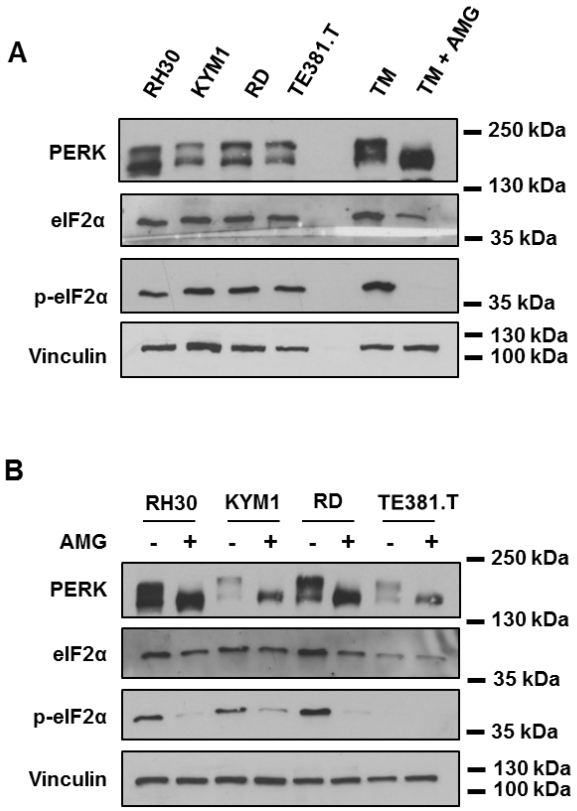

Figure 3.2: RMS cell lines display basal PERK activity – **(A)** PERK signalling was examined via Western blot in two ARMS cell lines (RH30, KYM1) and two ERMS cell lines (RD, TE381.T). PERK, eIF2α and p-eIF2α protein expression levels were examined. RH30 cells treated with TM (5 µg/ml for 5 h) served as a positive control and RH30 cells treated with TM plus AMGEN44 (TM: 5 µg/ml, AMG: 2 µM for 5 h) served as a negative control. Vinculin was used as a loading control. **(B)** Untreated and AMGEN44 (2 µM) treated RMS cells were collected at 72 h and PERK activity was examined by Western blot. PERK inhibition via AMGEN44 is indicated by a downshift in PERK band. eIF2α and p-eIF2α protein expression levels were examined. Vinculin was used as a loading control. The Western blots shown are representative of three independent sets of experiments.

3.2.3 RMS cell lines display basal IRE1 activity

Since XBP1s protein levels were difficult to detect using Western blot, conventional RT-PCR was performed to identify the presence of *XBP1s* mRNA and assess IRE1 splicing activity. Treatment of RH30 cells with TM was used as a positive control and treatment of RH30 cells with TM in combination with IRE1 inhibitor MKC8866

was used as a negative control. *XBP1s* mRNA was expressed in all four cell lines (Fig. 3.3A). Several concentrations of IRE1 RNase inhibitor MKC8866 were tested to confirm IRE1 RNase inhibition (See Fig. 3.4 for RH30 and RD, data not shown for KYM1 and TE381.T). Addition of MKC8866 to each of the four cell lines completely abolished *XBP1s* mRNA expression confirming basal IRE1 activity (Fig. 3.3B).

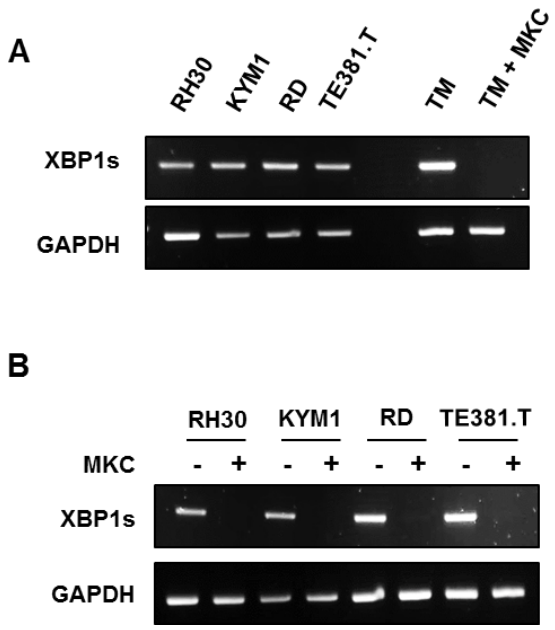

Figure 3.3: RMS cell lines display basal IRE1 activity - (A) IRE1 signalling was assessed by detecting *XBP1s* mRNA levels using RT-PCR. For RT-PCR detection of *XBP1s*, RH30 cells treated with TM (5 µg/ml for 5 h) served as a positive control and RH30 cells treated with TM plus MKC8866 (TM: 5 µg/ml, MKC8866: 20 µM for 5 h) served as a negative control. GAPDH was used as a loading control. **(B)** Untreated and MKC8866 (20 µM) treated RMS cells were collected at 72 h and *XBP1s* mRNA levels were examined by RT-PCR. GAPDH was used as a loading control. The RT-PCR images shown are representative of three independent sets of experiments.

It can be concluded that RMS cell lines possess basal IRE1 and PERK signalling. Since activation of both the IRE1 and PERK arms of the UPR is evident in RMS cell lines, the purpose of this signalling in these cells and the reliance of these cells on this signalling was next investigated. As previously described in Section 1.8.3, the UPR can be utilised in cancer cells to evade cell death and promote cell survival. It was hypothesised that pharmacological inhibition of the UPR, using IRE1 and PERK inhibitors, could induce cell death in RMS cells and/or impact the survival of RMS

cells. Two cell lines, RH30 (ARMS) and RD (ERMS) were chosen as representatives for each subtype for this investigation.

3.2.4 IRE1 RNase inhibitor MKC8866 induces cell death and reduces viability in RH30 cells

RH30 and RD cells were treated with a range of MKC8866 concentrations (5-40 μM) for 72 h. *XBP1s* mRNA levels were diminished by 5 μM MKC8866 in RH30 cells and by 10 μM MKC8866 in RD cells after 72 h (Fig. 3.4A). A range of concentrations of MKC8866 were applied to RH30 and RD cells for different timepoints and cell death and viability was measured. In order to measure cell death, we used fluorescence microscopy to measure PI uptake caused by membrane permeabilisation, a prototypic characteristic of cell death [87]. RH30 cells were sensitive to higher concentrations of MKC8866, as this resulted in the induction of cell death as demonstrated by PI uptake (Fig. 3.4B). On the other hand, RD cells appear to be resistant to MKC8866-mediated cell death as demonstrated by lack of PI uptake (Fig. 3.2B). We also wanted to evaluate the effect of UPR inhibition on cell viability. To test this, a CTG assay was used that determines the number of metabolically active cells by measuring the amount of ATP present [298], enabling an estimation of the number of viable cells. MKC8866 markedly reduced cell viability in RH30 cells, whereas MKC8866 had no effect on RD cell viability (Fig. 3.4C). To validate the results seen with CTG and avoid misinterpretation, another non-metabolic assay was also be implemented. A cell count was performed in parallel using DAPI staining which revealed reduced cell number in MKC8866 treated RH30 cells (Fig. 3.4D). These data suggest that IRE1 could play an important role in RH30 cells and not in RD cells.

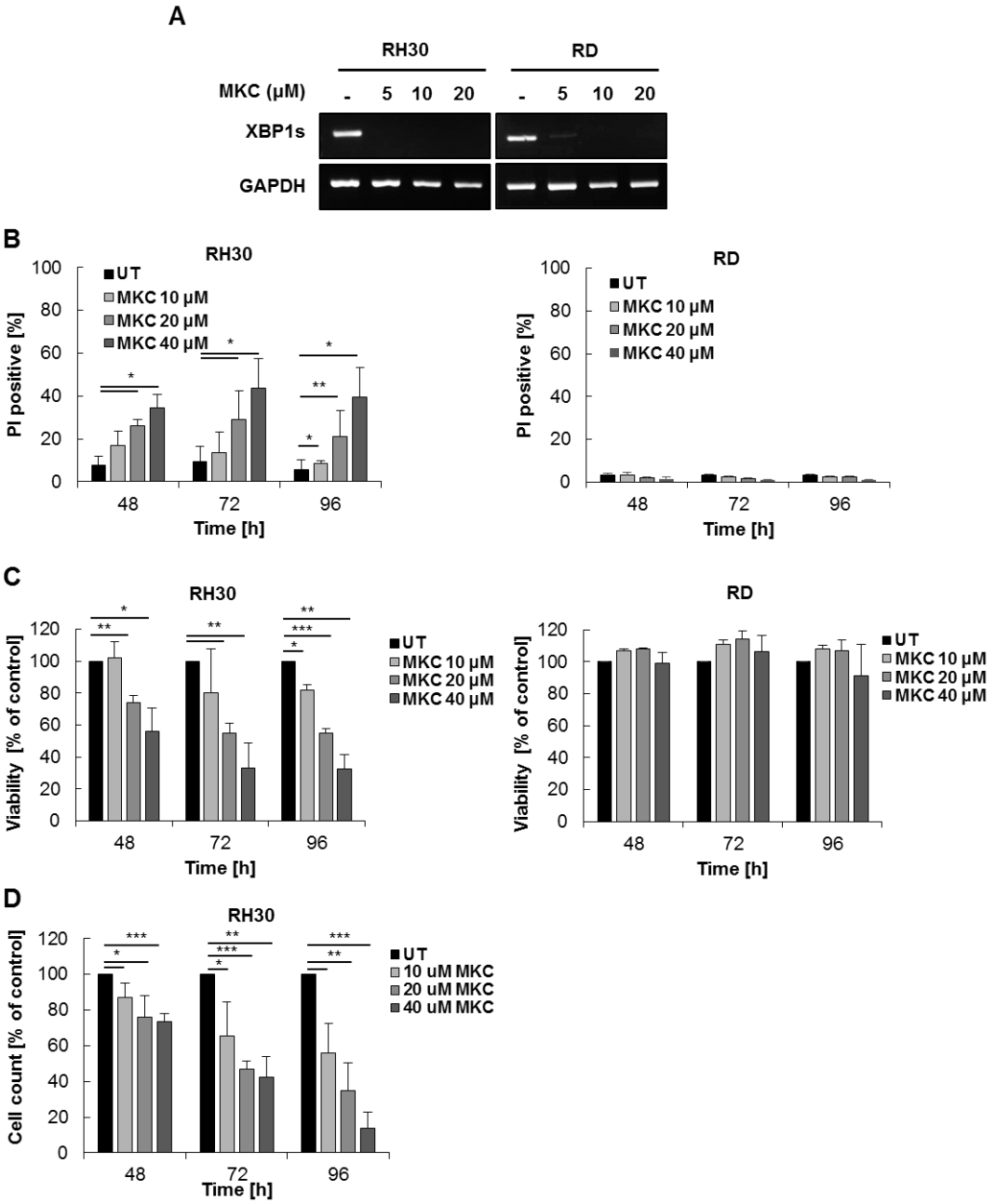

Figure 3.4: IRE1 RNase inhibitor MKC8866 induces cell death and reduces viability in RH30 cells - RH30 and RD cells were treated with indicated concentrations of MKC8866 (5-40 μM) for the indicated timepoints. **(A)** Following 72 h of treatment with MKC8866, IRE1 RNase inhibition was confirmed using RT-PCR showing *XBP1s* mRNA levels. GAPDH was used as a loading control. **(B)** RH30 and RD cells were treated with indicated concentrations of MKC8866 for up to 96 h and cell death was determined by measuring PI/Hoechst stained cells using a Molecular Device Microscope with an automated analysis using MetaXpress Software. **(C)** Cell viability was assessed using CTG and is expressed as a percentage of untreated controls. **(D)** Cell number was determined by measuring Hoechst stained cells using a Molecular Device Microscope with an automated analysis using MetaXpress Software. The RT-PCR image shown is representative of three independent sets

of experiments. Mean ± SD of three independent experiments performed in triplicate are shown; *P < 0.05; **P < 0.01, ***P < 0.001.

3.2.5 PERK inhibitor AMGEN44 reduces cell viability of RH30 and RD cells

RH30 and RD cells were treated with a range of AMGEN44 concentrations (1-10 μM) for 72 h. PERK phosphorylation was reduced (indicated by an downshift in PERK band) by all concentrations of AMGEN44 in both cell lines (Fig. 3.5A). A range of concentrations of AMGEN44 were applied to RH30 and RD cells for indicated times and cell death and viability was measured. The addition of AMGEN44 did not induce any cell death in RH30 and RD cells as demonstrated by lack of PI uptake (Fig. 3.5B). On the other hand, AMGEN44 slightly decreased cell viability in RH30 cells and markedly reduced cell viability in RD cells (Fig. 3.5C). The number of RH30 and RD cells correlated with reduced viability, as cell number was markedly reduced in both cell lines following AMGEN44 treatment (Fig. 3.5D). These data suggest that RMS cells utilise and rely on PERK signalling.

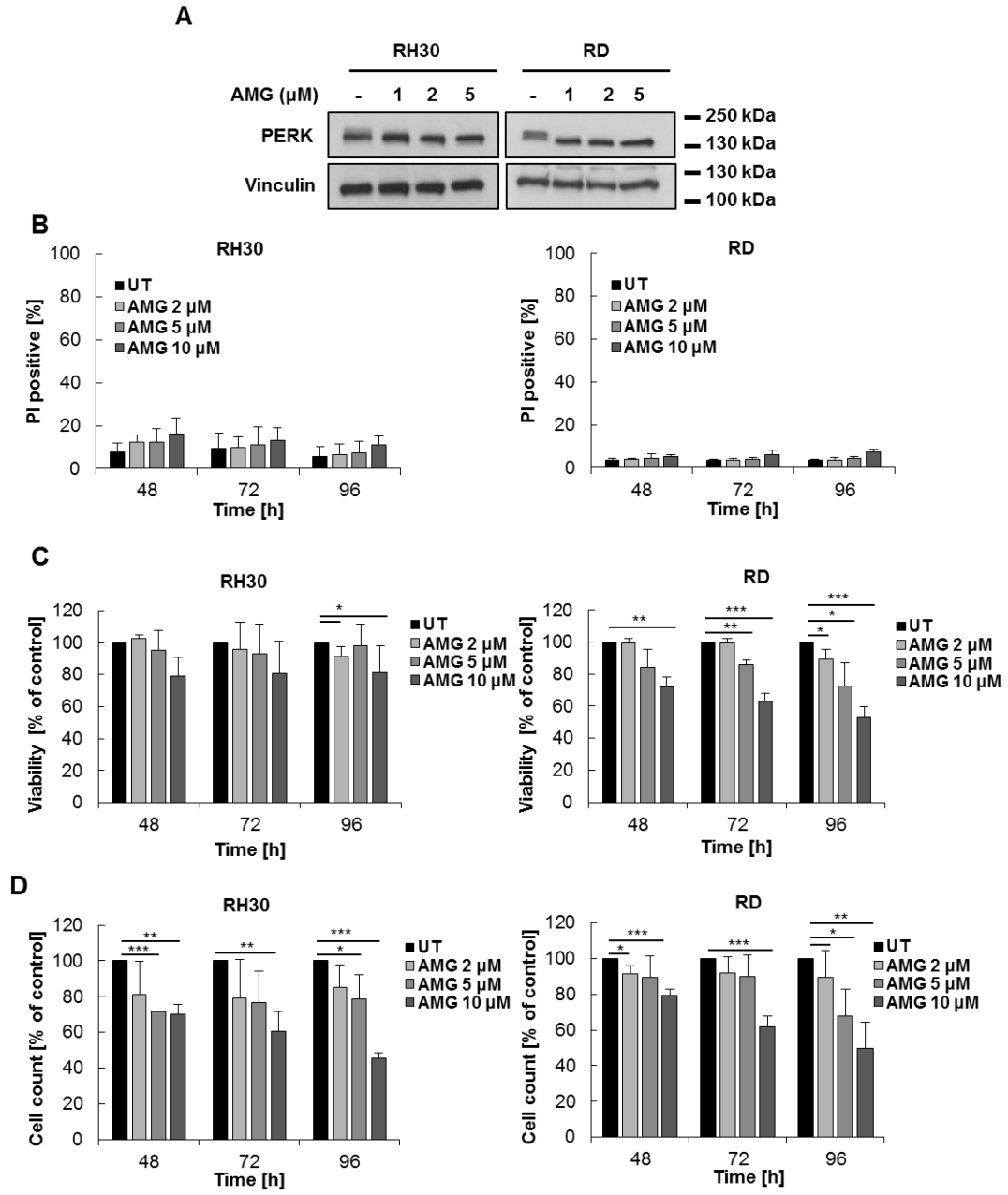

Figure 3.5: PERK inhibitor AMGEN44 reduces cell viability of RH30 and RD cells - RH30 and RD cells were treated with a range of concentrations of AMGEN44 (1-10 μM) for the indicated times. **(A)** PERK inhibition, following 72 h of AMGEN44 (2 μM) treatment, was demonstrated using Western blot and vinculin was used as a loading control. **(B)** RH30 and RD cells were treated with indicated concentrations of AMGEN44 for up to 96 h and cell death was determined by measuring PI/Hoechst stained cells using a Molecular Device Microscope with an automated analysis using MetaXpress Software. **(C)** Cell viability was assessed using CTG and is expressed as a percentage of untreated controls. **(D)** Cell number was determined by measuring Hoechst stained cells using a Molecular Device Microscope with an automated analysis using MetaXpress Software. The Western blots shown are representative of three independent sets of experiments. Mean ± SD of three independent experiments performed in triplicate are shown; *P < 0.05; **P < 0.01, ***P < 0.001.

3.2.6 MKC8866 and AMGEN44 combination treatment reduces viability of RH30 and RD cells

Since MKC8866 and AMGEN44 treatment reduced cell viability in RH30 and RD cells, it was hypothesized that the combination of the two could have a synergistic effect on viability, or even induce cell death. Concentrations chosen for this combination were based on previous dose ranges revealing that 20 μM MKC8866 was sufficient for *XBP1s* reduction (Fig. 3.4A) and 2 μM AMGEN44 was adequate for PERK dephosphorylation (Fig. 3.5A). RH30 and RD cells were treated with MKC8866 (20 μM) and/or AMGEN44 (2 μM) for 72 h and Western blot confirmed IRE1 and PERK inhibition. In cells treated with AMGEN44, alone or in combination with MKC8866, PERK phosphorylation was reduced (indicated by a downshift in PERK band) and p-eIF2α protein levels were diminished (Fig. 3.6A). In cells treated with MKC8866, alone or in combination with AMGEN44, XBP1s protein expression was completely abolished (Fig. 3.6A). Cells were treated with MKC8866 and/or AMGEN44 for the indicated times and cell death and viability were examined. Combination of MKC8866 and AMGEN44 did not increase cell death when compared with single agent treatments in either RH30 or RD cells (Fig. 3.6B). There was a further decrease in cell viability in combination treatment compared to MKC8866 alone in RH30 cells at 96 h (Fig. 3.6C). For RD cells, cell viability was further decreased in MKC8866/AMGEN44 cotreated cells in comparison to AMGEN44 alone at 96 h (Fig. 3.6C). These results confirm that combined inhibition of IRE1 and PERK in RH30 and RD cells also reduce RMS cell viability.

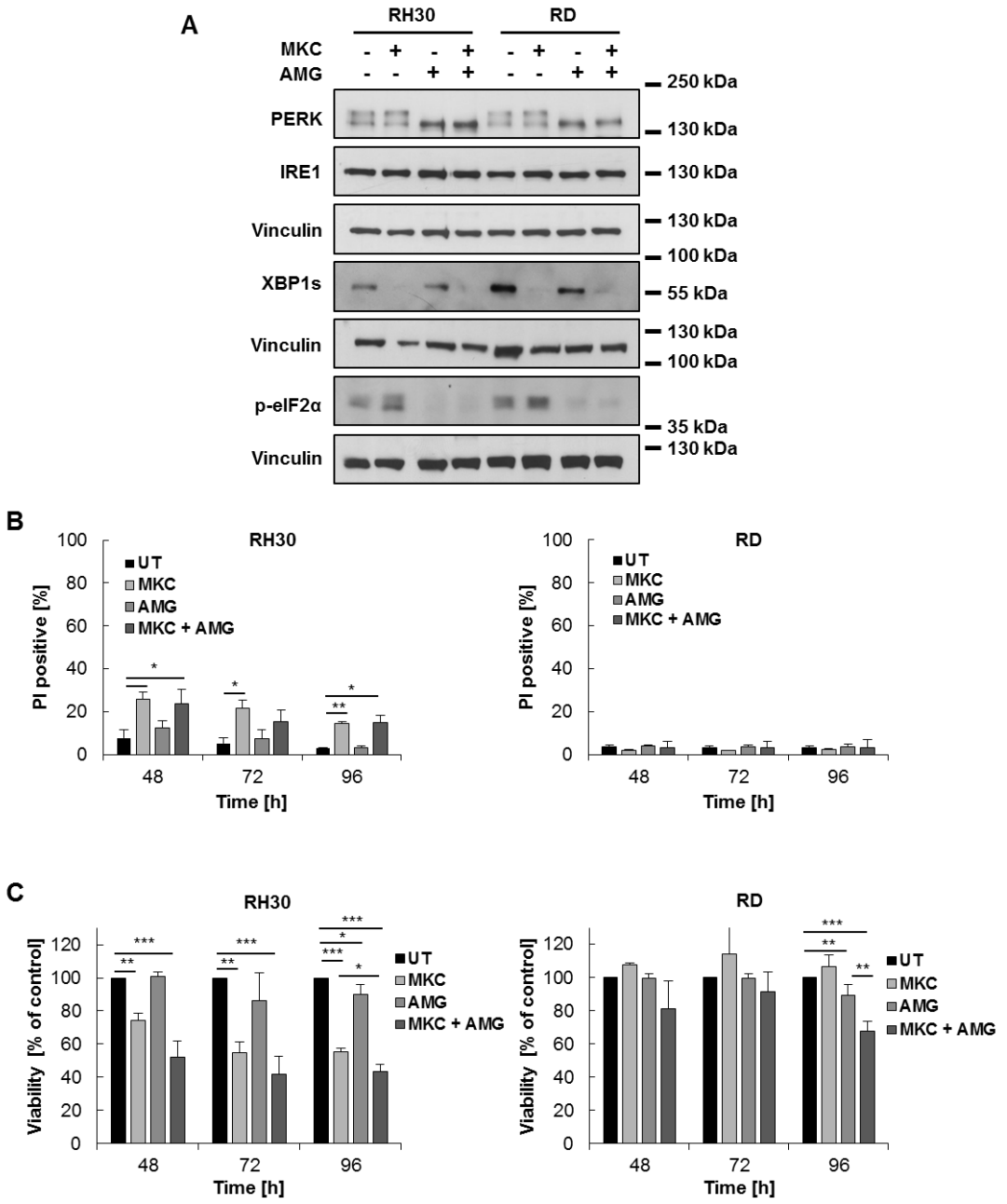

Figure 3.6: MKC8866 and AMGEN44 combination treatment reduces viability of RH30 and RD cells – (A) RH30 and RD cells were treated with MKC8866 (20 µM) and/or AMGEN44 (2 µM) for 72 h and PERK, IRE1, p-eIF2α and XBP1s protein expression levels were detected via Western blot. Vinculin was used as a loading control. **(B)** Cells were treated with MKC8866 (20 µM) and/or AMGEN44 (2 µM) for indicated times and cell death and viability were investigated. Cell death was determined by measuring PI/Hoechst stained cells using a Molecular Device Microscope with an automated analysis using MetaXpress Software. **(C)** Cell viability was assessed using CTG and is expressed as a percentage of untreated controls. The Western blots shown are representative of three independent sets of experiments.. Mean ± SD of three independent experiments performed in triplicate are shown; *P < 0.05; **P < 0.01, ***P < 0.001.

3.2.7 MKC8866 and AMGEN44 reduce RMS cell proliferation

Next, since cell viability was reduced following IRE1 and PERK inhibition, the long-term effect of MKC8866 and/or AMGEN44 on proliferation was studied. Cells were treated with MKC8866 (20 μM) and/or AMGEN44 (2 μM) for up to six days. Using a Casy cell counter, cells were counted every two days. A significant reduction in cell proliferation was observed in RH30 cells following MKC8866 and combination treatment as well as a reduction in proliferation following AMGEN44 treatment (Fig. 3.5A). RD cells displayed reduced proliferation following AMGEN44 and MKC8866/AMGEN44 combination treatment (Fig. 3.7A). Bar chart representation for cell count at six days of treatment indicated significant difference between treated and untreated cells (Fig. 3.7B). These results demonstrate that IRE1 and PERK inhibition reduces proliferation in RMS cells.

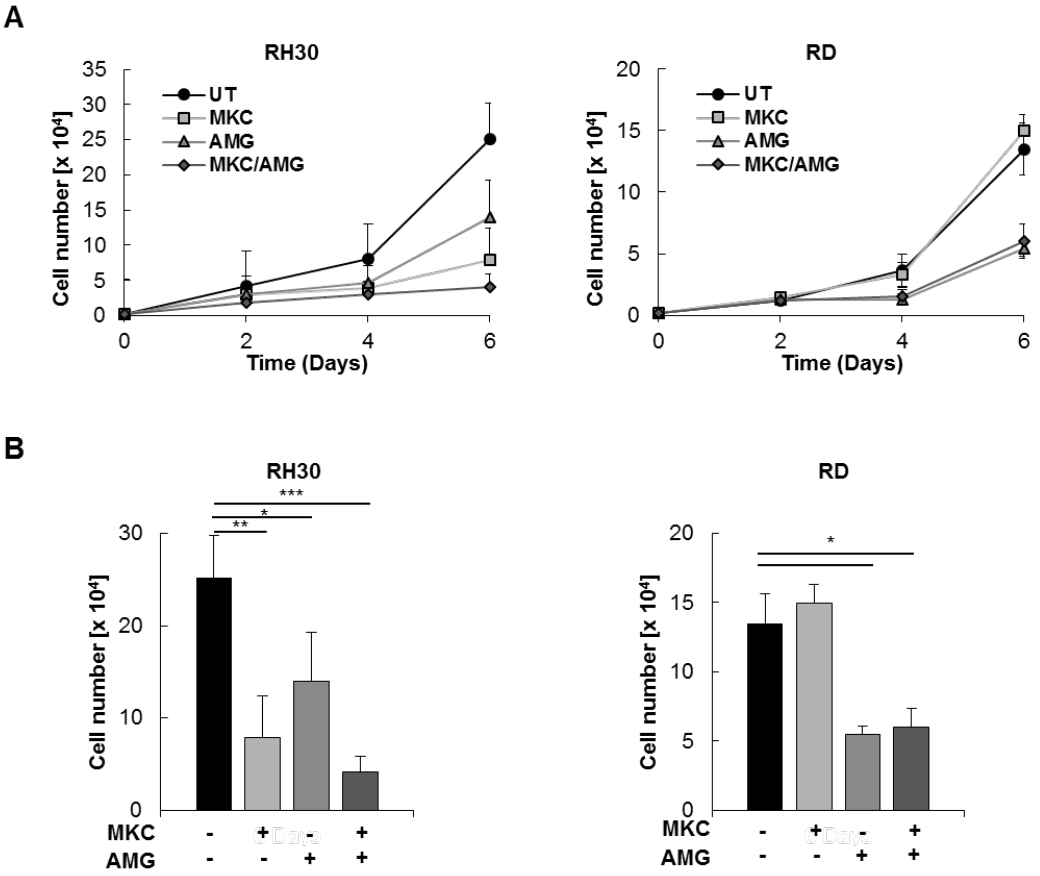

Figure 3.7: MKC8866 and AMGEN44 reduce RMS cell proliferation - (A) MKC8866 (20 μM) and AMGEN44 (2 μM) single and combination treatments were added to RH30 and RD cells and treatment was reapplied at 72 h. Cells were counted at 2, 4 and 6 days using a

Casy counter to generate cell growth curves. **(B)** Cell numbers for Day 6 are represented in bar chart form. Mean ± SD of three independent experiments performed in triplicate are shown; *P < 0.05; **P < 0.01, ***P < 0.001.

3.2.8 MKC8866 and AMGEN44 reduce colony formation in RMS cell lines

Another method of testing the long-term effect of treatments on cells is to perform clonogenic assays. Here, cells are seeded at a density that is low enough to isolate them. If cells possess replicative potential, they eventually form colonies after a number of days [277]. RH30 and RD cells (seeded at 400 cells/well) were treated with MKC8866 (20 μM) and/or AMGEN44 (2 μM) for up to 12 days. Similar to the responses seen in viability and proliferation assays following MKC8866 and AMGEN44 single and combination treatments, treatment of RH30 cells with IRE1 and PERK inhibitors significantly reduced colony formation compared to untreated cells (Fig. 3.8A, C). Moreover, treatment of RD cells with PERK inhibitor, alone or in combination with MKC8866, significantly reduced colony formation compared to untreated RD cells (Fig. 3.8B, D). Again, RD cells were unaffected by MKC8866 single treatment (Fig. 3.8B, D).

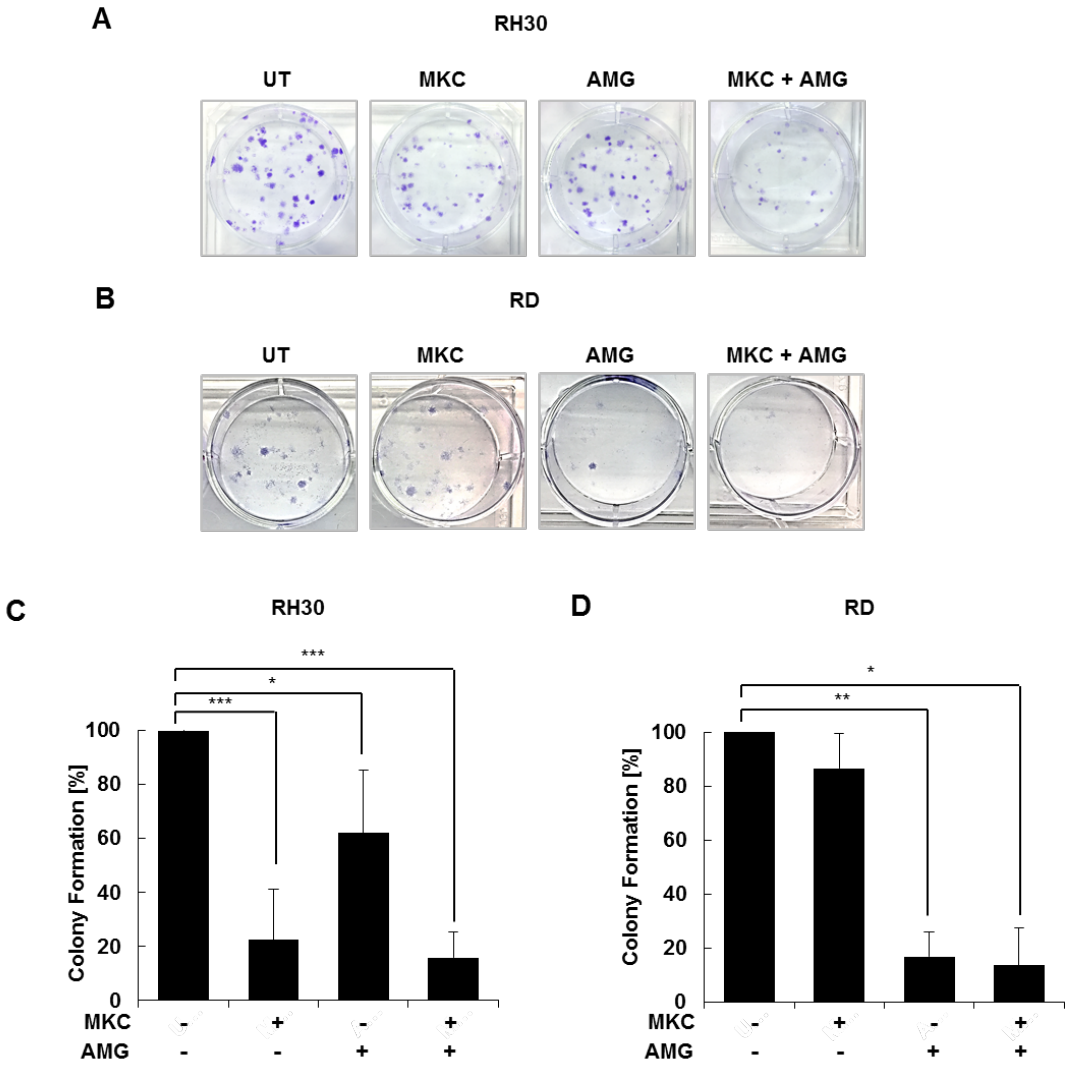

Figure 3.8: MKC8866 and AMGEN44 reduce colony formation in RMS cell lines, RH30 and RD - Long-term survival following UPR inhibition was tested using clonogenic assays. RH30 and RD cells were treated with MKC8866 (20 µM) and/or AMGEN44 (2 µM) and treatment was reapplied every 72 h. **(A & B)** Following 12 days of treatment, cells were stained with 0.5% CV displaying fully formed colonies. One representative experiment is shown for each cell line. **(C & D)** The percentage of colony formation compared to untreated control is displayed in bar chart representation. Mean ± SD of three independent experiments performed are shown; *P < 0.05; **P < 0.01, ***P < 0.001.

Since MKC8866 and AMGEN44 significantly reduced the long-term survival of RH30 and RD cells, respectively, it was decided to test whether this proliferation inhibition was seen in other RMS cell lines. The study was extended to a number of other RMS cell lines including ARMS cell lines, KYM1, RMS13 and RH41, and ERMS cell lines, TE381.T, RH36 and T174. Following MKC8866 and AMGEN44 treatment, all ARMS cell lines displayed reduced colony formation in both single

and combination treatment conditions (Fig. 3.9 (LEFT)). For ERMS cell lines, reduced colony formation was observed in AMGEN44 treated cells (Fig. 3.9 (RIGHT)). Two ERMS cell lines, RH36 and T174, also showed sensitivity to MKC8866 in which colony formation was reduced. Overall, the same trend was seen in RMS cell lines, where ARMS appeared particularly sensitive to IRE1 inhibition, whereas ERMS displayed a higher sensitivity to PERK inhibition. These data confirm that MKC8866 and AMGEN44 do not selectively affect RH30 and RD cells, and that inhibition of IRE1 and PERK has the potential to be used therapeutically on all RMS entities.

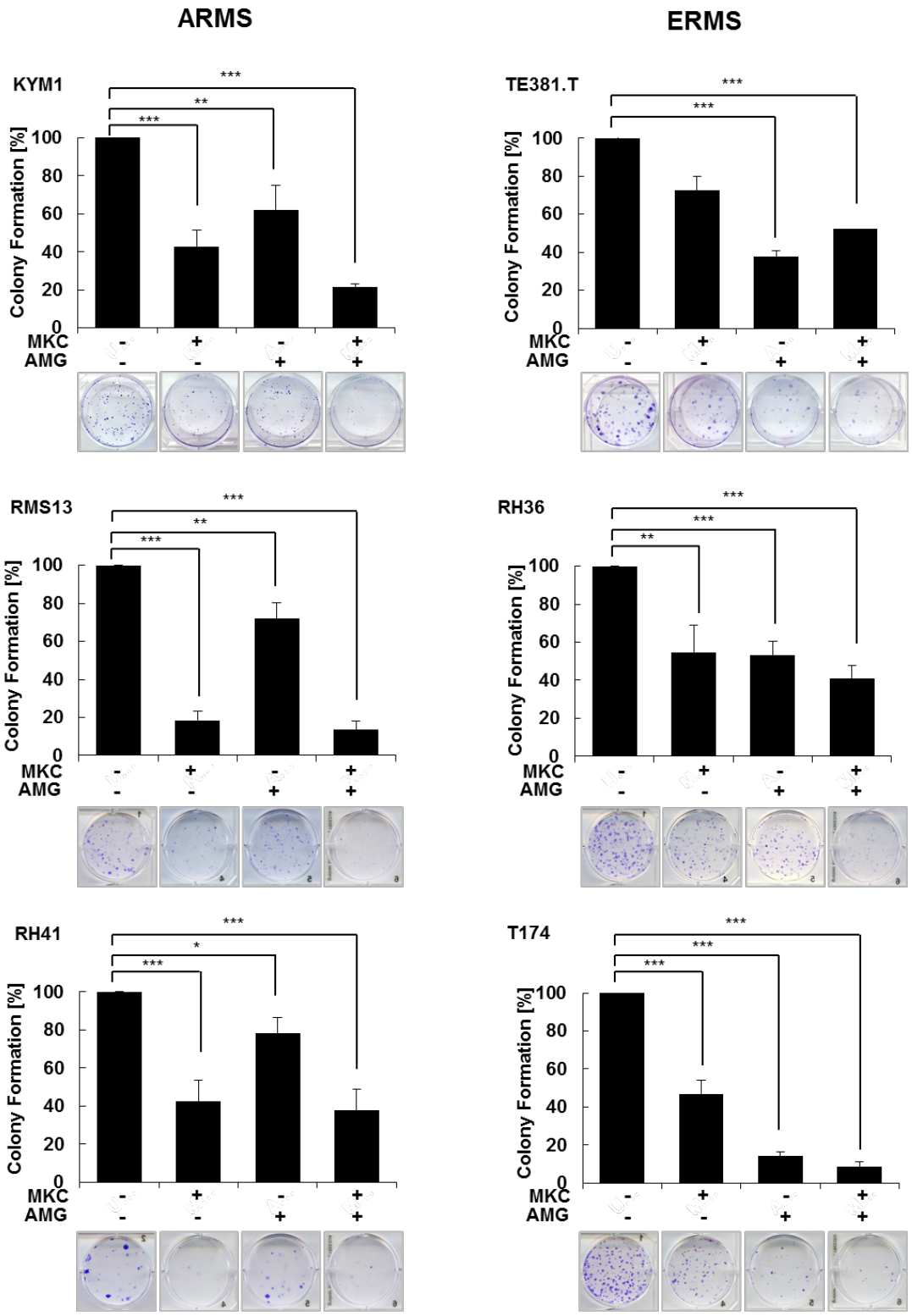

Figure 3.9: MKC8866 and AMGEN44 reduce colony formation in a number of RMS cell lines - Long-term survival following UPR inhibition using clonogenic assays was carried out in three ARMS cell lines; KYM1, RMS13 and RH41 (LEFT) and three ERMS cell lines; TE381.T, RH36 and T174 (RIGHT). Cells were treated with MKC8866 (20 μM) and/or AMGEN44 (2 μM) and treatment was reapplied every 72 h. Following 12 days of

treatment, cells were stained with 0.5% CV displaying fully formed colonies. One representative experiment is shown for each cell line and the percentage of colony formation compared to untreated control is displayed in bar chart representation. Mean ± SD of three independent experiments are shown; *P < 0.05; **P < 0.01, ***P < 0.001.

3.2.9 MKC8866 and AMGEN44 do not negatively affect the viability or survival of non-malignant cell lines, MRC5 and C2C12

To test the effects of MKC8866 and AMGEN44 on non-malignant cells, MKC8866 and AMGEN44 were applied to two non-malignant cell lines, MRC5 and C2C12. These two control cell lines are typically used for testing RMS treatments [299].The MRC5 cell line is derived from a human non-malignant lung fibroblast and the C2C12 cell line is derived from mouse non-malignant myoblasts [299]. Cells were treated with MKC8866 (20 μM) and/or AMGEN44 (2 μM) and cell death and viability were analysed. Cell death was not induced by either MKC8866 or AMGEN44 treatments in either of the cell lines as demonstrated by lack of PI uptake (Fig. 3.10A). In addition, cell viability was also unaffected (Fig. 3.10B). To test the longer-term effects of the treatments, cells were treated with MKC8866 (20 μM) and/or AMGEN44 (2 μM) for up to six days. Using a Casy cell counter cells were counted every two days. As seen in Fig. 3.10C, neither MKC8866 nor AMGEN44 had a significant effect on cell number in both non-malignant cell lines, suggesting no toxic effects.

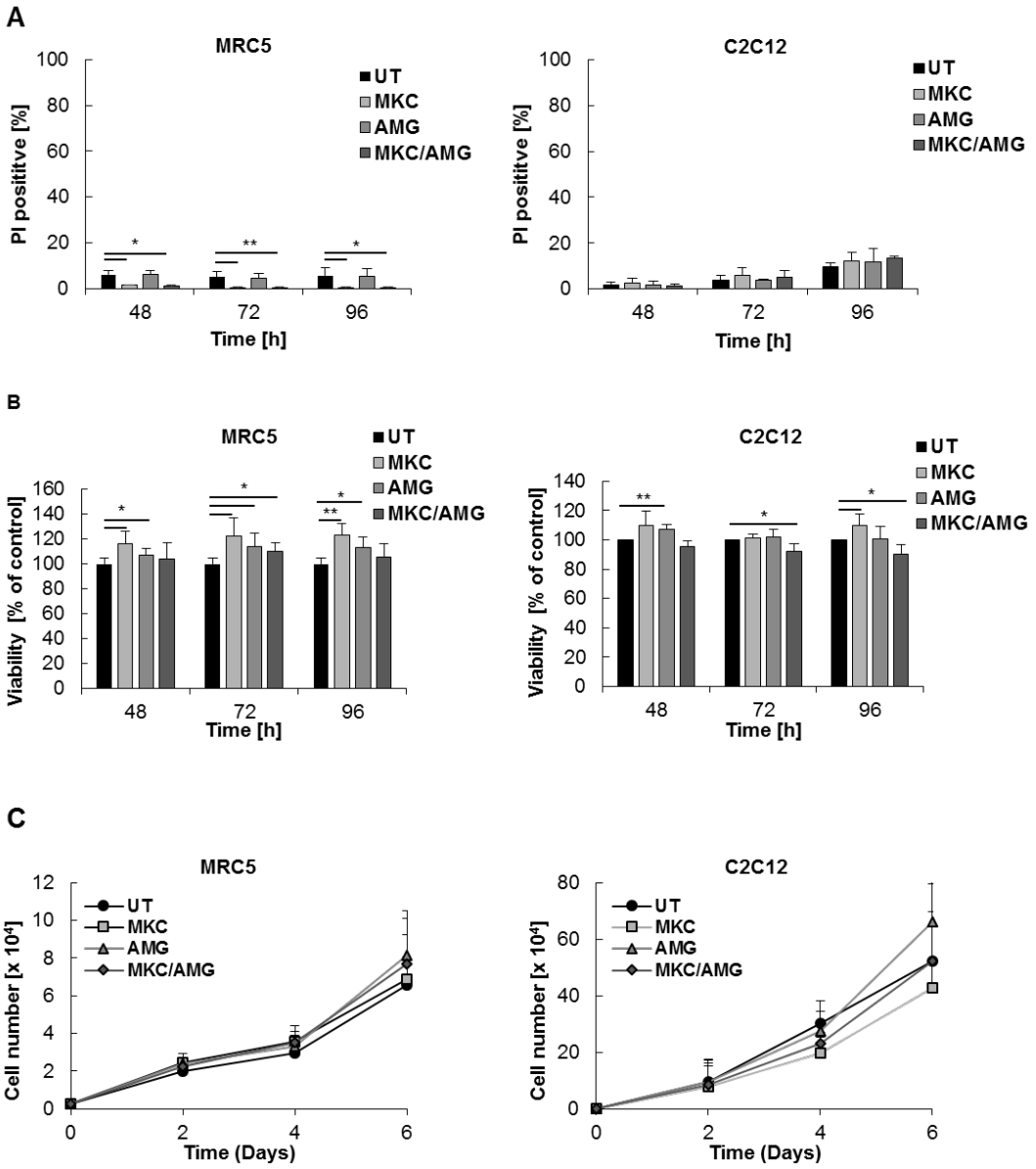

Figure 3.10: MKC8866 and AMGEN44 do not negatively affect the viability or survival of non-malignant cell lines, MRC5 and C2C12 - Human non-malignant lung fibroblast cell line MRC5 and mouse non-malignant myoblast cell line C2C12 were treated with MKC8866 (20 μM) and/or AMGEN44 (2 μM) and treatment was reapplied at 72 h. **(A)** Cell death and viability were examined at indicated timepoints. Cell death was determined by measuring PI/Hoechst stained cells using a Molecular Device Microscope with an automated analysis using MetaXpress Software. **(B)** Cell viability was assessed using CTG and is expressed as the percentage of untreated controls. **(C)** MKC8866 (20 μM) and/or AMGEN44 (2 μM) was added to MRC5 and C2C12 cells and reapplied at 72 h. Cells were counted at 2, 4 and 6 days using a Casy counter to generate cell growth curves. Mean ± SD of three independent experiments performed in triplicate are shown; *P < 0.05; **P < 0.01, ***P < 0.001.

3.2.10 Genetic inhibition of IRE1 and PERK reduces viability of RMS cell lines

To confirm the specificity of MKC8866 and AMGEN44 and their effect on RMS viability and colony formation, a knockdown of IRE1 and PERK in RH30 and RD cells was performed. Western blot confirmed a robust IRE1 and PERK knockdown at several timepoints after transfection (Fig. 3.11A and 3.12A). Knockdown of IRE1 and PERK did not result in cell death induction in either RH30 or RD cells compared to siCtrl (Fig. 3.11B and 3.12B). In contrast, IRE1 and PERK knockdown resulted in a reduction in cell viability in both RH30 and RD cells (Fig. 3.11C and 3.12C).

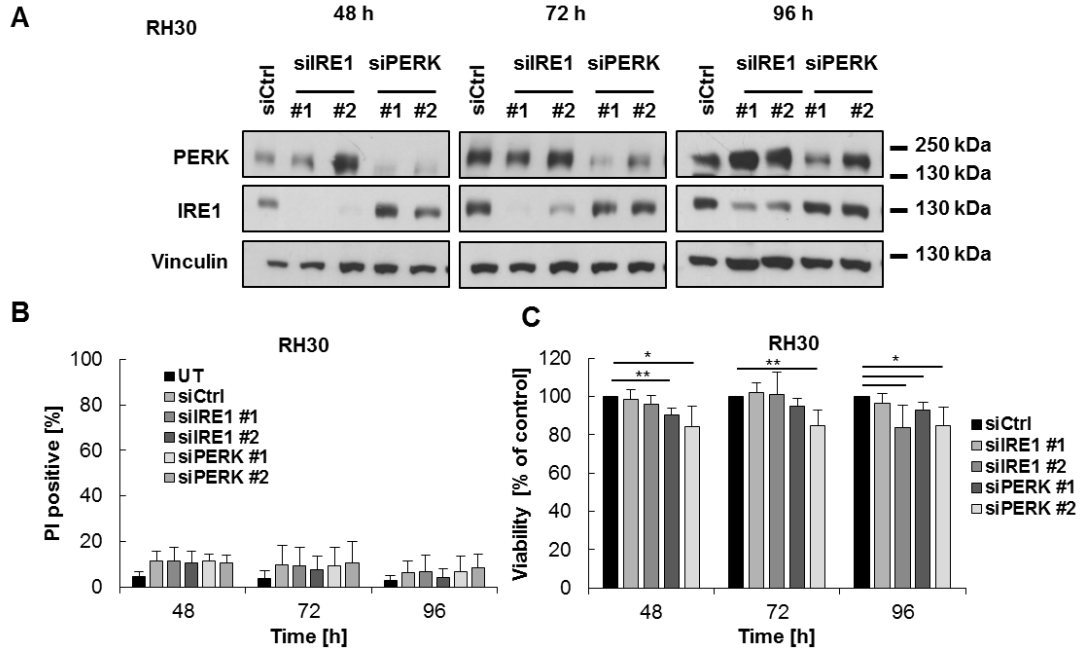

Figure 3.11: Genetic inhibition of IRE1 and PERK reduces viability of RH30 cells - RH30 cells were transiently transfected with non-silencing siRNA (siCtrl) and siRNA constructs targeting IRE1 (siIRE1) and PERK (siPERK). **(A)** Western blots confirmed this knockdown at indicated timepoints. Vinculin was used as a loading control. The Western blots shown are representative of three independent sets of experiments. **(B)** Cell death was determined by measuring PI/Hoechst stained cells using a Molecular Device Microscope with an automated analysis using MetaXpress Software. **(C)** Cell viability was assessed using CTG and is expressed as a percentage of untreated controls. Mean ± SD of three independent experiments performed in triplicate are shown; *P < 0.05; **P < 0.01.

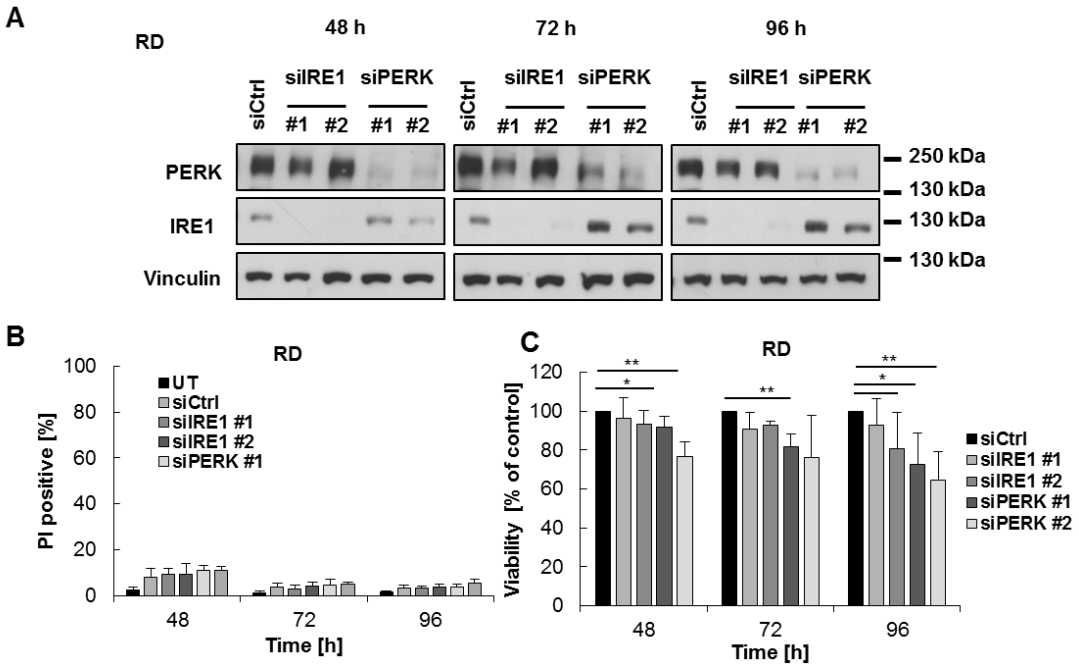

Figure 3.12: Genetic inhibition of IRE1 and PERK reduces viability of RD cells - RD cells were transiently transfected with non-silencing siRNA (siCtrl) and siRNA constructs targeting IRE1 (siIRE1) and PERK (siPERK). **(A)** Western blots confirmed this knockdown at indicated timepoints. Vinculin was used as a loading control. **(B)** The Western blots shown are representative of three independent sets of experiments. Cell death was determined by measuring PI/Hoechst stained cells using a Molecular Device Microscope with an automated analysis using MetaXpress Software. **(C)** Cell viability was assessed using CTG and is expressed as a percentage of untreated controls. Mean ± SD of three independent experiments performed in triplicate are shown; *P < 0.05; **P < 0.01.

A combinatorial knockdown of both IRE1 and PERK was also carried out. This time, in order to increase efficiency of IRE1 and PERK knockdown in cells, siRNA was reapplied at 48 h. Western blot confirmed an efficient knockdown of IRE1 and PERK in both cell lines at all timepoints (Fig. 3.13A and 3.14A). For RH30 cells, there was no induction of cell death following IRE1 knockdown (Fig. 3.13B). Single knockdown of IRE1 and PERK did not significantly reduce viability in RH30 cells (Fig. 3.13C), which differs from the significantly reduced viability observed following single knockdowns in Fig. 3.11C. Combination knockdown of IRE1 and PERK resulted in a significant reduction in cell viability in RH30 cells Fig. (3.13C). The reduction in viability following IRE1 and PERK inhibition corresponds to the reduction in viability seen in RH30 cells following MKC8866 and AMGEN44 combination treatment (Fig. 3.6C). For RD cells, no cell death induction was observed following PERK inhibition, alone or in combination with an IRE1

knockdown (Fig. 3.14A) which is consistent with previous results observed in RD cells following treatment with AMGEN44 and MKC8866. PERK and IRE1/PERK combination knockdowns resulted in a substantial reduction in cell viability in RD cells (Fig. 3.14C). These results correspond to the effects seen in RD cells following treatment with AMGEN44 and MKC8866/AMGEN44 (Fig. 3.6).

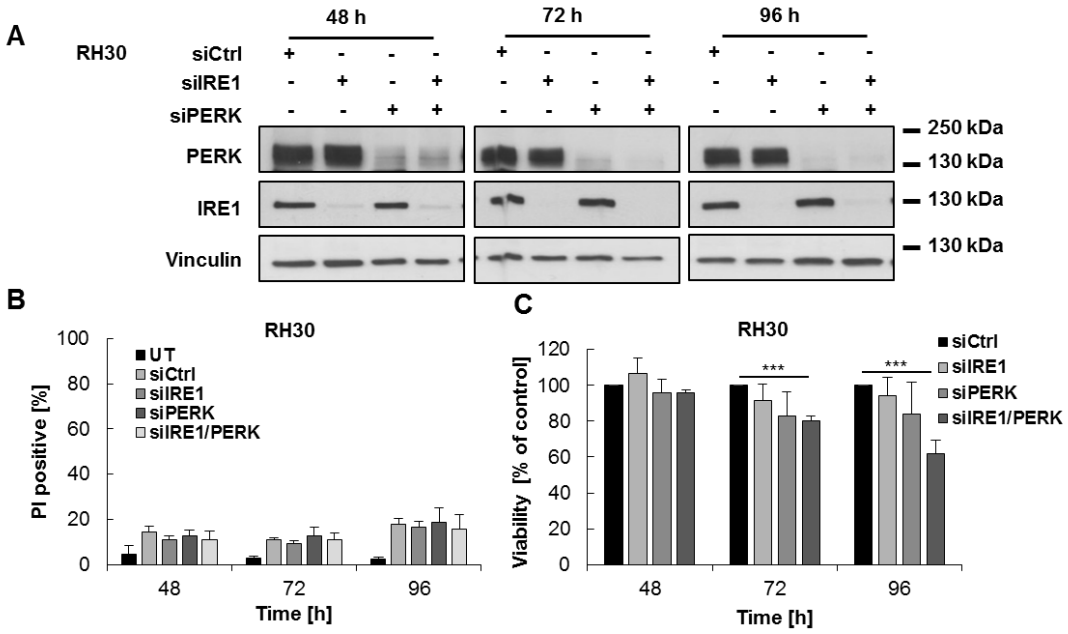

Figure 3.13: Combined genetic inhibition of IRE1 and PERK reduces viability of RH30 cells - RH30 cells were transiently transfected with non-silencing siRNA (siCtrl) and siRNA constructs targeting IRE1 (siIRE1) and PERK (siPERK). Both single and double knockdown of IRE1 and PERK were performed. **(A)** Western blots confirmed knockdowns at indicated timepoints and vinculin was used as a loading control. **(B)** The Western blots shown are representative of three independent sets of experiments. Cell death was determined by measuring PI/Hoechst stained cells using a Molecular Device Microscope with an automated analysis using MetaXpress Software. **(C)** Cell viability was assessed using CTG and is expressed as a percentage of untreated controls. Mean ± SD of three independent experiments performed in triplicate are shown; ***P < 0.001.

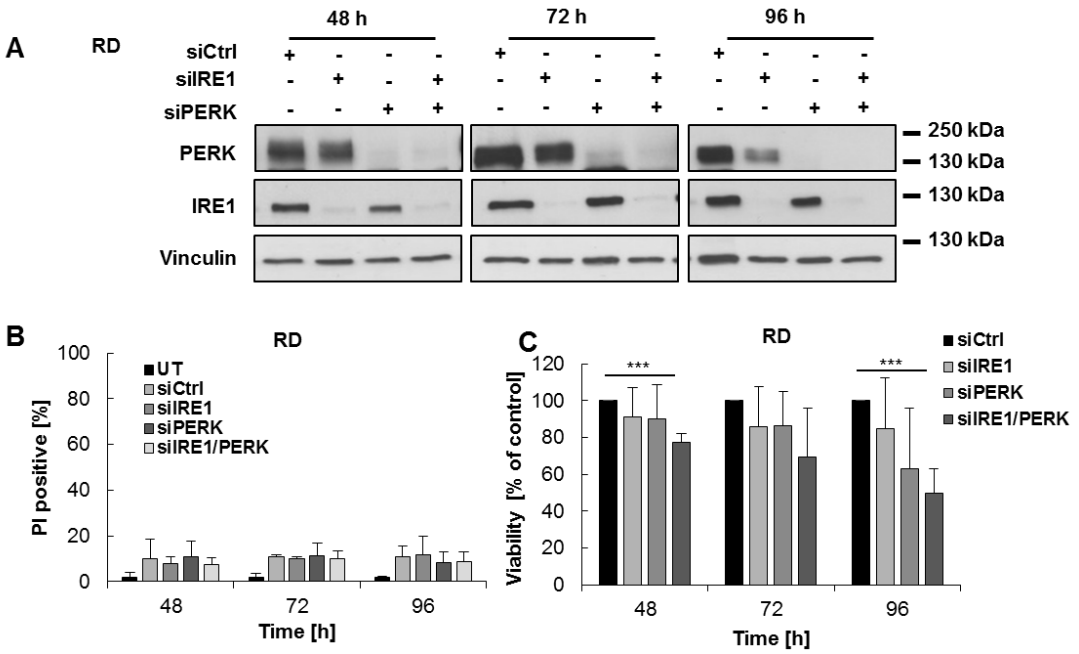

Figure 3.14: Combined genetic inhibition of IRE1 and PERK reduces viability of RD cells - RD cells were transiently transfected with non-silencing siRNA (siCtrl) and siRNA constructs targeting IRE1 (siIRE1) and PERK (siPERK). Both single and double knockdown of IRE1 and PERK were performed. **(A)** Western blots confirmed knockdowns at indicated timepoints and vinculin was used as a loading control. The Western blots shown are representative of three independent sets of experiments. **(B)** Cell death was determined by measuring PI/Hoechst stained cells using a Molecular Device Microscope with an automated analysis using MetaXpress Software. **(C)** Cell viability was assessed using CTG and is expressed as a percentage of untreated controls. Mean ± SD of three independent experiments performed in triplicate are shown; ***P < 0.001.

3.2.11 Genetic inhibition of IRE1 and PERK reduces colony formation ability of RH30 and RD cells

Next, it was decided to test the knockdown effect of IRE1 and PERK on long-term survival of RH30 and RD cells. IRE1 and PERK protein levels were returned to a basal state six days after transfection in both cell lines (Fig. 3.15A). Nonetheless, initial knockdown of IRE1 and PERK was sufficient to impede the ability of RMS cells to form colonies. RH30 cells respond in a similar manner to that of treatment with MKC8866 and/or AMGEN44 in which colony formation was significantly hindered (Fig. 3.15B, D). Likewise, following IRE1 and PERK knockdown, RD cells responded similarly to AMGEN44 and combinatorial MKC8866 and AMGEN44 treatments where there was reduced colony formation (Fig. 3.15C, E).

These experiments confirm that the effects seen with MKC8866 and AMGEN44 are in fact a result of inhibition of IRE1 and PERK, respectively.

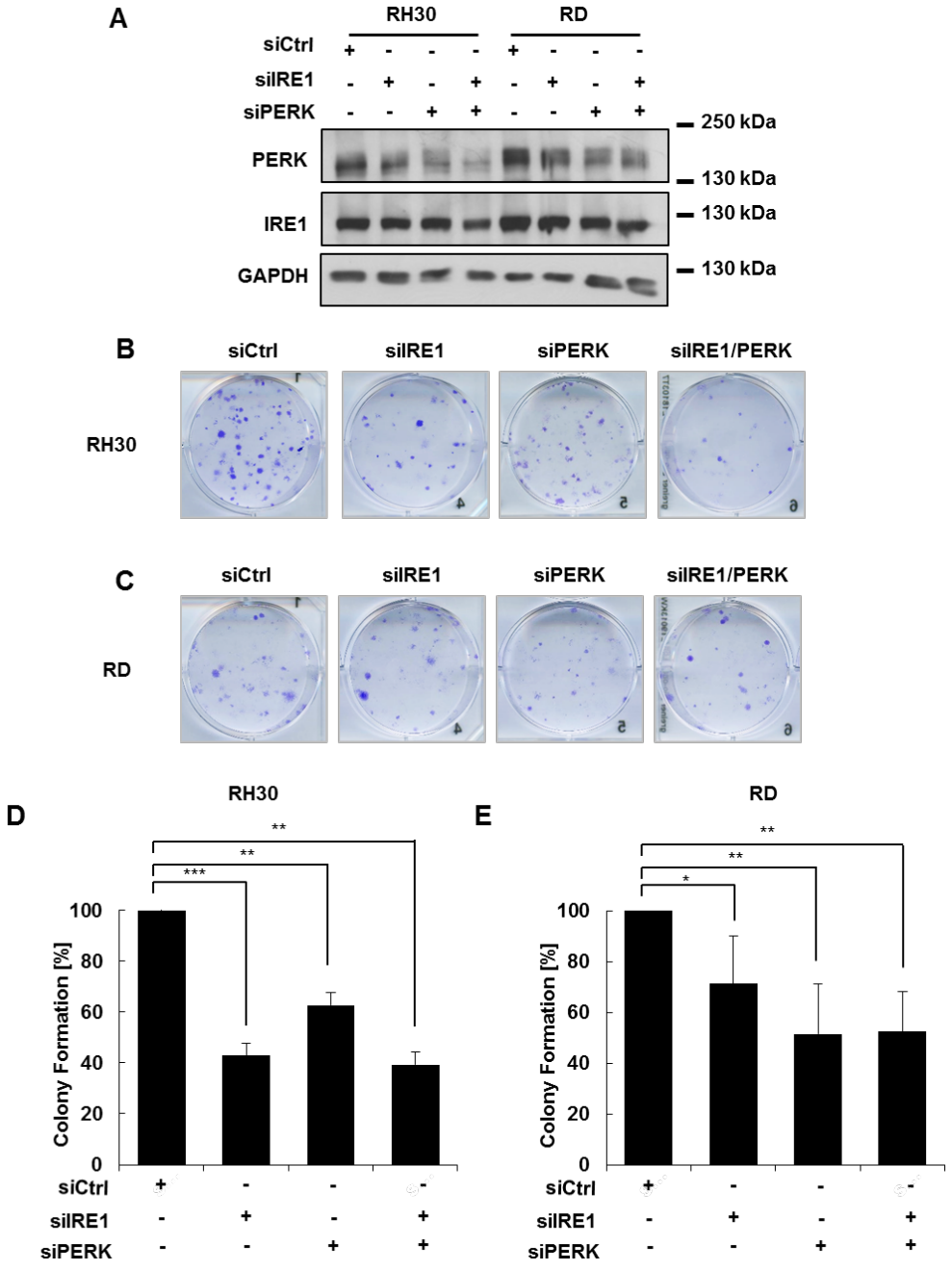

Figure 3.15: Genetic inhibition of IRE1 and PERK reduces colony formation ability of RH30 and RD cells - RH30 and RD cells were transiently transfected with non-silencing siRNA (siCtrl) and siRNA constructs targeting IRE1 (siIRE1) and PERK (siPERK). Both single and double knockdown of IRE1 and PERK were performed. **(A)** IRE1 and PERK protein levels were examined via Western blot 6 days after transfection was carried out. Vinculin was used as a loading control. The Western blot shown is representative of three independent sets of experiments. **(B, C)** Long-term survival using CV colony staining assay

investigated the effect of the knockdown. After 12 days of knockdown, cells were stained with 0.05% CV displaying fully formed colonies. One of three independent experiments are shown for the clonogenic assay. **(D, E)** Graphs averaging all three experiments are shown. Mean ± SD of three independent experiments performed are shown; *P < 0.05; **P < 0.01, ***P < 0.001.

3.2.12 RAS mutated RMS13 cell lines have higher sensitivity to UPR inhibition

RAS proteins are GTPases that control a variety of critical cellular activities and in normal cells their function is tightly regulated [300]. In cancer, *RAS* genes are frequently mutated which subsequently allows uncontrolled proliferation and survival of the tumour cells [301]. As discussed in section 1.8.1, UPR signalling is linked to oncogene activation in several cancers [191]. Since the majority of ERMS tumours possess RAS mutations including *HRAS, KRAS and NRAS* mutations, it was hypothesized that these mutations are responsible for PERK activity and subsequent sensitivity to PERK inhibition [168, 173, 175]. The introduction of RAS mutations into an ARMS cell line may identify a role for RAS in response to specific UPR inhibitor treatments. RMS13 cells, an ARMS cell line expressing wildtype RAS, were transfected to ectopically express mutant *RAS* genes, *NRAS12V*, *KRAS12V*, or *HRAS12V* [276]. The RAS mutated cell lines were then treated with MKC8866 (20 μM) and/or AMGEN44 (2 μM) for up to six days. After six days of treatment, cells were counted using a Casy cell counter. RMS13 cells with NRAS mutations were more sensitive to MKC8866 and AMGEN44 single and combination treatment as demonstrated by reduced cell number (Fig. 3.16). RMS13 cell lines with KRAS and HRAS mutations were more sensitive to MKC8866 and AMGEN44 cotreatment compared to EV cells as demonstrated by reduced cell number (Fig. 3.16).

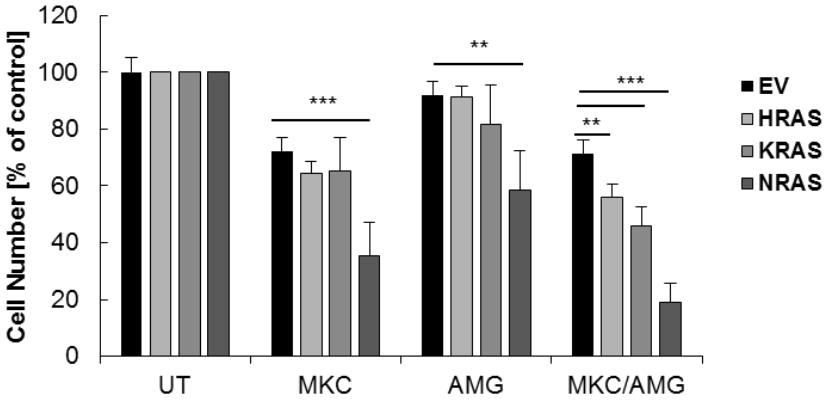

Figure 3.16: RAS mutated RMS13 cell lines have increased sensitivity to UPR inhibition - RMS13 cells expressing EV, HRAS12V, KRAS12V, or NRAS12V were treated with MKC8866 (20 μM) and AMGEN44 (2 μM) single and combination treatments and treatment was reapplied at 72 h. Cells were counted at 6 days using a Casy counter to generate cell number. Mean ± SD of three independent experiments performed in triplicate are shown; *P < 0.05; **P < 0.01, ***P < 0.001.

3.2.13 ATF4 is not crucial for KYM1 cells survival

During initial investigation of UPR signalling activity in RMS cell lines, unusually high levels of ATF4 were observed in KYM1 cells compared to other RMS cell lines (Fig. 3.17A). A number of experiments were performed to determine the importance of ATF4 in these cells. A genetic knockdown of ATF4 using siRNA and electroporation was performed and cell death, viability and colony formation were investigated. ATF4 knockdown was confirmed using Western blot (Fig. 3.17B). ATF4 knockdown did not induce cell death in KYM1 cells as demonstrated by lack of PI uptake (Fig. 3.17C). However, knockdown of ATF4 did significantly reduce viability (Fig. 3.17D). Cell number corroborated viability results in which the number of cells was significantly reduced in ATF4 knockdown cells (Fig. 3.17E). Since there was a reduction in viability, long-term survival was subsequently investigated. There was no difference in colony formation in ATF4 knockdown cells compared with control cells (Fig. 3.17F, G). Overall, ATF4 does not seem to be essential to the cells as death was not induced and long-term colony formation was unaffected. Therefore, this line of enquiry was not investigated further.

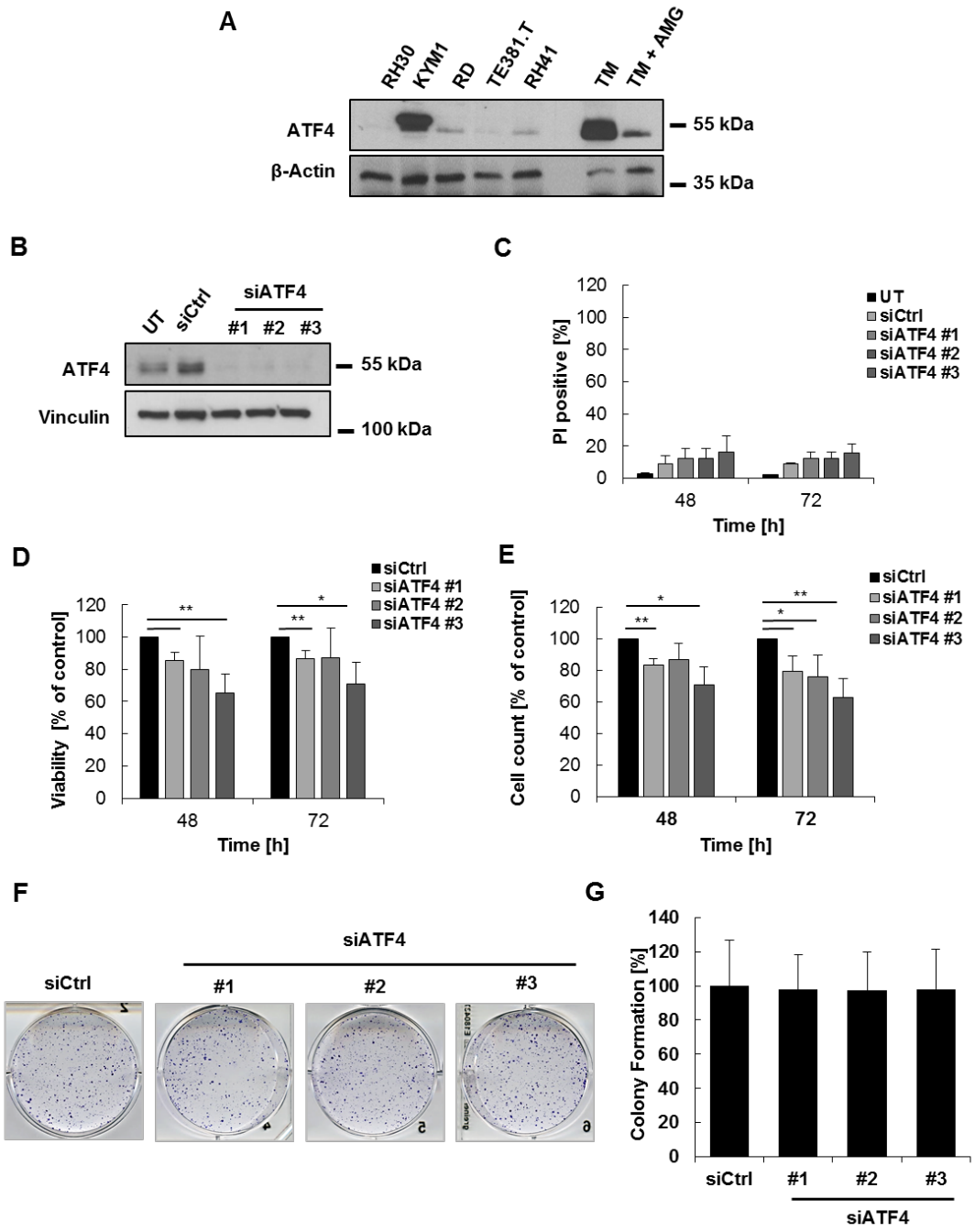

Figure 3.17: ATF4 is not crucial for KYM1 cells survival - (A) ATF4 protein levels were examined in four RMS cell lines (RH30, KYM1, RD, TE381.T and RH41). RH30 cells treated with TM (5 µg/ml for 5 h) served as a positive control, TM plus AMGEN44 (TM: 5 µg/ml and AMG: 2 µM for 5 h) served as a negative control and β-actin was used as a loading control. **(B)** KYM1 cells were transfected with non-silencing siRNA (siCtrl) and siRNA constructs targeting ATF4 (siATF4) using electroporation. Western blots confirmed this knockdown 72 h after transfection. Vinculin was used as a loading control. The Western blots shown are representative of three independent sets of experiments. **(C)** Cell death in KYM1 ATF4 knockdown cells was determined by measuring PI/Hoechst stained cells using a Molecular Device Microscope with an automated analysis using a Molecular Device

Microscope with an automated analysis using MetaXpress Software. **(D)** Cell viability was assessed using CTG and is expressed as the percentage of untreated controls. **(E)** Cell count was determined by measuring Hoechst stained cells using a Molecular Device Microscope with an automated analysis using MetaXpress Software. Mean ± SD of three independent experiments performed in triplicate are shown; *P < 0.05; **P < 0.01. **(F)** Long-term survival using CV colony staining assay investigated the effect of the knockdown in KYM1 cells. After 12 days of knockdown, cells were stained with 0.5% CV displaying fully formed colonies. One representative experiment is shown. **(G)** The percentage of colony formation compared to untreated control is displayed in bar chart representation. Mean ± SD of three independent experiments are shown.

3.2.14 Nicoletti assay reveals no difference in cell cycle following treatment with MKC8866 and AMGEN44

Due to a reduction in viability, proliferation and colony formation, cell cycle was subsequently investigated. To investigate cell cycle following MKC8866 and AMGEN44 treatment in RMS cells, a Nicoletti assay was used. Nicoletti assays can be used to measure the sub-G1 fraction of cells, which can be subsequently used to derive cell cycle data [302]. RH30 and RD cells were treated with MKC8866 (20 μM) and/or AMGEN44 (2 μM) for up to six days. Analysis of DNA content of cells after four and six days of treatment displayed no difference in cell cycle between untreated and MKC8866 and/or AMGEN44 treated RH30 and RD cells (Fig. 3.18A, B) suggesting that MKC8866 and AMGEN44 do not prompt a cell cycle arrest.

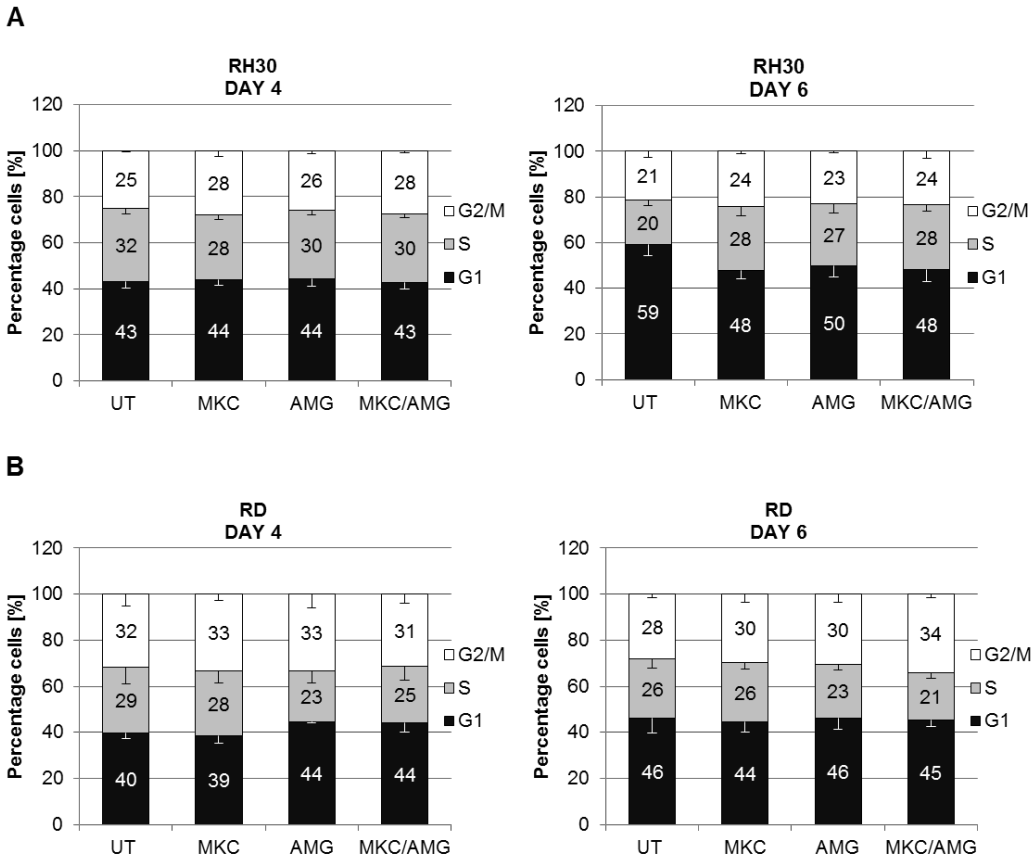

Figure 3.18: Nicoletti assay reveals no difference in cell cycle following treatment with MKC8866 and AMGEN44 - MKC8866 (20 μM) and AMGEN44 (2 μM) single and combination treatments were added to RH30 and RD cells and reapplied at 72 h. After 4 and 6 days of treatment, cells were incubated with Nicoletti buffer and DNA content was measured using flow cytometry. FACS measured DNA data were analysed using FlowJo to render specific cell phases **(RH30: A, RD: B)**. Mean ± SD of three independent experiments performed in triplicate are shown.

3.2.15 A portion of RMS cells enter a non-proliferating state following treatment with MKC8866 and AMGEN44

KI67, a commonly used proliferation marker, can also be used for cell cycle analysis [303]. Using fluorescence microscopy and a FITC-tagged KI67 antibody, KI67 levels were analysed in MKC8866 and AMGEN44 treated RH30 and RD cells. The number of KI67 positive cells was significantly reduced in MKC8866 and AMGEN44 treated RH30 cells compared to untreated cells at both four and six days (Fig. 3.19A). In RD cells, there was a decrease in KI67 levels in AMGEN44 and MKC8866/AMGEN44 cotreated cells at four and six days (Fig. 3.19B). The reduced

KI67 levels observed in these samples correspond to reduced proliferation following treatment with the UPR inhibitors.

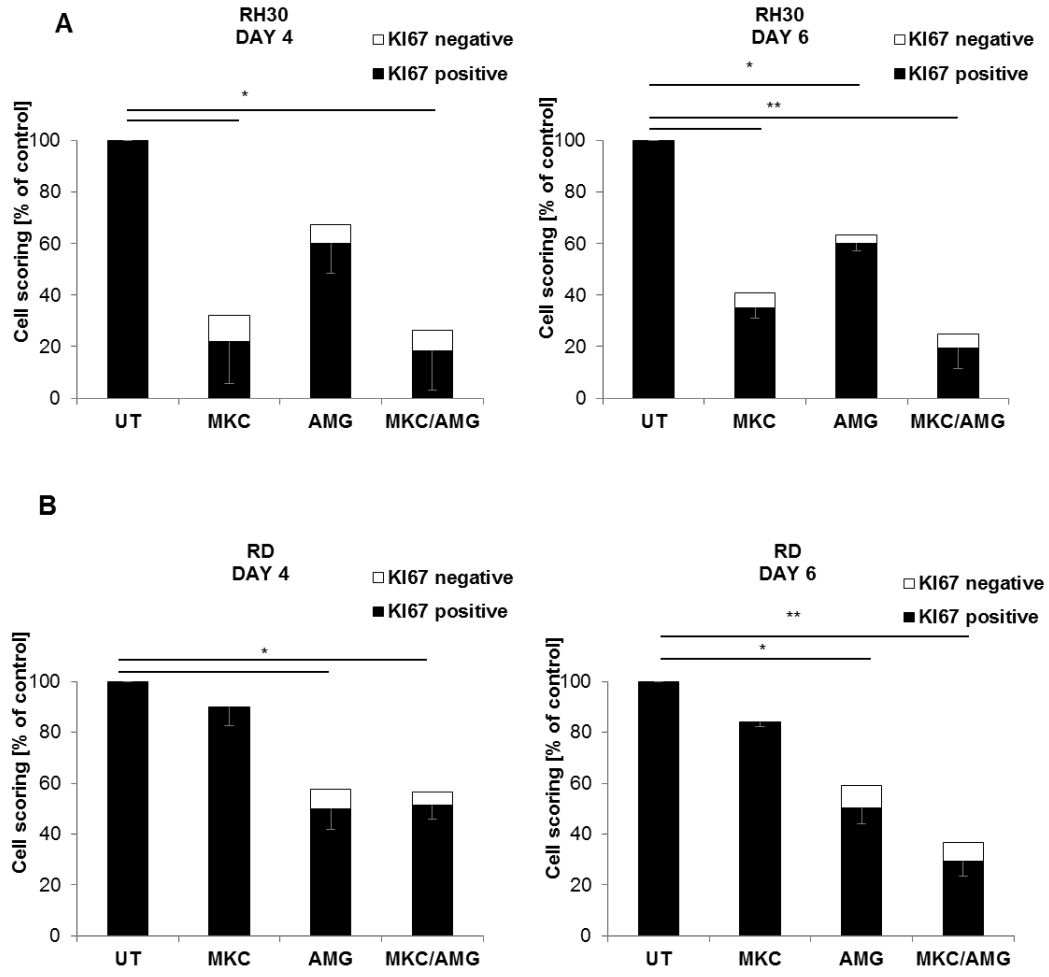

Figure 3.19: A portion of RMS cells enter a G0 non-proliferating state following treatment with MKC8866 and AMGEN44 - MKC8866 (20 μM) and AMGEN44 (2 μM) single and combination treatments were added to RH30 and RD cells and reapplied at 72 h. Following six days of treatment, cells were fixed and stained with a KI67 antibody. Fluorescence of KI67 positive cells was measured at a Molecular Device Microscope with an automated analysis using MetaXpress Software. The percentage of KI67 compared to untreated control is displayed as a percentage of the cell number **(RH30: A, RD: B)**. Mean ± SD of three independent experiments performed are shown. Statistical significance compares positively stained KI67 cells; *P < 0.05; **P < 0.01.

3.2.16 IRE1 and PERK inhibition, using MKC8866 and AMGEN44, induces senescence in RMS cells

3.2.16.1 MKC8866 and AMGEN44 cause an increase in senescence marker β-Gal in RMS cells

KI67 is also an indicator of senescence [304]. In RMS cells the induction of senescence is associated with decreased KI67 levels [305]. Since the UPR can contribute to senescence evasion in cancer cells (described in section 1.8.5), I next decided to investigate whether senescence is involved in the reduction in proliferation observed in MKC8866 and AMGEN44 treated RH30 cells and AMGEN44 treated RD cells. Senescent cells possess high levels of β-Gal and β-Gal staining is one of the most commonly used markers for senescence detection [216]. In the presence of β-Gal, senescent cells are stained bright green following the addition of β-Gal staining. Positive controls for β-Gal staining using etoposide were first tested in RH30 and RD cells (see Appendix A, Fig. A1). RH30 and RD cells were treated with MKC8866 (20 μM) and/or AMGEN44 (2 μM) for up to six days. After six days of treatment, cells were stained with β-Gal. β-Gal positive cells were observed in MKC8866 and AMGEN44 treated RH30 cells and in AMGEN44 treated RD cells (Fig. 3.20A). Quantification of these images shown in Fig. 3.20B reveal a significant increase in β-Gal in MKC8866 and AMGEN44 treated RH30 cells compared to untreated cells and in AMGEN44 treated RD cells compared to untreated cells. These data imply that MKC8866 and AMGEN44 induce senescence in RMS cells.

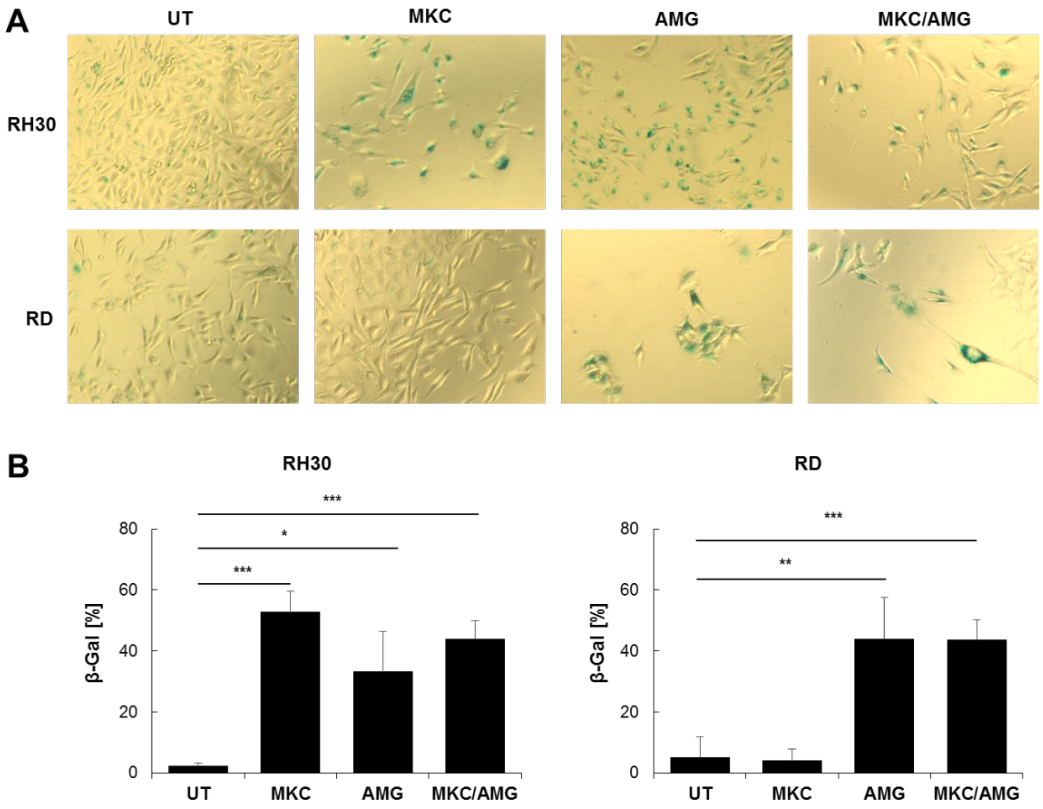

Figure 3.20: MKC8866 and AMGEN44 cause an increase in senescence marker β-Gal in RMS cells - MKC8866 (20 μM) and AMGEN44 (2 μM) single and combination treatments were added to RH30 and RD cells and treatments were reapplied at 72 h. **(A)** Following 6 days of treatment, cells were fixed, and β-Gal staining was applied to cells and left overnight, before being imaged with an IX71 microscope using a 10X objective. One of three independent experiments performed in triplicate are shown. **(B)** Graphs for all three experiments are shown. Mean ± SD of three independent experiments in triplicate performed are shown; *P < 0.05; **P < 0.01, ***P < 0.001.

3.2.16.2 MKC8866 and AMGEN44 upregulate the senescence marker miR146 in RMS cells

Another marker used for the detection of senescence is the presence of the miRNA, miR146. miR146 is upregulated during senescence in response to several different inducers, and in many different cell types [275]. To investigate miR146 expression levels following the treatment of cells with MKC8866 and AMGEN44, GFP-tagged miR146-plasmids were introduced into RH30 and RD cells. The plasmid included a BSD resistance gene, therefore, selection with the antibiotic BSD ensured that all cells retained the plasmid. Following expression of miR146, the GFP promoter would be activated. Thus, following activation of miR146 associated senescence,

GFP is expressed. Using fluorescence microscopy, GFP positive cells could then be imaged and quantified. Positive controls for miR146 upregulation using etoposide was first tested in RH30-miR146-GFP and RD-miR146-GFP cells (see Appendix A, Fig. A2). RH30-miR146-GFP and RD-miR146-GFP cells were treated with MKC8866 (20 μM) and/or AMGEN44 (2 μM) for up to six days. GFP positive cells were observed in MKC8866 and AMGEN44 treated RH30-miR146-GFP cells and in AMGEN44 treated RD-miR146-GFP cells (Fig. 3.21A). Quantification of these images are shown in Fig. 3.21B which reveal a significant increase in GFP positivity in MKC8866 treated RH30-miR146-GFP cells compared to untreated cells. Likewise, there was a significant increase in GFP positive cells in AMGEN44 treated RD-miR146-GFP cells compared to untreated cells (Fig. 3.21B). These data coincide with the β-Gal staining results, confirming senescence induction following IRE1 and PERK inhibition in RMS cells.

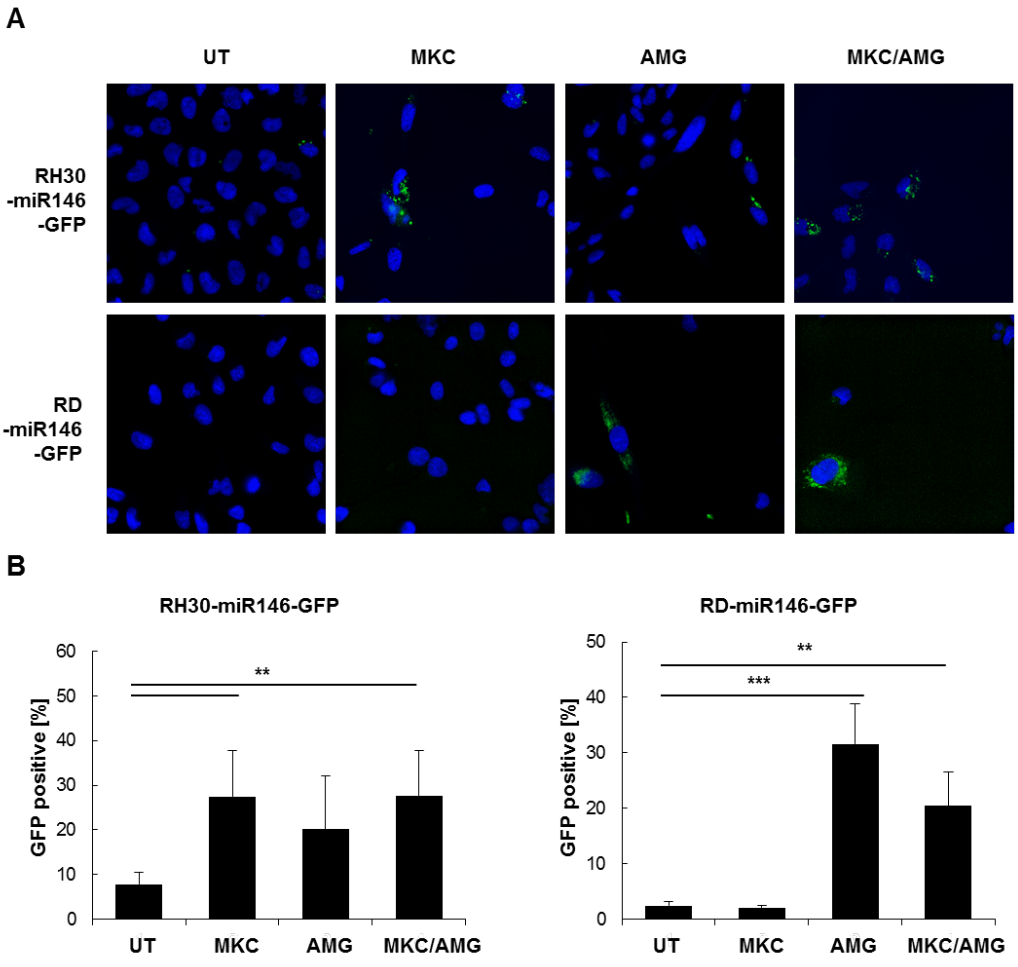

Figure 3.21: MKC8866 and AMGEN44 upregulate the senescence marker miR146 in RMS cells - RH30-miR146-GFP and RD-miR146-GFP cells were treated with MKC8866 (20 μM) and/or AMGEN44 (2 μM) and treatment was reapplied at 72 h. **(A)** Following 6 days of treatment, fluorescence was measured at a Molecular Device Microscope with an automated analysis using MetaXpress Software. DAPI-FITC overlay images were generated; Blue: DAPI/Hoechst stained cells, Green: GFP positive cells. One of three independent experiments are shown. **(B)** Graphs for all three experiments are shown. Mean ± SD of three independent experiments in triplicate performed are shown; *P < 0.05; **P < 0.01, ***P < 0.001.

3.2.16.3 MKC8866 and AMGEN44 do not upregulate E2F1 or p53 proteins in RMS cells

Depending on the type of senescence involved, several molecular markers including DNA damage markers and cell cycle regulators can be upregulated following senescence induction such as E2F1, pRB, p16, p21 and p53 [217, 306, 307]. The accumulation of molecular senescence markers following senescence induction in MKC8866 and AMGEN44 treated RH30 and RD cells was next investigated. RH30 and RD cells were treated with MKC8866 (20 μM) and/or AMGEN44 (2 μM) for 72 and 144 h and protein expression levels of E2F1, p53 and p-p53 were investigated using Western blot. No noticeable changes in protein levels were observed for these senescence markers and no conclusions can be made on the effect of MKC8866 and AMGEN44 on p53 and E2F1 in RMS cells (Fig. 3.22A, B). p21 and p16 protein expression levels were also probed, however, these proteins were not successfully detected. These results imply that p53 and E2F1 are not involved in MKC8866- and AMGEN44-induced senescence. However, small changes in proteins expression levels of these proteins are difficult to detect via Western blot and so they cannot be ruled out [304, 308]. Nevertheless, morphological changes, reduced proliferation, increased β-Gal and increased miR146 expression are sufficient proof to confirm senescence induction in MKC8866 and AMGEN44 treated RMS cells.

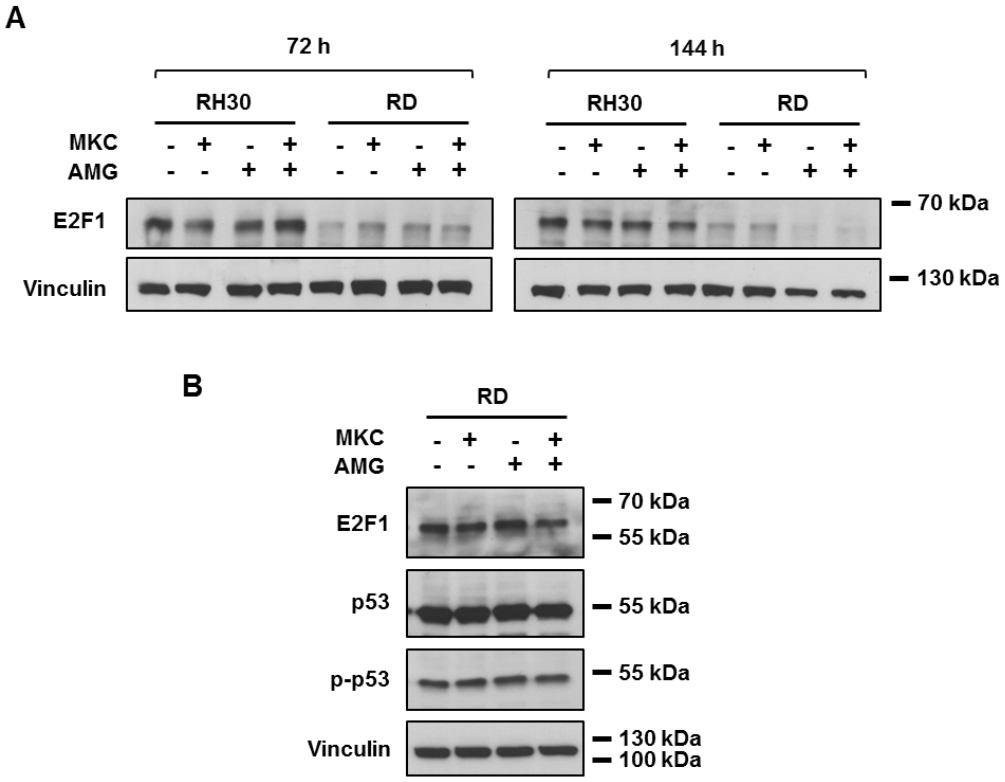

Figure 3.22: MKC8866 and AMGEN44 do not upregulate E2F1 or p53 proteins in RMS cells - RH30 and RD cells were treated with MKC8866 (20 μM) and/or AMGEN44 (2 μM) for 72 and 144 h. **(A)** E2F1, p53 and phospho-p53 protein expression levels were detected via Western blot. Vinculin was used as a loading controls. **(A)** RD cells were treated with MKC8866 (20 μM) and/or AMGEN44 (2 μM) for 144 h and E2F1, p53 and phospho-p53 (Ser15) protein expression levels were detected via Western blot. Vinculin was used as a loading control. The Western blots shown are representative of three independent sets of experiments.

3.2.17 MKC8866 and AMGEN44 alter the expression of apoptotic proteins in RMS cells

Senescent cells develop apoptosis resistance in which they prevent cell death induction by upregulating proteins that prevent apoptosis [221, 309]. It is common to see the upregulation of anti-apoptotic proteins such as Mcl-1 and Bcl-xL following the induction of senescence [221, 310, 311]. Western blot analysis was performed to assess the expression levels of a number of apoptotic proteins. RH30 and RD cells were treated with MKC8866 (20 μM) and/or AMGEN44 (2 μM) for 72 h. There was no upregulation of anti-apoptotic proteins Mcl-1, Bcl-2, or Bcl-xL. In fact, a decrease in Mcl-1 and Bcl-xL protein levels were observed in MKC8866 treated RH30 cells. On the other hand, decreased levels of pro-apoptotic proteins PUMA

and NOXA were detected in RH30 cells treated with MKC8866, alone or in combination with AMGEN44 (Fig. 3.23). In RD cells treated with AMGEN44, alone or in combination with MKC8866, p-ERK protein levels were increased (Fig. 3.23). The downregulation of pro-apoptotic proteins such as PUMA and NOXA and upregulation of p-ERK may promote senescence and contribute to cell death evasion.

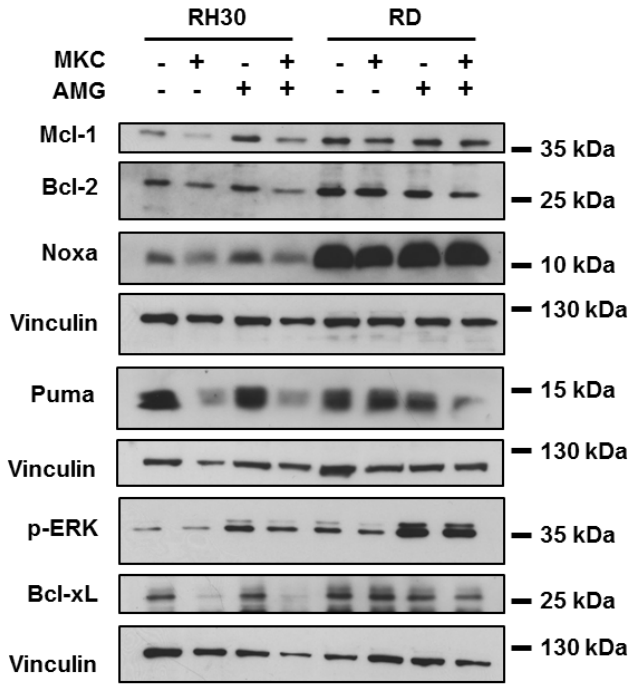

Figure 3.23: MKC8866 and AMGEN44 alter the expression of apoptotic proteins in RMS cells - RH30 and RD cells were treated with MKC8866 (20 μM) and/or AMGEN44 (2 μM) for 72 h. PUMA, NOXA, Mcl-1, Bcl-2, Bcl-xL and p-ERK protein expression levels were detected via Western blot and vinculin was used as a loading control. The Western blot shown is representative of three independent sets of experiments.

Ultimately, complete destruction and elimination of cancer cells is desirable for cancer therapies to ensure removal of the entire tumour. Thus, to induce cell death in RMS cells, it was next decided to search for a suitable drug to combine with UPR inhibitors.

3.2.18 AMGEN44 and MEK inhibitor cotreatment reduces the viability of RD cells

The Ras-MEK-ERK signalling cascade is activated in response to different extracellular stimuli and is known to be involved in differentiation, proliferation and survival [312]. The MEK-ERK pathway has also been linked to senescence [192, 313]. In Fig. 3.23, p-ERK protein levels were upregulated in AMGEN44 treated RD cells. Since ERK is phosphorylated during Ras-MEK-ERK signalling, increased p-ERK in PERK inhibited RD cells is indicative of activation of the Ras-MEK-ERK signalling pathway [314, 315]. Trametinib is a MEK inhibitor that prevents ERK phosphorylation [316]. Previously published studies have demonstrated that the MEK-ERK signalling pathway plays an important role in ERMS and that ERMS cell lines are sensitive to MEK inhibition in which MEK inhibitors induce cell death in these cells [317]. It was hypothesized that AMGEN44 treated RD cells would have increased sensitivity to MEK inhibition and that inhibition of MEK would induce cell death. Trametinib concentrations (0.1-0.5 μM) were chosen based on concentrations used in previous publications in which low amounts of cell death are induced and the mechanism of action is confirmed [316]. As seen from the data in Fig. 3.24A, AMGEN44 and trametinib cotreatment did not induce cell death in RD cells anymore than with trametinib alone. However, AMGEN44 further reduced viability in combination with trametinib compared to trametinib alone (Fig. 3.24B) implying that AMGEN44 and trametinib show some promise as a potential combination therapy to inhibit RMS cell survival.

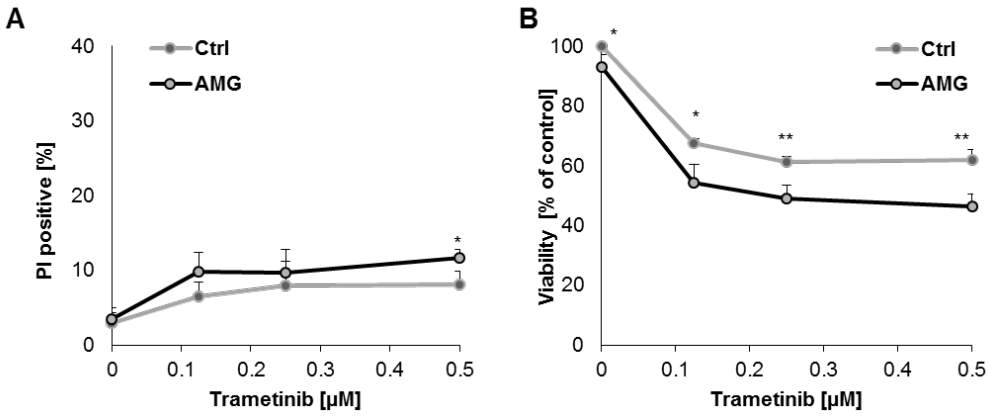

Figure 3.24: AMGEN44 and MEK inhibitor cotreatment reduces the viability of RD cells - RH30 cells were treated with a range of trametinib (0.125-0.5 μM) for 72 h in the present or absence of AMGEN44 (2 μM). Cell death was determined by measuring PI/Hoechst stained cells using a Molecular Device Microscope with an automated analysis using a Molecular Device Microscope with an automated analysis using MetaXpress Software (A). Cell viability was assessed using CTG and is expressed as the percentage of untreated controls (B). Mean ± SD of three independent experiments performed in triplicate are shown; *P < 0.05, **P < 0.01.

3.2.19 MKC8866 and aurora A kinase inhibitor cotreatment induce cell death and reduce viability in RH30 cells

Aurora kinases are serine/threonine kinases that are essential for cell division and cell proliferation [318]. Aurora A kinase has been shown to regulate *PAX3-FOXO1* in fusion positive RMS cells [287]. Alisertib (MLN8237), an Aurora A kinase inhibitor, has cytotoxic effects against RMS cells as a single agent [286, 287]. The combinatorial effects of alisertib and MKC8866 in RH30 cells was next investigated. Alisertib concentrations (0.25-1 μM) were chosen based on concentrations used in previous publications in which low levels of cell death are induced and the mechanism of action is confirmed [287]. The data in Fig. 3.25 revealed that MKC8866 induced cell death and reduced viability in combination with alisertib in RH30 cells. These data suggest that the combination of MKC8866 with alisertib shows potential as a combination therapy to induce cell death in RMS.

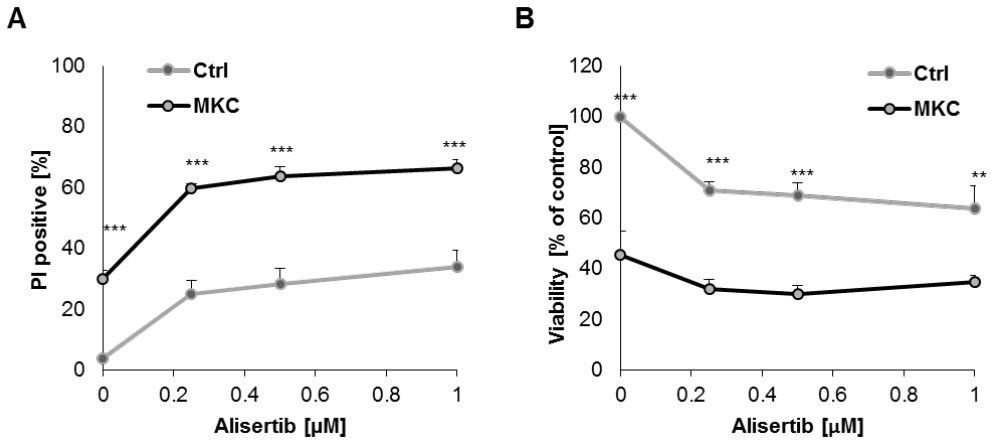

Figure 3.25: MKC8866 and aurora A kinase inhibitor cotreatment induce cell death and reduce viability in RH30 cells - RH30 cells were treated with a range of alisertib (0.25-1 μM) for 72 h in the present or absence of MKC8866 (20 μM). Cell death was determined by measuring PI/Hoechst stained cells using a Molecular Device Microscope

with an automated analysis using a Molecular Device Microscope with an automated analysis using MetaXpress Software (A). Cell viability was assessed using CTG and is expressed as the percentage of untreated controls (B). Mean ± SD of three independent experiments performed in triplicate are shown; *P < 0.05, **P < 0.01, ***P < 0.001.

3.2.20 Proteasome inhibitors, Btz and Carf, induce apoptosis in RMS cell line RH30

Proteasome inhibitors such as Btz have demonstrated cytotoxic effects against a number of cancer cell types including breast, lung, colon and prostate cancer [282-285]. Previously, a study demonstrated that proteasome inhibitor MG132 decreased senescence and induced cell death in doxorubicin treated leukemia cells [319]. Furthermore, a recent study demonstrated that the combination of IRE1 RNase inhibitors with proteasome inhibitors synergistically induced cell death in leukemia cells [250]. Thus, the effect of proteasome inhibitors against RMS, alone and in combination with UPR inhibitors, was investigated.

To examine the effects of proteasome inhibitors Btz and Carf on RMS, a cell death assay was initially carried out. A range of Btz and Carf concentrations (1-30 nM) were applied to the RMS cell line, RH30. Btz- and Carf-induced cell death occurred both in a time- and dose-dependent manner in RH30 cells, as demonstrated by PI-uptake (Fig. 3.26A). The specific mode of cell death involved was also investigated. Since caspases play a major role in apoptosis, blocking caspase activity can reveal apoptosis involvement. zVAD.fmk is a pan caspase inhibitor, regularly used to confirm apoptosis [299]. The addition of zVAD.fmk to Btz and Carf treated RH30 cells significantly, albeit not completely, rescued cells from cell death, suggesting apoptosis is the main cell death pathway activated upon treatment with Btz (Fig. 3.26B). To identify the potential involvement of necroptosis, Necrostatin1s (Nec1s), a specific RIP1 and necroptosis inhibitor [320], was added to Btz and Carf treated RH30 cells. Nec1s did not reduce cell death levels alone or in combination with zVAD.fmk, ruling out any involvement of necroptosis upon Btz treatment (Fig. 3.26B).

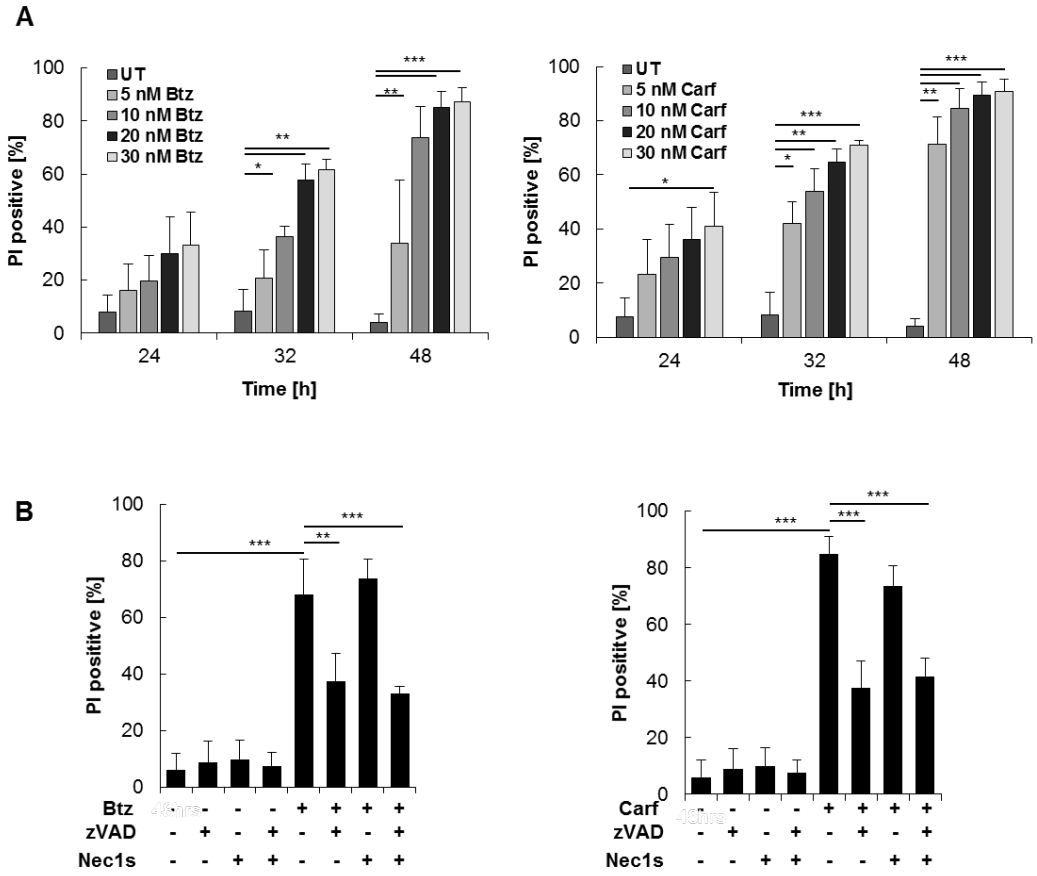

Figure 3.26: Proteasome inhibitors, Btz and Carf, induce apoptosis in RH30 cells - RH30 cells were treated with indicated concentrations of Btz and Carf for up to 72 h. Cell death was determined by measuring PI/Hoechst stained cells using a Molecular Device Microscope with an automated analysis using a Molecular Device Microscope with an automated analysis using MetaXpress Software (A). RH30 cells were treated with Btz (10 nM) and Carf (10 nM) for 36 h in the presence or absence of 20 µM zVAD.fmk, 1 µM Nec1s or a combination of zVAD.fmk (20 µM) and Nec1s (1 µM). Cell death was determined by measuring PI/Hoechst stained cells using a Molecular Device Microscope with an automated analysis using a Molecular Device Microscope with an automated analysis using MetaXpress Software (B). Mean ± SD of three independent experiments performed in triplicate are shown; *P < 0.05; **P < 0.01, ***P < 0.001.

3.2.21 Btz and Carf induce ER stress and UPR signalling in RH30 cells

Using Western blot, protein levels of ER stress markers including GRP78, PERK, p-eIF2α and CHOP were investigated following Btz and Carf treatment. RH30 cells were treated with Btz (10 nM) and Carf (10 nM) for up to 24 h and UPR signalling was investigated via Western blotting (Fig. 4A). TM (5 µg/ml) served as a positive control for ER stress and UPR induction. Activation of PERK (indicated by an upward band shift), phosphorylation of eIF2α and increased CHOP protein levels

were all observed following Btz and Carf treatment, implying activation of the PERK arm of the UPR (Fig. 3.27A). RH30 cells were treated with Btz (10 nM) and Carf (10 nM) for 8 h and p-JNK protein levels were investigated via Western blotting. Increased p-JNK levels were observed in RH30 cells following treatment with both Btz and Carf (Fig. 3.27B).

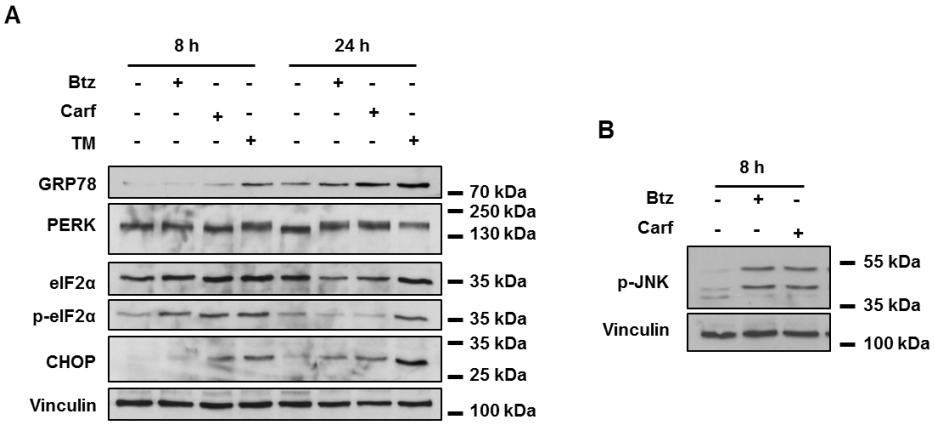

Figure 3.27: Btz and Carf induce ER stress and UPR signalling in RH30 cells - RH30 cells were treated with Btz (10 nM) and Carf (10 nM) for 8 and 24 h. Expression levels of PERK (phosphorylation indicated by upward band shift), p-eIF2α, eIF2α, CHOP and GRP78 were evaluated by Western blot analysis. TM (5 µg/ml) served as a positive control and vinculin was used as a loading control (A). RH30 cells were treated with Btz (10 nM) and Carf (10 nM) for 8 h. Expression levels of -pJNK were evaluated using Western blot analysis and vinculin was used as a loading control (B). The Western blots shown are representative of three independent sets of experiments.

3.2.22 MKC8866 and proteasome inhibitor cotreatment induces cell death in RH30 cells

RH30 cells were treated with 20 µM MKC8866 alone or in combination with 10 nM Btz or 10 nM Carf for up to 32 h. Combination of MKC8866 with both proteasome inhibitors increased the induction of cell death in RH30 cells (Fig. 3.28).

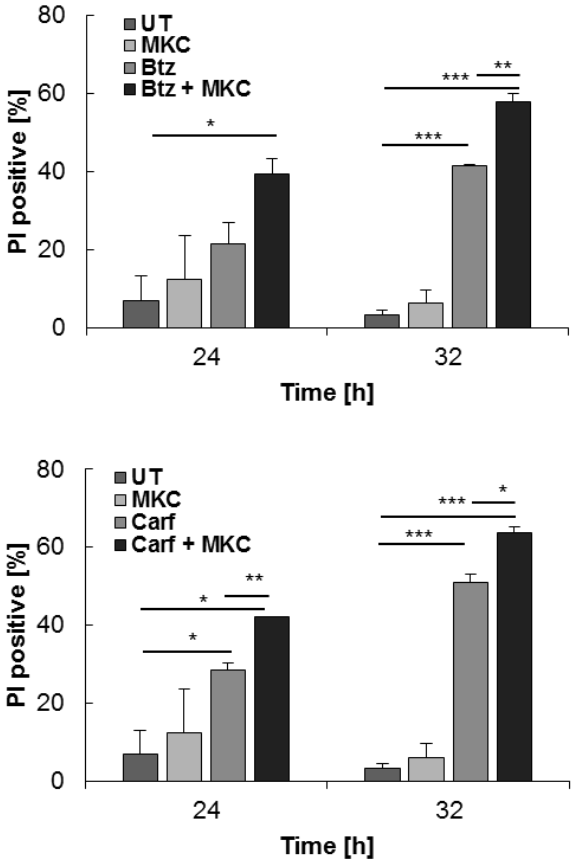

Figure 3.28: MKC8866 and proteasome inhibitor cotreatment induces cell death in RH30 cells - RH30 cells were treated with Btz (10 nM) or Carf (10 nM) for the indicated times in the presence or absence of MKC8866 (20 μM). Cell death was determined by measuring PI/Hoechst stained cells using a Molecular Device Microscope with an automated analysis using a Molecular Device Microscope with an automated analysis using MetaXpress Software. Mean ± SD of three independent experiments performed in triplicate are shown; *P < 0.05, **P < 0.01, ***P < 0.001.

3.2.23 AMGEN44, does not enhance the cytotoxicity of proteasome inhibitor Btz in RD cells

A combination of Btz and AMGEN44 was also tested in RD cells. Treatment of RD cells with Btz and AMGEN44 did not have an increased cytotoxic effect compared to Btz alone (Fig. 3.29).

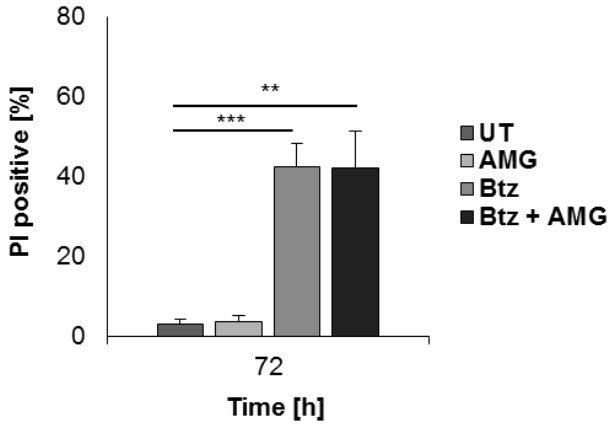

Figure 3.29: AMGEN44, does not enhance the cytotoxicity of proteasome inhibitor Btz in RD cells - RD cells were treated with Btz (20 nM) for 72 h in the presence or absence of AMGEN44 (2 μM). Cell death was determined by measuring PI/Hoechst stained cells using a Molecular Device Microscope with an automated analysis using a Molecular Device Microscope with an automated analysis using MetaXpress Software. Mean ± SD of three independent experiments performed in triplicate are shown; *P < 0.05, **P < 0.01, ***P < 0.001.

3.3 Discussion

In this chapter, the aim was to investigate basal UPR activity in RMS cell lines and to modulate this activity, using UPR inhibitors, to determine the role of the UPR in RMS. Basal activation of IRE1 and PERK was observed in RMS cell lines, which was diminished upon addition of the IRE1 inhibitor MKC8866, or PERK inhibitor AMGEN44. Further investigation into this IRE1 and PERK inhibition demonstrated a reduction in cell viability, cell proliferation and inhibition of long-term colony formation in both ARMS and ERMS subtypes of RMS. These effects were confirmed by genetic knockdown of IRE1 and PERK using siRNA. It was also discovered that ARMS cell lines are highly sensitive to IRE1 inhibition whereas ERMS cell lines are more sensitive to PERK inhibition. Additionally, it was established that these UPR inhibitors did not induce any cell death in non-malignant cell lines, nor did they reduce cell viability or proliferation of these healthy cell lines. Further exploration revealed a robust activation of senescence following UPR inhibition in both RMS subtypes, where cells displayed senescence-associated morphological changes and increased senescence markers such as β-Gal and miR146.

Previous studies have confirmed that RMS cells possess a competent UPR signalling network that can be activated in response to external stresses [141, 278-280]. For example, ER stress inducers and HSP inhibitors promote the activation of IRE1 and PERK and their downstream signalling elements including ATF4 and XBP1s [278, 280]. The data in this chapter suggest that RMS cells exhibit basal UPR activity. Since basal UPR signalling has not yet been investigated in RMS primary samples, it is not possible to corroborate these findings with other studies. Other sarcomas including Ewing sarcoma, fibrosarcoma and osteosarcoma have been associated with basal UPR signalling. For instance, Ewing sarcoma cell lines and surgical samples have elevated mRNA expression of *XBP1s* [321]. Likewise, osteosarcoma cells have upregulated *XBP1s* mRNA levels when compared with osteoblastic cells [322]. Fibrosarcoma, another type of soft tissue sarcoma, demonstrates PERK signalling that protects fibrosarcoma cells from cell death and promotes metastasis [323]. The findings in this chapter confirm basal UPR signalling activity in RMS cell lines only.

Since patient samples were not included in the present study and UPR signalling was instead only investigated in RMS cell lines, it remains to be shown whether UPR signalling is also basally active in primary RMS samples. Unfortunately, due to the low incidence of RMS, it is difficult to obtain primary RMS tissue samples and so it was not possible to investigate this aspect in the present thesis. Alternatively, when patient samples are unavailable, bioinformatic analysis of publicly available data sets can be performed to investigate UPR activity in patient tumours. At this present time, a computational approach is not feasible as there are currently very few databases on RMS. Nonetheless, RMS-derived cell lines are a good representation of RMS cancer biology, genetic background and cellular signalling, providing a reliable model for basic research and the development of novel therapeutics [324].

In cancer, the UPR can be activated by various external or internal stresses such as the tumour microenvironment, pharmacological and radiation treatments, oncogenic transformations and high secretory demands [325]. Stresses such as hypoxia and glucose deprivation caused by the TME have been shown to induce ER stress in cancer cells [207]. For example, hypoxia has been reported to induce activation of IRE1 signalling in TNBC [210, 326]. Since our *in vitro* model is a 2D *in vitro* culture system, it is unlikely that hypoxia or glucose deprivation is the cause of the observed basal UPR activity in the RMS cell lines. Another source of UPR activation in cancer cells is rapid cell division which dramatically enhances protein synthesis rates and overwhelms the protein folding capacity of the ER, generating ER stress and triggering UPR activation [192]. Increased protein demands due to higher proliferation rates could be the driver behind high RMS basal UPR activity. The activation of oncogenes has also been linked to IRE1 and PERK activation in a number of cancer models such as melanoma and lymphoma [195, 327]. Since ARMS and ERMS are associated with increased MYCN and RAS activity and signalling [180, 328], these oncogenes may be responsible for UPR activation. This will be discussed further, later in the discussion.

Consistently, long-term IRE1 and PERK inhibition significantly reduced proliferation and colony formation in RMS cells. These data confirm that UPR signalling plays a vital role in RMS and that inhibition of the UPR signalling

pathways prevents long-term reproducibility and survival of RMS cells. Until now, the effect of UPR inhibitors on RMS had not been explored. However, many studies have been published demonstrating the effects of IRE1 and PERK inhibitors on other cancers. For example, IRE1 RNase inhibitors induce cell death in MM, Ewing sarcoma and leukemia cells [249, 250, 321]. IRE1 RNase inhibitors also reduce growth in cancer cells including breast cancer, MM, leukemia and prostate cancer [198, 199, 201, 249, 250, 252]. Although PERK inhibitors have not been evaluated in the context of RMS, studies have shown that inhibition of PERK reduces tumour growth in MM and pancreatic cancer mouse models [258, 259]. Together, these data support the hypothesis that targeting IRE1 and PERK signalling in RMS could be an attractive therapeutic option.

We confirmed MKC8866-mediated prevention of XBP1 splicing and that AMGEN44-mediated prevention phosphorylation of eIF2α were correlated with reduced proliferation in RMS cells. However, the signalling elements downstream of IRE1 and PERK involved in the reduced proliferation response MKC8866 and AMGEN44 were not evaluated. To further investigate the response by RMS following MKC8866 and AMGEN44 treatment, a microarray analysis could be performed to highlight changes in gene expression following treatment with UPR inhibitors. This could enable the identification of important players involved in the signalling response to IRE1 and PERK inhibition. Previously, mRNA microarray analysis of IRE1-inhibited cells derived from TNBC cell lines produced an *IRE1* gene signature that highlighted components involved in the response to IRE1 inhibition [198]. Using this gene signature approach, Logue and colleagues revealed that IRE1 activity strongly correlates with the expression of genes involved in inflammatory responses such as *IL-6* and *IL-8*. Following IRE1 inhibition using MKC8866 in these TNBC cells, they discovered that these pro-tumourigenic factors were downregulated, highlighting their involvement in the response to IRE1 inhibition in TNBC [198].

In this study, we did not investigate ATF6 signalling in RMS cells. The ATF6 pathway has been shown to overlap with IRE1 and PERK signalling as it promotes the transcription of *XBP1*, *CHOP* and *ATF4* [34]. ATF6 signalling could be

implicated in the IRE1 and PERK signalling observed in RMS cells. It can therefore not be excluded that the IRE1 and PERK activity detected in RMS cells could be partially enhanced by ATF6 signalling. To investigate ATF6 signalling in RMS, genetic silencing or pharmacological inhibition of ATF6 using ceapins should be performed [262]. Additionally, inhibition of ATF6 during MKC8866 and AMGEN44 treatment could identify potential roles of ATF6 during the RMS response to IRE1 and PERK inhibition. Moreover, inhibition of ATF6 in combination with the IRE1 and PERK inhibitors could have synergistic cytostatic and/or cytotoxic effects in RMS cells.

IRE1 and PERK inhibition have both been linked to cell cycle arrest in cancer cells. For example, IRE1 inhibitors induced a G1 cell cycle arrest in TNBC and leukemic cells which correlated with a significant decrease in proliferation [198, 201]. On the other hand, PERK inhibition in breast cancer cells caused a delay in cell cycle progression at the G2/M phase which resulted in reduced proliferation [203]. The KI67 protein is present in all proliferating cells, at any stage of the cell cycle. If cells do not possess KI67, this likely indicates that they are in the G0 non-proliferating stage of the cell cycle [303]. The reduced proliferation seen in MKC8866 and AMGEN44 treated cells could be explained by these cells entering a G0 state of arrest, as demonstrated by reduced KI67 levels [303]. Upon analysis of cell cycle, if cells are in G0 stage of the cell cycle a G1 arrest should be observed [329]. Analysis of cell cycle phases using the Nicoletti assay, showed no difference in cell cycle in MKC8866 or AMGEN44 treated cells compared to untreated cells for both RH30 and RD cells. This suggests that there is no disruption to the cell cycle. Therefore, these data from the KI67 analysis and Nicoletti analysis do not support each other and a conclusion cannot be drawn regarding the effects that MKC8866 and AMGEN44 have on RMS cell cycle. Perhaps the Nicoletti assay is not sensitive enough to detect changes as there was still a portion of proliferating cells that mask the cells halted in G0. To detect small changes in cell cycle it is often necessary to synchronise cells so that they are all in the same phase of the cell cycle at the beginning of the assay. Frequently used techniques used to synchronise cells include cell cycle inhibitor nocodazole or serum deprivation [330, 331]. In addition, other cell cycle analysis techniques could be utilised to validate the Nicoletti assay results

such as BrdU staining, another convenient and inexpensive method to analyse cell cycle [332]. To differentiate between cells in G1 or G0, RNA levels would need to be analysed as cells in G0 have lower levels of RNA compared to proliferating cells [329]. This technique involves a Hoechst-3342 and Pyronin Y double staining allowing RNA levels to be distinguished from DNA and thus, allowing the identification of resting or senescent cells [329].

When using small molecule inhibitors there is always the possibility that they exhibit off-target effects. It is important to validate any results obtained with appropriate genetic approaches. For this, an siRNA approach was used to genetically silence IRE1 and PERK. In general, single and combinatorial knockdown of IRE1 and PERK correlated with results obtained using pharmacological inhibitors, MKC8866 and AMGEN44 respectively, such as reduced cell viability and colony formation. There were a number of inconsistencies between the results seen with UPR inhibitors and IRE1 and PERK silencing. For example, MKC8866 demonstrated cytotoxic effects against RH30 whereas IRE1 knockdown did not. However, MKC8866 was sufficient at blocking *XBP1* splicing at a concentration as low as 5 μM and cytotoxicity was only observed at higher concentrations of MKC8866. This result could have been an outcome of using high and nonspecific concentrations of the inhibitor and not as a result of inhibition of IRE1 signalling alone. Since IRE1 possesses both RNase and kinase activity, knockdown of IRE1 prevents both of these activities whereas MKC8866 selectively blocks RNase activity. IRE1 kinase activity has been linked to pro-death signalling through ASK1 and JNK phosphorylation and activation [145-147]. Differences in responses between MKC8866 and IRE1 genetic silencing could be as a result of kinase inhibition following IRE1 silencing. Nonetheless, genetic inhibition of IRE1 significantly reduced long-term colony formation in RH30 cells. Furthermore, pharmacological and genetic inhibition of IRE1 and PERK in RH30 and RD cells produced comparable results for viability and colony formation assays. These data indicate that the effects observed using MKC8866 and AMGEN44 are due to their inhibition of IRE1 and PERK, respectively.

In order for drugs to be considered for use in clinics, it is necessary for them to be cancer cell-specific and have no harmful effects on healthy cells. Non-malignant cell lines, MRC5 and C2C12, were unaffected by MKC8866 and AMGEN44, underlining the lack of toxicity of these compounds against non-cancerous cells. This is particularly important for the progression of drugs as potential therapeutics in order to avoid unwanted side effects. Many cells in the body depend on UPR signalling for physiological processes and some specific cell types require increased UPR signalling for their functions. For example, insulin-secreting β-cells place high demands on ER function [333]. Hence, these cells are potentially more sensitive to UPR inhibition which could result in severe side effects. Therefore, the use of UPR inhibitors requires a careful therapeutic strategy. The next step for testing the effects of UPR inhibition on RMS cell survival would be *in vivo* testing. Chicken chorioallantoic membrane (CAM) assay is one type of *in vivo* model which could be used in further investigations that is inexpensive and readily available. CAM assays involve placing tumour cells onto the chorioallantoic membrane of fertilised chicken eggs where they can subsequently be monitored for tumour growth, invasion, angiogenesis and metastasis *in vivo* [334]. Additionally, RMS mouse models have been developed that mimic the multiple aberrant molecular events associated with RMS [335]. The use of these mouse models would enable investigation of tumour environment factors such as nutrient and oxygen deprivation, which could in theory intensify UPR activity and enhance the results seen following UPR inhibition. In addition, mouse models would allow the identification of any potential side effects of the UPR inhibitors. Side effects associated with UPR inhibitors and potential side effects of MKC8866 and AMGEN44 are discussed in detail in chapter 5.

To confirm the broader relevance of UPR inhibition in RMS, the study was extended to six additional RMS cell lines giving a total of four cell lines for each subtype. Experiments in these cell lines confirmed that the cytostatic effects of IRE1 and PERK inhibition observed in RH30 and RD cells also occur in other RMS cell lines. Following UPR inhibition, an interesting pattern among the investigated cell lines was observed. According to this trend, ARMS cell lines were found to be more sensitive to IRE1 inhibition than PERK inhibition. Although some ERMS cell lines responded to IRE1 inhibition more than RD cells, in general, ERMS are more

sensitive to PERK inhibition. Based on our *in vitro* data, we propose that ARMS rely heavily on IRE1 and have a high sensitivity to IRE1 inhibition, whereas ERMS have a high dependency on PERK, resulting in their increased sensitivity to PERK inhibition.

Differences in responsiveness between ARMS and ERMS to UPR inhibition could be due to genetic variations between the two subtypes. Neoplastic transformation due to loss of tumour suppressors or activation of oncogenes has been linked to UPR activation in a number of cancers [191-193]. ARMS cases are typically characterised by expression of the *PAX3/7- FOXO1* hybrid gene [177, 178]. RH30, RMS13, and RH41 cell lines possess the *PAX3-FOXO1* hybrid gene. The high sensitivity of ARMS subtypes to IRE1 inhibition could be indicative of a connection between *PAX3/7-FOXO1* and IRE1 signalling. A knockdown of *PAX3-FOXO1* in fusion positive ARMS could be utilised to determine if *PAX3-FOXO1* expression sensitizes ARMS cells to MKC8866 treatment. *PAX3-FOXO1* knockdown ARMS cells have been previously generated by other groups [336, 337]. Alternatively, the expression of the *PAX3/7-FOXO1* hybrid in an ERMS cell line could reveal whether this fusion protein causes these cells to become more sensitive to IRE1 inhibition. High sensitivity of ARMS to IRE1 inhibition could also be due to a connection between *Myc* and IRE1/XBP1s signalling pathways. A large portion of ARMS cases have high activity of *Myc*, which is a direct transcriptional target of *PAX3-FOXO1* hybrid gene [180, 181]. ARMS cell lines RH30, RMS13, and RH41 have increased *c-Myc* and *MYCN*. ERMS, on the other hand, have significantly lower expression of the *Myc* oncogene compared to ARMS [181]. In recent years, a number of studies have been published linking *Myc* and the IRE1/XBP1s pathway. For instance, Zhao and colleagues discovered that oncogenic *Myc* upregulates the IRE1/XBP1 branch of the UPR in breast cancer and that genetic and pharmacological inhibition of IRE1 RNase activity reduced tumour growth *in vitro* and *in vivo* [251].

ERMS cases are typically accompanied by *HRAS, KRAS and NRAS* mutations [168, 173, 175]. ERMS cell lines used in this thesis, RD, TE381.T, T174 and RH36, all possess *RAS* mutations; RD, TE381.T and T174 have an *NRAS* mutation and RH36 has a *HRAS* mutation. The higher sensitivity of ERMS subtypes to PERK inhibition

could be due to the presence of these *RAS* mutations. A previous study by Horiguchi *et al*., disovered that knockdown of ATF4 in HRAS transformed MEFs resulted in slower growing tumours *in vivo* when compared to their non-transformed wildtype counterparts with an ATF4 knockdown [290]. In this study, the aim was to investigate the involvement of RAS in ERMS sensitivity to PERK inhibition. Experiments using ARMS cell line RMS13 with ectopic overexpression of different mutated *RAS*, demonstrate that RMS13 cells with mutated NRAS have increased sensitivity to PERK inhibition which is otherwise not seen in wildtype RMS13. RD, T174 and TE381.T ERMS cell lines used in this study all possess NRAS mutations. These *NRAS* mutations may be responsible for ERMS higher sensitivity to PERK inhibition. However, the *NRAS* mutated RMS13 cell line also had enhanced sensitivity to IRE1 inhibition by MKC8866. Therefore, no definitive conclusion can be drawn from these results. Further studies will be required to understand ERMS high sensitivity to PERK inhibition.

This study also highlights the potential role of the UPR in promoting the indefinite replicative ability of RMS cancer cells. Senescence is defined as a cellular growth arrest driven by a range of mechanisms including telomere shortening and stresses such as chemotherapeutic stressors [214, 215]. Senescence is recognised as a critical process for cancer prevention and cancer cells require mechanisms that allow them to avoid senescence and gain indefinite replication abilities [220]. The findings observed in this chapter, including senescence-related morphological changes, and increased β-Gal and miR146 following UPR inhibition, suggest that the UPR could be contributing to senescence evasion in RMS. The upregulation of miR146 following the induction of senescence has been linked to NF-κB signalling. In fact, the mir146 reporter used in this study operates in a context-dependent manner in which it is highly dependent on miR146 promoter regulatory mechanisms such as GATA4 or NF-κB [275]. The transcription factor GATA4 is normally degraded by autophagy. During senescence autophagy-mediated degradation of GATA4 is suppressed, thereby stabilizing GATA4 [275]. In turn, GATA4 activates NF-κB to promote senescence [275]. Since NF-κB and GATA4 are associated with miR146 upregulation in senescence models, increased levels of miR146 following treatment

of RMS cells with MKC8866 and AMGEN44 suggests the involvement of GATA4 and NF-κB in response to UPR inhibition [275].

The induction of senescence observed in UPR inhibited cells is a compelling explanation for the reduced proliferation observed. A number of studies have indicated that the UPR contributes to senescence evasion [215] where blockade of UPR signalling results in senescence induction. For example, inhibition of PERK induced senescence in both MCF-7 and HT1080 cells [291]. Likewise, ATF4 deletion in transformed fibroblasts triggered senescence, resulting in slower tumour growth and significantly smaller tumours *in vivo* [290]. It is important to note that although reduced proliferation and reduced tumour growth is beneficial in cancer therapy, senescent cells must be safely destroyed and removed to prevent future re-entry into cell cycling and division, which could lead to relapse. It has been argued that some cases of senescence are not irreversible and in fact, some studies have demonstrated that senescent cells can re-enter the cell cycle and resume growth [338, 339]. In addition, SASP signalling from senescent cells could have detrimental effects on surrounding cells by releasing pro-inflammatory cytokines and chemokines that can be potentially harmful and pro-tumourigenic [340, 341]. Hence, senolytics, which selectively kill senescent cells, or other cytotoxic drugs are necessary in combination with these UPR inhibitors in order to kill the senescent cells and ensure complete removal [341].

A significant portion of cells had proliferative capabilities even after UPR inhibition. To eliminate these remaining cells as well as the senescent population, a combination treatment is required. Previous studies have demonstrated a synergistic anticancer effect of UPR inhibitors combined with current chemotherapeutics and targeted therapies. For example, combination of MKC8866 with chemotherapeutic paclitaxel had increased cytostatic effects in TNBC [198]. Thus, the combination of UPR inhibitors with chemotherapeutics or targeted drugs in RMS should be tested. In a hypothesis-driven approach, this was further explored by combining MKC8866 and AMGEN44 with drugs that have previously shown cytotoxic effects against RMS cells. MKC8866 and aurora A kinase inhibitor increased cell death and reduced cell viability in RH30 cells. Aurora A kinase inhibitors are known to induce

cell death in RMS cells [286, 287], however, the combined effect of targeting and inhibiting aurora A kinase and IRE1 have not previously been investigated. Likewise, MEK inhibition has cytotoxic effects against ERMS cells [317]. Although increased PERK signalling has been observed in a number of RAS transformed cell lines, combined inhibition of RAS and PERK in cancer cells also remains unexplored [290, 342]. Here, combination of trametinib with AMGEN44 decreases the viability of ERMS cells. Combining UPR inhibitors with other anticancer drugs is discussed further in chapter 5 (section 5.5.1).

Proteasome inhibitor Btz is used for the treatment of MM which is a tumour type associated with high basal IRE1 activity [343]. Btz induces apoptosis in MM cells, reduces tumour growth *in vivo* and prolongs the overall survival in patients with relapsed or refractory MM [344-347]. In this chapter, it was established that Btz induces cell death in RMS cells as a single agent and in combination with MKC8866. These data corroborate previously published data demonstrating the toxicity of Btz against RMS [348, 349]. Previously, ER stress inducers, including TG and 2-DG, have been shown to inhibit PAX3-FOXO1 activity in RMS cells [141, 350]. Since Btz also induces ER stress, inhibition of PAX3-FOXO1 activity by Btz in ARMS cells could be a valid explanation for their increased sensitivity to Btz. Examining the expression of PAX3-FOXO1 target genes following the treatment of ARMS cells with Btz could reveal the effects of Btz on PAX3-FOXO1. Moreover, it was confirmed that the combination of MKC8866 and Btz has additive cytotoxic effects in RMS cells. Combination treatment with Btz and IRE1 RNase inhibitors have previously been tested; combination of the IRE1 RNase inhibitor MKC-3946 and Btz significantly blocked MM tumour growth and increased survival in mice [199]. Likewise, combination of MKC8866 and Btz resulted in a marked cytotoxic response in mast cell leukemia [250]. Wilhelm *et al.* demonstrated that Btz induces IRE1 signalling which promotes the activation of the JNK/JUN pathway which subsequently induces XBP1 splicing and the transcription of CHOP [250]. Both Btz and Carf induced phosphorylation of JNK in RH30 cells could be due to IRE1 signalling. The increase in CHOP protein levels may also, in part, be a result of IRE1 activation [250]. However, this is not confirmation of IRE1 activity and further investigation such as XBP1s expression must be performed. This could provide a

suitable explanation for increased sensitivity to IRE1 inhibition following Btz treatment as increased p-JNK was also observed in Btz and Carf-treated RH30 cells. The co-treatment of RMS cells with Btz and IRE1 RNase inhibitors demonstrates a clinical potential for RMS.

In summary, the data in this chapter highlight the important role of UPR signalling in RMS cells and that inhibition of this signalling has significant potential therapeutic value in RMS.

Chapter 4: The anti-apoptotic effect of Smac mimetic BV6 on tunicamycin-induced apoptosis

Publications

The data from this chapter has been published in two manuscripts:

1. Behnaz Ahangarian Abhari, **Nicole McCarthy***, Marie Le Berre, Michelle Kilcoyne, Lokesh Joshi, Patrizia Agostinis and Simone Fulda (2019) Smac mimetic suppresses tunicamycin-induced apoptosis via resolution of ER stress. Cell Death and Disease, volume 10, article number 155. DOI: 10.1038/s41419-019-1381-z.
   * Shared first author

2. Behnaz Ahangarian Abhari, **Nicole McCarthy**, Patrizia Agostinis, Simone Fulda (2019) NF-κB contributes to Smac mimetic-conferred protection from tunicamycin-induced apoptosis. Apoptosis, volume 24, pages 269-277. DOI: 10.1007/s10495-018-1507-2.

Contributions

Behnaz Ahangarian Abhari made significant contributions to the work in this chapter. Contributions made include data in the following figures: 4.1, 4.2(B, C), 4.3, 4.4(B, C), 4.10, 4.12 and 4.13.

4.1 Introduction

Neuroblastoma, the fourth most frequently occurring childhood cancer, accounts for approximately 15% of all childhood cancer deaths [182]. Low survival rates and short- and long-term adverse effects from current treatments indicate that novel treatments are urgently needed for neuroblastoma patients [182, 185].

As previously discussed, treatment of cells with agents that stimulate ER stress and drive the UPR towards pro-death signalling is a potential therapeutic strategy in cancer treatment (see section 1.10.1.1) [76, 81, 243]. A number of ER stress inducers such as TM and Btz induce apoptosis in many cancer cell lines including MM, leukemia, colon, cervical cancer and prostate cancer [7, 243].

IAP proteins also serve as a potential therapeutic target in cancer as they are heavily involved in the regulation of cell death and survival [126, 274] (described in Chapter 1, section 1.5). Moreover, IAP proteins are dysregulated in a number of cancers including liver cancer, cervical cancer, MM and glioma [227-232]. Inhibition of IAPs is beneficial as a cancer treatment as it removes the negative impact of IAPs on caspase activity in cancer cells, thereby allowing the progression of cell death in tumour cells [119, 269]. Smac mimetics, which are inhibitors of IAPs, demonstrate cytotoxic effects against several cancers. For example, Smac mimetics induce apoptosis in melanoma, breast cancer, lung cancer and acute lymphoblastic leukemia (ALL) cells [351, 352].

Since both ER stress inducers and Smac mimetics are known to induce cell death in cancer cells, it was hypothesized that the combination of the two may have an additive or synergistic effect. Additionally, IAPs have been shown to play a pro-survival role in the UPR response to ER stress where the UPR promotes IAP activity [60, 61, 353]. The induction of anti-apoptotic IAPs is important for cell survival, as it delays the onset and activation of apoptosis. For example, the upregulation of *IAP* mRNA via PERK signalling during ER stress protects cells from ER stress-induced apoptosis [60-62]. Accordingly, addition of Smac mimetics during ER stress should not only prevent IAP inhibition of caspases but also impede their pro-survival role

during ER stress, sensitizing the cells to ER stress and driving the cells towards cell death.

To investigate this combination in neuroblastoma, TM was chosen as a prototypic ER stress inducer (see section 1.10.1) and BV6, was chosen as a Smac mimetic (see section 1.11) which antagonizes cIAP1, cIAP2 and XIAP. Cell death, cell viability and colony formation assays will be used to explore the combined effect of TM and BV6 treatment.

4.2 Results

4.2.1 Smac mimetic BV6 rescues paediatric cancer cells from TM-induced cell death

A combination of BV6 (4 μM) and a range of TM concentrations were applied to a number of cancer cell lines including neuroblastoma and RMS as well as glioblastoma (GBM). SubG1 fraction analysis, allows the fraction of apoptotic cells in a sample to be determined. The addition of BV6 significantly attenuated TM-induced cell death in all cell lines (Fig. 4.1).

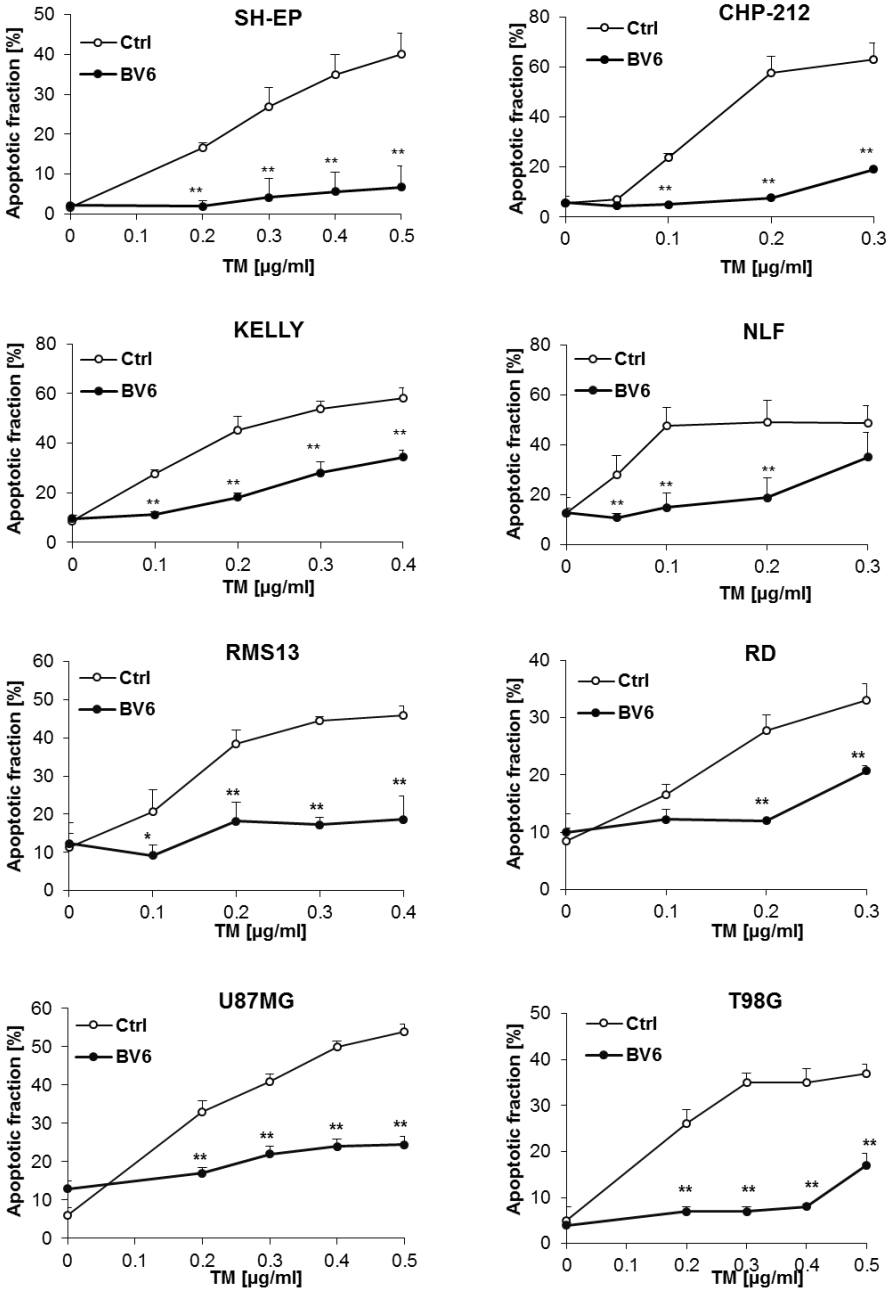

Figure 4.1: Smac mimetic BV6 rescues paediatric cancer cells from TM-induced cell death - Neuroblastoma cells (SH-EP, CHP-212, KELLY, NLF), RMS cells (RMS13, RD) and GBM cells (U87MG, T98G) were treated for 72 h with indicated concentrations of TM and/or 4 μM BV6. Apoptotic fraction of cells was determined using Nicoletti assay by measuring subG1 DNA content of PI-stained nuclei using flow cytometry. Mean ± SD of three independent experiments performed in triplicate are shown; *P < 0.05, **P < 0.01

4.2.2 BV6 protects neuroblastoma cells against TM-induced apoptosis

A time kinetic analysis showed that BV6 protected SH-EP cells against TM-induced apoptosis at all time points up to 72 h (Fig. 4.2A). Next, the precise mode of cell death involved was investigated. Treatment of SH-EP cells with TM increased subG1 fraction (apoptotic fraction) which is indicative of ongoing apoptosis (Fig. 4.2A). The addition of pan caspase inhibitor zVAD.fmk to TM treated cells significantly reduced the apoptotic fraction of cells from cell death, suggesting apoptosis is the main cell death pathway activated upon treatment with TM (Fig. 4.2B). Since caspases are major components of apoptotic signalling [84, 85], caspase cleavage and activation were also evaluated using Western blotting. TM treatment induced caspase-3, -8 and -9 activation, which was diminished following the addition of BV6 (Fig. 4.2C). The inhibition of apoptosis and caspase activation following the addition of BV6 suggests an anti-apoptotic effect of BV6.

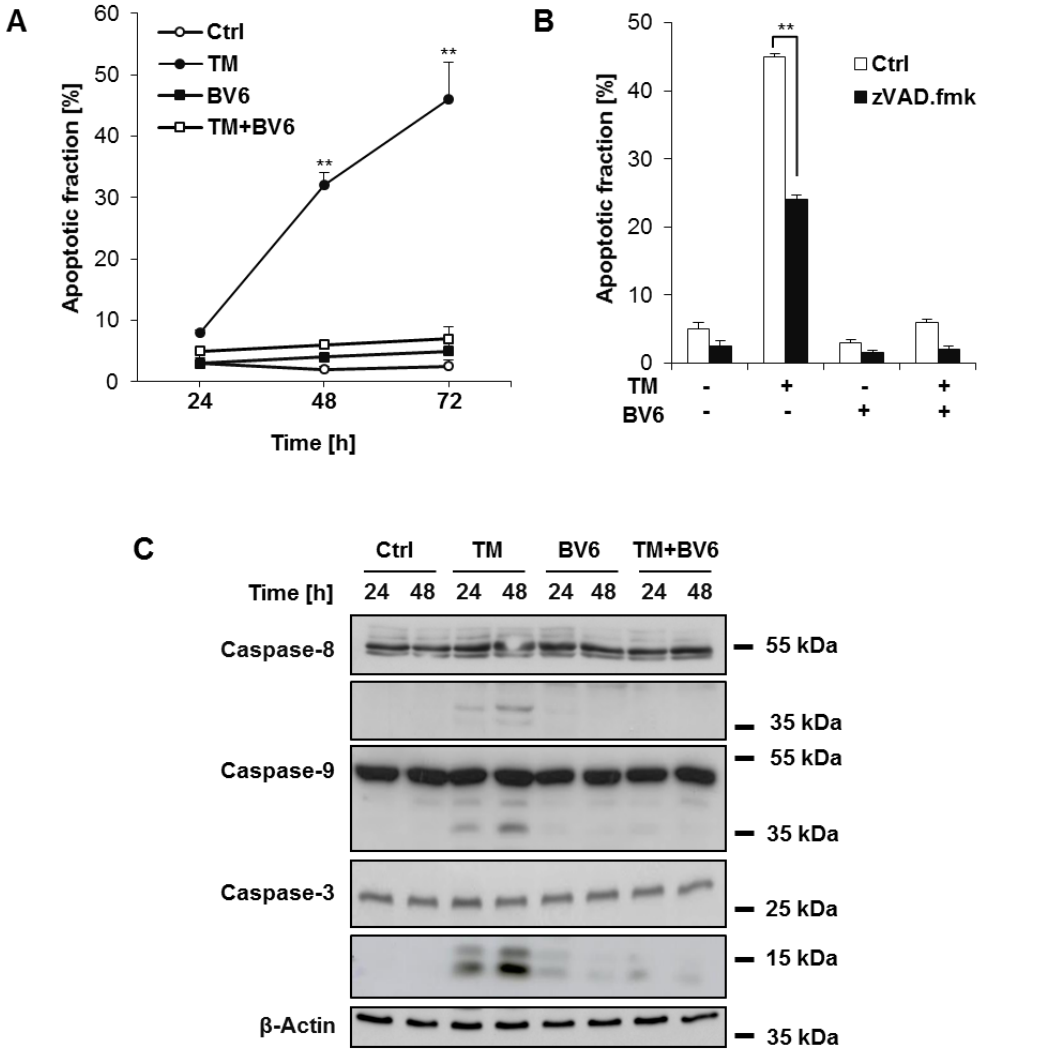

Figure 4.2: BV6 protects neuroblastoma cells against TM-induced apoptosis – (A) SH-EP cells were treated with 0.4 µg/ml TM and/or 4 µM BV6 for indicated times. Apoptotic fraction of cells was determined using Nicoletti assay by measuring subG1 DNA content of PI-stained nuclei using flow cytometry. **(B)** SH-EP cells were treated for 72 h with 0.4 µg/ml TM and/or 4 µM BV6 in the presence or absence of caspase inhibitor zVAD.fmk (40 µM). Apoptotic fraction of cells was determined using Nicoletti assay by measuring subG1 DNA content of PI-stained nuclei using flow cytometry. Mean ± SD of three independent experiments performed in triplicate are shown; **P < 0.01. **(C)** Caspase activation, following 0.4 µg/ml TM and/or 4 µM BV6 treatment of SH-EP cells for indicated times, was analysed by Western blot. β-Actin was used as a loading control. The Western blot shown is representative of three independent sets of experiments.

4.2.3 BV6 protects neuroblastoma cells from TM-reduced colony formation

To test the long-term effect of BV6 on TM treatment, a clonogenic assay was performed. BV6 significantly improved long-term survival of cells by preventing TM-induced loss of colony formation (Fig. 4.3).

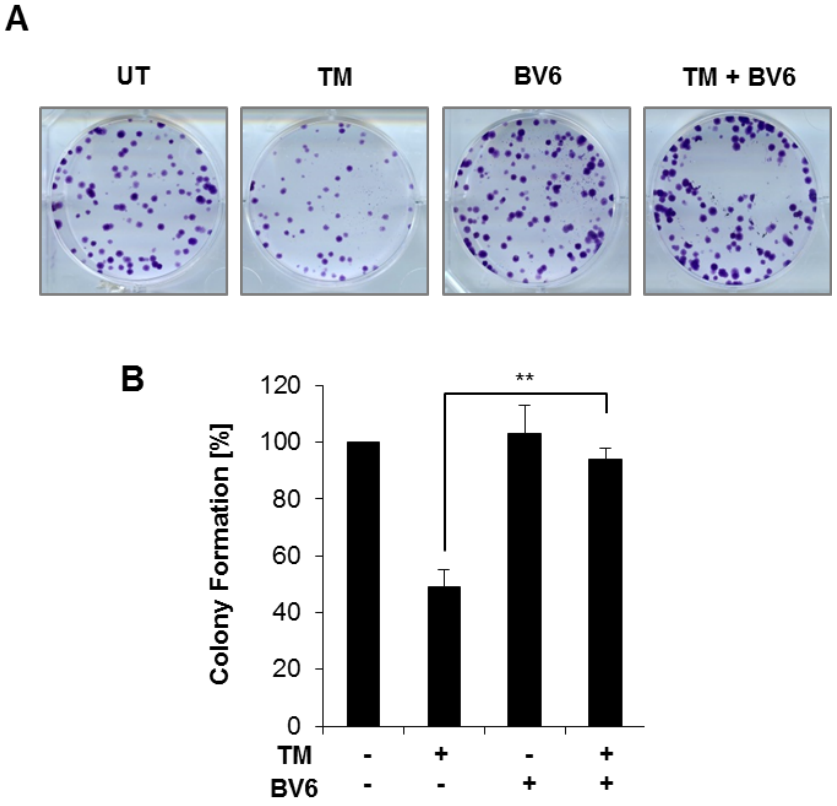

Figure 4.3: BV6 protects neuroblastoma cells from TM-reduced colony formation - SH-EP cells were treated with 0.4 µg/ml TM and/or 4 µM BV6 for 48 h. After 48 h, cells were reseeded to equal densities in regular media and colonies were left to form for 12 days. **(A)** After 12 days, cells were stained with 0.5% CV displaying fully formed colonies. One of three representative experiment is shown. **(B)** The percentage of colony formation compared to untreated control is displayed in bar chart representation Mean ± SD of three independent experiments are shown; **P < 0.01.

4.2.4 Different Smac mimetics rescue SH-EP cells from TM-induced cell death

Smac mimetics are known to stimulate auto-ubiquitination and subsequent proteasomal degradation of cIAP1 and cIAP2 [119]. To confirm that the concentration of BV6 used efficiently inhibits cIAPs, a Western blot detecting cIAP1 and 2 was performed (Fig. 4.4A). cIAP1 protein levels were diminished after treatment with BV6. cIAP2 levels were also depleted after 1 h treatment with BV6, however, protein levels were returned after 6 h. It should be noted that due to the rapid effects of BV6 on cIAP proteins, cIAP1 and 2 protein levels were only measured at early timepoints following TM and BV6 treatment and not later. XIAP protein levels were also investigated in which there was no change in XIAP protein

levels following TM or BV6 treatment (Fig. 4.4A). No change in XIAP levels was expected as Smac and Smac mimetics inhibit XIAP through direct binding, but do not result in its degradation [118, 238]. To ensure that the observed effects of BV6 are attributed to its Smac mimetic activity, additional Smac mimetics including IAP inhibitor 2, IAP inhibitor 3 and birinipant were used to assess the broader relevance of Smac mimetics. These other Smac mimetics inhibited TM-triggered apoptosis and loss of cell viability similar to BV6 (Fig. 4.4B, C), supporting the observed pro-survival effect of Smac mimetics is due to its IAP inhibition.

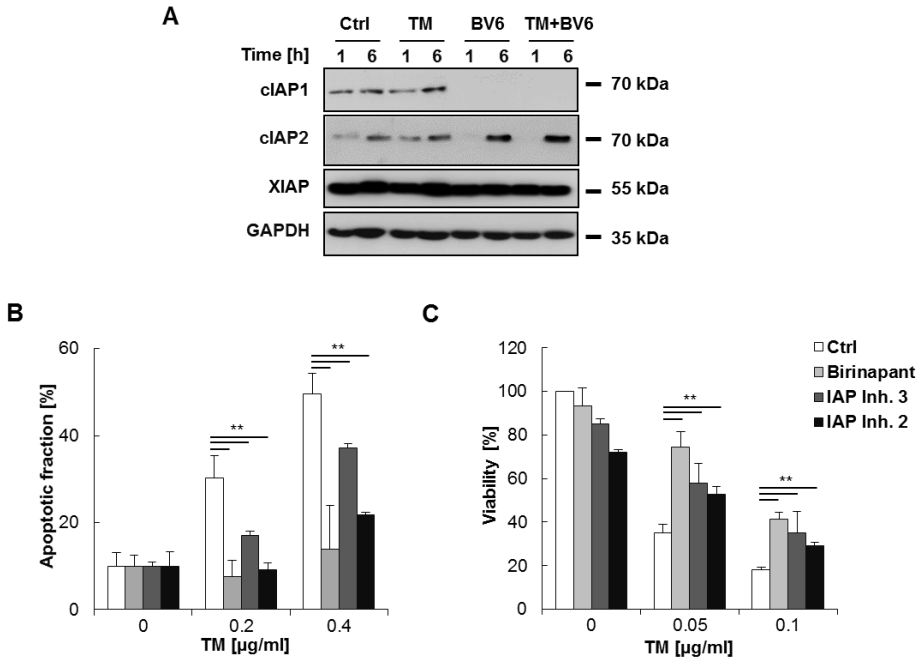

Figure 4.4: Different Smac mimetics rescue SH-EP cells from TM-induced cell death - (A) SH-EP cells were treated with TM (0.4 µg/ml) and/or BV6 (4 µM) for the indicated times (1 and 6 h). cIAP1, cIAP2 and XIAP protein level were analysed by Western blot analysis and GAPDH was used as a loading control. **(B)** SH-EP cells were treated with indicated concentrations of TM and/or different Smac mimetics (birinapant: 30 µM; IAP inhibitor 3: 40 µM; IAP inhibitor 2: 20 µM) for 72 h. Apoptotic fraction of cells was determined using Nicoletti assay by measuring subG1 DNA content of PI-stained nuclei using flow cytometry. **(C)** Cell viability was assessed using CTG and is expressed as the percentage of untreated controls. Mean ± SD of three independent experiments performed in triplicate are shown; **P < 0.01. The Western blot shown is representative of three independent sets of experiments.

4.2.5 Genetic silencing of cIAP1 and cIAP2 rescues SH-EP cells from TM-induced cell death

Due to the nature of BV6 and its inhibitory effects on cIAPs, a cIAP1/2 double knockdown was carried out to prove that genetic inhibition of IAPs induces the same anti-apoptotic effect as pharmacological inhibition. To test this, cIAP1 and cIAP2 were simultaneously knocked down using siRNAs against these genes. Efficient silencing of *cIAP1* and *cIAP2* was confirmed by detecting protein levels using Western blotting (Fig. 4.5A). As expected, combined silencing of both *cIAP1* and *cIAP2* mimicked BV6 activity and significantly rescued cells from TM-induced cell death (Fig. 4.5B). This highlights the importance of cIAP protein depletion for BV6-mediated protection against TM-induced apoptosis.

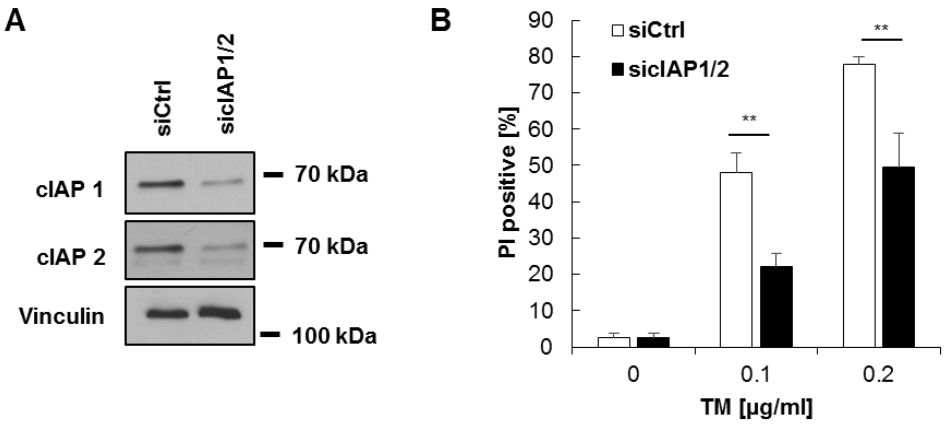

Figure 4.5: Genetic silencing cIAP1 and cIAP2 rescues SH-EP cells from TM-induced cell death - (A) SH-EP cells were transiently transfected with cIAP1 and cIAP2 (sicIAP1/2) siRNA or with control siRNA (siCtrl). cIAP1 and cIAP2 protein level were analysed by Western blot analysis and Vinculin was used as a loading control. **(B)** Following treatment of knockdown cells with 0.1 or 0.2 µg/ml TM for 72 h, cell death was determined by measuring PI/Hoechst stained cells using a Molecular Device Microscope with an automated analysis using MetaXpress Software. Mean ± SD of three independent experiments performed in triplicate are shown; **P < 0.01. The Western blot shown is representative of three independent sets of experiments.

Since other Smac mimetics and genetic inhibition of cIAPs rescued TM-induced cell death, this confirms that the anti-apoptotic effect of BV6 is specific to IAP inhibition.

4.2.6 BV6 inhibits TM-induced ER stress and UPR signalling

Next, it was decided to investigate the mechanism by which BV6 prevents TM-induced cell death and whether BV6 has a specific inhibitory effect on the UPR signalling involved in TM-induced cell death. Using Western blot, ER stress markers were investigated where TG (10 μM) served as a positive control. PERK phosphorylation, demonstrated by an upward band shift of PERK, was observed in TM treated cells. Remarkably, the addition of BV6 to TM-treated cells reduced this upward band shift of PERK indicating reduced PERK activity (Fig. 4.6A). Protein levels of GRP78 and CHOP, two key ER stress markers, were also assessed. Likewise, GRP78 and CHOP protein levels were increased following TM treatment. This upregulation was markedly reduced following BV6 addition (Fig. 4.6A). Next, IRE1 activity was investigated by detecting *XBP1s* mRNA levels using RT-PCR. TM treatment also activated the IRE1 arm of the UPR, demonstrated by increased *XBP1* splicing. Similar to its effect on PERK activation, IRE1 activity was also abolished following BV6 addition (Fig. 4.6B). Together, these results indicate that BV6 resolves TM-triggered ER stress response pathways. The observed reduction in UPR signalling correlates with BV6-mediated inhibition of TM-induced apoptosis

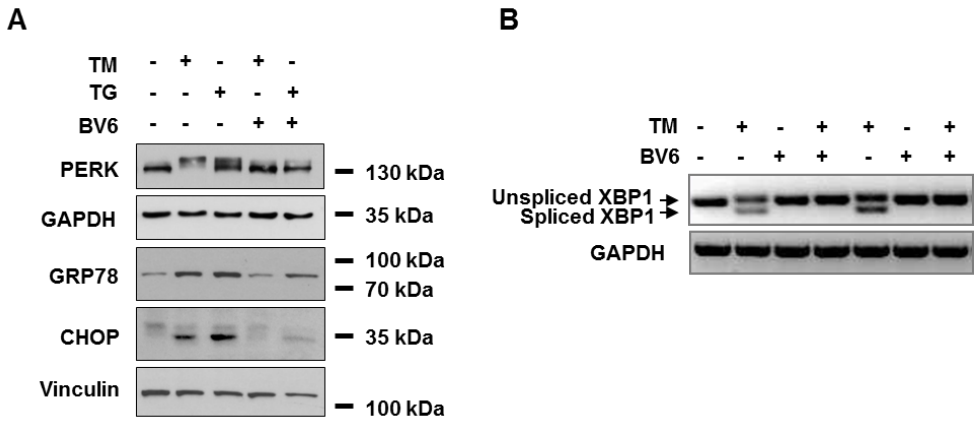

Figure 4.6: BV6 inhibits TM-induced ER stress and UPR signalling - (A) SH-EP cells were treated with 0.4 μg/ml TM and/or 4 μM BV6 for 9 h. Treatment with 10 μM TG was used as a positive control. Protein expression levels of CHOP and GRP78 were evaluated by Western blot analysis. PERK PERK activity was also examined by Western blot (indicated by an upward band shift). GAPDH was used as a loading control. The Western blot shown is representative of three independent sets of experiments. **(B)** Expression levels of *XBP1* mRNA (spliced (263 bp) and unspliced (289 bp) isoforms) were evaluated using RT-PCR.

GAPDH was used as a loading control. The RT-PCR shown is representative of three independent sets of experiments.

4.2.7 BV6-mediated protection against ER stress-induced cell death is limited to TM-induced ER stress

Since BV6 abolishes TM-induced ER stress and subsequently diminishes ER stress induced cell death, it was next asked if BV6 had the same anti-apoptotic effect on cell death induced by other ER stress inducers. For that reason, the study was extended to additional ER stress inducers with different modes of primary action such as TG, DTT, 2-DG and BFA. In contrast to its effect on TM, BV6 failed to rescue cells from cell death in response to all other ER stress inducers including TG, DTT, 2-DG and BFA (Fig. 4.7A). In fact, addition of BV6 to cells with ER stress inducers TG, DTT and 2-DG, increased cytotoxicity demonstrating a combined effect (Fig. 4.7A). To ensure that the concentrations used were comparable to the ER stress and UPR induction triggered by TM, a Western blot comparing GRP78 upregulation and PERK phosphorylation was performed comparing TM- and TG-induced ER stress. Indeed, similar ER stress and UPR induction levels were observed in both TM and TG treated cells (Fig. 4.7C) at concentrations that caused a comparable percentage of cell death (Fig. 4.7B). These data suggest that BV6-mediated protection is specific to TM provoked ER stress-induced cell death.

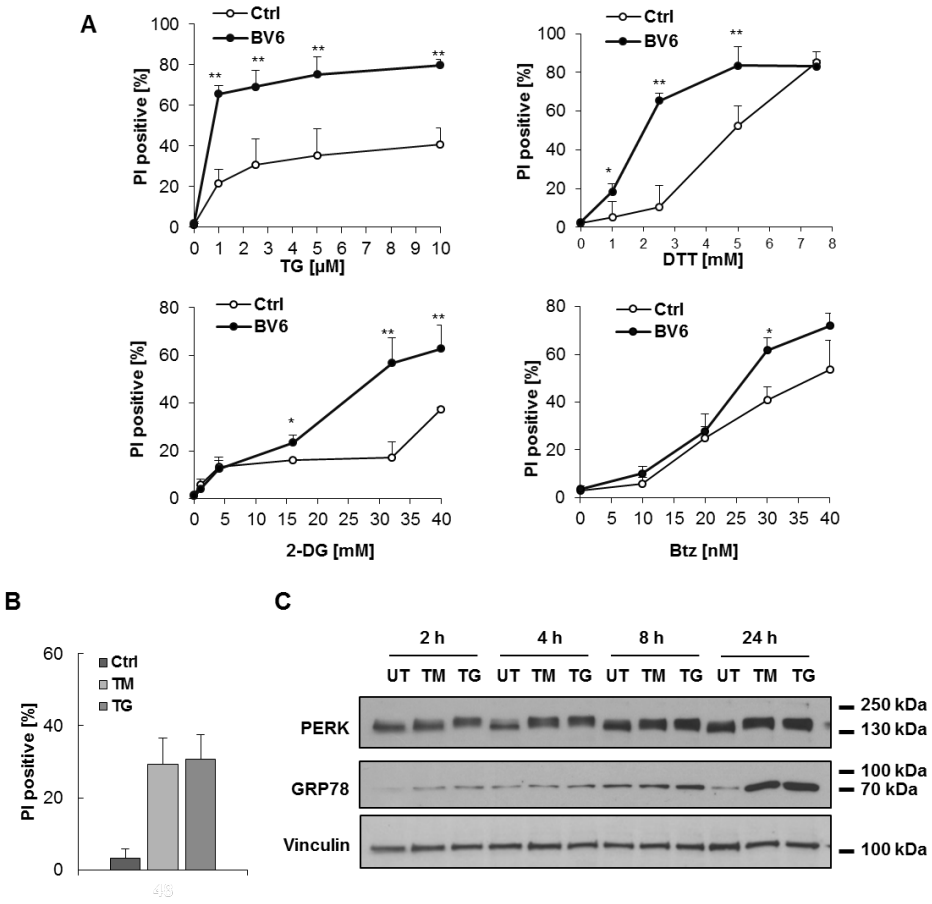

Figure 4.7: BV6-mediated protection against ER stress-induced cell death is limited to TM-induced ER stress - (A) SH-EP cells were treated with different ER stress inducers, TG, DTT, 2-DG and Btz, at indicated concentrations with or without 5 µM BV6 for 72 h. Cell death was determined by measuring PI/Hoechst stained cells using a Molecular Device Microscope with an automated analysis using MetaXpress Software. **(B)** SH-EP cells were treated with 0.4 µg/ml TM or 2.5 µM TG for indicated times. Cell death was determined by measuring PI/Hoechst stained cells using a Molecular Device Microscope with an automated analysis using MetaXpress Software. **(C)** Expression of GRP78 and activation of PERK (indicated by upward band shift) was analysed by Western Blot. Vinculin was used as loading control. The Western blot shown is representative of three independent sets of experiments. Mean ± SD of three independent experiments performed in triplicate are shown.

4.2.8 BV6 activates non-canonical and canonical NF-κB signalling in SH-EP cells

A major role of IAPs is regulating NF-κB signalling (see section 1.5). cIAPs are responsible for the activation of canonical NF-κB pathway by stimulating the removal of the IkBα inhibitory subunit from NF-κB (RelA/p50) allowing a free NF-κB dimer to translocate to the nucleus [122, 125]. The noncanonical NF-κB pathway

is normally suppressed by the continuous proteasomal degradation of NIK by cIAP1 and cIAP2 [126]. Smac mimetics, such as BV6, have been previously linked to NF-κB activation in which they activate both the canonical and non-canonical pathways [119]. Therefore, the potential role of NF-κB in this process was next investigated. Consistently, BV6 treatment caused NIK accumulation, processing of p100 to p52 and phosphorylation of IkB in the presence and absence of TM, indicative of ongoing canonical and non-canonical NF-κB signalling (Fig. 4.8A). Single treatment with TM did not affect NF-κB signalling (Fig. 4.8A). Double knockdown of cIAP1 and 2 also activated the non-canonical NF-κB signalling pathways in the presence and absence of TM confirming that IAP inhibition, both pharmacologically and genetically, induces NF-κB signalling (Fig. 4.8B).

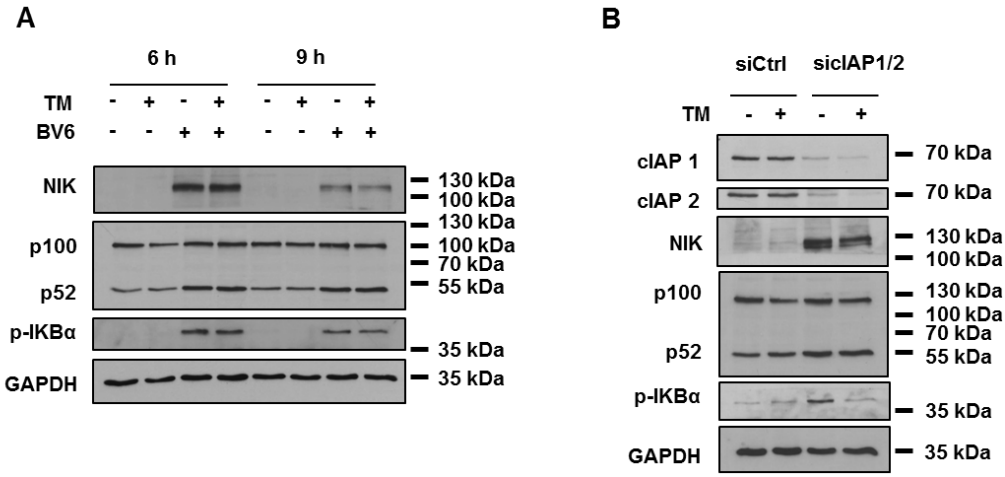

Figure 4.8 BV6 activates non-canonical and canonical NF-κB signalling in SH-EP cells - (A) SH-EP cells were treated with 0.4 μg/ml TM and/or 4 μM BV6 for the indicated times. Protein expression levels of NIK, p100/p52 and p-IKBα were evaluated by Western blot analysis and GAPDH was used as a loading control. **(B)** SH-EP cells were transiently transfected with cIAP1 and cIAP2 (sicIAP1/2) siRNA or with control siRNA (siCtrl). sicIAP1/2 and siCtrl cells were treated with 0.4 μg/ml TM and cIAP1, cIAP2, NIK, p100/p52 and p-IKBα protein levels were analysed by Western blot analysis. GAPDH was used as a loading control. The Western blots shown are representative of three independent sets of experiments.

4.2.9 BV6 activation of NF-κB signalling reduces CHOP in TM treated SH-EP cells

A direct comparison between TM/BV6 and TG/BV6 treated cells revealed a higher activation of the NF-κB components in TM/BV6 treated cells (Fig. 4.9). This NF-κB

activation, including p52 processing and IκBα phosphorylation, corresponded with a reduction in CHOP (Fig. 4.9). These data suggest that NF-κB could be an important factor involved in the prevention of TM-induced cell death in SH-EP cells as it correlates with reduced CHOP, a key pro-death signalling component of the UPR. These data imply that NF-κB may contribute to BV6-mediated suppression of TM-stimulated UPR and protection from TM-induced apoptosis

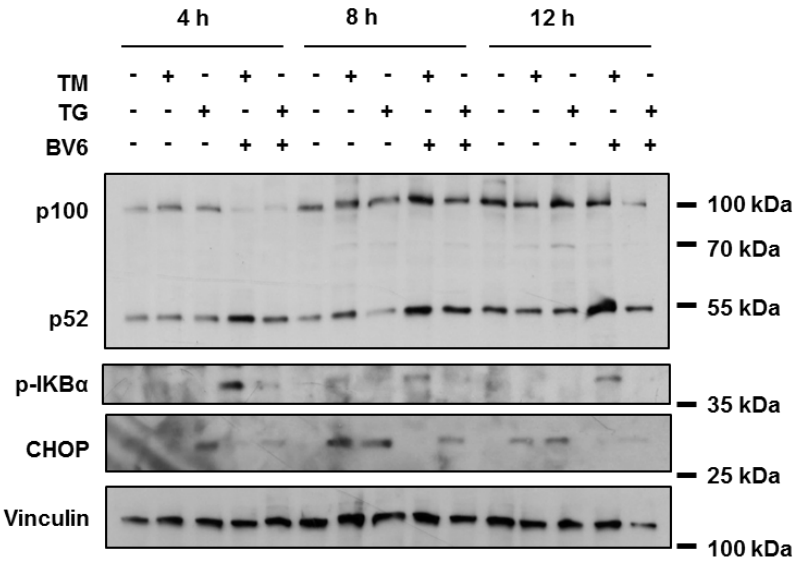

Figure 4.9: BV6 activation of NF-κB signalling reduces CHOP in TM treated SH-EP cells - SH-EP cells were treated with 0.4 μg/ml TM or 2.5 μM TG and BV6 (4 μM) for the indicated times. Expression of CHOP, p100, p52 and p-IKBα proteins were analysed using Western Blot analysis. Vinculin was used as a loading control. The Western blots shown are representative of three independent sets of experiments.

4.2.10 NF-κB contributes to BV6-mediated suppression of TM-stimulated UPR and is involved in BV6-conferred protection against TM-induced apoptosis

Since ongoing NF-κB signalling appears to decrease CHOP protein levels, we next explored whether NF-κB might be involved in the BV6-conferred protection against TM-induced UPR and ER stress. To investigate the functional impact of NF-κB, a dominant-negative super-repressor (IκBα-SR), which blocks canonical and non-canonical NF-κB signalling, was stably expressed [354]. Western blot analysis confirmed a robust overexpression of IκBα-SR and validated that it potently suppressed IκBα phosphorylation upon treatment with BV6 alone or in combination

with TM, in contrast to control empty vector (EV) cells (Fig. 4.10A). NF-κB inhibition lessened, although not completely, the BV6-imposed suppression of CHOP and GRP78 protein levels in TM/BV6 treated cells (Fig. 4.10A). These findings suggest that NF-κB contributes in part to the BV6-mediated suppression of TM-stimulated upregulation of CHOP and GRP78. As expected, BV6 significantly reduced apoptosis and restored viability in TM treated control EV cells (Fig. 4.10B, C). Importantly, this BV6-mediated protection against TM was significantly reversed in IκBα-SR cells (Fig. 4.10B, C), demonstrating that NF-κB contributes to the BV6-conferred protection from TM-induced apoptosis.

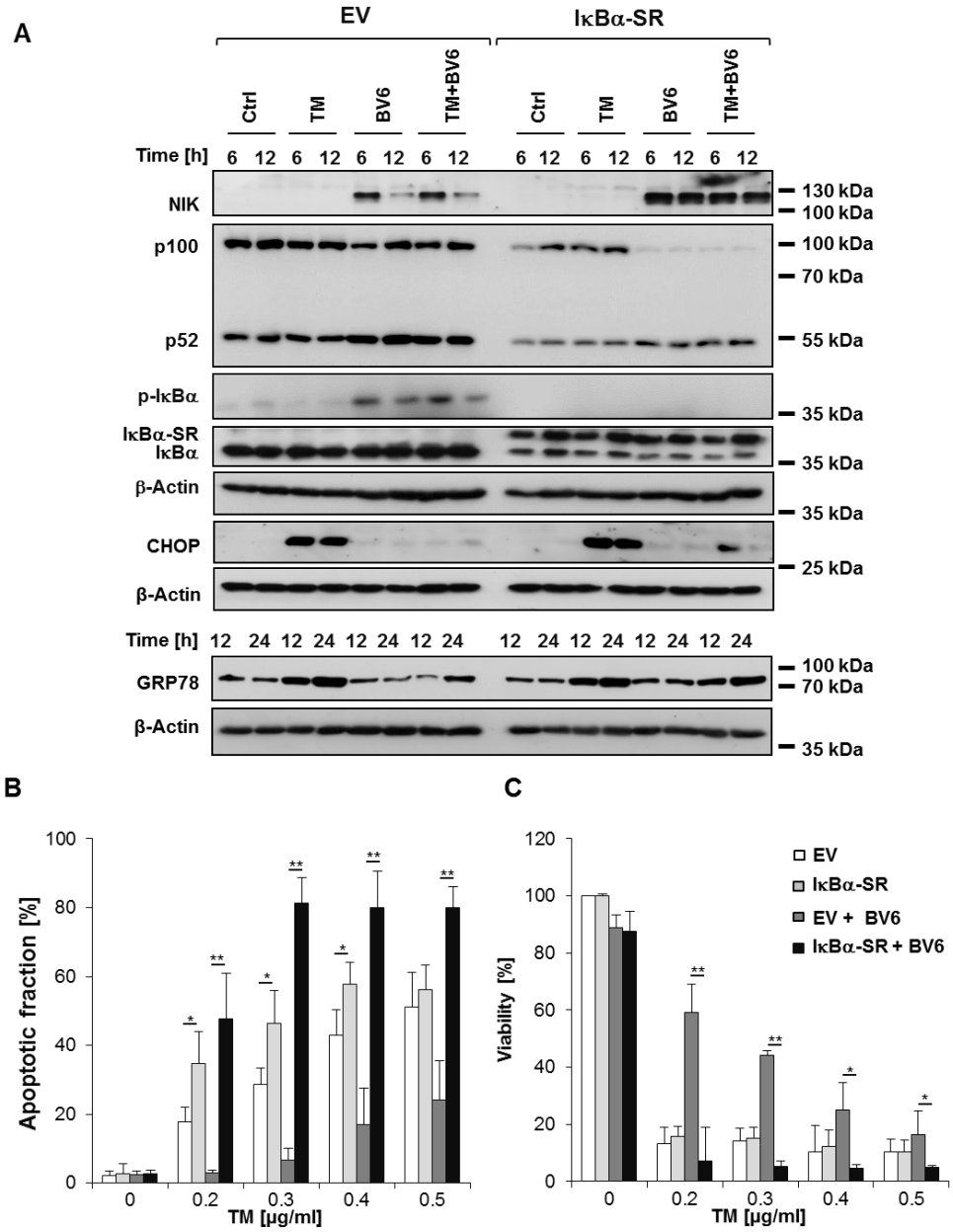

Figure 4.10: NF-κB contributes to BV6-mediated suppression of TM-stimulated UPR and is involved in BV6-conferred protection against TM-induced apoptosis - (A) SH-EP cells stably expressing IκBα-SR or vector control were treated with 0.4 μg/ml TM and/or 4 μM BV6 for the indicated times. Protein expression levels of NIK, p100, p52, p-IKBα, IκBα-SR IκBα and CHOP were analysed using Western blot analysis. β-Actin was used as a loading control. **(B)** The Western blot shown is representative of three independent sets of experiments. SH-EP cells stably expressing IκBα-SR or vector control were treated with 0.4 μg/ml TM and/or 4 μM BV6 for 72 h. Apoptotic fraction of cells was determined using Nicoletti assay by measuring subG1 DNA content of PI-stained nuclei using flow cytometry. **(C)** Cell viability was assessed using CTG and is expressed as the percentage of untreated controls. Mean ± SD of three independent experiments performed in triplicate are shown; *P < 0.05; **P < 0.01.

4.2.11 NIK contributes to BV6-conferred protection against TM-induced apoptosis

BV6-mediated depletion of cIAP proteins has been previously reported to cause NIK accumulation [119]. Consistent with this, NF-κB activation in TM/BV6 treated cells displayed considerable NIK accumulation (Fig. 4.8A and 4.11A). Knockdown of cIAP1 and cIAP2 also promoted NIK accumulation alone or in combination with TM (Fig. 4.8B and 4.11B). Therefore, the contribution of NIK to BV6-mediated protection against TM was explored next. NIK was transiently silenced using two distinct siRNAs. Efficient NIK knockdown was confirmed by measuring NIK proteins using Western blot, in the presence or absence of TM (Fig. 4.11D). Knockdown of NIK significantly inhibited the BV6-mediated protection against TM-induced apoptosis (Fig. 4.11C). This finding highlights that NIK also contributes to BV6-conferred protection against TM-induced apoptosis.

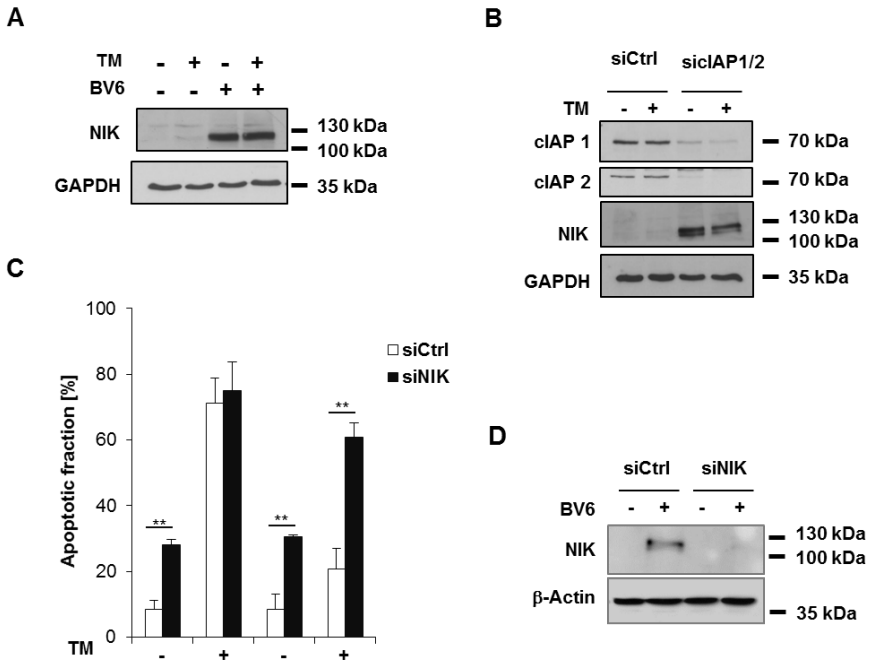

Figure 4.11: NIK contributes to BV6-conferred protection against TM-induced apoptosis - (A) SH-EP cells were treated with 0.4 µg/ml TM and/or 4 µM BV6 for 6 h. Expression of NIK protein was analysed by Western blot. GAPDH served as loading control. **(B)** SH-EP cells were transiently transfected with siRNAs against cIAP1 and cIAP2 (sicIAP1/2) or with control siRNA (siCtrl). Expression of NIK protein was analysed using Western blot analysis after 6 h of TM (0.4 µg/ml) treatment. GAPDH served as loading control. One of three representative experiments is shown for Western blots. **(C)** siCtrl and sicIAP1/2 cells were treated with 0.4 µg/ml TM and/or 4 µM BV6 and at 48 h, the apoptotic fraction of cells was determined using Nicoletti assay by measuring subG1 DNA content of PI-stained nuclei using flow cytometry. Mean ± SD of three independent experiments performed in triplicate are shown; $^{**}P < 0.01$. **(D)** siCtrl and siNIK cells were treated with 4 µM BV6 for 3 h and expression of NIK protein was analysed using Western blotting. β-Actin was used as a loading control. The Western blots shown are representative of three independent sets of experiments.

4.2.12 Upregulation of cIAP2 via NF-κB contributes to BV6-conferred protection from TM-induced apoptosis

At the beginning of this study, the expression levels of IAP proteins were analysed following BV6 treatment (Fig. 4.4A). As expected, BV6 caused rapid downregulation of cIAP1 and cIAP2 after just 1 h. cIAP2 was upregulated again after six h of BV6 treatment (Fig. 4.4A). *cIAP2* is a known NF-κB target gene [355, 356], thus, it was hypothesized that NF-κB could play a role in its upregulation following BV6 treatment. Therefore, cIAP2 protein levels were examined upon exposure to BV6 and/or TM in IκBα-SR-overexpressing and EV control cells.

Noticeably, NF-κB inhibition in IκBα-SR-overexpressing cells completely abolished cIAP2 upregulation following BV6 treatment (Fig. 4.12A), proving an involvement of NF-κB in cIAP2 upregulation. To investigate the contribution of cIAP2 to BV6-conferred protection against TM, a cIAP2 knockdown was performed using shRNA. Efficiency of the knockdown was demonstrated using Western blot (Fig. 4.12B). Importantly, apoptosis was significantly increased in cIAP2 knockdown cells following TM/BV6 treatment compared to control cells (Fig. 4.12C) demonstrating that upregulation of cIAP2 by NF-κB, contributes to the BV6-conferred protection from TM-induced apoptosis.

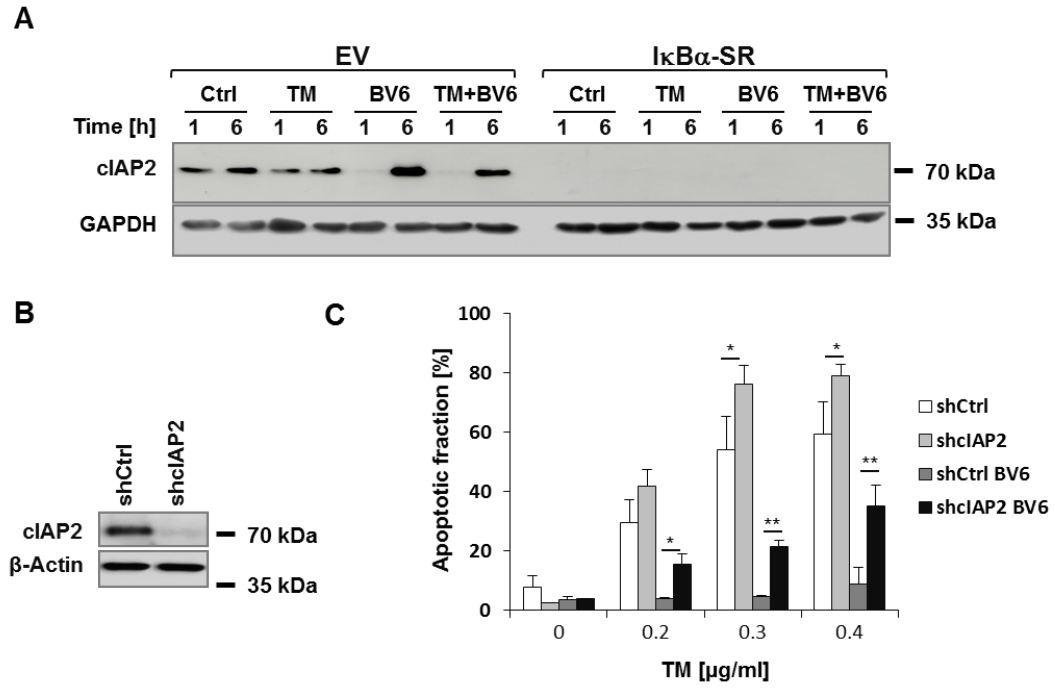

Figure 4.12: Upregulation of cIAP2 via NF-κB contributes to BV6-conferred protection against TM-induced apoptosis - (A) SH-EP cells stably expressing IκBα-SR or EV were treated with 0.4 µg/ml TM and/or 4 µM BV6 for the indicated times. Protein expression of cIAP2 was assessed using Western blot analysis. GAPDH was used as a loading control. **(B)** SH-EP cells were transduced with shRNA against cIAP2 (shcIAP2) or with an empty vector (shCtrl). Protein expression of cIAP2 was analysed by Western blotting and β-Actin was used as a loading control. The Western blots shown are representative of three independent sets of experiments. **(C)** shCtrl and shcIAP2 cells were treated with 4 µM BV6 and/or indicated concentrations of TM for 72 h. Apoptotic fraction of cells was determined using Nicoletti assay by measuring subG1 DNA content of PI-stained nuclei using flow cytometry. Mean ± SD of three independent experiments performed in triplicate are shown; *P < 0.05; **P < 0.01.

4.2.13 Upregulation of Mcl-1 contributes to BV6-conferred protection from TM-induced apoptosis

Mcl-1 is typically downregulated during ER stress due to translation inhibition [140, 141]. However, *Mcl-1* is also an NF-κB target gene that has been reported to protect cells from ER stress-induced apoptosis [59, 357]. Mcl-1 protein levels were downregulated in TM treated cells allowing apoptosis (Fig. 4.13A). Conversely, Mcl-1 was upregulated in BV6 and TM/BV6 treated cells (Fig. 4.13A). To test the functional relevance of Mcl-1 for BV6-mediated protection against TM, Mcl-1 was transiently silenced using shRNA. Knockdown of Mcl-1 was confirmed by measuring Mcl-1 protein levels using Western blot (Fig. 4.13B). Mcl-1 downregulation partially inhibited BV6-mediated protection from TM- induced apoptosis (Fig. 4.13C). It can be concluded that Mcl-1, as well as NIK and cIAP2, also contributes to BV6-mediated rescue of TM-induced apoptosis.

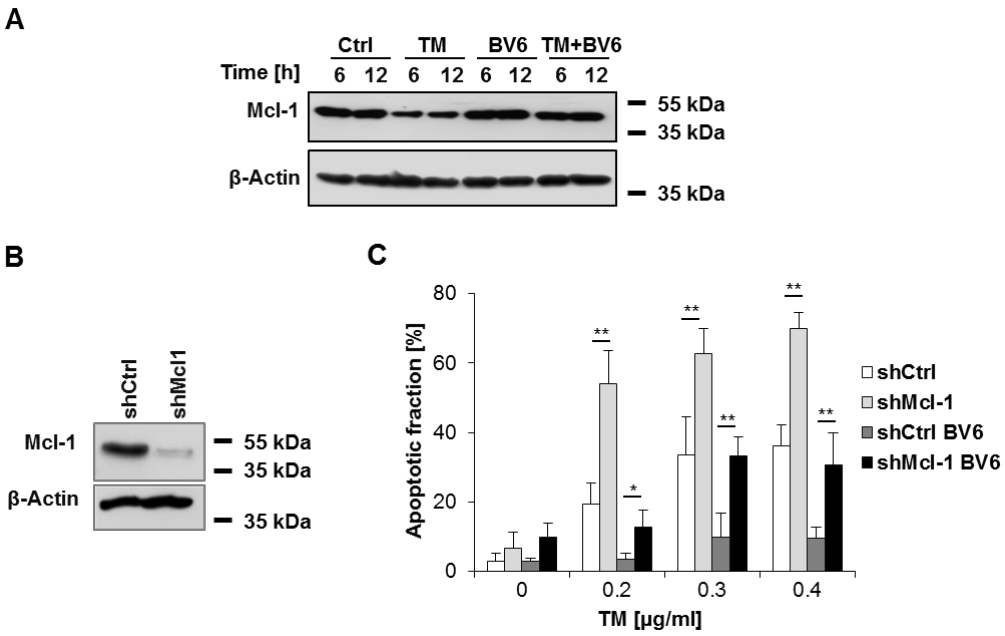

Figure 4.13: Upregulation of Mcl-1 contributes to BV6-conferred protection against TM-induced apoptosis - (A) SH-EP cells were treated with 0.4 µg/ml TM and/or 4 µM BV6 for the indicated times. Mcl-1 protein expression was evaluated by Western blot analysis. β-Actin was used as a loading control. **(B)** SH-EP cells were transduced with shRNA against Mcl-1 (shMcl-1) or with an empty vector (shCtrl). Expression of Mcl-1 protein was analysed by Western blot analysis. β-Actin was used as a loading control. The Western blots shown are representative of three independent sets of experiments. **(C)** shCtrl and shMcl-1 cells were treated with 0.4 µg/ml TM and/or 4 µM BV6 for 72 h and the

apoptotic fraction of cells was determined using Nicoletti assay by measuring subG1 DNA content of PI-stained nuclei using flow cytometry. Mean ± SD of three independent experiments performed in triplicate are shown; *P < 0.05; **P < 0.01.

4.3 Discussion

In this chapter, the effects of combined treatment of the neuroblastoma cell line, SH-EP, with TM and BV6 were investigated. Initially, we combined treatment with ER stress inducers and Smac mimetics in neuroblastoma as a potential therapeutic strategy. Unexpectedly, combination of BV6 with TM did not cause further cytotoxic effect, rather it reduced cell death under such conditions. This observation of protection against cell death was not exclusive to neuroblastoma cells, as BV6 provided protection against TM-induced cell death in additional paediatric cancer cell lines including RMS. This directed the study towards investigating the unexpected effect of BV6 on TM-induced cell death. The combination of TM with Smac mimetics or genetic inhibition of cIAPs rescued SH-EP cells from cell death by inhibiting apoptosis and preventing the activation of caspases, suggesting an anti-apoptotic effect of Smac mimetics on TM-induced cell death. In contrast, BV6 did not rescue cells from cell death induced by other prototypic ER stressors (TG, DTT, 2-DG or Btz) indicating that the BV6-mediated reduction of ER stress and cell death is specific to TM's mechanism of action. BV6 specifically abolished TM-stimulated ER stress and UPR signalling. It was revealed that pharmacological and genetic IAP inhibition stimulated activation of NF-κB signalling which contributed to the cell death rescue observed in SH-EP cells. Additionally, NF-κB-mediated upregulation of Mcl-1 and cIAP2 served an important role in this pro-survival process.

In general, mild ER stress results in an upregulation of IAPs to promote survival. Following detrimental ER stress, the UPR downregulates IAPs to promote apoptosis. Previously, this downregulation of IAPs during ER stress was thought to only be pro-death, mediating the activation of caspases and apoptosis [60]. Here, we demonstrated for the first time that inhibition of IAPs had a pro-survival role rather than a pro-apoptotic role. The data in this chapter indicate that IAPs may contribute to cell death signalling following TM-induced ER stress, as inhibition of IAPs correlated with reduced cell death induction as demonstrated by pharmacological inhibition with BV6 and combined genetic silencing of cIAP1/ and 2. . Indeed, the rapid re-expression of cIAP2 protein following BV6 treatment promoted the pro-

survival response to ER stress during TM/BV6 cotreatment.. However, a potential role of cIAP1 in ER stress-mediated cell death, that is not pro-survival, has been uncovered.

Investigation into the effect of IAP antagonist BV6 on ER stress and UPR signalling revealed that BV6 abolishes TM-stimulated ER stress and UPR signalling. To date, there are no published studies demonstrating that Smac mimetics regulate ER stress and UPR signalling or that IAP inhibition suppresses ER stress-induced apoptosis. For the first time, an important role of Smac mimetics and IAP antagonists in the regulation of ER stress signalling has been uncovered.

Previous published studies have demonstrated the combined cytotoxic effects of Smac mimetics and ER stress inducers. Ramakrishnan and colleagues demonstrated the combinatory cytotoxic effects of Smac mimetic and ER stress induction in MM. In said study, they discovered that BH3 mimetic obatoclax induced a strong UPR response in MM cells. Combining obatoclax and the Smac mimetic LCL161 demonstrated a synergistic induction of cell death in which LCL161 inhibition of IAPs was responsible for overcoming obatoclax-induced UPR pro-survival signalling [358]. Likewise, another published study demonstrated that combination of ER stress inducer Btz with the Smac mimetic birinipant induced apoptosis in MM cells [359]. In fact, in this chapter increased cytotoxic effects were observed following the addition of BV6 upon treatment with other ER stress inducers including Btz, TG, DTT and 2-DG. These data agree with the results published by Ramakrishnan *et al.,* and Zhou *et al*. [358, 359].

Activation of both the canonical and non-canonical NF-κB pathways was observed following BV6 treatment. NF-κB signalling pathways play an important role in cell survival signalling (described in section 1.5.1). The data in this chapter supports previous findings demonstrating that IAP antagonists induce NF-κB signalling via IAP inhibition [269]. Both canonical and non-canonical NF-κB signalling pathways were required for BV6-conferred protection from TM-induced apoptosis and this BV6-induced activation of NF-κB contributed to reduced ER stress activation and UPR signalling. These data are supported by previous studies that demonstrate that

NF-κB provides resistance to ER stress-induced cell death [360, 361]. Nozaki and colleagues demonstrated that NF-κB inhibits CHOP activation in breast cancer cells treated with TM, subsequently inhibiting cell death induction. The same study also revealed that the p65 subunit of NF-κB is specifically responsible for repressing CHOP promoter activity [360]. This study would imply that p65 is involved in BV6/NF-κB-mediated pro-survival signalling during TM/BV6 cotreatment. Burikhanov and colleagues discovered that the anti-apoptotic mechanism of NF-κB was due to the upregulation of UACA, a pro-inflammatory protein. UACA subsequently prevents the translocation of GRP78 from the ER to the cell surface, attenuating ER stress [361]. This would suggest that UACA may be responsible for reduced GRP78 and ER stress levels following Smac mimetic-induced NF-kB activation.

Furthermore, it was discovered that NF-κB target genes such as anti-apoptotic *cIAP2* and *Mcl-1* are upregulated following BV6 addition, as both proteins were upregulated following BV6 treatment. NF-κB can upregulate the expression of anti-apoptotic proteins such as c-IAP2 which promote cell survival [360, 362]. NF-κB signalling has also been linked to the regulation of anti-apoptotic Mcl-1 protein, promoting its expression [363, 364]. Here, the addition of BV6 restored Mcl-1 levels during TM treatment. The simultaneous upregulation of cIAP2 and Mcl-1 contribute to the BV6-mediated rescue of TM-induced cell death, as genetic knockdown of either of the two proteins significantly blocked the BV6-triggered rescue of TM-induced cell death. Knockdown of these proteins significantly rescued cells from cell death, albeit not completely. Incomplete protection from cell death could be due to knockdown inefficiency or compensation from the other key proteins involved in the process such as Mcl-1 in the case of cIAP2 knockdown and cIAP2 in the case of Mcl-1 knockdown. Interestingly, in the previously mentioned study which demonstrated that ER stress induced-cell death by Obatoclax was enhanced when combined with Smac mimetic LCL161, the ER stress inducing compound obatoclax is an inhibitor of Mcl-1 [358]. Thus, unlike in TM/BV6 treated SH-EP cells in which Mcl-1 is upregulated following TM/BV6 treatment, Mcl-1 is inhibited allowing cell death induction. These data support an important pro-survival role for Mcl-1 in BV6-

mediated pro-survival signalling and that removal of this anti-apoptotic protein promotes cell death.

In this chapter, the ATF6 arm of the UPR was not investigated. Therefore, we cannot comment on the involvement of ATF6 in this BV6-mediated suppression of TM induced ER stress. Several studies have demonstrated ATF6 activation following TM treatment in cells [365-367]. To identify any potential role of ATF6 in this process, ATF6f protein levels in addition to expression levels of its target genes, could be investigated. Previous studies have demonstrated that ATF6 activates NF-κB in cells [368, 369]. If ATF6 signalling is not completely attenuated by BV6, it could potentially promote and contribute to NF-κB signalling observed in this study.

Taken together, these data are the first to show that Smac mimetics protect cells from TM-triggered apoptosis by resolving the UPR and ER stress. These data provide insights into the regulation of cellular stress responses by Smac mimetics and the context-dependent role of NF-κB in the cellular response to Smac mimetics. The anti-apoptotic function of NF-κB on TM-induced ER stress response has important implications for developing Smac mimetics as cancer therapeutics. This protective function of Smac mimetics on TM-induced apoptosis has a broad relevance not only for structurally different Smac mimetics, but also for several cancer entities. Altogether, the findings in this chapter point to a potential pitfall for cancer treatment, and emphasize that the combination of ER stress inducers such as TM with Smac mimetics in cancer treatment must be carefully evaluated. Nonetheless, several ER stress inducers including TG, 2-DG and Btz displayed cytotoxic effects against neuroblastoma alone or in combination with the Smac mimetic BV6. In fact, the cytotoxic effect of BV6 on neuroblastoma cells was enhanced with 2-DG, TG and Btz. Recently, similar results were published where combination of Btz and the Smac mimetic birinipant synergistically induced apoptosis in MM [359]. Although Smac mimetics prevent TM toxicity against neuroblastoma cells, these data reveal that the BV6 combination with other ER stressors is still a potential therapeutic strategy for neuroblastoma.

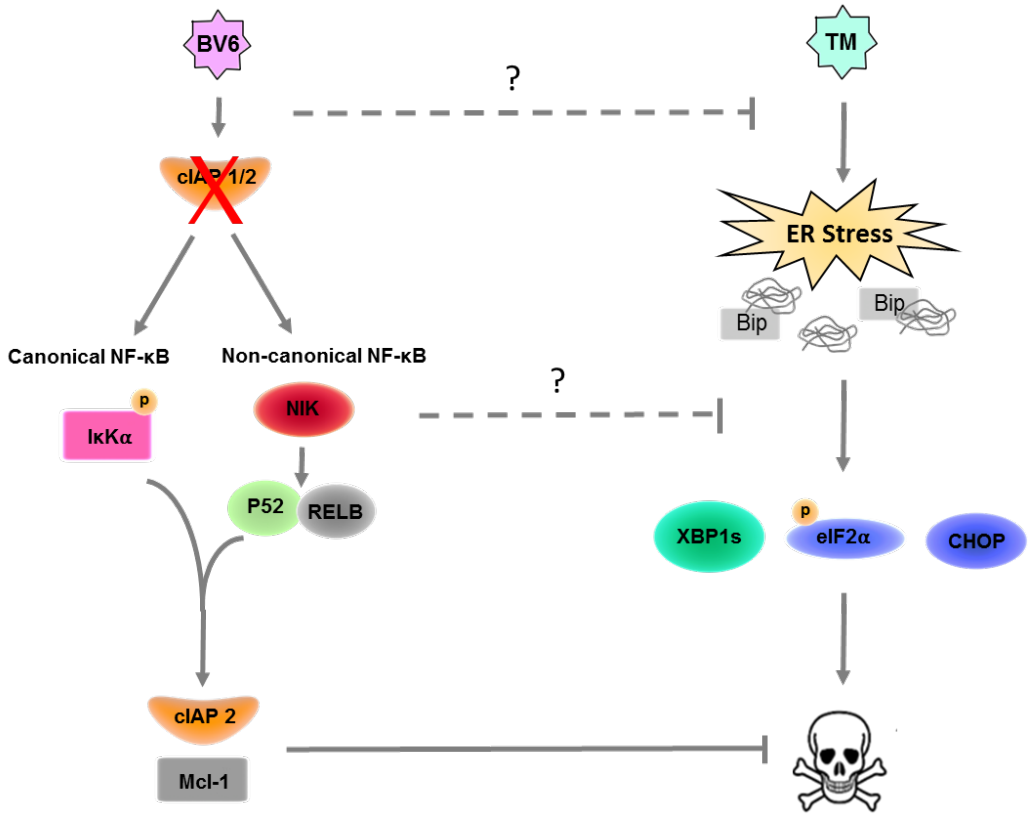

Figure 4.14: The anti-apoptotic effect of Smac mimetic BV6 on TM-induced cell death

Schematic diagram representing the data uncovered in this chapter. BV6 prevents ER stress induction by blocking TM induced ER stress and subsequent UPR activation. BV6 simultaneously upregulates both the canonical and non-canonical NF-κB pathways. NF-κB promotes pro-survival signalling through upregulation of anti-apoptotic proteins including cIAP2 and Mcl-1.

Chapter 5: General Discussion and Outlook

5.1 Research Challenges for Paediatric Cancer Therapy

One of the major problems associated with paediatric cancer treatment progression is drug identification. Normally, cancer drug research focuses on frequently occurring adult cancers such as breast cancer, lung cancer, prostate cancer and colon cancer [370]. Childhood carcinomas differ greatly from adult cancers so many target agents developed to inhibit specific pathways in adult carcinomas have little or no effect against childhood malignancies [165]. Thus, it is necessary to generate novel agents that specifically target childhood cancers. Since childhood cancers occur in such low numbers, they are not considered a focus in research or a priority for research funding [371, 372]. The potential for financial return for pharmaceutical companies from developing specific childhood cancer drugs is also 'low', making them less likely to invest in drug research and development specifically targeting these childhood cancers [372, 373]. The insufficient efforts in paediatric cancer research needed to produce new drugs as well as generate preclinical information for novel or previously identified drugs, contributes greatly to the lack of improvements in childhood cancer care [372]. Since there is shortage of novel and specific drugs for childhood cancers, paediatric oncologists and researchers turn to clinically approved adult cancer drugs to be used in the treatment of children with cancer [165]. A number of agents effective against adult malignancies can have anticancer effects against some childhood cancers [165, 374]. To address some of the difficulties associated with paediatric cancer treatment development, in this thesis the aim was to identify potential compounds that could have therapeutic value and potential uses in paediatric cancers. To this end, pre-clinical testing of several compounds were performed on paediatric cell lines. Several compounds were identified that could have the potential to progress towards further testing in paediatric cancer i.e. UPR inhibitor treatment of RMS in Chapter 3 and ER stress inducers in Chapter 3 and 4.

For years now, cancer therapy has relied heavily on cytotoxic treatment approaches such as chemotherapy and radiation. Currently, radiation, chemotherapy and surgery are the most commonly used treatment methods for paediatric cancer [374]. Such

cytotoxic treatments aim to eradicate tumours by ensuring complete destruction and removal of all tumour cells. Although these approaches have been successful in total tumour eradication and overall increased patient survival, they are also associated with acute- and long-term adverse effects in patient [164]. This is mainly due to their lack of specificity and their detrimental toxic effects on healthy non-malignant cells, resulting in severe side effects. To overcome the harsh side effects associated with generic cytotoxic agents in children with cancer, new targeted and non-toxic compounds need to be developed and/or tested. To tackle this issue, in this thesis, we identified compounds that could potentially replace the current conventional cytotoxic treatments and therefore hold the potential to be more effective while presenting less side effects. UPR inhibitors, ER stress inducers and other drugs targeting cell survival and cell death pathways were investigated, alone or in combination, in a number of paediatric cancer cell lines.

The use of targeted therapies is assumed to confer greater specificity and fewer side effects compared to chemotherapeutics. Side effects of new therapies are most commonly identified in *in vivo* models [375]. One of the major limitations in this thesis is the fact that all studies were carried out *in vitro*. Systemic side effects were not assessed and we were unable to confirm whether the compounds tested would have lower side effects than conventionally used drugs. Nonetheless, in chapter 3, UPR inhibitors were tested on non-malignant cell lines which displayed no altered viability or proliferation, which is promising regarding potential side-effects on healthy tissue. To confirm the effects of a drug and its potential as a therapeutic agent, primary sample testing and *in vivo* tests are necessary. A number of mouse models have been established for RMS [335] and neuroblastoma cancers [376]. CAM assays, which monitor tumour growth, invasion, angiogenesis and metastasis *in vivo*, could also be used to validate the potential clinical effects of the compounds used in this study [334]. However, the focus of this thesis was cell-based only which is why *in vivo* testing was not performed. *In vitro* studies are important tools in cancer research as they are imperative for investigating the molecular mechanisms of tumour cells and for identifying therapeutic targets for cancer treatments. Cancer cell lines and *in vitro* studies are of significant value for drug development as they provide substantial supportive evidence for their potential use in therapy.

5.2 Targeting the UPR in Cancer

In recent years, the UPR has been implicated in cancer (described in Chapter 1 section 1.8) and has become a topic of interest in cancer therapy research due to its connection and contribution to various hallmarks of cancer, in addition to its potential as a cell death inducer. In this thesis, the potential of UPR targeting drugs as paediatric cancer treatments was explored. There are two ways to target the UPR in cancer: First, the inhibition of UPR signalling to block pro-survival signalling or second, induction of UPR signalling to drive the cell towards cell death. In theory, targeted therapies with either of these mechanism of actions could be used in the treatment of paediatric cancers. To investigate this, different UPR inhibitors and inducers were tested on a range of different paediatric cancers including RMS and neuroblastoma.

TME characteristics, such as oxygen and nutrient deprivation, are known to be major cancer cell stressors, resulting in UPR signalling activation [208, 377]. Consistently, the studies in this thesis confirm that UPR modulators, both inducers and inhibitors, affect a panel of paediatric cell lines by either inducing cell death or blocking proliferation. It should be noted that since the present study relied heavily on the use of *in vitro* testing, additional stresses induced by the TME were not accounted for. Added stress from the TME could contribute to the effects seen with the treatments used in this thesis. For example, cancer cells that are dependent on increased UPR pro-survival signalling provoked by TME stresses could be much more sensitive to UPR inhibitors. On the other hand, ER stress induction and UPR activation from the TME in addition to ER stress inducers could intensify UPR signalling and subsequently enhance cell death signalling [208]. In both instances, lower doses could perhaps be used to increase specificity and decrease side effects. Conversely, activation of the UPR by TME could activate pro-death signalling which, following the addition of UPR inhibitors, could be prevented, giving rise to increased cancer cell survival [208]. Therefore, it is important to use experimental models which account for the complex surrounding dynamics in tumours, mimicking actual tumour environments in order to investigate the effect of these extracellular conditions on treatment responses. Again, one way to investigate this is the use of *in vivo* models.

5.3 Inhibiting the UPR as a Cancer Therapy

Innovative targeted anticancer drugs concentrate on targeting cellular elements and pathways that are involved in the transformation and/or progression of the cancer. The use of anticancer drugs that target specific qualities in paediatric cancers could hold the key to successfully treating paediatric cancers, raising survival rates and reducing detrimental side effects that are associated with current conventional chemotherapy. Since the UPR is upregulated in several cancers and is linked to the development, progression and survival of a number of cancers, then direct targeting of the UPR is an attractive therapeutic target in cancer. A plethora of research has demonstrated that UPR inhibition has robust anticancer effects including reduced growth, reduced proliferation, reduced invasion and reduced angiogenesis. For example, PERK inhibitor GSK2656167 preclinical testing demonstrated reduced tumour growth of MM and pancreatic tumours in mouse models [258, 259]. IRE1 inhibitors STF-083010, MKC3946 and 4μ8c also reduce growth in a number of cancer cells including breast cancer, MM and prostate cancer [198, 199, 201, 249, 250, 252]. In chapter 3 of this thesis, it was confirmed that UPR inhibitors reduced proliferation and replicative ability of RMS cells following IRE1 and PERK inhibition.

In order for UPR inhibitors to be successful as an anticancer therapy, then it is important that the tumour entity possesses basal UPR activity, as otherwise, UPR inhibitors may have no effect. Prior to treatment with UPR inhibitors, it is necessary to test and confirm that the tumour entity displays a robust UPR activity. This can be achieved with the use of biopsies, which will allow the prediction of treatment responses. Biopsy analysis are not only useful for predicting treatment responses but can also be valuable for predicting patient outcomes. For instance, increased UPR signalling has been shown to dictate tumour phenotypes and patient outcomes. Thus, identifying aberrant UPR signalling can be used as a prognostic tool. For example, Lhomond and colleagues discovered that increased IRE1 signalling is associated with increased tumour angiogenesis, invasion and migration in GBM tumour cells. In addition, this higher IRE1 activity correlated shorter patient survival [378].

Not only has inhibition of the UPR revealed a potential therapeutic target in RMS, but it has also enabled a better understanding of UPR signalling in the context of this disease. In this thesis, through the use of UPR inhibitors, it was discovered that the UPR is involved in promoting the indefinite replicative ability in RMS cells (Chapter 3). This study focused on the effect of UPR inhibition on death, survival, replication and proliferation. As discussed in Chapter 1 section 1.8, the UPR is also implicated in several other cancer characteristics. For example, UPR signalling has been shown to promote angiogenesis, invasion and metastasis in cancer [6]. In the case of angiogenesis, the IRE1 and PERK arms of the UPR upregulate VEGF and promote angiogenesis which in turn supplies cancers with sufficient blood and nutrients [209]. For example, IRE1 signalling has been shown to promote VEGFA production and angiogenesis in TNBC and glioblastoma, rendering IRE1 inhibition an attractive therapeutic target to prevent angiogenesis [210, 326, 379]. Impeded IRE1 signalling in *in vivo* xenografts results in reduced levels of VEGFA, reduced blood vessel formation and significantly smaller xenograft sizes compared to their wildtype counterparts [210, 326, 380, 381]. On the other hand, the RIDD activity of IRE1 has been shown to play an anti-tumourigenic role by reducing tumour angiogenesis and tumour cell invasiveness [378]. Thus, inhibition of IRE1 signalling could have contradictory effects. Investigation of RIDD activity and angiogenesis and invasion following IRE1 inhibition in RMS would underline any critical roles of RIDD in these processes. The investigation of angiogenesis, invasion and metastasis was beyond the scope of this thesis and was not evaluated. To fully characterise the role of the UPR in RMS, and the consequences of UPR inhibition in RMS, investigation into other hallmarks of cancer following UPR inhibition may provide additional insights into UPR involvement in RMS biology.

Targeting the UPR in the clinic presents a number of challenges. One of the potential pitfalls of using UPR inhibitors is unwanted side effects. Many cells rely on the UPR for managing ER stress and maintaining homeostasis. For example, certain cell types such as antibody-producing B-cells or insulin-secreting β-cells place high demands on ER function [333, 382]. The UPR is also necessary for the protection of cells from acute injury and pathogens [4, 383]. In addition to the immediate actions of UPR in response to misfolded or unfolded proteins, there are many broader roles of

the UPR such as in cell differentiation, development and metabolism [1]. Thus, inhibition of this response could be detrimental to healthy tissue cells. For example, the IRE1 RNase inhibitor 4μ8c function was found to introduce non-specific effects such as insulin secretion inhibition and antioxidant activity in mouse models [384, 385]. Likewise, PERK inhibitors, GSK2606414 and GSK2656167 were also described to have off-target effects such as pancreatic toxicity and hyperglycemia as a result of loss of acinar and β-cells which are highly dependent on PERK for viability [253, 254, 386]. Since MKC8866 and AMGEN44 are relatively new compounds, their long-term effects in humans are currently unknown. Indeed, studies have confirmed that MKC8866 is not toxic in mouse models following long-term administration [198, 251], thus displaying promising clinical potential. Currently, MKC8866 is in clinical trial where it has so far not shown any adverse side effects (NCT: 03950570). PERK inhibitor, AMGEN44 has been shown to be more specific than GSK2606414 and GSK2656167, hopefully reducing the unwanted side effects that were previously associated with GSK2606414 and GSK2656167. Nonetheless, this study as well as other literature have highlighted the potential of UPR inhibitors in cancer therapy due to their undeniable anticancer effects in preclinical studies. It was also confirmed that this UPR inhibition has no effect on the survival of genetically similar non-malignant cell lines. However, as demonstrated by unwanted side effects associated with previous UPR inhibitors, caution must certainly be taken during progression to clinical settings.

5.4 Inducing Cell Death as a Cancer Therapy

For many paediatric cancer therapies, including radiation and chemotherapy, the main mechanism of action is cell death induction by ultimate poisoning of cancer cells [387]. For years, this has been the desired mode of action for cancer therapy and is still a main focus of research efforts as it ensures the complete destruction of the tumour. However, the need for less severe and less toxic compounds is huge. Two approaches in which cell death can be induced in paediatric cancer cells include direct targeting of cell death signalling pathways or by provoking ER stress-induced cell death. A better understanding of the regulatory mechanisms that control these cell death signalling pathways is necessary for the identification of new targets for

cancer treatment and to also identify potential strategies to overcome therapy resistance [388].

5.4.1 Targeting cell death pathways for cancer therapy

Apoptosis is commonly dysregulated in human cancers [225]. Manipulation of the apoptotic pathway not only facilitates tumour formation and progression, but also enables treatment resistance [388]. Therapeutic opportunities to exploit apoptosis for cancer therapies involve either targeting cell death receptors to activate extrinsic pathway or by targeting key players involved in the intrinsic pathway of apoptosis [388]. Intrinsic apoptosis is tightly regulated by a number of factors including pro-apoptotic and anti-apoptotic Bcl-2 family proteins [389, 390]. Thus, two strategies for targeting and promoting intrinsic apoptosis in cancer cells is by either enhancing pro-apoptotic signals or neutralising anti-apoptotic proteins [390]. Several small-molecule inhibitors have been developed to target anti-apoptotic Bcl-2 proteins such as BH3 mimetics that inhibit anti-apoptotic Bcl-2 proteins including Mcl-1, Bcl-2 and Bcl-xL [390, 391]. BH3 mimetics are a promising new class of anticancer agents that exhibit cytotoxic effects on a number of cancer cell types. For example, BH3 mimetics activate apoptosis as a single agent in neuroblastoma [392]. Combination of BH3 mimetics with other anticancer drugs also show promising therapeutic value. For example, BH3 mimetics such as ABT-199 sensitise RMS cells to apoptosis when combined with chemotherapeutic agents including vincristine, actinomycin D, cyclophosphamide, etoposide and doxorubicin [391].

IAP proteins are also major negative regulators of apoptosis and are upregulated in several different cancer types making them an attractive therapeutic targets in cancer [227, 390]. Smac mimetics that antagonise IAP proteins such as BV6 have demonstrated cytotoxic effects against cancer cell types including, leukmeia, MM, fibrosarcoma and lung cancer [238, 270, 271]. Smac mimetics are not yet used in clinics, however, there are a number of ongoing clinical trials testing Smac mimetics as anticancer treatments [227]. These clinical trials include Smac mimetic treatment of patients with MM, advanced solid tumours and hematological malignancies (NCT0195543, NCT04122625, NCT03386526) [125, 393]. Phase 1 clinical trials revealed complete remissions of patients with ovarian carcinoma and mucosa-

associated lymphoid tissue lymphoma following administration of the Smac mimetic GDC-0917 (NCT01226277) [394]. Although various Smac mimetics are well tolerated as single agents, a number of Smac mimetics have demonstrated adverse side effects such as nausea, vomiting and rashes when used as a single agent [125, 227]. Nonetheless, both pre-clinical testing and clinical trials show promising potential for the use of Smac mimetics in targeting cancer cells for cell death. Furthermore, treatment of cancer cells with Smac mimetics in combination with other treatments such as radiation, chemotherapeutics, death receptor agonists, demonstrate particular promise as an anticancer strategy [95, 238, 239]. Thus, the combinatory effects of Smac mimetic BV6 with ER stress inducers was investigated in Chapter 4. This is discussed further in section 5.5.2.

In this thesis, only apoptotic cell death is investigated, however, there are several other forms of cell death with therapeutic potential for cancer treatment such as ferroptosis, an iron dependent form of cell death, or necroptosis, a caspase independent form of cell death [7]. Previous studies demonstrate that necroptosis and ferroptosis inducing agents have potential clinical value. Daechert *et al*., revealed that oxidative stress-inducer Erastin induces ferroptotic cell death in RMS cells [395]. Frank and colleagues discovered that treatment of HT29 cells with interferons and cell cycle arrest-inducing agents induces necroptosis [396]. Thus, for cancer cells resistant to apoptosis these cell death inducing mechanism are an alternative approach to inducing cell death. Since ER stress inducers including Btz and TM preferentially activate apoptotic signalling pathways (as demonstrated in chapter 4 and chapter 5), we did not delve further into any other forms of cell death.

5.4.2 Inducing ER stress as a cancer therapy

Since the UPR is known to induce cell death following prolonged or extensive stress, the application of ER stress inducers to cancer cells could drive the cells towards death. In both chapters 3 and 4, proteasome inhibitors Btz and Carf had cytotoxic effects against RMS and neuroblastoma cell lines. These data are supported by a number of studies that demonstrate that proteasome inhibitors induce apoptosis in paediatric cancer cell lines including neuroblastoma [345, 397-403]. Although Btz is FDA approved for the use against MM [344-347] it has been linked to having

negative side effects such as GI symptoms, fatigue, nerve damage and platelet deficiency when used as a single treatment [404]. In Chapter 4, TM induced cell death in a number of different paediatric cancer cell lines. These findings are supported by vast amounts of literature where TM treatment of several cancer cell lines leads to ER stress induced cell death [7]. Unfortunately, TM is also not favoured for use in clinics due to lack of specificity and high toxicity [404-407]. The development of newer ER stressors that are more specific to cancer cells would be beneficial. For example, disulfide bond disrupting agents (DDAs) are promising agents for cancer treatment since they are potent ER stress inducers and are shown to be more selective for cancer cells [7, 408, 409]. On the other hand, combination therapies involving ER stress inducers could serve as potential therapeutic strategies (discussed further in Section 5.5.2). If combined with other commonly used cancer treatment drugs, lower doses could be used for both, consequently reducing unwanted side effects.

5.5 Combining UPR targeting drugs with other anticancer drugs

The potential success of either ER stress inducers or UPR inhibitors as single anticancer agents remains uncertain. Nevertheless, both inducers and inhibitors of the UPR have been shown beneficial in combination with other anticancer drugs in a number of different cancers where combinations can induce cell death or reduce tumour growth.

5.5.1 Combining UPR inhibitors with anticancer drugs

In chapter 3, UPR inhibition in RMS cells resulted in a considerable reduction in cell proliferation. This reduced proliferation corresponded with a significant number of senescent cells, suggesting that IRE1 and PERK inhibition induces senescence in RMS cells. TIS is associated with reduced tumour growth and size which is undoubtedly promising as an anticancer therapy as it enhances patient survival [293]. TIS could be utilised for the chronic management of some cancers or prior to surgery in order to prevent tumour growth and/or reduce the tumour size, for example, in patients who are not immediately suitable for surgery due to age or illness complications [410]. Furthermore, TIS is also promising in relation to cancer cells

with compromised cell death pathways [222]. However, senescence is in some ways controversial due to its potentially harmful properties including its ability to be reversed, the potential of cell cycle re-entry, its SASP signalling effect on surrounding cells, and its ability to induce inflammation [338-341]. Combination therapies are suggested as a precaution to ensure complete removal of the senescent cells to avoid cancer cell recurrence or damaging side effects. Agents capable of inducing cell death in senescent cells are known as senolytics [222]. For example, BH3 mimetic and BCL-W and BCL-xL inhibitor ABT-737 specifically induces apoptosis in senescent cells [311]. A two-hit synthetic lethal approach that first evokes senescence and then subsequently eliminates the senescent cancer cells shows great promise as a new therapeutic strategy for cancer treatment [341]. Two drugs were identified in which cytotoxicity was enhanced following the addition of the IRE1 RNase inhibitor MKC8866. It is important to note that UPR signalling can be both pro- and anti-senescence as mentioned in Chapter 1 section 1.8.5. Here, it was determined that the UPR plays an anti-senescence role in RMS and inhibition of this results in senescence induction. Senescence is still relatively uncharted territory and caution must be taken when considering it as a therapeutic approach. Further characterisation of senescence and investigation into its effects will determine its potential as a therapeutic strategy.

Cancer treatments such as chemotherapy and radiation likely act as severe stress stimuli on cancer cells, which potentially induces ER stress and UPR signalling. The UPR is known to act as an adaptive mechanism of cancer cells following pharmacological treatment, allowing the cell to endure, adapt and survive, thus encouraging cancer treatment resistance [190, 191]. The UPR has become an attractive target in cancer treatment where tumours display resistance to conventional treatments. The chemotherapeutic agent paclitaxel upregulates XBP1s in TNBC, while addition of the IRE1 inhibitor MKC8866 induced a synergistic cytostatic effects with paclitaxel, both *in vitro* or *in vivo* [198]. Another study described that the IRE1 RNase inhibitor 4μ8C was able to trigger cell death when combined with cisplatin in cervical cancer stem cells [411]. These studies confirm that combination of UPR inhibitors with chemotherapeutics may provide valuable cancer therapies. This is addressed in Chapter 3 in which UPR inhibitors were

combined with other anticancer drugs including Btz, alisertib and trametinib. Again, since many cells rely on a properly functioning UPR to survive, the specificity of the UPR inhibitors must be verified and potential side effects must be closely monitored following administration. Combination of UPR inhibitors with chemotherapeutics could also lower the dose of chemotherapeutics required, reducing toxic side effects associated with these drugs.

5.5.2 Combining ER stress inducers with anticancer drugs

Combination of currently used cancer therapies with UPR inhibitors is not the only strategy to manipulate the UPR in combination therapies. As described in Chapter 1, section 1.6, following extensive stress, UPR signalling eventually switches to pro-death signalling. Additional ER stress from anticancer drugs in combination with ER stress inducers could overwhelm the UPR and drive the UPR towards pro-death signalling in tumour cells. Thus, combination of anticancer drugs with UPR inducers is also a viable option. Consistently, it was confirmed that Btz and TM induce cell death in a number of paediatric cancer cell lines. Unfortunately, their therapeutic values as single treatments are debated (previously discussed in 5.4.2) [404]. Nevertheless, if combined with other therapies, then lower concentrations could potentially be used. As previously discussed (section 5.4.1), in cancer therapy, Smac mimetics show promise as single agents but also in combination with other drugs. Smac mimetics have been reported to enhance apoptosis in combination with death receptor ligands, chemotherapeutics and radiation in various childhood cancers, such as leukemia, neuroblastoma, RMS, and glioblastoma [239, 390, 412-414]. Furthermore, a number of Smac mimetics are in clinical trial in combination with anticancer drugs in advanced solid tumours, lung cancer and multiple myeloma (NCT01573780, NCT03270176, NCT03111992). For this reason, ER stress inducers were tested in combination with Smac mimetic BV6 in paediatric cancers.

Combination of ER stress inducer Btz with other anticancer drugs show promising therapeutic value for cancer treatment. For example, combination treatments of Btz with chemotherapeutics such as vincristine, dexamethasone, pegylated L-asparaginase, and doxorubicin successfully increased patient remission and displayed acceptable toxicity in ALL patients [415, 416]. In this thesis, it was

confirmed that combination of Btz with the anticancer drug BV6 had additive effects against neuroblastoma and leukemic cells. This is in line with other published studies where ER stress induction combined with IAP inhibitors induce cell death in cancer cells [358, 359]. These data show promise for ER stress inducers and IAP antagonists as a therapeutic strategy for cancer.

There has also been several success cases where TM has been combined with chemotherapeutics, subsequently increasing cytotoxic effects of chemotherapeutic drugs [367, 417, 418]. For example, TM decreased the EC_{50} for doxorubicin and vincristine in ovarian cancer, enhancing their cytotoxicity [417]. Likewise, TM also dramatically increased vincristine-induced apoptosis in multidrug-resistance gastric cancer cells by inducing ER stress [367]. TM combined with cisplatin induced a relatively higher growth inhibition rate compared to cisplatin alone in breast cancer [418]. In this thesis, we evaluated the combined effects of TM with the IAP inhibitor BV6 as an anticancer therapy in paediatric cancers including neuroblastoma. In contrast to the favourable cytotoxic combination observed with BV6 and numerous ER stress inducers such as Btz, combination of TM with Smac mimetics did not increase the cytotoxic effects but rather reduced them, dismissing its potential as a therapeutic combination. Nonetheless, it was identified that NF-κB plays a significant role in this BV6-mediated pro-survival signalling. Although BV6 specifically protected cells from TM-induced cell death and not other ER stress inducers, the upregulation of NF-κB and the pro-survival effect of NF-κB following ER stress needs to be considered when combining ER stress inducers and IAP antagonists. For example, NF-κB direct inhibition of pro-apoptotic CHOP and upregulation of anti-apoptotic Mcl-1 observed in this thesis and in literature [360, 363, 364]. Therefore, caution should be taken, not just with TM but potentially also other ER stress inducing agents including chemotherapeutics as IAP antagonists may incur treatment resistance through NF-κB signalling.

Inhibition of NF-κB pro-survival signalling can combat the anti-apoptotic effect of Smac mimetics during the UPR response to ER stress. Btz has been shown to inhibit NF-κB activity by blocking IκBα degradation and diminishing the expression of NF-κB target genes [419, 420]. The data in this thesis, as well as previously published

studies, confirm that loss of cIAPs caused by Smac mimetics induce NF-κB signalling [421]. Thus, Btz-inhibition of pro-survival NF-κB signalling during BV6 treatment could contribute to enhanced cytotoxicity in combination treatments compared to single agents. An example of this is when the proteasome inhibitor Carf enhanced the cytotoxic effect of doxorubicin in neuroblastoma cells by inhibiting doxorubicin induced NF-κB activation by stabilizing IκBα [422].

It is important to be cautionary when overwhelming the UPR via ER stress induction as there are particular concerns surrounding this method. The combination of cytotoxic drugs with ER stress inducers could confer excess stress on healthy non-malignant cells, potentially causing them to die. The ultimate goal of cancer therapies using ER stress inducers is to apply low, sub-toxic concentrations so that the stress does not reach a certain threshold in non-malignant cells and that the UPR induction is specific to cancer cells. To prevent the induction of excess ER stress, ER stress could be induced to activate the pro-survival UPR followed by UPR inhibition, to prevent pro-survival signalling, turning the UPR towards pro-death. For example, combination of ER stress inducer Btz with UPR inhibitors. In fact, a number of studies demonstrate that combination of IRE1 inhibitor and Btz has combined cytotoxic effects in cancer cells such as leukemia and MM [200, 250]. In Chapter 3, the potential of combining Btz with the IRE1 inhibitor MKC8866 as a cancer therapy in RMS cells was also identified.

5.6 Future Perspectives

This study uncovered a number of roles of cell stress and cell death signalling components in paediatric cells under normal conditions and following treatment with anticancer drugs. Several potential targets and therapies for paediatric cell lines including RMS and neuroblastoma were identified. As discussed, there are several pitfalls to the work in this study, for example, the lack of primary sample testing and *in vivo* testing. These limitations can certainly be overcome by further studies and testing including *in vivo* studies which will be vital for the progression of potential anticancer therapies such as UPR inhibitors or combination treatments. Since UPR inhibitors and inducers show promising effects in the paediatric cancer cells in this

thesis, it could also be worthwhile testing these therapeutic strategies on other paediatric cancers. For instance, extending these studies to other paediatric cancers, could involve a screening to identify paediatric cancers with high basal UPR activity that could be targeted with inhibitors. It is important to confirm the role of the UPR in cancer cells prior to treatments, in order to avoid unwanted effects and/or lack of desired effects. Basic and translational research on the cancer of interest with the drugs of interest are foremost important. Next, *in vivo* and clinical testing to confirm efficacy and toxicity of the anticancer agents is required. Lastly, it would be beneficial to determine UPR activity in patients by means of biopsies or biomarkers. In the case of combination treatments with UPR inhibitors or inducers, it could be beneficial to identify activation of UPR signalling following initial anticancer treatment. This is especially relevant for paediatric patients where heterogeneity is substantial between patients.

5.7 Conclusion

In conclusion, the primary goal of this thesis has been achieved. The aim was to investigate cell death and survival signalling associated with the UPR in paediatric cancers. This thesis has certainly broadened our knowledge on UPR signalling in several paediatric cancers and its potential involvement in cancer therapy. We believe that these findings will stimulate further research into developing anticancer drugs in paediatric cancers and fill in some of the existing gaps required for the transition from bench to bedside.

References

1. Almanza, A., et al., *Endoplasmic reticulum stress signalling - from basic mechanisms to clinical applications.* FEBS J, 2019. **286**(2): p. 241-278.
2. Park, S.W. and U. Ozcan, *Potential for therapeutic manipulation of the UPR in disease.* Semin Immunopathol, 2013. **35**(3): p. 351-73.
3. Oslowski, C.M. and F. Urano, *Measuring ER stress and the unfolded protein response using mammalian tissue culture system.* Methods Enzymol, 2011. **490**: p. 71-92.
4. Hetz, C., J.M. Axten, and J.B. Patterson, *Pharmacological targeting of the unfolded protein response for disease intervention.* Nat Chem Biol, 2019. **15**(8): p. 764-775.
5. Ricci, M.S. and W.X. Zong, *Chemotherapeutic approaches for targeting cell death pathways.* Oncologist, 2006. **11**(4): p. 342-57.
6. Urra, H., et al., *Endoplasmic Reticulum Stress and the Hallmarks of Cancer.* Trends Cancer, 2016. **2**(5): p. 252-262.
7. Wang, M., et al., *The unfolded protein response as a target for anticancer therapeutics.* Crit Rev Oncol Hematol, 2018. **127**: p. 66-79.
8. Palade, G.E. and K.R. Porter, *Studies on the endoplasmic reticulum. I. Its identification in cells in situ.* J Exp Med, 1954. **100**(6): p. 641-56.
9. Friedman, J.R. and G.K. Voeltz, *The ER in 3D: a multifunctional dynamic membrane network.* Trends Cell Biol, 2011. **21**(12): p. 709-17.
10. Palade, G.E., *The endoplasmic reticulum.* J Biophys Biochem Cytol, 1956. **2**(4 Suppl): p. 85-98.
11. Voeltz, G.K., M.M. Rolls, and T.A. Rapoport, *Structural organization of the endoplasmic reticulum.* EMBO Rep, 2002. **3**(10): p. 944-50.
12. Banjo, A.O., *Interactions between the rough endoplasmic reticulum and the nuclear membrane during increased proliferation of the endoplasmic reticulum.* Afr J Med Med Sci, 1983. **12**(3-4): p. 145-54.
13. Kaufman, R.J., *Stress signaling from the lumen of the endoplasmic reticulum: coordination of gene transcriptional and translational controls.* Genes Dev, 1999. **13**(10): p. 1211-33.
14. Braakman, I. and N.J. Bulleid, *Protein folding and modification in the mammalian endoplasmic reticulum.* Annu Rev Biochem, 2011. **80**: p. 71-99.
15. Hebert, D.N. and M. Molinari, *In and out of the ER: protein folding, quality control, degradation, and related human diseases.* Physiol Rev, 2007. **87**(4): p. 1377-408.
16. Drummond, D.A. and C.O. Wilke, *The evolutionary consequences of erroneous protein synthesis.* Nat Rev Genet, 2009. **10**(10): p. 715-24.
17. Meusser, B., et al., *ERAD: the long road to destruction.* Nat Cell Biol, 2005. **7**(8): p. 766-72.
18. Clapham, D.E., *Calcium signaling.* Cell, 2007. **131**(6): p. 1047-58.
19. Meldolesi, J. and T. Pozzan, *The endoplasmic reticulum Ca2+ store: a view from the lumen.* Trends Biochem Sci, 1998. **23**(1): p. 10-4.
20. Brown, M.S. and J.L. Goldstein, *A proteolytic pathway that controls the cholesterol content of membranes, cells, and blood.* Proc Natl Acad Sci U S A, 1999. **96**(20): p. 11041-8.

21. Noack, J., G. Brambilla Pisoni, and M. Molinari, *Proteostasis: bad news and good news from the endoplasmic reticulum.* Swiss Med Wkly, 2014. **144**: p. w14001.
22. Ron, D. and P. Walter, *Signal integration in the endoplasmic reticulum unfolded protein response.* Nat Rev Mol Cell Biol, 2007. **8**(7): p. 519-29.
23. Tabas, I. and D. Ron, *Integrating the mechanisms of apoptosis induced by endoplasmic reticulum stress.* Nat Cell Biol, 2011. **13**(3): p. 184-90.
24. Mori, K., *Tripartite management of unfolded proteins in the endoplasmic reticulum.* Cell, 2000. **101**(5): p. 451-4.
25. Schroder, M. and R.J. Kaufman, *The mammalian unfolded protein response.* Annu Rev Biochem, 2005. **74**: p. 739-89.
26. Bertolotti, A., et al., *Dynamic interaction of BiP and ER stress transducers in the unfolded-protein response.* Nat Cell Biol, 2000. **2**(6): p. 326-32.
27. Bertolotti, A., et al., *Increased sensitivity to dextran sodium sulfate colitis in IRE1beta-deficient mice.* J Clin Invest, 2001. **107**(5): p. 585-93.
28. Martino, M.B., et al., *The ER stress transducer IRE1beta is required for airway epithelial mucin production.* Mucosal Immunol, 2013. **6**(3): p. 639-54.
29. Mori, K., et al., *A transmembrane protein with a cdc2+/CDC28-related kinase activity is required for signaling from the ER to the nucleus.* Cell, 1993. **74**(4): p. 743-56.
30. Sidrauski, C. and P. Walter, *The transmembrane kinase Ire1p is a site-specific endonuclease that initiates mRNA splicing in the unfolded protein response.* Cell, 1997. **90**(6): p. 1031-9.
31. Shamu, C.E. and P. Walter, *Oligomerization and phosphorylation of the Ire1p kinase during intracellular signaling from the endoplasmic reticulum to the nucleus.* EMBO J, 1996. **15**(12): p. 3028-39.
32. Ali, M.M., et al., *Structure of the Ire1 autophosphorylation complex and implications for the unfolded protein response.* EMBO J, 2011. **30**(5): p. 894-905.
33. Liou, H.C., et al., *A new member of the leucine zipper class of proteins that binds to the HLA DR alpha promoter.* Science, 1990. **247**(4950): p. 1581-4.
34. Yoshida, H., et al., *XBP1 mRNA is induced by ATF6 and spliced by IRE1 in response to ER stress to produce a highly active transcription factor.* Cell, 2001. **107**(7): p. 881-91.
35. Lee, A.H., N.N. Iwakoshi, and L.H. Glimcher, *XBP-1 regulates a subset of endoplasmic reticulum resident chaperone genes in the unfolded protein response.* Mol Cell Biol, 2003. **23**(21): p. 7448-59.
36. Travers, K.J., et al., *Functional and genomic analyses reveal an essential coordination between the unfolded protein response and ER-associated degradation.* Cell, 2000. **101**(3): p. 249-258.
37. Hollien, J. and J.S. Weissman, *Decay of endoplasmic reticulum-localized mRNAs during the unfolded protein response.* Science, 2006. **313**(5783): p. 104-7.
38. Oikawa, D., et al., *Identification of a consensus element recognized and cleaved by IRE1 alpha.* Nucleic Acids Res, 2010. **38**(18): p. 6265-73.
39. Hollien, J., et al., *Regulated Ire1-dependent decay of messenger RNAs in mammalian cells.* J Cell Biol, 2009. **186**(3): p. 323-31.
40. Moore, K.A., et al., *Regulation of sumo mRNA during endoplasmic reticulum stress.* PLoS One, 2013. **8**(9): p. e75723.

41. Arensdorf, A.M., D. Diedrichs, and D.T. Rutkowski, *Regulation of the transcriptome by ER stress: non-canonical mechanisms and physiological consequences.* Front Genet, 2013. **4**: p. 256.
42. Shi, Y., et al., *Identification and characterization of pancreatic eukaryotic initiation factor 2 alpha-subunit kinase, PEK, involved in translational control.* Mol Cell Biol, 1998. **18**(12): p. 7499-509.
43. Ma, K., K.M. Vattem, and R.C. Wek, *Dimerization and release of molecular chaperone inhibition facilitate activation of eukaryotic initiation factor-2 kinase in response to endoplasmic reticulum stress.* J Biol Chem, 2002. **277**(21): p. 18728-35.
44. Lloyd, M.A., et al., *Characteristics of eukaryotic initiation factor 2 and its subunits.* J Biol Chem, 1980. **255**(3): p. 1189-93.
45. Adams, S.L., et al., *Eukaryotic initiation complex formation. Evidence for two distinct pathways.* J Biol Chem, 1975. **250**(23): p. 9083-9.
46. Harding, H.P., et al., *Regulated translation initiation controls stress-induced gene expression in mammalian cells.* Mol Cell, 2000. **6**(5): p. 1099-108.
47. Ameri, K. and A.L. Harris, *Activating transcription factor 4.* Int J Biochem Cell Biol, 2008. **40**(1): p. 14-21.
48. B'Chir, W., et al., *The eIF2alpha/ATF4 pathway is essential for stress-induced autophagy gene expression.* Nucleic Acids Res, 2013. **41**(16): p. 7683-99.
49. Novoa, I., et al., *Feedback inhibition of the unfolded protein response by GADD34-mediated dephosphorylation of eIF2alpha.* J Cell Biol, 2001. **153**(5): p. 1011-22.
50. Brush, M.H., D.C. Weiser, and S. Shenolikar, *Growth arrest and DNA damage-inducible protein GADD34 targets protein phosphatase 1 alpha to the endoplasmic reticulum and promotes dephosphorylation of the alpha subunit of eukaryotic translation initiation factor 2.* Mol Cell Biol, 2003. **23**(4): p. 1292-303.
51. Cullinan, S.B., et al., *Nrf2 is a direct PERK substrate and effector of PERK-dependent cell survival.* Mol Cell Biol, 2003. **23**(20): p. 7198-209.
52. Hayes, J.D. and M. McMahon, *Molecular basis for the contribution of the antioxidant responsive element to cancer chemoprevention.* Cancer Lett, 2001. **174**(2): p. 103-13.
53. Itoh, K., et al., *An Nrf2/small Maf heterodimer mediates the induction of phase II detoxifying enzyme genes through antioxidant response elements.* Biochem Biophys Res Commun, 1997. **236**(2): p. 313-22.
54. Shen, J., et al., *ER stress regulation of ATF6 localization by dissociation of BiP/GRP78 binding and unmasking of Golgi localization signals.* Dev Cell, 2002. **3**(1): p. 99-111.
55. Yamamoto, K., et al., *Transcriptional induction of mammalian ER quality control proteins is mediated by single or combined action of ATF6alpha and XBP1.* Dev Cell, 2007. **13**(3): p. 365-76.
56. Yoshida, H., et al., *ATF6 activated by proteolysis binds in the presence of NF-Y (CBF) directly to the cis-acting element responsible for the mammalian unfolded protein response.* Mol Cell Biol, 2000. **20**(18): p. 6755-67.
57. Hetz, C., E. Chevet, and H.P. Harding, *Targeting the unfolded protein response in disease.* Nat Rev Drug Discov, 2013. **12**(9): p. 703-19.

58. Wortel, I.M.N., et al., *Surviving Stress: Modulation of ATF4-Mediated Stress Responses in Normal and Malignant Cells.* Trends Endocrinol Metab, 2017. **28**(11): p. 794-806.
59. Jiang, C.C., et al., *Up-regulation of Mcl-1 is critical for survival of human melanoma cells upon endoplasmic reticulum stress.* Cancer Res, 2008. **68**(16): p. 6708-17.
60. Hamanaka, R.B., et al., *PERK-dependent regulation of IAP translation during ER stress.* Oncogene, 2009. **28**(6): p. 910-20.
61. Hu, P., et al., *Critical role of endogenous Akt/IAPs and MEK1/ERK pathways in counteracting endoplasmic reticulum stress-induced cell death.* J Biol Chem, 2004. **279**(47): p. 49420-9.
62. Muaddi, H., et al., *Phosphorylation of eIF2 alpha at Serine 51 Is an Important Determinant of Cell Survival and Adaptation to Glucose Deficiency.* Molecular Biology of the Cell, 2010. **21**(18): p. 3220-3231.
63. Qi, L., B. Tsai, and P. Arvan, *New Insights into the Physiological Role of Endoplasmic Reticulum-Associated Degradation.* Trends Cell Biol, 2017. **27**(6): p. 430-440.
64. Ruggiano, A., O. Foresti, and P. Carvalho, *Quality control: ER-associated degradation: protein quality control and beyond.* J Cell Biol, 2014. **204**(6): p. 869-79.
65. Lilley, B.N. and H.L. Ploegh, *Multiprotein complexes that link dislocation, ubiquitination, and extraction of misfolded proteins from the endoplasmic reticulum membrane.* Proc Natl Acad Sci U S A, 2005. **102**(40): p. 14296-301.
66. Adams, J., *The proteasome: structure, function, and role in the cell.* Cancer Treat Rev, 2003. **29 Suppl 1**: p. 3-9.
67. Hosokawa, N., et al., *A novel ER alpha-mannosidase-like protein accelerates ER-associated degradation.* Embo Reports, 2001. **2**(5): p. 415-422.
68. Klionsky, D.J. and S.D. Emr, *Autophagy as a regulated pathway of cellular degradation.* Science, 2000. **290**(5497): p. 1717-21.
69. Mizushima, N., T. Yoshimori, and Y. Ohsumi, *The role of Atg proteins in autophagosome formation.* Annu Rev Cell Dev Biol, 2011. **27**: p. 107-32.
70. Kouroku, Y., et al., *ER stress (PERK/eIF2alpha phosphorylation) mediates the polyglutamine-induced LC3 conversion, an essential step for autophagy formation.* Cell Death Differ, 2007. **14**(2): p. 230-9.
71. Deegan, S., et al., *A close connection between the PERK and IRE arms of the UPR and the transcriptional regulation of autophagy.* Biochem Biophys Res Commun, 2015. **456**(1): p. 305-11.
72. Deegan, S., et al., *Stress-induced self-cannibalism: on the regulation of autophagy by endoplasmic reticulum stress.* Cell Mol Life Sci, 2013. **70**(14): p. 2425-41.
73. Ogata, M., et al., *Autophagy is activated for cell survival after endoplasmic reticulum stress.* Mol Cell Biol, 2006. **26**(24): p. 9220-31.
74. Margariti, A., et al., *XBP1 mRNA splicing triggers an autophagic response in endothelial cells through BECLIN-1 transcriptional activation.* J Biol Chem, 2013. **288**(2): p. 859-72.
75. Metcalf, D.J., et al., *Autophagy and misfolded proteins in neurodegeneration.* Exp Neurol, 2012. **238**(1): p. 22-8.
76. Hetz, C., *The unfolded protein response: controlling cell fate decisions under ER stress and beyond.* Nat Rev Mol Cell Biol, 2012. **13**(2): p. 89-102.

77. Kerr, J.F., A.H. Wyllie, and A.R. Currie, *Apoptosis: a basic biological phenomenon with wide-ranging implications in tissue kinetics.* Br J Cancer, 1972. **26**(4): p. 239-57.
78. Lockshin, R.A. and Z. Zakeri, *Cell death in health and disease.* J Cell Mol Med, 2007. **11**(6): p. 1214-24.
79. Favaloro, B., et al., *Role of apoptosis in disease.* Aging (Albany NY), 2012. **4**(5): p. 330-49.
80. Saraste, A. and K. Pulkki, *Morphologic and biochemical hallmarks of apoptosis.* Cardiovasc Res, 2000. **45**(3): p. 528-37.
81. Fulda, S., et al., *Cellular stress responses: cell survival and cell death.* Int J Cell Biol, 2010. **2010**: p. 214074.
82. Locksley, R.M., N. Killeen, and M.J. Lenardo, *The TNF and TNF receptor superfamilies: integrating mammalian biology.* Cell, 2001. **104**(4): p. 487-501.
83. Kischkel, F.C., et al., *Cytotoxicity-dependent APO-1 (Fas/CD95)-associated proteins form a death-inducing signaling complex (DISC) with the receptor.* EMBO J, 1995. **14**(22): p. 5579-88.
84. Scaffidi, C., et al., *Two CD95 (APO-1/Fas) signaling pathways.* EMBO J, 1998. **17**(6): p. 1675-87.
85. Elmore, S., *Apoptosis: a review of programmed cell death.* Toxicol Pathol, 2007. **35**(4): p. 495-516.
86. Lutter, M., G.A. Perkins, and X. Wang, *The pro-apoptotic Bcl-2 family member tBid localizes to mitochondrial contact sites.* BMC Cell Biol, 2001. **2**: p. 22.
87. Brunelle, J.K. and A. Letai, *Control of mitochondrial apoptosis by the Bcl-2 family.* J Cell Sci, 2009. **122**(Pt 4): p. 437-41.
88. Giam, M., D.C. Huang, and P. Bouillet, *BH3-only proteins and their roles in programmed cell death.* Oncogene, 2008. **27 Suppl 1**: p. S128-36.
89. Chipuk, J.E., et al., *The BCL-2 family reunion.* Mol Cell, 2010. **37**(3): p. 299-310.
90. Slee, E.A., et al., *Ordering the cytochrome c-initiated caspase cascade: hierarchical activation of caspases-2, -3, -6, -7, -8, and -10 in a caspase-9-dependent manner.* J Cell Biol, 1999. **144**(2): p. 281-92.
91. Saelens, X., et al., *Toxic proteins released from mitochondria in cell death.* Oncogene, 2004. **23**(16): p. 2861-74.
92. Crook, N.E., R.J. Clem, and L.K. Miller, *An apoptosis-inhibiting baculovirus gene with a zinc finger-like motif.* J Virol, 1993. **67**(4): p. 2168-74.
93. Miller, L.K., *An exegesis of IAPs: salvation and surprises from BIR motifs.* Trends Cell Biol, 1999. **9**(8): p. 323-8.
94. Hay, B.A., *Understanding IAP function and regulation: a view from Drosophila.* Cell Death Differ, 2000. **7**(11): p. 1045-56.
95. Fulda, S. and D. Vucic, *Targeting IAP proteins for therapeutic intervention in cancer.* Nat Rev Drug Discov, 2012. **11**(2): p. 109-24.
96. Silke, J. and D. Vucic, *IAP family of cell death and signaling regulators.* Methods Enzymol, 2014. **545**: p. 35-65.
97. Vaux, D.L. and J. Silke, *IAPs, RINGs and ubiquitylation.* Nat Rev Mol Cell Biol, 2005. **6**(4): p. 287-97.
98. Hofmann, K., P. Bucher, and J. Tschopp, *The CARD domain: a new apoptotic signalling motif.* Trends Biochem Sci, 1997. **22**(5): p. 155-6.

99. Shiozaki, E.N., et al., *Mechanism of XIAP-mediated inhibition of caspase-9.* Mol Cell, 2003. **11**(2): p. 519-27.
100. Hurley, J.H., S. Lee, and G. Prag, *Ubiquitin-binding domains.* Biochem J, 2006. **399**(3): p. 361-72.
101. Deveraux, Q.L., et al., *X-linked IAP is a direct inhibitor of cell-death proteases.* Nature, 1997. **388**(6639): p. 300-4.
102. Suzuki, Y., Y. Nakabayashi, and R. Takahashi, *Ubiquitin-protein ligase activity of X-linked inhibitor of apoptosis protein promotes proteasomal degradation of caspase-3 and enhances its anti-apoptotic effect in Fas-induced cell death.* Proc Natl Acad Sci U S A, 2001. **98**(15): p. 8662-7.
103. MacFarlane, M., et al., *Proteasome-mediated degradation of Smac during apoptosis: XIAP promotes Smac ubiquitination in vitro.* J Biol Chem, 2002. **277**(39): p. 36611-6.
104. Schile, A.J., M. Garcia-Fernandez, and H. Steller, *Regulation of apoptosis by XIAP ubiquitin-ligase activity.* Genes Dev, 2008. **22**(16): p. 2256-66.
105. Srinivasula, S.M. and J.D. Ashwell, *IAPs: what's in a name?* Mol Cell, 2008. **30**(2): p. 123-35.
106. Sun, C., et al., *NMR structure and mutagenesis of the inhibitor-of-apoptosis protein XIAP.* Nature, 1999. **401**(6755): p. 818-22.
107. Vucic, D., V.M. Dixit, and I.E. Wertz, *Ubiquitylation in apoptosis: a post-translational modification at the edge of life and death.* Nat Rev Mol Cell Biol, 2011. **12**(7): p. 439-52.
108. Choi, Y.E., et al., *The E3 ubiquitin ligase cIAP1 binds and ubiquitinates caspase-3 and -7 via unique mechanisms at distinct steps in their processing.* J Biol Chem, 2009. **284**(19): p. 12772-82.
109. Blankenship, J.W., et al., *Ubiquitin binding modulates IAP antagonist-stimulated proteasomal degradation of c-IAP1 and c-IAP2(1).* Biochem J, 2009. **417**(1): p. 149-60.
110. Hu, S. and X. Yang, *Cellular inhibitor of apoptosis 1 and 2 are ubiquitin ligases for the apoptosis inducer Smac/DIABLO.* J Biol Chem, 2003. **278**(12): p. 10055-60.
111. Bertrand, M.J., et al., *cIAP1 and cIAP2 facilitate cancer cell survival by functioning as E3 ligases that promote RIP1 ubiquitination.* Mol Cell, 2008. **30**(6): p. 689-700.
112. Samuel, T., et al., *Distinct BIR domains of cIAP1 mediate binding to and ubiquitination of tumor necrosis factor receptor-associated factor 2 and second mitochondrial activator of caspases.* J Biol Chem, 2006. **281**(2): p. 1080-90.
113. Morizane, Y., et al., *X-linked inhibitor of apoptosis functions as ubiquitin ligase toward mature caspase-9 and cytosolic Smac/DIABLO.* J Biochem, 2005. **137**(2): p. 125-32.
114. Silke, J., et al., *Determination of cell survival by RING-mediated regulation of inhibitor of apoptosis (IAP) protein abundance.* Proc Natl Acad Sci U S A, 2005. **102**(45): p. 16182-7.
115. Conze, D.B., et al., *Posttranscriptional downregulation of c-IAP2 by the ubiquitin protein ligase c-IAP1 in vivo.* Mol Cell Biol, 2005. **25**(8): p. 3348-56.
116. Du, C., et al., *Smac, a mitochondrial protein that promotes cytochrome c-dependent caspase activation by eliminating IAP inhibition.* Cell, 2000. **102**(1): p. 33-42.

117. Wu, G., et al., *Structural basis of IAP recognition by Smac/DIABLO.* Nature, 2000. **408**(6815): p. 1008-12.
118. Yang, Q.H. and C. Du, *Smac/DIABLO selectively reduces the levels of c-IAP1 and c-IAP2 but not that of XIAP and livin in HeLa cells.* J Biol Chem, 2004. **279**(17): p. 16963-70.
119. Varfolomeev, E., et al., *IAP antagonists induce autoubiquitination of c-IAPs, NF-kappaB activation, and TNFalpha-dependent apoptosis.* Cell, 2007. **131**(4): p. 669-81.
120. Perkins, N.D., *The diverse and complex roles of NF-kappaB subunits in cancer.* Nat Rev Cancer, 2012. **12**(2): p. 121-32.
121. Karin, M., *NF-kappaB as a critical link between inflammation and cancer.* Cold Spring Harb Perspect Biol, 2009. **1**(5): p. a000141.
122. Rothwarf, D.M. and M. Karin, *The NF-kappa B activation pathway: a paradigm in information transfer from membrane to nucleus.* Sci STKE, 1999. **1999**(5): p. RE1.
123. Pahl, H.L., *Activators and target genes of Rel/NF-kappaB transcription factors.* Oncogene, 1999. **18**(49): p. 6853-66.
124. Varfolomeev, E., et al., *Cellular inhibitors of apoptosis are global regulators of NF-kappaB and MAPK activation by members of the TNF family of receptors.* Sci Signal, 2012. **5**(216): p. ra22.
125. Bai, L., D.C. Smith, and S. Wang, *Small-molecule SMAC mimetics as new cancer therapeutics.* Pharmacol Ther, 2014. **144**(1): p. 82-95.
126. Varfolomeev, E. and D. Vucic, *(Un)expected roles of c-IAPs in apoptotic and NFkappaB signaling pathways.* Cell Cycle, 2008. **7**(11): p. 1511-21.
127. Hayden, M.S. and S. Ghosh, *Signaling to NF-kappaB.* Genes Dev, 2004. **18**(18): p. 2195-224.
128. Dejardin, E., *The alternative NF-kappaB pathway from biochemistry to biology: pitfalls and promises for future drug development.* Biochem Pharmacol, 2006. **72**(9): p. 1161-79.
129. Iurlaro, R. and C. Munoz-Pinedo, *Cell death induced by endoplasmic reticulum stress.* FEBS J, 2016. **283**(14): p. 2640-52.
130. Rodriguez, D., D. Rojas-Rivera, and C. Hetz, *Integrating stress signals at the endoplasmic reticulum: The BCL-2 protein family rheostat.* Biochim Biophys Acta, 2011. **1813**(4): p. 564-74.
131. Wang, X.Z. and D. Ron, *Stress-induced phosphorylation and activation of the transcription factor CHOP (GADD153) by p38 MAP Kinase.* Science, 1996. **272**(5266): p. 1347-9.
132. McCullough, K.D., et al., *Gadd153 sensitizes cells to endoplasmic reticulum stress by down-regulating Bcl2 and perturbing the cellular redox state.* Mol Cell Biol, 2001. **21**(4): p. 1249-59.
133. Puthalakath, H., et al., *ER stress triggers apoptosis by activating BH3-only protein Bim.* Cell, 2007. **129**(7): p. 1337-49.
134. Reimertz, C., et al., *Gene expression during ER stress-induced apoptosis in neurons: induction of the BH3-only protein Bbc3/PUMA and activation of the mitochondrial apoptosis pathway.* J Cell Biol, 2003. **162**(4): p. 587-97.
135. Armstrong, J.L., et al., *Regulation of endoplasmic reticulum stress-induced cell death by ATF4 in neuroectodermal tumor cells.* J Biol Chem, 2010. **285**(9): p. 6091-100.

136. Ohoka, N., et al., *TRB3, a novel ER stress-inducible gene, is induced via ATF4-CHOP pathway and is involved in cell death.* EMBO J, 2005. **24**(6): p. 1243-55.
137. Yamaguchi, H. and H.G. Wang, *CHOP is involved in endoplasmic reticulum stress-induced apoptosis by enhancing DR5 expression in human carcinoma cells.* J Biol Chem, 2004. **279**(44): p. 45495-502.
138. Li, G., et al., *Role of ERO1-alpha-mediated stimulation of inositol 1,4,5-triphosphate receptor activity in endoplasmic reticulum stress-induced apoptosis.* J Cell Biol, 2009. **186**(6): p. 783-92.
139. Marciniak, S.J., et al., *CHOP induces death by promoting protein synthesis and oxidation in the stressed endoplasmic reticulum.* Genes Dev, 2004. **18**(24): p. 3066-77.
140. Allagnat, F., et al., *Mcl-1 downregulation by pro-inflammatory cytokines and palmitate is an early event contributing to beta-cell apoptosis.* Cell Death Differ, 2011. **18**(2): p. 328-37.
141. Ramirez-Peinado, S., et al., *2-deoxyglucose induces Noxa-dependent apoptosis in alveolar rhabdomyosarcoma.* Cancer Res, 2011. **71**(21): p. 6796-806.
142. Galehdar, Z., et al., *Neuronal apoptosis induced by endoplasmic reticulum stress is regulated by ATF4-CHOP-mediated induction of the Bcl-2 homology 3-only member PUMA.* J Neurosci, 2010. **30**(50): p. 16938-48.
143. Hiramatsu, N., et al., *Translational and posttranslational regulation of XIAP by eIF2 alpha and ATF4 promotes ER stress-induced cell death during the unfolded protein response.* Molecular Biology of the Cell, 2014. **25**(9): p. 1411-1420.
144. Urra, H., et al., *When ER stress reaches a dead end.* Biochim Biophys Acta, 2013. **1833**(12): p. 3507-3517.
145. Urano, F., et al., *Coupling of stress in the ER to activation of JNK protein kinases by transmembrane protein kinase IRE1.* Science, 2000. **287**(5453): p. 664-6.
146. Ichijo, H., et al., *Induction of apoptosis by ASK1, a mammalian MAPKKK that activates SAPK/JNK and p38 signaling pathways.* Science, 1997. **275**(5296): p. 90-4.
147. Tobiume, K., et al., *ASK1 is required for sustained activations of JNK/p38 MAP kinases and apoptosis.* EMBO Rep, 2001. **2**(3): p. 222-8.
148. Fan, M., et al., *Vinblastine-induced phosphorylation of Bcl-2 and Bcl-XL is mediated by JNK and occurs in parallel with inactivation of the Raf-1/MEK/ERK cascade.* J Biol Chem, 2000. **275**(39): p. 29980-5.
149. Wang, W., et al., *MCL-1 degradation mediated by JNK activation via MEKK1/TAK1-MKK4 contributes to anticancer activity of new tubulin inhibitor MT189.* Mol Cancer Ther, 2014. **13**(6): p. 1480-91.
150. Lei, K. and R.J. Davis, *JNK phosphorylation of Bim-related members of the Bcl2 family induces Bax-dependent apoptosis.* Proc Natl Acad Sci U S A, 2003. **100**(5): p. 2432-7.
151. Younce, C.W. and P.E. Kolattukudy, *MCP-1 causes cardiomyoblast death via autophagy resulting from ER stress caused by oxidative stress generated by inducing a novel zinc-finger protein, MCPIP.* Biochem J, 2010. **426**(1): p. 43-53.
152. Kim, B.J., S.W. Ryu, and B.J. Song, *JNK- and p38 kinase-mediated phosphorylation of Bax leads to its activation and mitochondrial*

translocation and to apoptosis of human hepatoma HepG2 cells. J Biol Chem, 2006. **281**(30): p. 21256-65.
153. Han, D., et al., *IRE1alpha kinase activation modes control alternate endoribonuclease outputs to determine divergent cell fates.* Cell, 2009. **138**(3): p. 562-75.
154. Upton, J.P., et al., *IRE1alpha cleaves select microRNAs during ER stress to derepress translation of proapoptotic Caspase-2.* Science, 2012. **338**(6108): p. 818-22.
155. Lerner, A.G., et al., *IRE1alpha induces thioredoxin-interacting protein to activate the NLRP3 inflammasome and promote programmed cell death under irremediable ER stress.* Cell Metab, 2012. **16**(2): p. 250-64.
156. Morishima, N., K. Nakanishi, and A. Nakano, *Activating transcription factor-6 (ATF6) mediates apoptosis with reduction of myeloid cell leukemia sequence 1 (Mcl-1) protein via induction of WW domain binding protein 1.* J Biol Chem, 2011. **286**(40): p. 35227-35.
157. Kim, R., et al., *Role of the unfolded protein response in cell death.* Apoptosis, 2006. **11**(1): p. 5-13.
158. Torre, L.A., et al., *Global cancer statistics, 2012.* CA Cancer J Clin, 2015. **65**(2): p. 87-108.
159. Steliarova-Foucher, E., et al., *International incidence of childhood cancer, 2001-10: a population-based registry study.* Lancet Oncol, 2017. **18**(6): p. 719-731.
160. Bhakta, N., et al., *Childhood cancer burden: a review of global estimates.* Lancet Oncol, 2019. **20**(1): p. e42-e53.
161. Ward, Z.J., et al., *Estimating the total incidence of global childhood cancer: a simulation-based analysis.* Lancet Oncol, 2019. **20**(4): p. 483-493.
162. Johnston, W.T., et al., *Childhood cancer: Estimating regional and global incidence.* Cancer Epidemiol, 2020: p. 101662.
163. Winther, J.F., et al., *Childhood cancer survivor cohorts in Europe.* Acta Oncol, 2015. **54**(5): p. 655-68.
164. Bryant, R., *Managing side effects of childhood cancer treatment.* J Pediatr Nurs, 2003. **18**(2): p. 113-25.
165. Smith, M.A., et al., *Declining childhood and adolescent cancer mortality.* Cancer, 2014. **120**(16): p. 2497-506.
166. Kopp, L.M., et al., *Late effects in adult survivors of pediatric cancer: a guide for the primary care physician.* Am J Med, 2012. **125**(7): p. 636-41.
167. Oeffinger, K.C. and M.M. Hudson, *Long-term complications following childhood and adolescent cancer: foundations for providing risk-based health care for survivors.* CA Cancer J Clin, 2004. **54**(4): p. 208-36.
168. Dasgupta, R., J. Fuchs, and D. Rodeberg, *Rhabdomyosarcoma.* Semin Pediatr Surg, 2016. **25**(5): p. 276-283.
169. Saab, R., S.L. Spunt, and S.X. Skapek, *Myogenesis and rhabdomyosarcoma the Jekyll and Hyde of skeletal muscle.* Curr Top Dev Biol, 2011. **94**: p. 197-234.
170. Ognjanovic, S., et al., *Trends in childhood rhabdomyosarcoma incidence and survival in the United States, 1975-2005.* Cancer, 2009. **115**(18): p. 4218-26.
171. van der Graaf, W.T.A., et al., *Soft tissue sarcomas in adolescents and young adults: a comparison with their paediatric and adult counterparts.* Lancet Oncol, 2017. **18**(3): p. e166-e175.

172. Tombolan, L., et al., *High IGFBP2 expression correlates with tumor severity in pediatric rhabdomyosarcoma.* Am J Pathol, 2011. **179**(5): p. 2611-24.
173. Hawkins, D.S., A.A. Gupta, and E.R. Rudzinski, *What is new in the biology and treatment of pediatric rhabdomyosarcoma?* Curr Opin Pediatr, 2014. **26**(1): p. 50-6.
174. Tostar, U., et al., *Reduction of human embryonal rhabdomyosarcoma tumor growth by inhibition of the hedgehog signaling pathway.* Genes Cancer, 2010. **1**(9): p. 941-51.
175. *Childhood Rhabdomyosarcoma Treatment (PDQ(R)): Health Professional Version*, in *PDQ Cancer Information Summaries*. 2002: Bethesda (MD).
176. Ruiz-Mesa, C., et al., *Rhabdomyosarcoma in adults: new perspectives on therapy.* Curr Treat Options Oncol, 2015. **16**(6): p. 27.
177. Shapiro, D.N., et al., *Fusion of PAX3 to a member of the forkhead family of transcription factors in human alveolar rhabdomyosarcoma.* Cancer Res, 1993. **53**(21): p. 5108-12.
178. Davis, R.J., et al., *Fusion of PAX7 to FKHR by the variant t(1;13)(p36;q14) translocation in alveolar rhabdomyosarcoma.* Cancer Res, 1994. **54**(11): p. 2869-72.
179. Parham, D.M. and F.G. Barr, *Classification of rhabdomyosarcoma and its molecular basis.* Adv Anat Pathol, 2013. **20**(6): p. 387-97.
180. Hachitanda, Y., et al., *N-myc gene amplification in rhabdomyosarcoma detected by fluorescence in situ hybridization: its correlation with histologic features.* Mod Pathol, 1998. **11**(12): p. 1222-7.
181. Marshall, A.D. and G.C. Grosveld, *Alveolar rhabdomyosarcoma - The molecular drivers of PAX3/7-FOXO1-induced tumorigenesis.* Skelet Muscle, 2012. **2**(1): p. 25.
182. Park, J.R., A. Eggert, and H. Caron, *Neuroblastoma: biology, prognosis, and treatment.* Hematol Oncol Clin North Am, 2010. **24**(1): p. 65-86.
183. Esiashvili, N., C. Anderson, and H.M. Katzenstein, *Neuroblastoma.* Curr Probl Cancer, 2009. **33**(6): p. 333-60.
184. Maris, J.M., *Recent advances in neuroblastoma.* N Engl J Med, 2010. **362**(23): p. 2202-11.
185. Saletta, F., L. Dalla Pozza, and J.A. Byrne, *Genetic causes of cancer predisposition in children and adolescents.* Transl Pediatr, 2015. **4**(2): p. 67-75.
186. Ishola, T.A. and D.H. Chung, *Neuroblastoma.* Surg Oncol, 2007. **16**(3): p. 149-56.
187. Arya, A., et al., *Rifampicin pharmacokinetics in children under the Revised National Tuberculosis Control Programme, India, 2009.* Int J Tuberc Lung Dis, 2015. **19**(4): p. 440-5.
188. Smith, V. and J. Foster, *High-Risk Neuroblastoma Treatment Review.* Children (Basel), 2018. **5**(9).
189. Ma, Y. and L.M. Hendershot, *The role of the unfolded protein response in tumour development: friend or foe?* Nat Rev Cancer, 2004. **4**(12): p. 966-77.
190. Avril, T., E. Vauleon, and E. Chevet, *Endoplasmic reticulum stress signaling and chemotherapy resistance in solid cancers.* Oncogenesis, 2017. **6**(8): p. e373.
191. Madden, E., et al., *The role of the unfolded protein response in cancer progression: From oncogenesis to chemoresistance.* Biol Cell, 2019. **111**(1): p. 1-17.

192. Tameire, F., Verginadis, II, and C. Koumenis, *Cell intrinsic and extrinsic activators of the unfolded protein response in cancer: Mechanisms and targets for therapy.* Semin Cancer Biol, 2015. **33**: p. 3-15.
193. Cubillos-Ruiz, J.R., S.E. Bettigole, and L.H. Glimcher, *Tumorigenic and Immunosuppressive Effects of Endoplasmic Reticulum Stress in Cancer.* Cell, 2017. **168**(4): p. 692-706.
194. Namba, T., et al., *Loss of p53 enhances the function of the endoplasmic reticulum through activation of the IRE1alpha/XBP1 pathway.* Oncotarget, 2015. **6**(24): p. 19990-20001.
195. Hart, L.S., et al., *ER stress-mediated autophagy promotes Myc-dependent transformation and tumor growth.* J Clin Invest, 2012. **122**(12): p. 4621-34.
196. Luo, B. and A.S. Lee, *The critical roles of endoplasmic reticulum chaperones and unfolded protein response in tumorigenesis and anticancer therapies.* Oncogene, 2013. **32**(7): p. 805-18.
197. Li, X.X., et al., *Knockdown of IRE1alpha inhibits colonic tumorigenesis through decreasing beta-catenin and IRE1alpha targeting suppresses colon cancer cells.* Oncogene, 2017. **36**(48): p. 6738-6746.
198. Logue, S.E., et al., *Inhibition of IRE1 RNase activity modulates the tumor cell secretome and enhances response to chemotherapy.* Nat Commun, 2018. **9**(1): p. 3267.
199. Mimura, N., et al., *Blockade of XBP1 splicing by inhibition of IRE1alpha is a promising therapeutic option in multiple myeloma.* Blood, 2012. **119**(24): p. 5772-81.
200. Harnoss, J.M., et al., *Disruption of IRE1alpha through its kinase domain attenuates multiple myeloma.* Proc Natl Acad Sci U S A, 2019. **116**(33): p. 16420-16429.
201. Sun, H., et al., *Inhibition of IRE1alpha-driven pro-survival pathways is a promising therapeutic application in acute myeloid leukemia.* Oncotarget, 2016. **7**(14): p. 18736-49.
202. Thorpe, J.A. and S.R. Schwarze, *IRE1alpha controls cyclin A1 expression and promotes cell proliferation through XBP-1.* Cell Stress Chaperones, 2010. **15**(5): p. 497-508.
203. Bobrovnikova-Marjon, E., et al., *PERK promotes cancer cell proliferation and tumor growth by limiting oxidative DNA damage.* Oncogene, 2010. **29**(27): p. 3881-95.
204. Rong, R., et al., *Oncogenic Ras-mediated downregulation of Gadd153/CHOP is required for Ras-induced cellular transformation.* Oncogene, 2005. **24**(30): p. 4867-72.
205. Cullinan, S.B. and J.A. Diehl, *PERK-dependent activation of Nrf2 contributes to redox homeostasis and cell survival following endoplasmic reticulum stress.* J Biol Chem, 2004. **279**(19): p. 20108-17.
206. Grivennikov, S.I. and M. Karin, *Dangerous liaisons: STAT3 and NF-kappaB collaboration and crosstalk in cancer.* Cytokine Growth Factor Rev, 2010. **21**(1): p. 11-9.
207. Sano, R. and J.C. Reed, *ER stress-induced cell death mechanisms.* Biochim Biophys Acta, 2013. **1833**(12): p. 3460-3470.
208. Asha, K. and N. Sharma-Walia, *Virus and tumor microenvironment induced ER stress and unfolded protein response: from complexity to therapeutics.* Oncotarget, 2018. **9**(61): p. 31920-31936.

209. Ghosh, R., et al., *Transcriptional regulation of VEGF-A by the unfolded protein response pathway.* PLoS One, 2010. **5**(3): p. e9575.
210. Chen, X., et al., *XBP1 promotes triple-negative breast cancer by controlling the HIF1alpha pathway.* Nature, 2014. **508**(7494): p. 103-107.
211. Hayflick, L., *The Limited in Vitro Lifetime of Human Diploid Cell Strains.* Exp Cell Res, 1965. **37**: p. 614-36.
212. Shay, J.W. and W.E. Wright, *Hayflick, his limit, and cellular ageing.* Nat Rev Mol Cell Biol, 2000. **1**(1): p. 72-6.
213. Cristofalo, V.J., et al., *Replicative senescence: a critical review.* Mech Ageing Dev, 2004. **125**(10-11): p. 827-48.
214. Salama, R., et al., *Cellular senescence and its effector programs.* Genes Dev, 2014. **28**(2): p. 99-114.
215. Pluquet, O., A. Pourtier, and C. Abbadie, *The unfolded protein response and cellular senescence. A review in the theme: cellular mechanisms of endoplasmic reticulum stress signaling in health and disease.* Am J Physiol Cell Physiol, 2015. **308**(6): p. C415-25.
216. Kuilman, T., et al., *The essence of senescence.* Genes Dev, 2010. **24**(22): p. 2463-79.
217. Coppe, J.P., et al., *Senescence-associated secretory phenotypes reveal cell-nonautonomous functions of oncogenic RAS and the p53 tumor suppressor.* PLoS Biol, 2008. **6**(12): p. 2853-68.
218. Serrano, M., et al., *Oncogenic ras provokes premature cell senescence associated with accumulation of p53 and p16INK4a.* Cell, 1997. **88**(5): p. 593-602.
219. Collado, M. and M. Serrano, *Senescence in tumours: evidence from mice and humans.* Nat Rev Cancer, 2010. **10**(1): p. 51-7.
220. Kim, N.W., et al., *Specific association of human telomerase activity with immortal cells and cancer.* Science, 1994. **266**(5193): p. 2011-5.
221. Hernandez-Segura, A., J. Nehme, and M. Demaria, *Hallmarks of Cellular Senescence.* Trends Cell Biol, 2018. **28**(6): p. 436-453.
222. Dorr, J.R., et al., *Synthetic lethal metabolic targeting of cellular senescence in cancer therapy.* Nature, 2013. **501**(7467): p. 421-5.
223. Denoyelle, C., et al., *Anti-oncogenic role of the endoplasmic reticulum differentially activated by mutations in the MAPK pathway.* Nat Cell Biol, 2006. **8**(10): p. 1053-63.
224. Zhu, B., et al., *The nuclear receptor peroxisome proliferator-activated receptor-beta/delta (PPARbeta/delta) promotes oncogene-induced cellular senescence through repression of endoplasmic reticulum stress.* J Biol Chem, 2014. **289**(29): p. 20102-19.
225. Plati, J., O. Bucur, and R. Khosravi-Far, *Dysregulation of apoptotic signaling in cancer: molecular mechanisms and therapeutic opportunities.* J Cell Biochem, 2008. **104**(4): p. 1124-49.
226. Hanahan, D. and R.A. Weinberg, *Hallmarks of cancer: the next generation.* Cell, 2011. **144**(5): p. 646-74.
227. Dubrez, L., J. Berthelet, and V. Glorian, *IAP proteins as targets for drug development in oncology.* Onco Targets Ther, 2013. **9**: p. 1285-304.
228. Imoto, I., et al., *Expression of cIAP1, a target for 11q22 amplification, correlates with resistance of cervical cancers to radiotherapy.* Cancer Res, 2002. **62**(17): p. 4860-6.

229. Weber, R.G., et al., *Characterization of genomic alterations associated with glioma progression by comparative genomic hybridization.* Oncogene, 1996. **13**(5): p. 983-94.
230. Zender, L., et al., *Identification and validation of oncogenes in liver cancer using an integrative oncogenomic approach.* Cell, 2006. **125**(7): p. 1253-67.
231. Keats, J.J., et al., *Promiscuous mutations activate the noncanonical NF-kappaB pathway in multiple myeloma.* Cancer Cell, 2007. **12**(2): p. 131-44.
232. Annunziata, C.M., et al., *Frequent engagement of the classical and alternative NF-kappaB pathways by diverse genetic abnormalities in multiple myeloma.* Cancer Cell, 2007. **12**(2): p. 115-30.
233. Tamm, I., et al., *High expression levels of x-linked inhibitor of apoptosis protein and survivin correlate with poor overall survival in childhood de novo acute myeloid leukemia.* Clin Cancer Res, 2004. **10**(11): p. 3737-44.
234. Hess, C.J., et al., *Activated intrinsic apoptosis pathway is a key related prognostic parameter in acute myeloid leukemia.* J Clin Oncol, 2007. **25**(10): p. 1209-15.
235. Sung, K.W., et al., *Overexpression of X-linked inhibitor of apoptosis protein (XIAP) is an independent unfavorable prognostic factor in childhood de novo acute myeloid leukemia.* J Korean Med Sci, 2009. **24**(4): p. 605-13.
236. Hundsdoerfer, P., et al., *XIAP expression is post-transcriptionally upregulated in childhood ALL and is associated with glucocorticoid response in T-cell ALL.* Pediatr Blood Cancer, 2010. **55**(2): p. 260-6.
237. Hussain, A.R., et al., *Prognostic significance of XIAP expression in DLBCL and effect of its inhibition on AKT signalling.* J Pathol, 2010. **222**(2): p. 180-90.
238. Li, W., et al., *BV6, an IAP antagonist, activates apoptosis and enhances radiosensitization of non-small cell lung carcinoma in vitro.* J Thorac Oncol, 2011. **6**(11): p. 1801-9.
239. Fulda, S., et al., *Smac agonists sensitize for Apo2L/TRAIL- or anticancer drug-induced apoptosis and induce regression of malignant glioma in vivo.* Nat Med, 2002. **8**(8): p. 808-15.
240. Pereira, D.M., et al., *Translating endoplasmic reticulum biology into the clinic: a role for ER-targeted natural products?* Nat Prod Rep, 2015. **32**(5): p. 705-22.
241. Teicher, B.A. and J.E. Tomaszewski, *Proteasome inhibitors.* Biochem Pharmacol, 2015. **96**(1): p. 1-9.
242. Maschek, G., et al., *2-deoxy-D-glucose increases the efficacy of adriamycin and paclitaxel in human osteosarcoma and non-small cell lung cancers in vivo.* Cancer Res, 2004. **64**(1): p. 31-4.
243. Yadav, R.K., et al., *Endoplasmic reticulum stress and cancer.* J Cancer Prev, 2014. **19**(2): p. 75-88.
244. Kubiczkova, L., et al., *Proteasome inhibitors - molecular basis and current perspectives in multiple myeloma.* J Cell Mol Med, 2014. **18**(6): p. 947-61.
245. Richardson, P.G., et al., *Bortezomib: proteasome inhibition as an effective anticancer therapy.* Annu Rev Med, 2006. **57**: p. 33-47.
246. Groen, K., et al., *Carfilzomib for relapsed and refractory multiple myeloma.* Cancer Manag Res, 2019. **11**: p. 2663-2675.
247. Ojha, R. and R.K. Amaravadi, *Targeting the unfolded protein response in cancer.* Pharmacol Res, 2017. **120**: p. 258-266.

248. Volkmann, K., et al., *Potent and selective inhibitors of the inositol-requiring enzyme 1 endoribonuclease.* J Biol Chem, 2011. **286**(14): p. 12743-55.
249. Papandreou, I., et al., *Identification of an Ire1alpha endonuclease specific inhibitor with cytotoxic activity against human multiple myeloma.* Blood, 2011. **117**(4): p. 1311-4.
250. Wilhelm, T., et al., *Infliction of proteotoxic stresses by impairment of the unfolded protein response or proteasomal inhibition as a therapeutic strategy for mast cell leukemia.* Oncotarget, 2018. **9**(3): p. 2984-3000.
251. Zhao, N., et al., *Pharmacological targeting of MYC-regulated IRE1/XBP1 pathway suppresses MYC-driven breast cancer.* J Clin Invest, 2018. **128**(4): p. 1283-1299.
252. Sheng, X., et al., *IRE1alpha-XBP1s pathway promotes prostate cancer by activating c-MYC signaling.* Nat Commun, 2019. **10**(1): p. 323.
253. Axten, J.M., et al., *Discovery of 7-methyl-5-(1-{[3-(trifluoromethyl)phenyl]acetyl}-2,3-dihydro-1H-indol-5-yl)-7H-p yrrolo[2,3-d]pyrimidin-4-amine (GSK2606414), a potent and selective first-in-class inhibitor of protein kinase R (PKR)-like endoplasmic reticulum kinase (PERK).* J Med Chem, 2012. **55**(16): p. 7193-207.
254. Axten, J.M., et al., *Discovery of GSK2656157: An Optimized PERK Inhibitor Selected for Preclinical Development.* ACS Med Chem Lett, 2013. **4**(10): p. 964-8.
255. Krishnamoorthy, J., et al., *Evidence for eIF2alpha phosphorylation-independent effects of GSK2656157, a novel catalytic inhibitor of PERK with clinical implications.* Cell Cycle, 2014. **13**(5): p. 801-6.
256. Rojas-Rivera, D., et al., *When PERK inhibitors turn out to be new potent RIPK1 inhibitors: critical issues on the specificity and use of GSK2606414 and GSK2656157.* Cell Death Differ, 2017. **24**(6): p. 1100-1110.
257. Smith, A.L., et al., *Discovery of 1H-pyrazol-3(2H)-ones as potent and selective inhibitors of protein kinase R-like endoplasmic reticulum kinase (PERK).* J Med Chem, 2015. **58**(3): p. 1426-41.
258. Atkins, C., et al., *Characterization of a novel PERK kinase inhibitor with antitumor and antiangiogenic activity.* Cancer Res, 2013. **73**(6): p. 1993-2002.
259. Moore, P.C., et al., *Parallel Signaling through IRE1alpha and PERK Regulates Pancreatic Neuroendocrine Tumor Growth and Survival.* Cancer Res, 2019. **79**(24): p. 6190-6203.
260. Nadanaka, S., et al., *Role of disulfide bridges formed in the luminal domain of ATF6 in sensing endoplasmic reticulum stress.* Mol Cell Biol, 2007. **27**(3): p. 1027-43.
261. Okada, T., et al., *A serine protease inhibitor prevents endoplasmic reticulum stress-induced cleavage but not transport of the membrane-bound transcription factor ATF6.* J Biol Chem, 2003. **278**(33): p. 31024-32.
262. Gallagher, C.M. and P. Walter, *Ceapins inhibit ATF6alpha signaling by selectively preventing transport of ATF6alpha to the Golgi apparatus during ER stress.* Elife, 2016. **5**.
263. Bu, L.J., et al., *Melatonin, a novel selective ATF-6 inhibitor, induces human hepatoma cell apoptosis through COX-2 downregulation.* World J Gastroenterol, 2017. **23**(6): p. 986-998.
264. Liston, P., et al., *Identification of XAF1 as an antagonist of XIAP anti-Caspase activity.* Nat Cell Biol, 2001. **3**(2): p. 128-33.

265. Hegde, R., et al., *Identification of Omi/HtrA2 as a mitochondrial apoptotic serine protease that disrupts inhibitor of apoptosis protein-caspase interaction.* J Biol Chem, 2002. **277**(1): p. 432-8.
266. Verhagen, A.M., et al., *HtrA2 promotes cell death through its serine protease activity and its ability to antagonize inhibitor of apoptosis proteins.* J Biol Chem, 2002. **277**(1): p. 445-54.
267. Srinivasula, S.M., et al., *A conserved XIAP-interaction motif in caspase-9 and Smac/DIABLO regulates caspase activity and apoptosis.* Nature, 2001. **410**(6824): p. 112-6.
268. Gao, Z., et al., *A dimeric Smac/diablo peptide directly relieves caspase-3 inhibition by XIAP. Dynamic and cooperative regulation of XIAP by Smac/Diablo.* J Biol Chem, 2007. **282**(42): p. 30718-27.
269. Vince, J.E., et al., *IAP antagonists target cIAP1 to induce TNFalpha-dependent apoptosis.* Cell, 2007. **131**(4): p. 682-93.
270. Opel, D., et al., *Targeting inhibitor of apoptosis proteins by Smac mimetic elicits cell death in poor prognostic subgroups of chronic lymphocytic leukemia.* Int J Cancer, 2015. **137**(12): p. 2959-70.
271. El-Mesery, M., M.E. Shaker, and A. Elgaml, *The SMAC mimetic BV6 induces cell death and sensitizes different cell lines to TNF-alpha and TRAIL-induced apoptosis.* Exp Biol Med (Maywood), 2016. **241**(18): p. 2015-2022.
272. Lu, J., et al., *SM-164: a novel, bivalent Smac mimetic that induces apoptosis and tumor regression by concurrent removal of the blockade of cIAP-1/2 and XIAP.* Cancer Res, 2008. **68**(22): p. 9384-93.
273. Sun, H., et al., *Potent bivalent Smac mimetics: effect of the linker on binding to inhibitor of apoptosis proteins (IAPs) and anticancer activity.* J Med Chem, 2011. **54**(9): p. 3306-18.
274. de Almagro, M.C. and D. Vucic, *The inhibitor of apoptosis (IAP) proteins are critical regulators of signaling pathways and targets for anti-cancer therapy.* Exp Oncol, 2012. **34**(3): p. 200-11.
275. Kang, C., et al., *The DNA damage response induces inflammation and senescence by inhibiting autophagy of GATA4.* Science, 2015. **349**(6255): p. aaa5612.
276. Schott, C., et al., *Oncogenic RAS Mutants Confer Resistance of RMS13 Rhabdomyosarcoma Cells to Oxidative Stress-Induced Ferroptotic Cell Death.* Front Oncol, 2015. **5**: p. 131.
277. Franken, N.A., et al., *Clonogenic assay of cells in vitro.* Nat Protoc, 2006. **1**(5): p. 2315-9.
278. Sannino, S., et al., *Compensatory increases of select proteostasis networks after Hsp70 inhibition in cancer cells.* J Cell Sci, 2018. **131**(17).
279. Sabnis, A.J., et al., *Combined chemical-genetic approach identifies cytosolic HSP70 dependence in rhabdomyosarcoma.* Proc Natl Acad Sci U S A, 2016. **113**(32): p. 9015-20.
280. Leon-Annicchiarico, C.L., et al., *ATF4 mediates necrosis induced by glucose deprivation and apoptosis induced by 2-deoxyglucose in the same cells.* FEBS J, 2015. **282**(18): p. 3647-58.
281. Briggs, J.W., et al., *Activation of the unfolded protein response in sarcoma cells treated with rapamycin or temsirolimus.* PLoS One, 2017. **12**(9): p. e0185089.

282. Kao, C., et al., *Bortezomib enhances cancer cell death by blocking the autophagic flux through stimulating ERK phosphorylation.* Cell Death Dis, 2014. **5**: p. e1510.
283. Thaler, S., et al., *The proteasome inhibitor Bortezomib (Velcade) as potential inhibitor of estrogen receptor-positive breast cancer.* Int J Cancer, 2015. **137**(3): p. 686-97.
284. Ando, M., et al., *Bortezomib sensitizes non-small cell lung cancer to mesenchymal stromal cell-delivered inducible caspase-9-mediated cytotoxicity.* Cancer Gene Ther, 2014. **21**(11): p. 472-482.
285. Uddin, S., et al., *Bortezomib (Velcade) induces p27Kip1 expression through S-phase kinase protein 2 degradation in colorectal cancer.* Cancer Res, 2008. **68**(9): p. 3379-88.
286. Niu, H., M. Manfredi, and J.A. Ecsedy, *Scientific Rationale Supporting the Clinical Development Strategy for the Investigational Aurora A Kinase Inhibitor Alisertib in Cancer.* Front Oncol, 2015. **5**: p. 189.
287. Ommer, J., et al., *Aurora A Kinase Inhibition Destabilizes PAX3-FOXO1 and MYCN and Synergizes with Navitoclax to Induce Rhabdomyosarcoma Cell Death.* Cancer Res, 2020. **80**(4): p. 832-842.
288. Yohe, M.E., et al., *MEK inhibition induces MYOG and remodels super-enhancers in RAS-driven rhabdomyosarcoma.* Sci Transl Med, 2018. **10**(448).
289. Almazan-Moga, A., et al., *Ligand-dependent Hedgehog pathway activation in Rhabdomyosarcoma: the oncogenic role of the ligands.* Br J Cancer, 2017. **117**(9): p. 1314-1325.
290. Horiguchi, M., et al., *Stress-regulated transcription factor ATF4 promotes neoplastic transformation by suppressing expression of the INK4a/ARF cell senescence factors.* Cancer Res, 2012. **72**(2): p. 395-401.
291. Kim, H.D., et al., *Phenylbutyric acid induces the cellular senescence through an Akt/p21(WAF1) signaling pathway.* Biochem Biophys Res Commun, 2012. **422**(2): p. 213-8.
292. Crose, L.E., et al., *Alveolar rhabdomyosarcoma-associated PAX3-FOXO1 promotes tumorigenesis via Hippo pathway suppression.* J Clin Invest, 2014. **124**(1): p. 285-96.
293. Ewald, J.A., et al., *Therapy-induced senescence in cancer.* J Natl Cancer Inst, 2010. **102**(20): p. 1536-46.
294. Ewald, J.A., et al., *A high-throughput method to identify novel senescence-inducing compounds.* J Biomol Screen, 2009. **14**(7): p. 853-8.
295. te Poele, R.H., et al., *DNA damage is able to induce senescence in tumor cells in vitro and in vivo.* Cancer Res, 2002. **62**(6): p. 1876-83.
296. Chang, B.D., et al., *A senescence-like phenotype distinguishes tumor cells that undergo terminal proliferation arrest after exposure to anticancer agents.* Cancer Res, 1999. **59**(15): p. 3761-7.
297. Roninson, I.B., *Tumor cell senescence in cancer treatment.* Cancer Res, 2003. **63**(11): p. 2705-15.
298. Crouch, S.P., et al., *The use of ATP bioluminescence as a measure of cell proliferation and cytotoxicity.* J Immunol Methods, 1993. **160**(1): p. 81-8.
299. Boedicker, C., et al., *Co-inhibition of BET proteins and PI3Kalpha triggers mitochondrial apoptosis in rhabdomyosarcoma cells.* Oncogene, 2020.
300. Takashima, A. and D.V. Faller, *Targeting the RAS oncogene.* Expert Opin Ther Targets, 2013. **17**(5): p. 507-31.

301. Pylayeva-Gupta, Y., E. Grabocka, and D. Bar-Sagi, *RAS oncogenes: weaving a tumorigenic web.* Nat Rev Cancer, 2011. **11**(11): p. 761-74.
302. Riccardi, C. and I. Nicoletti, *Analysis of apoptosis by propidium iodide staining and flow cytometry.* Nat Protoc, 2006. **1**(3): p. 1458-61.
303. Scholzen, T. and J. Gerdes, *The Ki-67 protein: from the known and the unknown.* J Cell Physiol, 2000. **182**(3): p. 311-22.
304. Lawless, C., et al., *Quantitative assessment of markers for cell senescence.* Exp Gerontol, 2010. **45**(10): p. 772-8.
305. Schilbach, K., et al., *Cancer-targeted IL-12 controls human rhabdomyosarcoma by senescence induction and myogenic differentiation.* Oncoimmunology, 2015. **4**(7): p. e1014760.
306. Pospelova, T.V., et al., *Pseudo-DNA damage response in senescent cells.* Cell Cycle, 2009. **8**(24): p. 4112-8.
307. Narita, M., et al., *Rb-mediated heterochromatin formation and silencing of E2F target genes during cellular senescence.* Cell, 2003. **113**(6): p. 703-16.
308. Noren Hooten, N. and M.K. Evans, *Techniques to Induce and Quantify Cellular Senescence.* J Vis Exp, 2017(123).
309. Wang, E., *Senescent human fibroblasts resist programmed cell death, and failure to suppress bcl2 is involved.* Cancer Res, 1995. **55**(11): p. 2284-92.
310. Childs, B.G., et al., *Senescence and apoptosis: dueling or complementary cell fates?* EMBO Rep, 2014. **15**(11): p. 1139-53.
311. Yosef, R., et al., *Directed elimination of senescent cells by inhibition of BCL-W and BCL-XL.* Nat Commun, 2016. **7**: p. 11190.
312. Nishida, E. and Y. Gotoh, *The MAP kinase cascade is essential for diverse signal transduction pathways.* Trends Biochem Sci, 1993. **18**(4): p. 128-31.
313. Deschenes-Simard, X., et al., *Tumor suppressor activity of the ERK/MAPK pathway by promoting selective protein degradation.* Genes Dev, 2013. **27**(8): p. 900-15.
314. Roberts, P.J. and C.J. Der, *Targeting the Raf-MEK-ERK mitogen-activated protein kinase cascade for the treatment of cancer.* Oncogene, 2007. **26**(22): p. 3291-310.
315. Ritt, D.A., et al., *Inhibition of Ras/Raf/MEK/ERK Pathway Signaling by a Stress-Induced Phospho-Regulatory Circuit.* Mol Cell, 2016. **64**(5): p. 875-887.
316. Lin, L., et al., *MEK inhibitors induce apoptosis via FoxO3a-dependent PUMA induction in colorectal cancer cells.* Oncogenesis, 2018. **7**(9): p. 67.
317. Dolgikh, N., et al., *NRAS-Mutated Rhabdomyosarcoma Cells Are Vulnerable to Mitochondrial Apoptosis Induced by Coinhibition of MEK and PI3Kalpha.* Cancer Res, 2018. **78**(8): p. 2000-2013.
318. Kollareddy, M., et al., *Aurora kinases: structure, functions and their association with cancer.* Biomed Pap Med Fac Univ Palacky Olomouc Czech Repub, 2008. **152**(1): p. 27-33.
319. Ortiz-Lazareno, P.C., et al., *Sensitization of U937 leukemia cells to doxorubicin by the MG132 proteasome inhibitor induces an increase in apoptosis by suppressing NF-kappa B and mitochondrial membrane potential loss.* Cancer Cell Int, 2014. **14**(1): p. 13.
320. Takahashi, N., et al., *Necrostatin-1 analogues: critical issues on the specificity, activity and in vivo use in experimental disease models.* Cell Death Dis, 2012. **3**: p. e437.

321. Tanabe, Y., et al., *IRE1alpha-XBP1 inhibitors exerted anti-tumor activities in Ewing's sarcoma.* Oncotarget, 2018. **9**(18): p. 14428-14443.
322. Chaiyawat, P., et al., *Protein profiling of osteosarcoma tissue and soft callus unveils activation of the unfolded protein response pathway.* Int J Oncol, 2019. **54**(5): p. 1704-1718.
323. Dey, S., et al., *ATF4-dependent induction of heme oxygenase 1 prevents anoikis and promotes metastasis.* J Clin Invest, 2015. **125**(7): p. 2592-608.
324. Mirabelli, P., L. Coppola, and M. Salvatore, *Cancer Cell Lines Are Useful Model Systems for Medical Research.* Cancers (Basel), 2019. **11**(8).
325. McGrath, E.P., et al., *The Unfolded Protein Response in Breast Cancer.* Cancers (Basel), 2018. **10**(10).
326. Drogat, B., et al., *IRE1 signaling is essential for ischemia-induced vascular endothelial growth factor-A expression and contributes to angiogenesis and tumor growth in vivo.* Cancer Res, 2007. **67**(14): p. 6700-7.
327. Croft, A., et al., *Oncogenic activation of MEK/ERK primes melanoma cells for adaptation to endoplasmic reticulum stress.* J Invest Dermatol, 2014. **134**(2): p. 488-497.
328. Langenau, D.M., et al., *Effects of RAS on the genesis of embryonal rhabdomyosarcoma.* Genes Dev, 2007. **21**(11): p. 1382-95.
329. Eddaoudi, A., S.L. Canning, and I. Kato, *Flow Cytometric Detection of G0 in Live Cells by Hoechst 33342 and Pyronin Y Staining.* Methods Mol Biol, 2018. **1686**: p. 49-57.
330. Schorl, C. and J.M. Sedivy, *Analysis of cell cycle phases and progression in cultured mammalian cells.* Methods, 2007. **41**(2): p. 143-50.
331. Yiangou, L., et al., *Method to Synchronize Cell Cycle of Human Pluripotent Stem Cells without Affecting Their Fundamental Characteristics.* Stem Cell Reports, 2019. **12**(1): p. 165-179.
332. Cecchini, M.J., M. Amiri, and F.A. Dick, *Analysis of cell cycle position in mammalian cells.* J Vis Exp, 2012(59).
333. Teodoro, T., et al., *Pancreatic beta-cells depend on basal expression of active ATF6alpha-p50 for cell survival even under nonstress conditions.* Am J Physiol Cell Physiol, 2012. **302**(7): p. C992-1003.
334. Lokman, N.A., et al., *Chick chorioallantoic membrane (CAM) assay as an in vivo model to study the effect of newly identified molecules on ovarian cancer invasion and metastasis.* Int J Mol Sci, 2012. **13**(8): p. 9959-70.
335. Zanola, A., et al., *Rhabdomyosarcomas: an overview on the experimental animal models.* J Cell Mol Med, 2012. **16**(7): p. 1377-91.
336. Hanna, J.A., et al., *PAX3-FOXO1 drives miR-486-5p and represses miR-221 contributing to pathogenesis of alveolar rhabdomyosarcoma.* Oncogene, 2018. **37**(15): p. 1991-2007.
337. Schmitt-Ney, M. and G. Camussi, *The PAX3-FOXO1 fusion protein present in rhabdomyosarcoma interferes with normal FOXO activity and the TGF-beta pathway.* PLoS One, 2015. **10**(3): p. e0121474.
338. Beausejour, C.M., et al., *Reversal of human cellular senescence: roles of the p53 and p16 pathways.* EMBO J, 2003. **22**(16): p. 4212-22.
339. Dirac, A.M. and R. Bernards, *Reversal of senescence in mouse fibroblasts through lentiviral suppression of p53.* J Biol Chem, 2003. **278**(14): p. 11731-4.
340. Coppe, J.P., et al., *The senescence-associated secretory phenotype: the dark side of tumor suppression.* Annu Rev Pathol, 2010. **5**: p. 99-118.

341. Lee, S. and C.A. Schmitt, *The dynamic nature of senescence in cancer.* Nat Cell Biol, 2019. **21**(1): p. 94-101.
342. Ma, X.H., et al., *Targeting ER stress-induced autophagy overcomes BRAF inhibitor resistance in melanoma.* J Clin Invest, 2014. **124**(3): p. 1406-17.
343. Nikesitch, N., et al., *Endoplasmic reticulum stress in the development of multiple myeloma and drug resistance.* Clin Transl Immunology, 2018. **7**(1): p. e1007.
344. Lancaster, S., *Bortezomib: the evidence of its clinical impact in multiple myeloma.* Core Evid, 2006. **1**(4): p. 265-77.
345. Hideshima, T., et al., *The proteasome inhibitor PS-341 inhibits growth, induces apoptosis, and overcomes drug resistance in human multiple myeloma cells.* Cancer Res, 2001. **61**(7): p. 3071-6.
346. LeBlanc, R., et al., *Proteasome inhibitor PS-341 inhibits human myeloma cell growth in vivo and prolongs survival in a murine model.* Cancer Res, 2002. **62**(17): p. 4996-5000.
347. Roccaro, A.M., et al., *Bortezomib mediates antiangiogenesis in multiple myeloma via direct and indirect effects on endothelial cells.* Cancer Res, 2006. **66**(1): p. 184-91.
348. Bersani, F., et al., *Bortezomib-mediated proteasome inhibition as a potential strategy for the treatment of rhabdomyosarcoma.* Eur J Cancer, 2008. **44**(6): p. 876-84.
349. Kahen, E., et al., *Identification of clinically achievable combination therapies in childhood rhabdomyosarcoma.* Cancer Chemother Pharmacol, 2016. **78**(2): p. 313-23.
350. Jothi, M., et al., *Small molecule inhibition of PAX3-FOXO1 through AKT activation suppresses malignant phenotypes of alveolar rhabdomyosarcoma.* Mol Cancer Ther, 2013. **12**(12): p. 2663-74.
351. Petersen, S.L., et al., *Autocrine TNFalpha signaling renders human cancer cells susceptible to Smac-mimetic-induced apoptosis.* Cancer Cell, 2007. **12**(5): p. 445-56.
352. Schirmer, M., et al., *Intrinsic and chemo-sensitizing activity of SMAC-mimetics on high-risk childhood acute lymphoblastic leukemia.* Cell Death Dis, 2016. **7**: p. e2052.
353. Warnakulasuriyarachchi, D., et al., *Translational induction of the inhibitor of apoptosis protein HIAP2 during endoplasmic reticulum stress attenuates cell death and is mediated via an inducible internal ribosome entry site element.* J Biol Chem, 2004. **279**(17): p. 17148-57.
354. Gilmore, T.D. and M. Herscovitch, *Inhibitors of NF-kappaB signaling: 785 and counting.* Oncogene, 2006. **25**(51): p. 6887-99.
355. Vallabhapurapu, S., et al., *Nonredundant and complementary functions of TRAF2 and TRAF3 in a ubiquitination cascade that activates NIK-dependent alternative NF-kappaB signaling.* Nat Immunol, 2008. **9**(12): p. 1364-70.
356. Zarnegar, B.J., et al., *Noncanonical NF-kappaB activation requires coordinated assembly of a regulatory complex of the adaptors cIAP1, cIAP2, TRAF2 and TRAF3 and the kinase NIK.* Nat Immunol, 2008. **9**(12): p. 1371-8.
357. Xu, H., et al., *N-alpha-acetyltransferase 10 protein inhibits apoptosis through RelA/p65-regulated MCL1 expression.* Carcinogenesis, 2012. **33**(6): p. 1193-202.

358. Ramakrishnan, V., et al., *Smac mimetic LCL161 overcomes protective ER stress induced by obatoclax, synergistically causing cell death in multiple myeloma.* Oncotarget, 2016. **7**(35): p. 56253-56265.
359. Zhou, L., et al., *The IAP antagonist birinapant potentiates bortezomib anti-myeloma activity in vitro and in vivo.* J Hematol Oncol, 2019. **12**(1): p. 25.
360. Nozaki, S., G.W. Sledge, Jr., and H. Nakshatri, *Repression of GADD153/CHOP by NF-kappaB: a possible cellular defense against endoplasmic reticulum stress-induced cell death.* Oncogene, 2001. **20**(17): p. 2178-85.
361. Burikhanov, R., et al., *Novel mechanism of apoptosis resistance in cancer mediated by extracellular PAR-4.* Cancer Res, 2013. **73**(2): p. 1011-9.
362. Patel, N.M., et al., *Paclitaxel sensitivity of breast cancer cells with constitutively active NF-kappaB is enhanced by IkappaBalpha super-repressor and parthenolide.* Oncogene, 2000. **19**(36): p. 4159-69.
363. Liu, H., et al., *Regulation of Mcl-1 by constitutive activation of NF-kappaB contributes to cell viability in human esophageal squamous cell carcinoma cells.* BMC Cancer, 2014. **14**: p. 98.
364. Jeyasuria, P., et al., *Elevated levels of uterine anti-apoptotic signaling may activate NFKB and potentially confer resistance to caspase 3-mediated apoptotic cell death during pregnancy in mice.* Biol Reprod, 2011. **85**(2): p. 417-24.
365. Wang, H., et al., *Tunicamycin-induced unfolded protein response in the developing mouse brain.* Toxicol Appl Pharmacol, 2015. **283**(3): p. 157-67.
366. Liu, C.Y., et al., *ER stress-related ATF6 upregulates CIP2A and contributes to poor prognosis of colon cancer.* Mol Oncol, 2018. **12**(10): p. 1706-1717.
367. Wu, J., et al., *Tunicamycin specifically aggravates ER stress and overcomes chemoresistance in multidrug-resistant gastric cancer cells by inhibiting N-glycosylation.* J Exp Clin Cancer Res, 2018. **37**(1): p. 272.
368. Yamazaki, H., et al., *Activation of the Akt-NF-kappaB pathway by subtilase cytotoxin through the ATF6 branch of the unfolded protein response.* J Immunol, 2009. **183**(2): p. 1480-7.
369. Rao, J., et al., *ATF6 mediates a pro-inflammatory synergy between ER stress and TLR activation in the pathogenesis of liver ischemia-reperfusion injury.* Am J Transplant, 2014. **14**(7): p. 1552-61.
370. Adamson, P.C., *Improving the outcome for children with cancer: Development of targeted new agents.* CA Cancer J Clin, 2015. **65**(3): p. 212-20.
371. Vassal, G., et al., *New drugs for children and adolescents with cancer: the need for novel development pathways.* Lancet Oncol, 2013. **14**(3): p. e117-24.
372. Adamson, P.C., et al., *Drug discovery in paediatric oncology: roadblocks to progress.* Nat Rev Clin Oncol, 2014. **11**(12): p. 732-9.
373. Dorsey, E.R., et al., *Funding of US biomedical research, 2003-2008.* JAMA, 2010. **303**(2): p. 137-43.
374. Norris, R.E. and P.C. Adamson, *Challenges and opportunities in childhood cancer drug development.* Nat Rev Cancer, 2012. **12**(11): p. 776-82.
375. Ireson, C.R., et al., *The role of mouse tumour models in the discovery and development of anticancer drugs.* Br J Cancer, 2019. **121**(2): p. 101-108.
376. Teitz, T., et al., *Preclinical models for neuroblastoma: establishing a baseline for treatment.* PLoS One, 2011. **6**(4): p. e19133.

377. Nagelkerke, A., et al., *The unfolded protein response as a target for cancer therapy.* Biochim Biophys Acta, 2014. **1846**(2): p. 277-84.
378. Lhomond, S., et al., *Dual IRE1 RNase functions dictate glioblastoma development.* EMBO Mol Med, 2018. **10**(3).
379. Harnoss, J.M., et al., *IRE1alpha Disruption in Triple-Negative Breast Cancer Cooperates with Antiangiogenic Therapy by Reversing ER Stress Adaptation and Remodeling the Tumor Microenvironment.* Cancer Res, 2020. **80**(11): p. 2368-2379.
380. Blais, J.D., et al., *Perk-dependent translational regulation promotes tumor cell adaptation and angiogenesis in response to hypoxic stress.* Mol Cell Biol, 2006. **26**(24): p. 9517-32.
381. Wang, Y., et al., *The unfolded protein response induces the angiogenic switch in human tumor cells through the PERK/ATF4 pathway.* Cancer Res, 2012. **72**(20): p. 5396-406.
382. Gass, J.N., et al., *The unfolded protein response of B-lymphocytes: PERK-independent development of antibody-secreting cells.* Mol Immunol, 2008. **45**(4): p. 1035-43.
383. Grootjans, J., et al., *The unfolded protein response in immunity and inflammation.* Nat Rev Immunol, 2016. **16**(8): p. 469-84.
384. Sato, H., et al., *4mu8C Inhibits Insulin Secretion Independent of IRE1alpha RNase Activity.* Cell Struct Funct, 2017. **42**(1): p. 61-70.
385. Chan, S.M.H., et al., *The inositol-requiring enzyme 1 (IRE1alpha) RNAse inhibitor, 4micro8C, is also a potent cellular antioxidant.* Biochem J, 2018. **475**(5): p. 923-929.
386. Yu, Q., et al., *Type I interferons mediate pancreatic toxicities of PERK inhibition.* Proc Natl Acad Sci U S A, 2015. **112**(50): p. 15420-5.
387. Westhoff, M.A., et al., *Cell death-based treatment of childhood cancer.* Cell Death Dis, 2018. **9**(2): p. 116.
388. Fulda, S., *Targeting apoptosis for anticancer therapy.* Semin Cancer Biol, 2015. **31**: p. 84-8.
389. Adams, J.M. and S. Cory, *The Bcl-2 apoptotic switch in cancer development and therapy.* Oncogene, 2007. **26**(9): p. 1324-37.
390. Fulda, S., *How to target apoptosis signaling pathways for the treatment of pediatric cancers.* Front Oncol, 2013. **3**: p. 22.
391. Faqar-Uz-Zaman, S.F., et al., *BCL-xL-selective BH3 mimetic sensitizes rhabdomyosarcoma cells to chemotherapeutics by activation of the mitochondrial pathway of apoptosis.* Cancer Lett, 2018. **412**: p. 131-142.
392. Goldsmith, K.C., et al., *BH3 peptidomimetics potently activate apoptosis and demonstrate single agent efficacy in neuroblastoma.* Oncogene, 2006. **25**(33): p. 4525-33.
393. Dean, E., et al., *Phase I trial of AEG35156 administered as a 7-day and 3-day continuous intravenous infusion in patients with advanced refractory cancer.* J Clin Oncol, 2009. **27**(10): p. 1660-6.
394. Fulda, S., *Promises and Challenges of Smac Mimetics as Cancer Therapeutics.* Clin Cancer Res, 2015. **21**(22): p. 5030-6.
395. Dachert, J., et al., *Targeting ferroptosis in rhabdomyosarcoma cells.* Int J Cancer, 2020. **146**(2): p. 510-520.
396. Frank, T., et al., *Cell cycle arrest in mitosis promotes interferon-induced necroptosis.* Cell Death Differ, 2019. **26**(10): p. 2046-2060.

397. Almond, J.B., et al., *Proteasome inhibitor-induced apoptosis of B-chronic lymphocytic leukaemia cells involves cytochrome c release and caspase activation, accompanied by formation of an approximately 700 kDa Apaf-1 containing apoptosome complex.* Leukemia, 2001. **15**(9): p. 1388-97.
398. Pahler, J.C., et al., *Effects of the proteasome inhibitor, bortezomib, on apoptosis in isolated lymphocytes obtained from patients with chronic lymphocytic leukemia.* Clin Cancer Res, 2003. **9**(12): p. 4570-7.
399. Miller, C.P., et al., *NPI-0052, a novel proteasome inhibitor, induces caspase-8 and ROS-dependent apoptosis alone and in combination with HDAC inhibitors in leukemia cells.* Blood, 2007. **110**(1): p. 267-77.
400. Colado, E., et al., *The effect of the proteasome inhibitor bortezomib on acute myeloid leukemia cells and drug resistance associated with the CD34+ immature phenotype.* Haematologica, 2008. **93**(1): p. 57-66.
401. Brignole, C., et al., *Effect of bortezomib on human neuroblastoma cell growth, apoptosis, and angiogenesis.* J Natl Cancer Inst, 2006. **98**(16): p. 1142-57.
402. Valentiner, U., et al., *Effects of bortezomib on human neuroblastoma cells in vitro and in a metastatic xenograft model.* Anticancer Res, 2009. **29**(4): p. 1219-25.
403. Luo, P., et al., *Bortezomib induces apoptosis in human neuroblastoma CHP126 cells.* Pharmazie, 2010. **65**(3): p. 213-8.
404. Foufelle, F. and B. Fromenty, *Role of endoplasmic reticulum stress in drug-induced toxicity.* Pharmacol Res Perspect, 2016. **4**(1): p. e00211.
405. Bourke, C.A. and M.J. Carrigan, *Experimental tunicamycin toxicity in cattle, sheep and pigs.* Aust Vet J, 1993. **70**(5): p. 188-9.
406. Morin, M.J. and R.J. Bernacki, *Biochemical effects and therapeutic potential of tunicamycin in murine L1210 leukemia.* Cancer Res, 1983. **43**(4): p. 1669-74.
407. Han, X., et al., *Tunicamycin enhances the antitumor activity of trastuzumab on breast cancer in vitro and in vivo.* Oncotarget, 2015. **6**(36): p. 38912-25.
408. Ferreira, R.B., et al., *Novel agents that downregulate EGFR, HER2, and HER3 in parallel.* Oncotarget, 2015. **6**(12): p. 10445-59.
409. Ferreira, R.B., et al., *Disulfide bond disrupting agents activate the unfolded protein response in EGFR- and HER2-positive breast tumor cells.* Oncotarget, 2017. **8**(17): p. 28971-28989.
410. Nardella, C., et al., *Pro-senescence therapy for cancer treatment.* Nat Rev Cancer, 2011. **11**(7): p. 503-11.
411. Fujimoto, A., et al., *Inhibition of endoplasmic reticulum (ER) stress sensors sensitizes cancer stem-like cells to ER stress-mediated apoptosis.* Oncotarget, 2016. **7**(32): p. 51854-51864.
412. Fakler, M., et al., *Small molecule XIAP inhibitors cooperate with TRAIL to induce apoptosis in childhood acute leukemia cells and overcome Bcl-2-mediated resistance.* Blood, 2009. **113**(8): p. 1710-22.
413. Loeder, S., et al., *Small molecule XIAP inhibitors sensitize childhood acute leukemia cells for CD95-induced apoptosis.* Int J Cancer, 2010. **126**(9): p. 2216-28.
414. Wagner, L., et al., *Smac mimetic sensitizes glioblastoma cells to Temozolomide-induced apoptosis in a RIP1- and NF-kappaB-dependent manner.* Oncogene, 2013. **32**(8): p. 988-97.

415. Messinger, Y., et al., *Phase I study of bortezomib combined with chemotherapy in children with relapsed childhood acute lymphoblastic leukemia (ALL): a report from the therapeutic advances in childhood leukemia (TACL) consortium.* Pediatr Blood Cancer, 2010. **55**(2): p. 254-9.
416. Bertaina, A., et al., *The combination of bortezomib with chemotherapy to treat relapsed/refractory acute lymphoblastic leukaemia of childhood.* Br J Haematol, 2017. **176**(4): p. 629-636.
417. Hiss, D.C., G.A. Gabriels, and P.I. Folb, *Combination of tunicamycin with anticancer drugs synergistically enhances their toxicity in multidrug-resistant human ovarian cystadenocarcinoma cells.* Cancer Cell Int, 2007. **7**: p. 5.
418. Zhong, J.T., et al., *Effects of endoplasmic reticulum stress on the autophagy, apoptosis, and chemotherapy resistance of human breast cancer cells by regulating the PI3K/AKT/mTOR signaling pathway.* Tumour Biol, 2017. **39**(5): p. 1010428317697562.
419. Wright, J.J., *Combination therapy of bortezomib with novel targeted agents: an emerging treatment strategy.* Clin Cancer Res, 2010. **16**(16): p. 4094-104.
420. Jiang, H.Y. and R.C. Wek, *Phosphorylation of the alpha-subunit of the eukaryotic initiation factor-2 (eIF2alpha) reduces protein synthesis and enhances apoptosis in response to proteasome inhibition.* J Biol Chem, 2005. **280**(14): p. 14189-202.
421. Wu, H., J. Tschopp, and S.C. Lin, *Smac mimetics and TNFalpha: a dangerous liaison?* Cell, 2007. **131**(4): p. 655-8.
422. Guan, S., et al., *Second-generation proteasome inhibitor carfilzomib sensitizes neuroblastoma cells to doxorubicin-induced apoptosis.* Oncotarget, 2016. **7**(46): p. 75914-75925.
423. Nagano, T., et al., *Identification of cellular senescence-specific genes by comparative transcriptomics.* Sci Rep, 2016. **6**: p. 31758.
424. Tamamori-Adachi, M., et al., *DNA damage response induced by Etoposide promotes steroidogenesis via GADD45A in cultured adrenal cells.* Sci Rep, 2018. **8**(1): p. 9636.

Appendix A

Low dose etoposide is commonly used as a positive control for senescence induction [423, 424]. RH30 and RD cells were treated with etoposide (0.25 µg/ml) for 72 h. After 72 h of treatment, treatment was removed and replaced with regular media. After 72 h cells were stained with β-Gal. β-Gal positive cells were observed in etoposide treated RH30 and RD cells (Fig. A1).

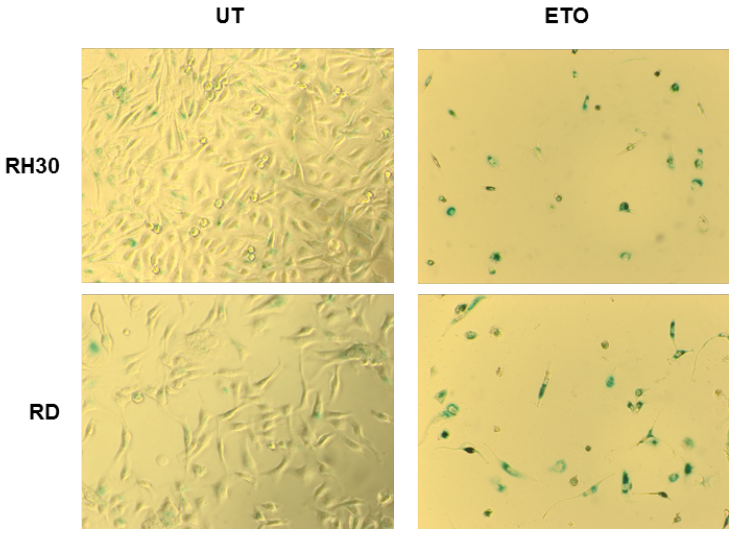

Figure A1: Etoposide increases β-Gal in RMS cells – Etoposide (0.25 µg/ml) was added to RH30 and RD cells for 72 h before being removed and replaced with regular media. After a total of 6 days, cells were fixed, and β-Gal staining was applied to cells and left overnight, before being imaged with an IX71 microscope using a 10X objective. One of three independent experiments performed in triplicate are shown.

Etoposide was also used as a positive control to investigate miR146 expression levels in RH30-miR146-GFP and RD-miR146-GFP cells. RH30-miR146-GFP and RD-miR146-GFP cells were treated with etoposide (0.25 µg/ml) for 72 h. After 72 h of treatment, treatment was removed and replaced with regular media. On day 6, GFP positive cells were observed in ETO treated RH30-miR146-GFP and RD-miR146-GFP cells (Fig. A2).

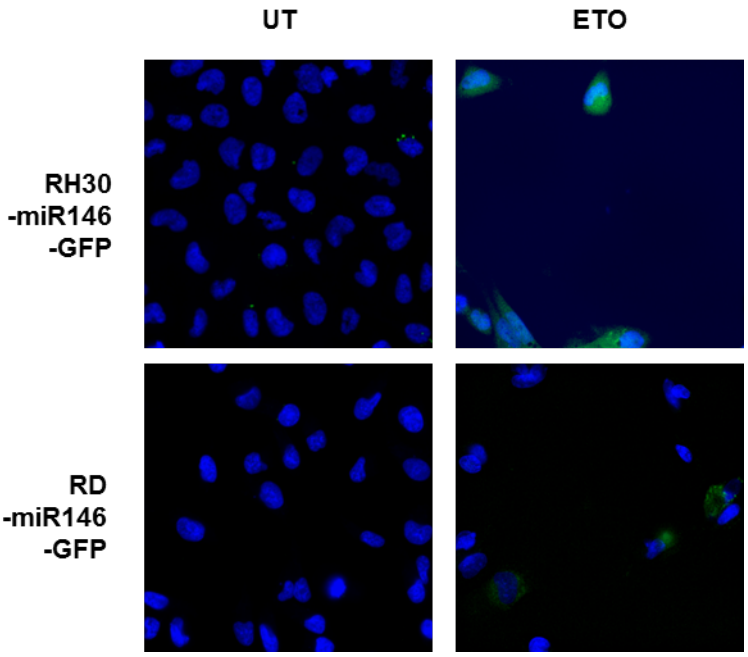

Figure A2: Etoposide upregulates the senescence marker miR146 in RMS cells - RH30-miR146-GFP and RD-miR146-GFP cells were treated with Etoposide (0.25 µg/ml) for 72 h before being replaced with regular media. After a total of 6 days, fluorescence was measured at a Molecular Device Microscope with an automated analysis using MetaXpress Software. DAPI-FITC overlay images were generated; Blue: DAPI/Hoechst stained cells, Green: GFP positive cells. One of three independent experiments are shown.